In vitro Ly6C^{high} monocyte generation as a novel tool for inflammatory diseases research

Juan Antonio Calatayud Subias

DOCTORAL THESIS

In vitro Ly6C^{high} monocyte generation as a novel tool for inflammatory diseases research

J. A. Calatayud-Subias

Barcelona 2016

In vitro Ly6C^{high} monocyte generation as a novel tool for inflammatory diseases research

(Generación *In vitro* de monocitos Ly6C^{high} para el estudio de enfermedades inflamatorias)

DOCTORAL THESIS
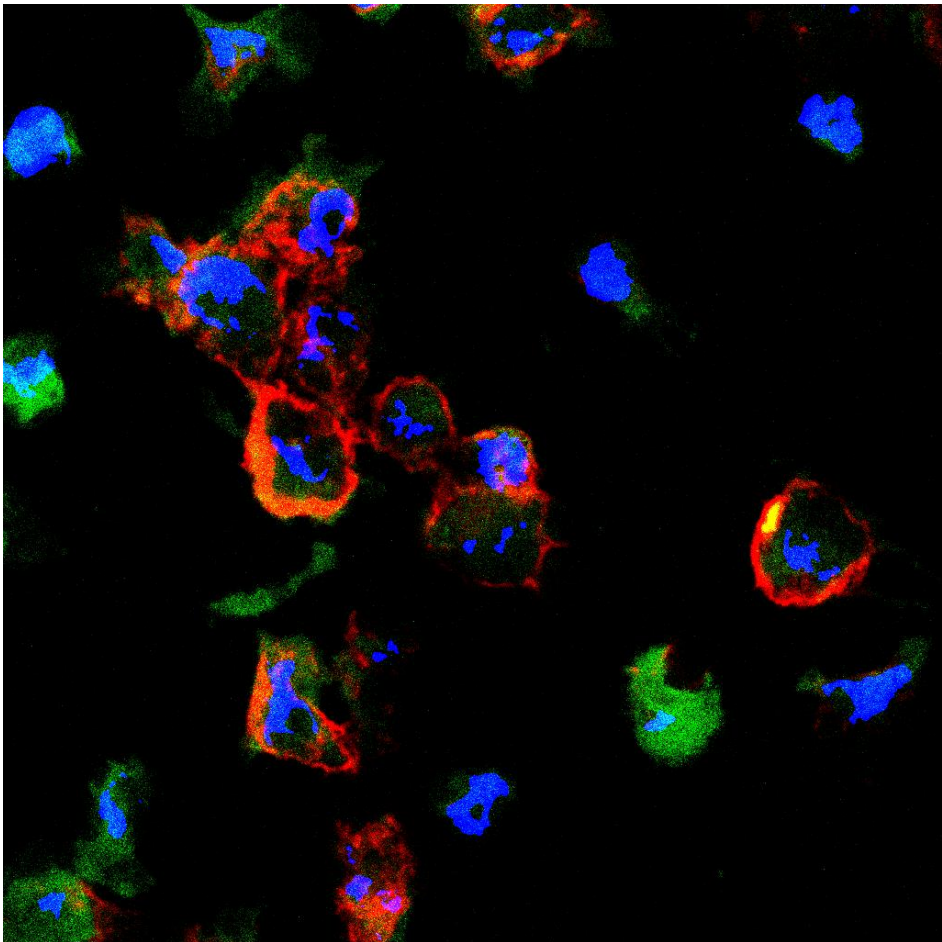
Juan Antonio Calatayud Subias

Barcelona 2016

PhD Programme in Biomedicine

Programa de Doctorado en Biomedicina

In vitro Ly6C^{high} monocyte generation as a novel tool for inflammatory diseases research

Generación *In vitro* de monocitos Ly6C^{high} para el estudio de enfermedades inflamatorias

Thesis submitted by – Memoria presentada por

Juan Antonio Calatayud Subias

To qualify for the Doctorate degree by – Para optar al grado de Doctor por la

University of Barcelona – Universidad de Barcelona

Department of Cell Biology, Physiology and Immunology –

Departamento de Biología Celular, Fisiología e Inmunología

Laboratory of Macrophage Biology – Laboratorio de Biología del Macrofago

Thesis Director
Director de tesis
Dr. Jorge Lloberas Cavero

Associate Professor

Die Wahrheit hat keine Grenzen, Formen oder Farben.

ACKNOWLEDGMENTS

INDEX

TABLE OF CONTENTS

LIST OF FIGURES & TABLES

I. INTRODUCTION

III.EXPERIMENTAL PROCEDURES

IV. RESULTS

VIII. SUPPLEMENTARY FIGURES

X

KEYWORDS AND ABREVIATIONS

APC: Antigen presenting cell

ARG1/*arg1*: Arginase 1 protein/gene

BMDM: Bone marrow-derived macrophages

BMDMo: Bone marrow-derived monocytes

CCR2: Chemokine receptor, MCP-1 receptor

CD115: Cluster of differentiation molecule 115, M-CSF receptor

CD11b: Cluster of differentiation molecule 11b, Integrin alpha M

CD11c: Cluster of differentiation molecule 11c, Integrin alpha X

CD14: Cluster of differentiation molecule 14, TLR4 co-receptor

$CD14^{hi}$: Human pro-inflammatory monocytes

CD16: Cluster of differentiation molecule 16, Fc receptor of low affinity FcγRIIIa/b

CD62L: Cluster of differentiation molecule 62L, L-selectin

CD68: Cluster of differentiation molecule 68, Macrosialin

CD80: Cluster of differentiation molecule 80, B7-1

CNS: Central nervous system

COX-2/*cox-2*: Inducible ciclooxygenase 2 protein/gene

CX3CR1: Chemokine receptor, Fraktalkine receptor

DAMPs: Damage-associated molecular patterns

DC: Dendritic cells

DiR: Dialkylcarbocyanine Lipophillic tracer

DMSO: Dimethylsulfoxide

DNFB: 1-Fluoro-2,4-dinitrofluorobenzene

EAE: Experimental autoimmune encephalopathy

EDTA: Ethylendiaminetetraacetic acid

F4/80: EGF-like module-containing mucin-like hormone receptor like 1

FACS: Flow activated cell sorting

FCS: Foetal calf serum

FIZZ-1/*fizz-1*: Found in inflammatory zone 1 protein/gene

G-CSF: Granulocyte colony stimulating factor

GM-CSF: Granulocyte macrophage colony stimulating factor

Gr-1: Granulocyte differentiation antigen 1

HEVs: High endothelial venules

HSC: Hematopoietic stem cell

IFN-γ/*ifn-γ*: Interferon gamma protein/gene

IL-10/*il-10*: Interleukin 10 protein/gene

IL-1β/*il-1β*: Interleukin 1 protein/gene

IL-4/*il-4*: Interleukin 4 protein/gene

IL-6/*il-6*: Interleukin 6 protein/gene

IL-8/*il-8*: Interleukin 8 protein/gene

KP: *Klebsiella pneumoniae* systemic infection model

LSCFM: Laser scanning confocal fluorescence microscopy

Ly6C: Cluster of leucocyte antigen 6 complex C locus

Ly6C^{hi}: Mice pro-inflammatory monocytes

Ly6G: Cluster of leucocyte antigen 6 complex G locus

Mθ: Macrophages

M1: Classically activated pro-inflammatory macrophages

M2: Alternatively activated anti-inflammatory macrophages

M-CSF: Macrophage colony stimulating factor

MHCII/IA^d/IAIE: Major histocompatibility complex II of BALB/C or C57B6

MOG: Myelin oligodendrocyte lipoprotein

MRC/*mrc*: Mannose receptor protein/gene

MS: Multiple sclerosis

NK: Natural killer cells

NKT: Natural killer T cells

NLR: Nod-like receptor

NO: Nitric oxide

NOS-2/*nos-2*: Inducible nitric oxide synthase 2 protein/gene

NTX: Notexin

OCT: Optimal cutting temperature compound

PAMPs: Pathogen-associated molecular patterns

PKH26: Lipophillic tracer

P-S: Penicillin-streptomycin

RLR: Rig-like receptor

RNS: Reactive nitrogen species

ROS: Reactive oxygen species

RT-PCR: Real-time polymerase chain reaction

STAT1/6: Signal transducer and activator of transcription 1/6

T CD4: T helper lymphocytes

T CD8: Cytotoxic T lymphocytes

T REG: Regulatory T lymphocytes

TAM: Tumour-associated macrophage

TGF-β/*tgf-β*: Transforming growth factor 1 beta protein/gene

TH$_1$: T helper 1 lymphocytes

TH$_{17}$: T helper 17 lymphocytes

TII: Thioglycollate-induced intraperitoneal aseptic inflammation model

TLR: Toll-like receptor

TNF-α/tnf-α: Tumour necrosis alpha protein/gene

YM1/ym1: Chitinase 3-like 3 protein/gene

INTRODUCTION

 I. INTRODUCTION

1. General introduction

1.1. Innate immune system

The innate immune system represents the oldest and the first line of defence against immune insults. Innate immune system has been shaped by evolution together with the microorganisms and parasites. There are two main functions of the innate immune system. The first function of the innate immunity is to provide the initial and fast response against infectious or non-infectious aggressions. The second function is to stimulate and guide the adaptive immune system response.

The innate immune system is composed by its humoral arm and its cellular arm mainly composed by phagocytes, it also includes epithelial barriers (Figure1). The soluble components of the innate immune system are the complement system, antimicrobial peptides and other opsonizing molecules. The cellular components include neutrophils, eosinophils, basophils, mastocytes, NK cells, $\gamma\delta$T cells, dendritic cells, monocytes and macrophages.
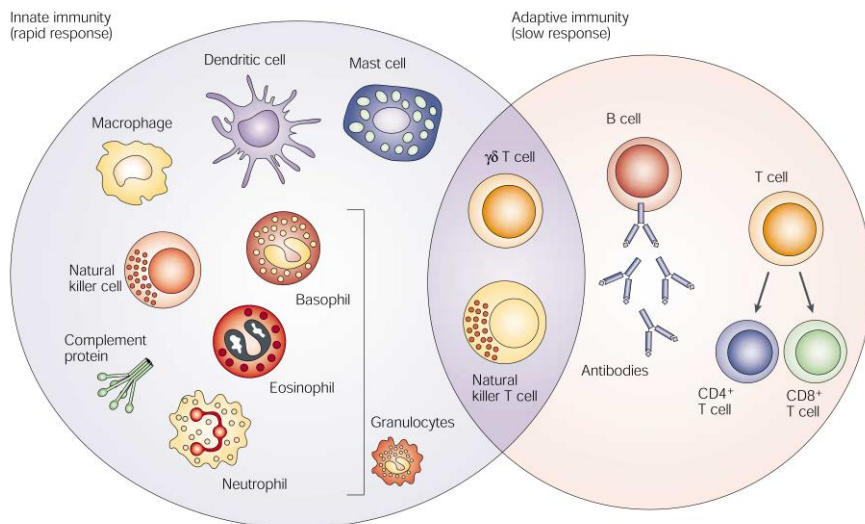
Figure1. Innate immune system versus adaptive immune system components (Dranoff 2004)

Macrophages and monocytes are in between the main actors of the innate immune system. These phagocytic cells are in charge to scavenge, internalize and digest toxic compounds or cells, produce inflammatory mediators, and contribute to the orchestration and coordination of other components of the immune system.

1

This capacity of the innate immune system to balance and determine the nature of future adaptive immune system responses makes it extremely attractive in order to understand how it is biased through one or another tendency.

2. Mononuclear phagocyte system

2.1. Definition of the mononuclear phagocyte system

Until recently, there was an established foundational dogma in immunology regarding the mononuclear phagocyte system (MPS) (van Furth and Cohn 1968). The MPS was considered a cell lineage englobing multiple cell subtypes that were though to originate from the same bone marrow precursors (Figure 2). The classic view of the MPS includes these hematopoietic pluripotent precursors and their descendants, the blood-derived monocytes, that would seed the organism with macrophages and dendritic cells (Geissmann, Manz et al. 2010; Chow, Brown et al. 2011; Onai and Ohteki 2014).
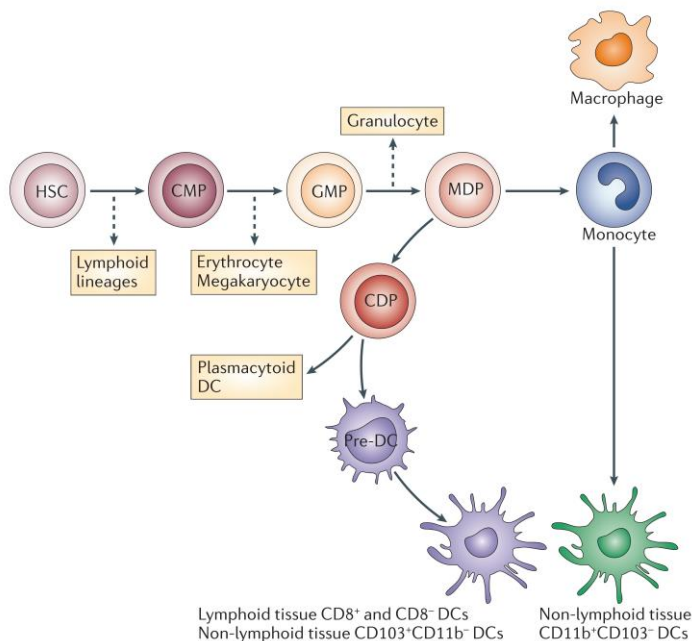
Figure2. Components of the mononuclear phagocyte system (Chow, Brown et al. 2011)

MPS components share distinct functional features including their proliferation and differentiation dependent on the M-CSF and IL-34 growth factors, their phagocytic activity and their extremely plastic gene expression (Jenkins and Hume 2014).

However, the MPS is currently under revision. Recent evidences suggest that dendritic cells and macrophages could be originate from distinct lineages and therefore distinct committed progenitors. Moreover, it has been recently proven that not all tissue macrophages derive from peripheral blood monocytes but are seeded during

2

development from the yolk sac and foetal liver and can also self-renew actively from previously established resident macrophage populations (Ginhoux and Jung 2014).

Nevertheless, even if some features may be shared by all cells belonging to the MPS still there is so much to unravel from the heterogeneity of this system. This can be explained by the fact that MPS components are highly adaptable and plastic cells, which results in extensive extracellular surface markers repertoire that may be shared by different types of cells. It is also explained by the fact that MPS components from non-lymphoid organs are poorly characterized compared to the lymphoid counterparts. More progress in unravelling the MPS system will be made as soon as genomic and gene product characterization will be performed (Geissmann, Gordon et al. 2010).

The novel view of the MPS is that it is clearly divided into separate cell lineages that arise at different stages of the embryonic development.

2.2. Monocyte and macrophages origin and ontogeny

Recent evidence demonstrate that macrophage populations do not depend entirely on the contribution from blood derived monocytes neither during homeostasis nor inflammation.
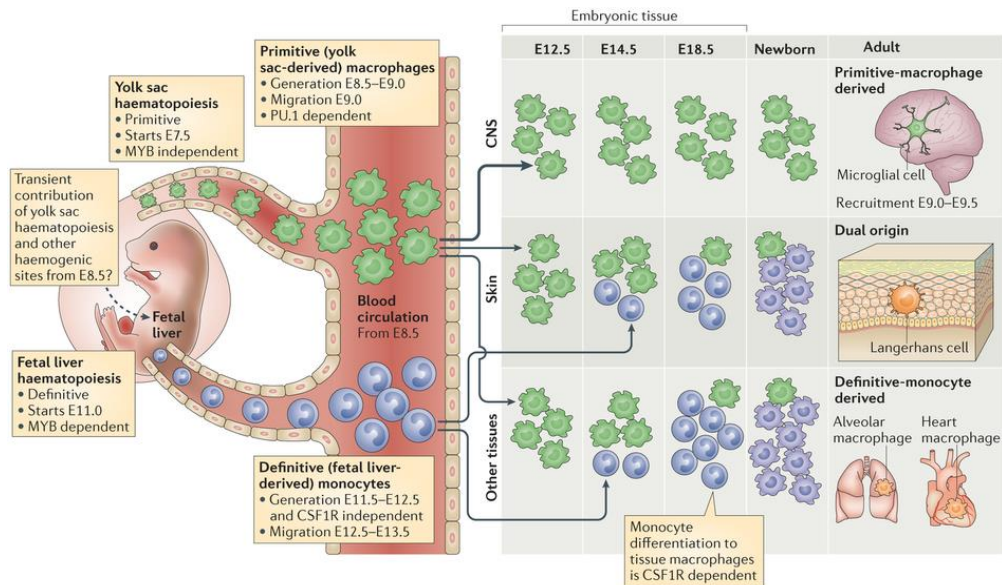
Nature Reviews | Immunology

Figure3. Primitive yolk-sac versus definitive fetal-liver or bone-marrow hematopoiesis (Ginhoux and Jung 2014).

The modern view of macrophage populations origin is that monocytes do not always substantially contribute to all tissue macrophage compartments, neither in steady-state or during inflammation (Epelman, Lavine et al. 2014; Ginhoux and Jung 2014).

Essentially, tissue resident macrophages present three possible types of origin, the embryonic, foetal or adult haematopoiesis (Figure 3). These three waves of colonizing cells are responsible for the generation of the peripheral pools of macrophages.

The first phase of embryonic haematopoiesis or the so called yolk-sac primitive haematopoiesis is restricted to myeloerythroid development. Yolk sac embryonic macrophages are the first to seed the tissues and give rise to resident populations of macrophages as soon as the circulatory system is fully established. The second phase of embryonic haematopoiesis or the so called aorta-gonads-mesonephros (AGM) definitive haematopoiesis is able to generate the hematopoietic stem cell precursors (HSCs) that seed the foetal liver together with yolk-sac precursors. This two processes are totally independent from blood monocytes recruitment and occur before birth.

Foetal liver definitive haematopoiesis is able to generate monocytes through the generation of pro-monocyte intermediates. These foetal liver-derived monocytes are released to the blood-flow and colonize foetal tissues originating a second wave population of recruited macrophages. This process also occurs before birth and it is already dependent on blood-monocytes, even thou they present a more immature state compared to monocytes coming from adult bone marrow haematopoiesis.
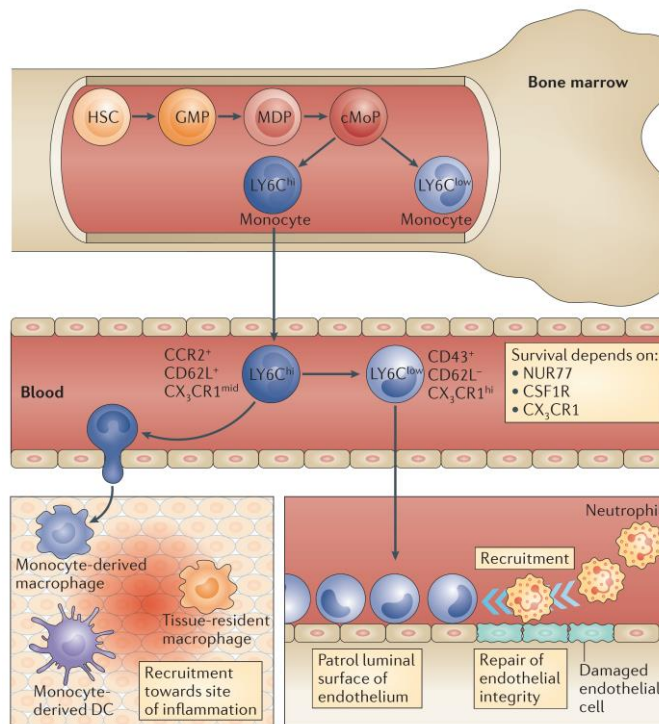
Figure4. Blood derived monocytes and adult bone marrow haematopoiesis in mice (Ginhoux and Jung 2014)

HSCs-derived monocytes originate during bone-marrow haematopoiesis occurred in adult individuals (Figure 4). Myeloid progenitor cells overcome successive steps of differentiation in response to the macrophage growth factor (M-CSF), the granulocyte-macrophage growth factor (GM-CSF), the granulocyte growth factor (G-CSF) and the interleukin 3 (IL-3), giving rise to multiple cell types including monocytes. Upon maturation, monocytes are released into the blood stream and scan the organism through the vascular system (Hume and MacDonald 2012).

Depending on the organs, yolk-sac-derived, foetal-liver-derived or bone-marrow derived monocytes sequentially migrate and colonize the tissues establishing the resident populations of macrophages. This fact creates different mosaics where the origin of resident cells may not be homogenous (Figure 5). Resident macrophage populations can in its turn maintain themselves through local proliferation with any substantial contribution from adult haematopoiesis.
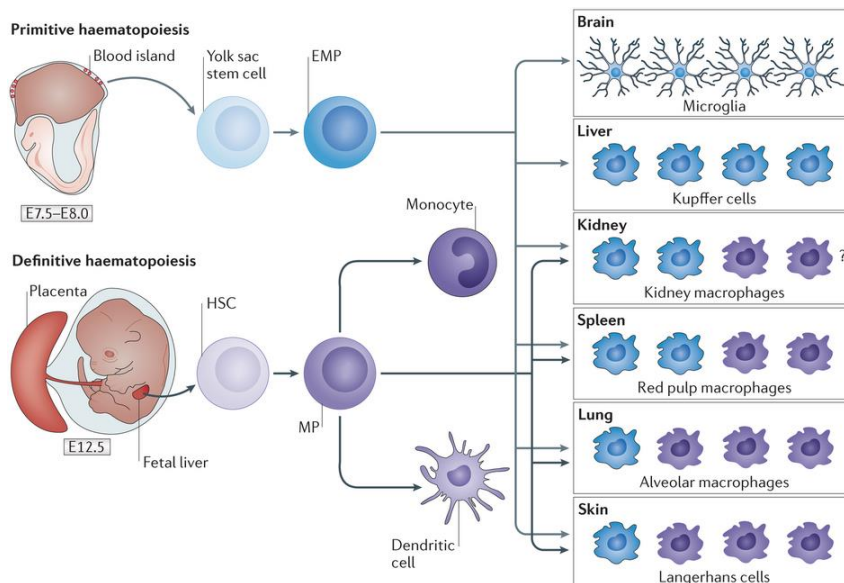
Nature Reviews | Neuroscience

Figure5. Macrophages originated from primitive or definitive haematopoiesis may coexist depending on the tissues (Prinz and Priller 2014).

In certain tissues, such as the brain with microglial cells, macrophages originate exclusively from the first wave of embryonic haematopoiesis. In other tissues, such as the skin with Langerhans cells, macrophages present a dual origin where contribution from embryonic haematopoiesis and foetal haematopoiesis coexist. However, in the majority of tissues, such as lung and heart macrophages, yolk-sac derived cells are fully replaced by the successive waves of blood-derived colonizing monocytes. Moreover,

resident macrophage populations can in its turn be partially or totally replaced by recruited populations from blood-derived monocytes (Figure 6) (Ginhoux and Jung 2014).

In the most recent models proposed, during mild inflammatory processes blood-derived monocytes infiltrate the tissues and give rise to recruited macrophages, but progressively these populations will disappear as they are not able to self-renovate. Only the resident macrophage populations will be able to proliferate and maintain the pool of tissue macrophages once the inflammatory insults have overcome.

In the case of moderate inflammatory pathologies there is a possibility that some populations of monocyte derived macrophages can self-maintain themselves even after inflammation is resolved. In this case endogenous populations and recruited populations can coexist forming a chimera of macrophages with dual embryonic or adult origin.
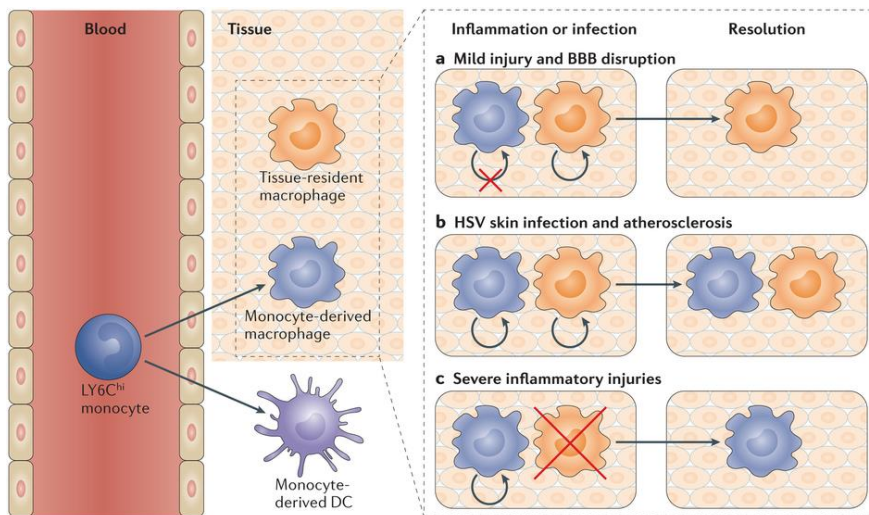
Nature Reviews | Immunology

Figure6. Resident versus recruited macrophage population dynamics during inflammation (Ginhoux and Jung 2014)

In severe inflammatory processes there is a partial or complete loss of the resident macrophage populations with embryonic origin. Consequently, the system has the ability to recover homeostasis by a complete macrophage repopulation from blood-derived monocytes (Ginhoux and Jung 2014).

2.3. Monocyte subsets and classification

Monocytes are considered a population of mononuclear leukocytes originated in the bone marrow during adulthood from dividing monoblasts. Once released into the bloodstream as non-dividing cells, monocytes seed peripheral tissues. Therefore,

monocytes can be considered a non-negligible systemic reservoir of myeloid precursors (Geissmann, Jung et al. 2003).

They can be classified into separate populations. According to their extracellular markers they have been commonly divided into two main subtypes (Figure 7). These two different subsets of bloodstream monocytes have been found in humans and mice sharing their phenotype, homing potential and function. Human and mice monocytes are classified regarding their CD14/CD16 and Ly6C expression respectively (Gordon and Taylor 2005; Yona and Jung 2010; Ziegler-Heitbrock 2014).

Antigen	Human CD14^{hi}CD16^{-} 'inflammatory' monocytes	Human CD14^{+}CD16^{+} 'resident' monocytes	Mouse CCR2^{+} CX$_3$CR1^{low} 'inflammatory' monocytes	Mouse CCR2^{-} CX$_3$CR1^{hi} 'resident' monocytes
Chemokine receptors				
CCR1	+	–	ND	ND
CCR2[‡]	+	–	+	–
CCR4	+	–	ND	ND
CCR5	–	+	ND	ND
CCR7	+	–	ND	ND
CXCR1	+	–	ND	ND
CXCR2	+	–	ND	ND
CXCR4	+	++	ND	ND
CX$_3$CR1[‡]	+	++	+	++
Other receptors				
CD4	+	+	ND	ND
CD11a	ND	ND	+	++
CD11b	++	++	++	++
CD11c[‡]	++	+++	–	+
CD14	+++	+	ND	ND
CD31	+++	+++	++	+
CD32	+++	+	ND	ND
CD33	+++	+	ND	ND
CD43	ND	ND	–	+
CD49b	ND	ND	+	–
CD62L[‡]	++	–	+	–
CD80	ND	ND	ND	ND
CD86	+	++	ND	ND
CD115	++	++	++	++
CD116	++	++	++[§]	++[§]
CD200R	ND	ND	ND	ND
F4/80	ND	ND	+	+
Ly6C	ND	ND	+	–
7/4	ND	ND	+	–
MHC class II	+	++	–	–

Figure7. Human and mouse monocyte surface markers (Gordon and Taylor 2005)

Besides actual classification of monocytes and macrophages relying on surface markers and ontogeny, further classification systems based also on localization may be

improved in order to permit a better understanding of each subpopulations and their function (Figure 8) (Guilliams, Ginhoux et al. 2014).

Classical, $Ly6C^{low}$ or $CD14^{low}/CD16^{high}$ patrolling monocytes are a long-lived subset of blood monocytes that keep under surveillance and maintain integrity of the endothelial layer. Given the possibility of monocyte conversion it is still not clear weather classical patrolling monocytes derive from non-classical monocyte differentiation in the blood or if there is a direct release of this cell subtype in its mature form from the bone marrow. Some authors consider both possibilities as complementary mechanisms for classical and non-classical monocyte homeostasis. Patrolling or resident monocytes present a characteristic CX3CR1-faciliated transmigration system. This subtype is also responsible of refilling the pool of resident macrophages and dendritic cells during homeostasis. Even more, new functions in pathogenic states such as early responses to inflammation have been proposed during the last years.
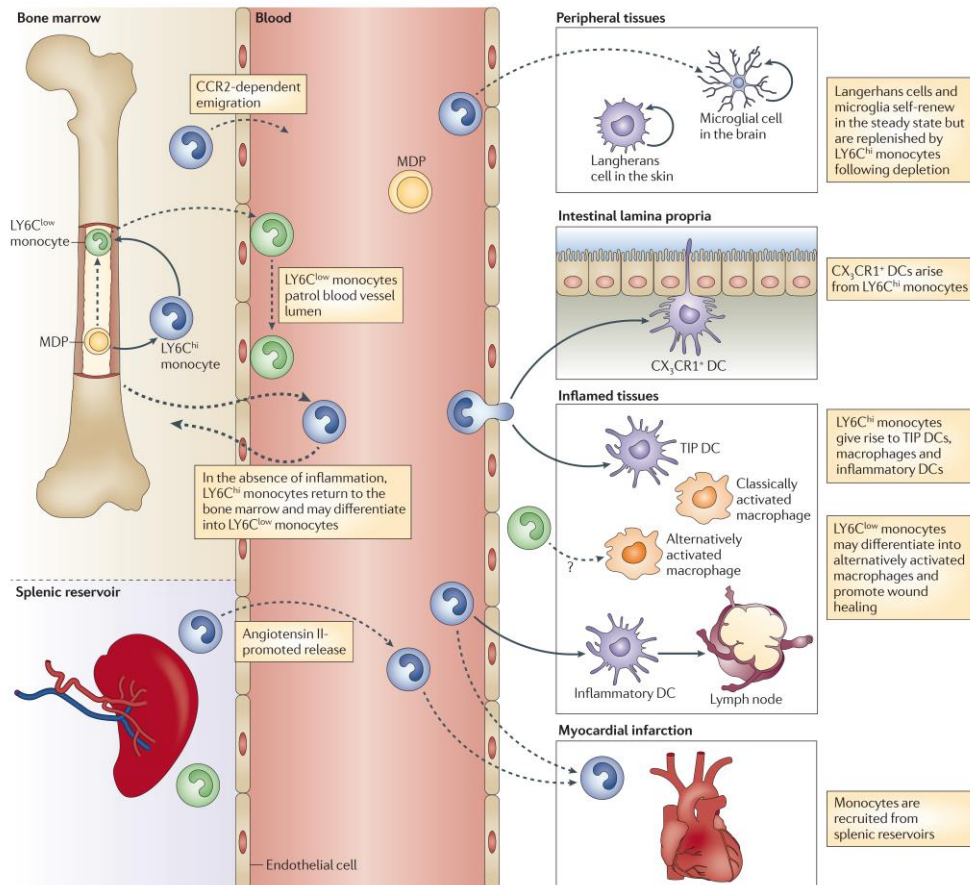
Figure8. Monocyte subsets, heterogeneity and function (Gordon and Taylor 2005)

Non-classical, Ly6C^{high} or CD14^{high}/CD16^{low} recruited monocytes consist of a specific short-lived subset that is actively recruited to sites of inflammation where its presence is required for an immune response. Non-classical monocytes are able to migrate through chemokine signalling into the inflammatory loci. The infiltration process needs the presence of diverse recruiting molecules expressed by the endothelium. Those recruiting molecules, including MCP-1 ligand for CCR2 receptor, are only synthesized when required for a specific and usually short time window. The initial inflammatory process activates the endothelial cells and makes possible the transmigration of pro-inflammatory monocytes.

Once established into the tissues and relying on the microenvironment recruited monocytes differentiate into effector cells including recruited macrophages and dendritic cells. Then, they polarize acquiring differential pro-inflammatory or anti-inflammatory capacities. Depending on the signals encountered within the tissues, monocytes are able to establish a pro-inflammatory and antimicrobial microenvironment or oppositely an anti-inflammatory and pro-fibrotic niche.

Multiple specific and sometimes opposite functional roles have been proposed for blood-derived pro-inflammatory monocytes. Taking in account the previous information, monocytes can be considered as cells with high plasticity potential. The specific migratory ability of monocytes, their plasticity and their critical role makes them extremely attractive as a tool for understanding inflammation. However, the mechanism how this cell subtype is able to replenish the inflammatory sites and trigger the illness is poorly understood.

2.4. Macrophage subsets and classification

Macrophages are divided into multiple subpopulations based on their origin and ontogeny, functional phenotype and anatomical location (Figure 9) (Murray and Wynn 2011).

Classification following their origin or ontogeny has been reviewed previously and divides macrophage populations in two main categories. Resident macrophage populations are established during embryogenesis and foetal stages. Resident tissue specific macrophages are in charge to maintain homeostasis of the tissues ingesting apoptotic cells and foreign materials. They also produce in collaboration with other cell types the initial chemoattractant signals that will recruit additional macrophage populations to the site of inflammation during infection or injury. Recruited macrophages originate from blood-derived monocytes and boost the inflammatory or anti-inflammatory reactions when required (Epelman, Lavine et al. 2014).
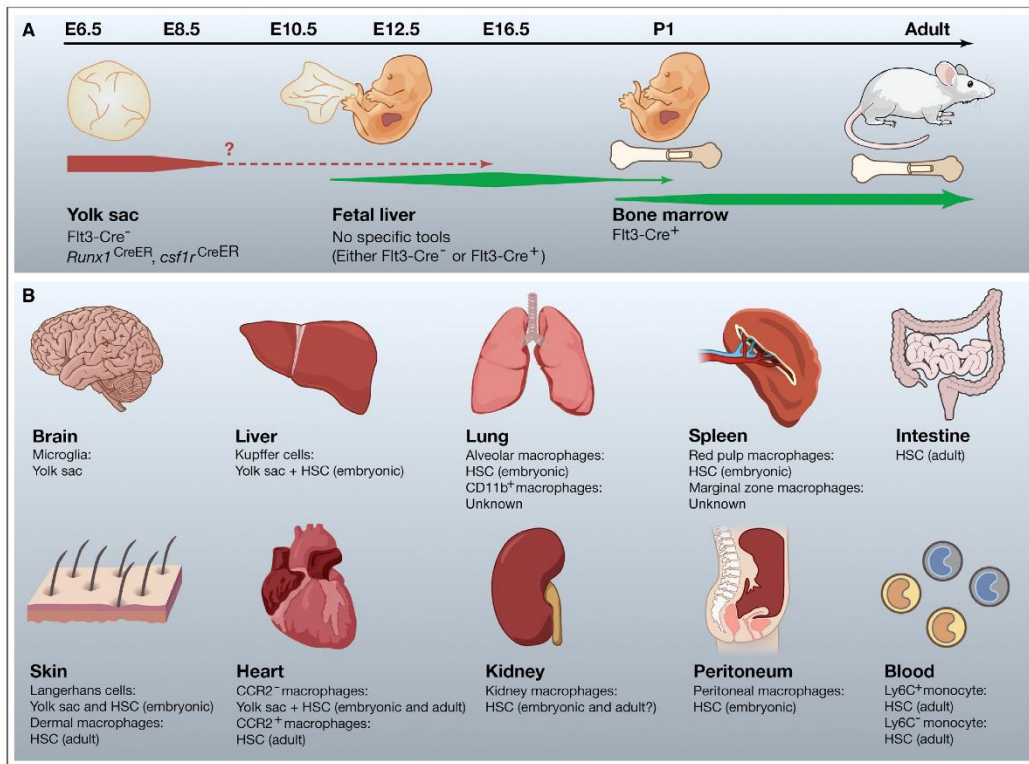
Figure9. Macrophage classification following lineages and ontogeny (Epelman, Lavine et al. 2014).

Classification based on their anatomical location may be confusing since multiple subtypes of macrophages with radically different functions and phenotypes may be found in a same tissue. However, diverse tissue-specific subpopulations of macrophages sharing specific functions have been clearly identified (Figure 10). In any case, macrophages can be considered sentinel cells in the tissues able to detect foreign or self-danger signals (Murray and Wynn 2011).

Classification based on their function, phenotype or state of activation is a complex matter. Given their extreme plasticity and flexibility in their programming, macrophages are well considered to represent a wide spectrum of activated phenotypes rather than stable populations (Figure 11). Here we present an extremely simplified view of macrophage heterogeneity (Mosser and Edwards 2008).

M0-like non-activated macrophages consist in subsets of macrophages that exist in a resting state prior to any kind of activation state.

M1-like or pro-inflammatory macrophages or classically activated macrophages are in charge to mediate defence against pathogens such as viruses, protozoa and bacteria as well as to create the pro-inflammatory microenvironment following aseptic injury or chronic/autoimmune inflammatory processes. M1-like pro-inflammatory

macrophages synthetize a broad range of pro-inflammatory compounds including cytokines, prostaglandins, reactive oxygen and nitrogen species and chemoatractants which boost the pro-inflammatory reaction. They are also key players in driving adaptive immune system reactions, actively producing mediators like IL-12 or IL-23 which are decisive during Th1 and Th17 polarization, driving inflammation forward.
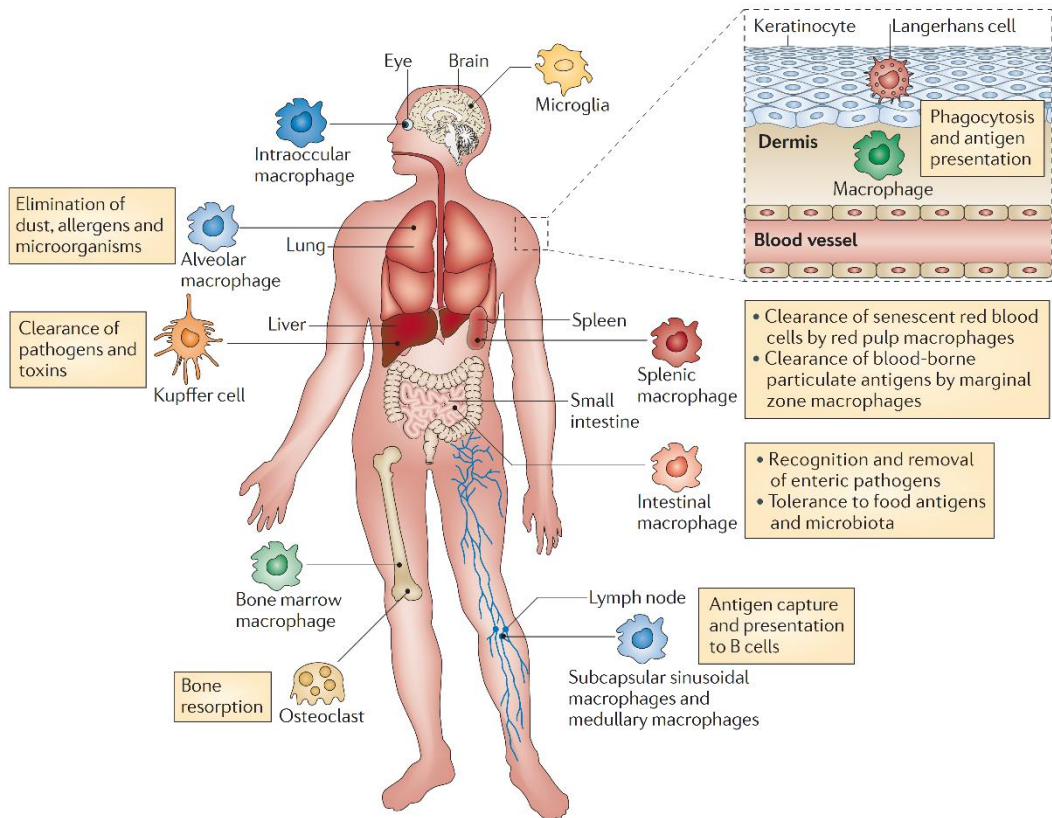
Figure10. Macrophage classification following anatomical location (Murray and Wynn 2011).

M2-like or anti-inflammatory macrophages or alternatively activated macrophages are in charge present regeneration, wound-healing, pro-fibrotic and angiogenic functions. M2-like anti-inflammatory macrophages secrete large amounts of anti-inflammatory and wound healing mediators such as extracellular matrix and vasculature remodelling factors, growth-factors, profibrotic factors and chemoatractants that enhance tissue regeneration and recovery of homeostasis. Once more, being decisive in polarizing adaptive immune system reactions, they actively produce mediators such as IL-4 or TGF-β crucial during Th2 polarization and resolution of the inflammation.

Regulatory macrophages consist on small subsets of macrophages secreting large amount of IL-10 in response to signalling from the Fc receptor γ. This subtype is

believed to present suppressive functions towards the other subpopulations, maintaining an equilibrium between the pro-inflammatory and anti-inflammatory forms of macrophages during inflammation. During homeostasis they also silence inflammatory reactions. Colonic macrophages inhibit immune reactions against host natural bacterial populations and their products. Marginal zone macrophages from the spleen mute immune reactions against apoptotic cells and their residues. However, the concept of regulatory macrophages is still being reviewed (Murray, P. J., J. E. Allen, S. K. Biswas, E. A. Fisher, D. W. Gilroy, S. Goerdt, S. Gordon, *et al.* 2014).
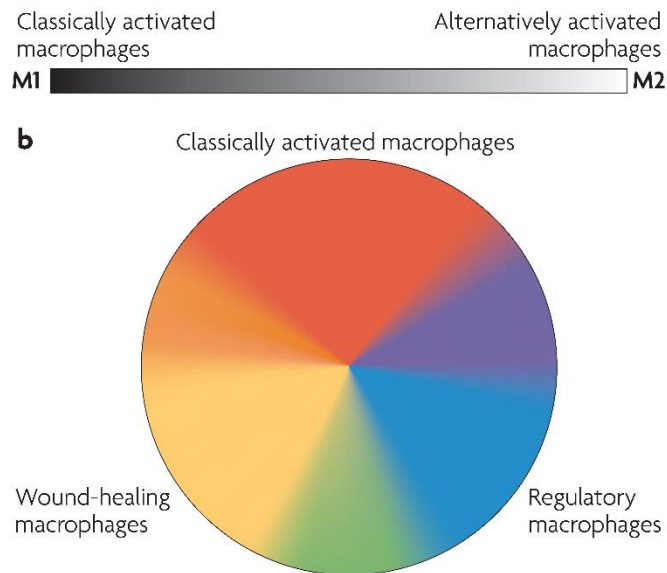
Figure11. Macrophage polarization classification (Mosser and Edwards 2008).

Tumour-associated macrophages (TAM) are believed to supress antitumor immunity. Isolated TAMs from solid and metastatic tumours present preferentially and M2-like phenotype. There is accumulating evidences that macrophages contribute to tumour progression, promoting anti-tumour activities, angiogenesis, metastasis and malignancy (Franklin and Li 2016).

Myeloid-derived suppressor cells (MDSC) are closely linked to TAMs and may be their precursors. Increasing numbers in TAMs and MDSCs always correlate with poor prognosis and survival (Peranzoni, Zilio et al. 2010).

Nowadays several macrophage subsets that do not fit in this simplified classification have been identified. Surface marker expression presents great overlap between populations that have been clearly separated in function or gene expression. The diversity in terminology and inconsistency in the use of markers for classification

impedes clear analysis and identification of the complex macrophage heterogeneity. Therefore, other methods for macrophage subpopulations identification have to be implemented such as gene expression profiles following cytokine or microbial activation and standardized methods (Murray, Allen et al. 2014).

3. The mononuclear phagocyte system role in inflammation

3.1. Inflammatory response

The inflammatory response is initiated after the release of danger signals from the damaged tissues that surround the lesion (Figure 12). Danger signals are classified into damage associated molecular pattern signals (DAMPs) and pathogen associated molecular pattern signals (PAMPs). DAMPs include endogenous intracellular molecules released by activated or necrotic cells and extracellular matrix molecules upregulated or degraded upon injury. PAMPs include a broad range of molecules belonging to foreign organisms during infectious insult such as bacteria and virus structural compounds or nucleic acids. DAMPs and PAMPs are vital danger signals that alert our immune system to tissue damage upon both infectious and sterile aggressions.
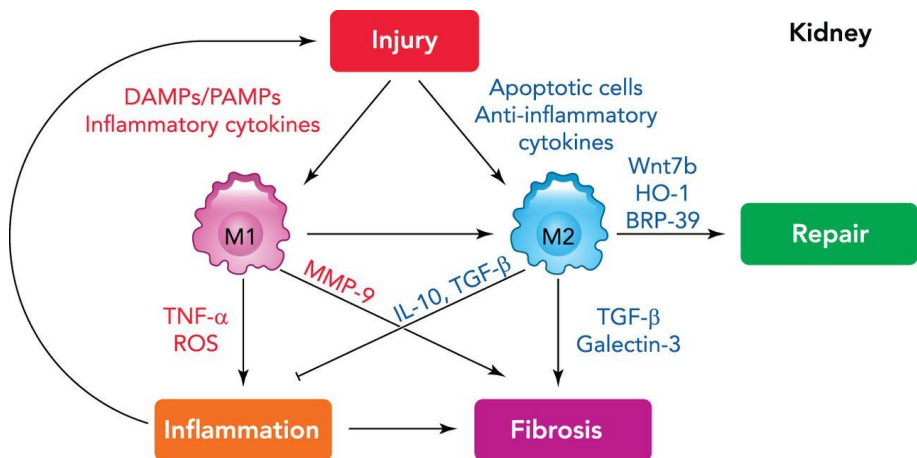
Figure12. Danger sensing, inflammatory response and resolution (Cao, Harris et al. 2015)

Toll-like receptors (TLRs), Nod-like receptors (NLRs), Rig-like receptors (RLRs), Scavenger receptors and Lectin-type receptors are the key players of DAMPs and PAMPs recognition and signalling. TLRs, NLRs, RLRs, Scavenger and Lectin-type receptors are expressed by a broad range of cell types including non-immune cells which allows ubiquitous and fast detection of danger signals. These recognition molecules are localized in different cellular compartments such as the cell surface, endosome, lysosome or cytoplasm and initiate signal transduction pathways. Once activated, these

13

signalling pathways trigger the expression of genes controlling the innate immune system responses and further instruct the development of antigen-specific adaptive immune system responses.

On the other hand, the inflammation caused by the activation of the innate immune system has its side effects. Inflammation produces in long term tissue damage to the host and contributes to the development of inflammatory diseases. Therefore, inflammatory diseases could be considered as long-term natural consequence of the innate immune activation in context with environmental enhancers and genetic predisposition (Auffray, Sieweke et al. 2009).

3.2. Monocyte and macrophage functions

Monocytes and macrophages display a wide range of functions during development, homeostasis and inflammation (Figure 13). They play extremely important roles in development and tissue homeostasis. They are in charge of tissue remodelling not only during developmental processes through removal of apoptotic cells and scavenging of toxic compound, but also during complex tissue remodelling occurred during adulthood for example during pregnancy-related endometrium myometrium remodelling (Mackler, Green et al. 2000; Poon, Lucas et al. 2014).
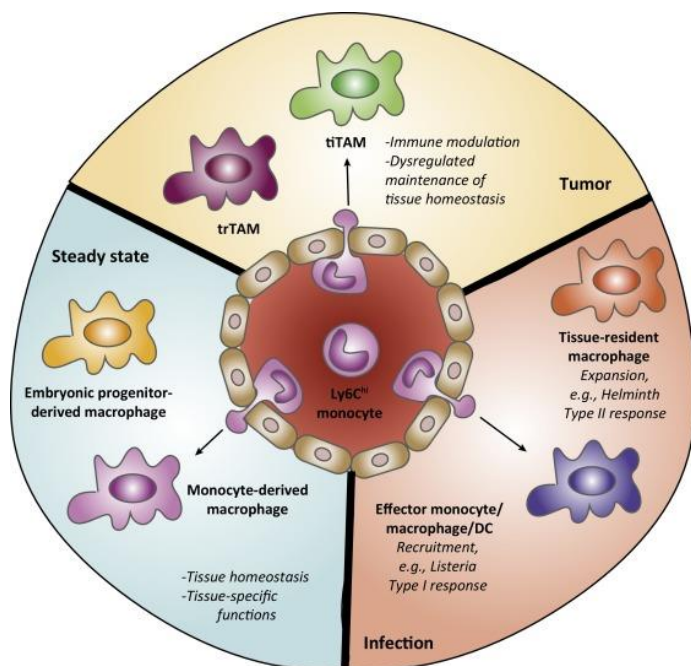
Figure13. Monocyte and macrophage functions (Franklin and Li 2016).

14

Blood monocytes can be considered as well as the largest pool of scavenger and potential effector cells inside the vascular system. Recent identification of a major monocytic reservoir in the spleen has shed light into how monocyte release can occur with such speed during inflammatory reactions. Monocyte release from the spleen following immune assaults is mediated in an angiotensin-mediated manner, which explains further the speediness of this process. Functional, morphologic and transcriptomic studies have made clear that splenic monocytes correspond to conventional blood monocytes generated in the bone marrow and accumulated locally in the spleen (Swirski, Nahrendorf et al. 2009; Yona and Jung 2010).

Monocytes and macrophages represent essential players during inflammation and immune assaults. Monocyte-macrophages-mediated inflammation is composed by four stages, tissue recruitment, differentiation and activation in situ, conversion to anti-inflammatory and restauration of tissue homeostasis (Murray and Wynn 2011).

Monocytes and macrophages also represent accessory cells that are able to link inflammation and innate defence against foreign microorganisms with the establishment of adaptive immune responses. These myeloid cells are able to link the innate immune responses to the adaptive immune reactions through antigen presentation processes and production of large quantities of effector molecules involved in the immune defence.

Given the plasticity of monocytes to give rise to macrophage and dendritic cell populations, with opposite pro-inflammatory or anti-inflammatory functions, understanding the biology of monocytes and macrophages may be of extreme relevance to control, delay or treat the long-term detrimental effects of sustained inflammation.

3.3. Monocyte and macrophage roles during acute inflammation

In response to the initial inflammatory signals recognized by the TLRs, NLRs and RLRs, resident immune and non-immune cells secrete vasodilator molecules which will increase blood-flow into the tissue (Figure 14). Simultaneously, the expression of chemoattractant proteins like CCL2 (MCP-1), CCL3 (MIP1α) and CCL5 is upregulated. Myeloid-derived cells such as pro-inflammatory monocytes, expressing the CCR2, CCR5 and CCR1 receptors for those mentioned chemokines initiate the infiltration process that will boost the inflammatory response occurred in the damaged loci (Imhof and Aurrand-Lions 2004).

Once infiltrated, pro-inflammatory monocytes themselves and the cell subtypes resulting from their differentiation, such as recruited pro-inflammatory macrophages and dendritic cells, perform a wide range of functions.

Infiltrated monocytes are responsible for the synthesis of pro-inflammatory soluble molecules like complement factors, prostaglandins, TNF-α, IL-6, IL-1β and IL-12

cytokines, but also for the upregulation of intracellular components implicated in inflammation and oxidative stress such as COX-2 and NOS-2. Tissue monocytes are also in charge of secreting additional chemoattractant proteins like CCL2, CCL3, CCL5 and CXCL8 (IL-8). Infiltrated monocytes can also secrete vascular and extracellular matrix remodelling factors such as vascular endothelial growth factors and proteolytic enzymes like metalloproteases (Yona and Jung 2010).
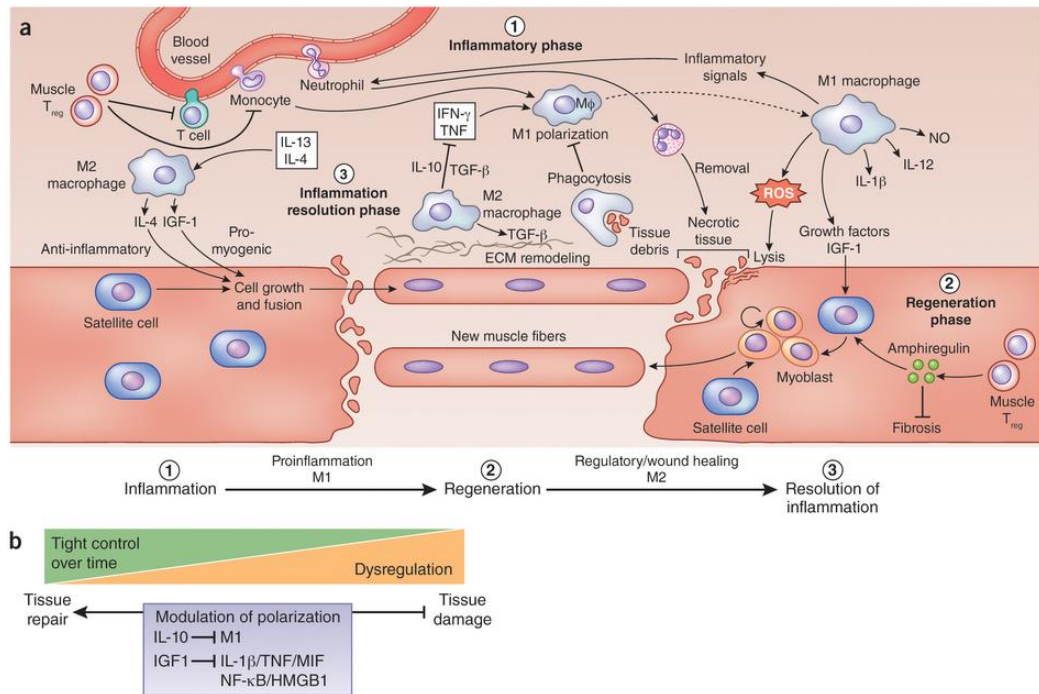
Figure14. Monocyte and macrophage functions during inflammation after muscle damage (Forbes and Rosenthal 2014).

After differentiation, monocytes give rise to a population of recruited macrophages and inflammatory dendritic cells that amplify the inflammatory response by secreting further pro-inflammatory soluble and intracellular mediators. Furthermore, recruited macrophages and inflammatory dendritic cells amplify the chemoattractant signal for successive waves of other monocyte-derived myeloid cells or neutrophils, and also for other immune cell lineages such as the T and B lymphocytes.

Nevertheless, extensive populations of resident cells such as resident macrophages and dendritic cells perform essential functions during inflammatory processes as well. Resident tissue macrophages can undergo massive proliferation in a Th2-dependent manner boosting parasite clearance in the peritoneum (Jenkins, Ruckerl et al. 2011). Resident populations of macrophages could also have an essential role in

proliferating and performing a role in pathologies such as asthma and allergic lung inflammation, liver inflammation during *Schistosoma* egg deposition or muscle inflammation during *Trichinella spiralis* invasion (Nascimento, Huang et al. 2014; Ruckerl and Allen 2014; Zaslona, Przybranowski et al. 2014).

Even thou it is clear that resident populations of macrophages have an important role during Th2-mediated inflammation, it is not so clear how important is the contribution of resident macrophage populations to inflammation resolution during Th1-mediated processes.

3.4. Monocytes and macrophage roles during chronic inflammation

Monocyte-derived cell infiltration is essential in all pathologies to establish an initial pro-inflammatory and chemoattractant microenvironment. This initial step allows the adaptive immune system to trigger a secondary immune response when inflammation cannot be resolved by the innate immune system (Figure 15).
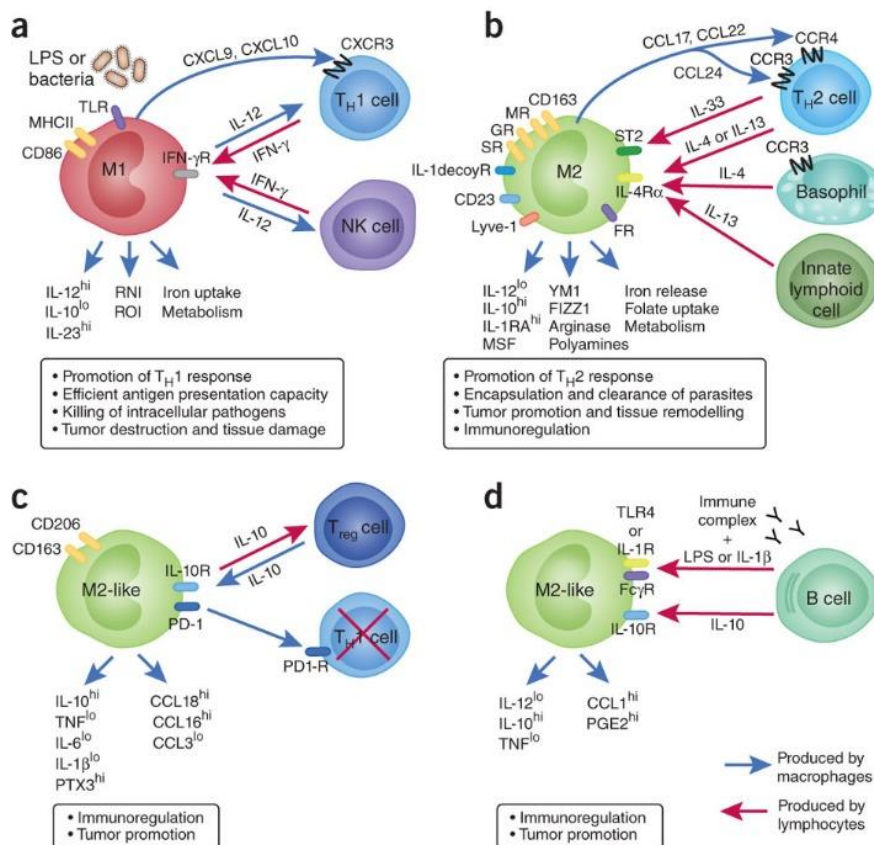
Figure15. Macrophage orchestration of the adaptive immune response during chronic inflammation (Biswas and Mantovani 2010)

In advanced stages of inflammation soluble and cellular components of the adaptive immune system take part in the response. Recruited macrophages and dendritic cells derived from infiltrating monocytes together with the resident populations initiate antigen presentation through major histocompatibility complex (MHC) class II within the inflamed tissue and surrounding lymph nodes. Afterwards, naïve T cells are polarized along pathogenic Th1, Th2 and Th17 lineages or the regulatory Treg lineage. In coordination, B lymphocytes get also activated and differentiate into plasmatic cells that initiate the secretion of specific antibodies.

The adaptive and innate immune system coordination, through sequential expression of chemokine ligands and receptors, allows the generation of a self-maintained vicious circle. In this process chemoattractant microenvironment, cellular infiltration, inflammatory microenvironment and tissue damage increase progressively during chronic inflammation.

3.5. Animal models

3.5.1. Thyoglicollate-induced inflammation model (TII)

Thyoglicollate-induced inflammation is generated by single intraperitoneal injection of thyoglicollate broth as described in the experimental procedures section.

Under steady-state conditions resident populations of macrophages and dendritic cells, but also T cells, B cells, NK cells and mastocytes are in charge of the basal immune surveillance. Thus, there is a strong controversy regarding the role of resident peritoneal macrophages during thyoglicollate-elicited peritonitis. However, their contribution to inflammation and recruitment of leucocyte populations appears to be minimal in this specific model (Ajuebor, Das et al. 1999).

During thyoglicollate-induced peritoneal inflammation the peritoneal cavity is colonized with peripheral blood-derived leukocytes. In a first step thyoglicollate elicits a robust neutrophil influx which reaches its peak levels between 4 and 24 hours after treatment. Afterwards blood-derived monocytes are recruited and their numbers start to increase reaching its peak around 48h. Macrophages influx resulting from monocyte in-situ differentiation is at peak around 72h. Massive myeloid infiltration within the peritoneal cavity makes this model an appropriate model for the study of the inflammatory events including inflammatory mediator production and leukocyte accumulation (Boring, Gosling et al. 1997; Henderson, Hobbs et al. 2003; Bradfield, Scheiermann et al. 2007; Handel, Johnson et al. 2008; Takahashi, Galligan et al. 2009; Lam, Harris et al. 2013).

3.5.2. Dinitrofenolbenzene contact-induced inflammation model (DNFB)

DNFB contact-induced inflammation model consists in a delayed-type hypersensitivity response to cutaneous contact with the chemical irritant 2,4-dinitrofluorobenzene (DNFB). DNFB is applied in the right ear of mice and acetone is applied in the left ear as a control, all this is performed as described in the experimental procedures section.

DNFB exposure induce an increase in the expression of adhesion molecules from the activated endothelium. Endothelial activation enhances leukocyte binding from the circulation, transmigration and trafficking to the site of inflammation. Furthermore, in this skin model of inflammation, DNFB diffuses from the epidermis to the dermis and reacts with amino-acid chains of extracellular proteins. Langerhans cells process this modified proteins and migrate to the regional lymph nodes through the lymphatic vessels. This process enables the generation of hapten-specific T lymphocytes.

This model provides a fast and useful tool to study inflammation and extravasation of leukocytes to the site of DNFB application (Klimuk, Semple et al. 1999; Tuckermann, Kleiman et al. 2007; Tang, Zou et al. 2012; Tamoutounour, Guilliams et al. 2013; Christensen, Skov et al. 2014).

3.5.3. Notexin-induced myoinjury model (NTX)

Notexin-induced myoinjury model is based on intramuscular injection of the Notexin venom from *Notechis scutatus* or Australian Tiger snake, which is detailed in the experimental procedures section.

Notexin venom exerts both neurotoxic and myotoxic activities. Neurotoxicity of Notexin is mediated by its phospholipase A2 (PLA2) activity that blocks neuromuscular transmission by decreasing the presynaptic release of acetylcholine. Myotoxicity of Notexin is due to its capacity to inhibit Ca2+ uptake into fragmented sarcoplasmic reticulum from skeletal muscle, causing muscle myofibers necrosis. Monocytes and macrophages are the major inflammatory cell populations recruited into injured skeletal muscle in this model, which makes it extremely useful for studying monocyte infiltration and differentiation.

Initially, resident mastocyte populations degranulate preformed pro-inflammatory mediators which will cause the accumulation of neutrophils. Neutrophils are in charge to amplify the pro-inflammatory and chemoattractant microenvironment as well as to start muscle fibbers digestion and phagocytosis.

Following the initial cellular events, blood derived pro-inflammatory Ly6C^{hi} monocytes infiltrate the tissues and give rise to a population of pro-inflammatory

macrophages. Initial monocyte/macrophage populations were associated with the production of pro-inflammatory cytokines and removal of necrotic tissue. Once the pro-inflammatory and degeneration phase overcomes macrophages switch to an anti-inflammatory phenotype and start producing anti-inflammatory mediators associated with tissue repair and regeneration of muscle fibbers.

Nevertheless, it is not clear whether subsequent waves of resident Ly6C^{lo} monocytes could infiltrate damaged tissues and exert an anti-inflammatory effect which would enhance muscle regeneration. In a similar way, it is not determined which is the real influence of resident populations of macrophages in muscle fibbers regeneration in this model (Helmke and Howard 1986; Yang and Chang 1991; Arnold, Henry et al. 2007; Chazaud, Brigitte et al. 2009; Brigitte, Schilte et al. 2010; Wang, Melton et al. 2014; Arnold, Perrin et al. 2015).

3.5.4. *Klebsiella pneumoniae* systemic infection model (KP)

Klebsiella pneumoniae systemic infection model is generated by intranasal injection of known concentrations of living *Klebsiella pneumoniae* Bacteria as followed in the experimental procedures section.

Klebsiella pneumoniae is a Gram negative bacteria common cause of nosocomial infections including urinary tract, respiratory, and wound infections. Contrary to many bacterial pathogens, *K. pneumoniae* is ubiquitous in nature. Its natural habitat includes mucosal surfaces of animals and environmental sources such as vegetation, soil and surface waters.

After intranasal infection with *Klebsiella pneumoniae*, bacteria start reproducing fast in the pulmonary tract of mice. Resident populations of alveolar macrophages and mast cells initiate the inflammatory response synthetizing pro-inflammatory and chemoattractant mediators. Alveolar macrophages, followed by infiltrated neutrophils initiate killing and phagocytosis of bacteria. This pro-inflammatory and chemoattractant microenvironment allows the subsequent infiltration of blood derived pro-inflammatory Ly6C^{hi} monocytes. Infiltrated Ly6C^{hi} monocytes and recruited macrophages are then able to contribute to control the infection and amplify the synthesis of pro-inflammatory and chemoattractant mediators. Myeloid cells including monocytes, macrophages and neutrophils play critical roles in bacterial clearance the infected tissues by their capacity for phagocytosis and killing. Depletion of either neutrophils or alveolar macrophages results in reduced killing of *K. pneumoniae* in vivo.

All this, makes this model a useful tool for the study of monocyte infiltration and function during infection (Rukavina, Ticac et al. 1997; Yu, Hansen et al. 2007; Regueiro,

Moranta et al. 2009; Moranta, Regueiro et al. 2010; March, Cano et al. 2013; Roger, Delaloye et al. 2013).

3.5.5. Experimental autoimmune encephalitis model (EAE)

Experimental Autoimmune Encephalomyelitis or EAE mice model was generated by active immunization with myelinic oligodendrocyte glycoprotein in emulsion with complete Freund´s adjuvant, and intravenous injection of *Bordetella pertussis* toxin as described in the experimental procedures section.

EAE mice model corresponds to a chronic relapsing brain and spinal cord disease widely used in Multiple Sclerosis (MS) research. EAE is a T cell-mediated autoimmune disease of the central nervous system. EAE can be induced in susceptible mice strains by active immunization with CNS myelin antigens or passively transferred via antigen-stimulated autoreactive T CD4$^+$ cell infusions. The immune system mechanisms involved in both EAE and MS present multiple similarities but also differences. The clinical course of the disease is characterized by weight loss and progressive ascendant paralysis. There are three existing MS animal models, the MBP-induced EAE model that leads to a self-limiting form of the pathology, the MOG-induced EAE model that leads to a chronic form of the pathology and the PLP-induced EAE model that leads to a relapsing remitting form of the pathology.

For this study we had chosen the chronic EAE model mainly because its lineal progression and non-self-limiting characteristics. As a chronic progressive disease, the CNS progresses from an initial mild inflammatory state to an established high inflammation. During the first phase of the EAE an initial wave of infiltrating immune cells triggers the establishment of an inflammatory chemoattractant microenvironment. Once the acute phase of the illness overcomes the chronic phase takes place. During the chronic phase the inflammation rises which is related to the auto destructive neural response. In this phase an inflammatory loop occurs where cells increasingly infiltrate and destroy axonal myelin causing illness progression.

The linearity of the illness progression and the capacity to reach an elevated inflammation state before remitting makes this model an optimal tool to study neural inflammation. Therefore, this model facilitates the study of bone-marrow myeloid cell migration during a complex autoimmune pathology in contrast with the self-limiting or the relapsing-remitting forms of the EAE (Miller and Karpus 2007; King, Dickendesher et al. 2009; Mildner, Mack et al. 2009; Ajami, Bennett et al. 2011; Jung and Schwartz 2012; Mishra, Wang et al. 2012).

4. Therapeutic roles of the mononuclear phagocyte system

Therapeutic and anti-inflammatory potential of monocytes resides as mentioned before in its extreme plasticity but also in different potential activities that belong specific to certain monocyte subsets (Figure 16). There are two main approximations about how monocytes may represent a therapeutic potential.
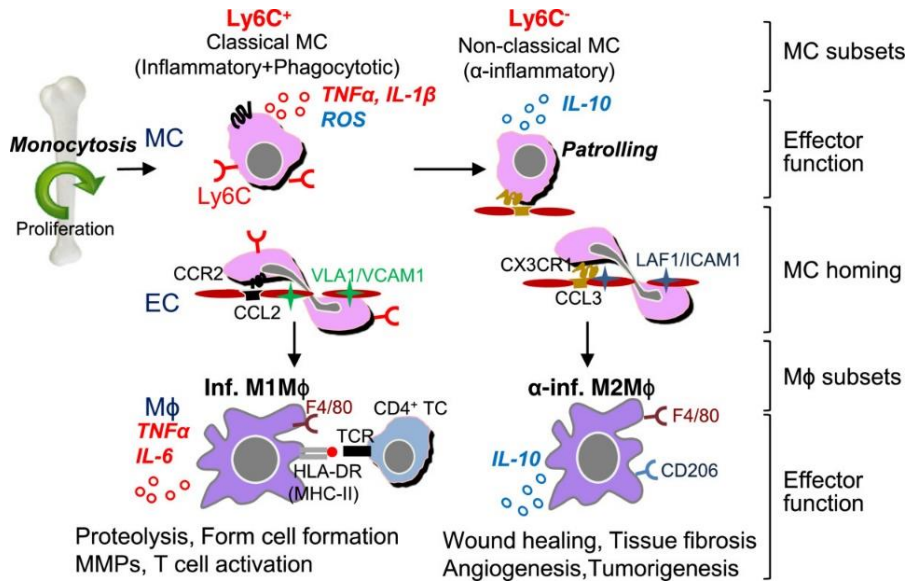
Figure16. Therapeutic anti-inflammatory potential of distinct subsets of monocytes (Yang, Zhang et al. 2014)

The first explanation is that colonizing monocytes may correspond to different subsets depending on the phase of the pathology. Wide range of studies established the possibility that during inflammatory processes distinct waves of monocytes colonize the tissues to perform sometimes opposite or complementary functions. It is also proposed that during the anti-inflammatory phase waves of classic and regulatory monocytes may infiltrate the tissues *de novo* giving rise to tolerogenic dendritic cells and anti-inflammatory macrophages that will boost the anti-inflammatory reaction.

Studies involving myocardial infarction damage and resolution found that two distinct waves of blood monocytes are recruited in this model. There was a specific early recruitment of classical Ly6C^{hi} monocytes that exhibited phagocytic, proteolytic and inflammatory activities. This was followed by delayed recruitment of Ly6C^{lo} monocytes which displayed anti-inflammatory, angiogenic and tissue remodelling properties (Nahrendorf, Swirski et al. 2007).

In a similar manner, studies involving *Listeria monocytogenes* intraperitoneal infection show that two distinct waves of Ly6C^{hi} and Ly6C^{lo} monocytes infiltrate the

tissues during inflammation. The wave of Ly6C^{hi} monocytes is believed to participate in the pro-inflammatory M1-like response where phagocytosis, bacterial clearance and increase of inflammation overcome. The wave of Ly6C^{lo} monocytes is believed to participate in an early pro-inflammatory M1-like response in which monocytes actively phagocyte and enhance inflammation, but also in delayed anti-inflammatory M2-like response with tissue remodelling, wound repair and immunomodulation (Auffray, Fogg et al. 2007).

When studying the implication of recruited myeloid cells in models of central nervous system encephalopathies, contradictory or perhaps complementary results come up. Indeed, infiltration of blood-derived monocytes and its differentiation towards M1-like macrophages boosts the inflammatory reaction in the CNS, axonal damage and worsens its prognosis (Hendriks, Teunissen et al. 2005; King, Dickendesher et al. 2009; Mildner, Mack et al. 2009; Ajami, Bennett et al. 2011; Jung and Schwartz 2012; Mishra, Wang et al. 2012).

Contradictory, again in a model of experimental autoimmune encephalopathy, recruited pro-inflammatory immature Ly6C^{hi} monocytes differentiate in situ into regulatory subpopulations that are able to present suppressor activity towards T cell pathogenic populations (Zhu, Kennedy et al. 2011). Furthermore, in this same model, recruited myeloid cells producing IL-23 and stimulating the production of GM-CSF by T helper cells are able to regulate the disease progression and severity (Codarri, Gyulveszi et al. 2011; El-Behi, Ciric et al. 2011).

In studies involving spinal cord injury an initial transmigration of pro-inflammatory Ly6C^{hi} monocytes into the injury site was observed with detrimental effects. However, a second wave of Ly6C^{lo} monocytes that was specific for resolution could also be detected

The second explanation is that plasticity of colonizing monocytes may allow the differentiation of one subtype of monocytes to another, or simply the differentiation into pro-inflammatory or anti-inflammatory recruited macrophages depending on the microenvironment of cytokines.

In a model of skeletal muscle injury and repair there was a rapid and specific infiltration of classical Ly6C^{hi} monocytes. In this case Ly6C^{hi} monocytes presented an inflammatory profile expressing pro-inflammatory cytokines. However, during the subsequent resolving phase infiltrating Ly6C^{hi} monocytes gave rise into proliferating macrophages that acquired anti-inflammatory profiles and stimulated muscle regeneration (Arnold, Henry et al. 2007).

Additional studies involving spinal cord injury showed similar results with an initial transmigration of classical Ly6C^{hi} monocytes into the injury site. Differentiation *in situ* of Ly6C^{hi} monocytes again established a population of recruited macrophages showing anti-

inflammatory and regulatory properties that suppressed detrimental activated resident microglia populations through IL-10 production (Shechter, London et al. 2009).

Extensive experimental data can be also found in relation with cancer models. In this case of solid tumours, Ly6C^{hi} monocytes differentiate into tumour-associated macrophages (TAM) that enhance tumorigenesis, tumour invasion, angiogenesis and progression to malignancy (Sunderkotter, Goebeler et al. 1991; De Palma, Venneri et al. 2005; Condeelis and Pollard 2006; Du, Lu et al. 2008; Pucci, Venneri et al. 2009).

Indeed, once the inflammatory trigger disappears monocyte-derived recruited macrophages switch into anti-inflammatory macrophage phenotypes (Figure 17). Anti-inflammatory macrophages together with Treg lymphocytes are responsible for the active synthesis of anti-inflammatory soluble molecules such as TGF-β, IL-4 and IL-10 cytokines implicated in the resolution of the inflammation. Alternatively activated macrophages also synthesize extracellular matrix remodeling and angiogenic molecules which contribute actively to tissue repair. Secreted anti-inflammatory molecules will reverse in its turn the phenotype of other pro-inflammatory macrophages to an anti-inflammatory phenotype creating a loop to control and resolve inflammation.
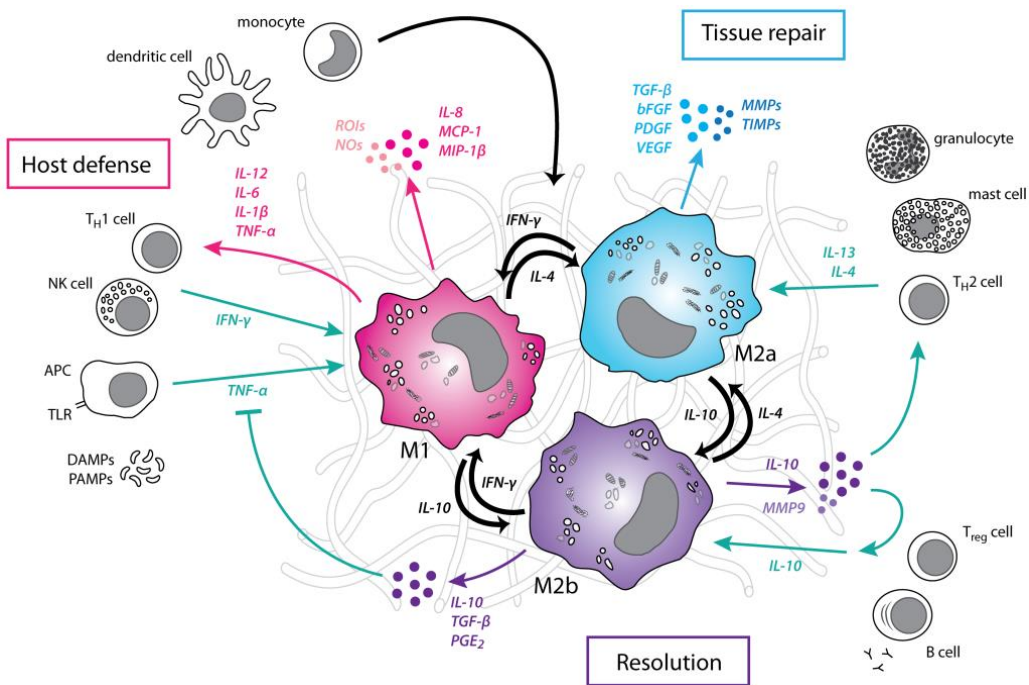
Figure17. Therapeutic anti-inflammatory potential of macrophages due to their plasticity (Biswas and Mantovani 2010)

5. Research and therapeutic potential of Ly6C^{hi} monocytes

Our experimental project is based on the effectiveness of our novel technique for *in vitro* generation Ly6C^{hi} monocytes. Until that moment, monocytes could not be generated *in vitro* and had to be isolated from peripheral blood. The efficiency of monocyte purification from blood was very poor and scarce amounts of cells were recovered as only 2-5% of blood leucocytes correspond to this subtype. This novel technique allows us to generate large amounts of completely functional *in vitro* produced Ly6C^{hi} monocytes.

We further confirm that these cells display the appropriate phenotypic and functional properties, particularly with regard to downstream compatibility and their complex role *in vivo*. Taking advantage on the ability of non-classical monocytes to infiltrate selectively into inflamed regions, our results indicate that we could open the door for new cell-based and classic therapeutic strategies. Similarly, we may be able to achieve induction of new immune balances, drug delivery treatments, and therapeutic targeting.

During the entire extension of this thesis, if not specified differently, the "Ly6C^{hi} monocytes" will correspond to the *in vitro* bone marrow-derived Ly6C^{hi} monocytes.

OBJECTIVES

II. HYPOTHESIS

The improvement of the *in vitro* generation of Ly6C^{hi} monocytes allows the manipulation of their phenotype and their potential application in diverse inflammatory processes.

III. OBJECTIVES

To optimize the differentiation, production and purification of *in vitro* Ly6C^{hi} monocytes from bone marrow cultures.

To characterize phenotypically and functionally the *in vitro* generated Ly6C^{hi} cells through comparative analysis with natural populations found in mice.

To determine the migratory capacity of *in vitro* Ly6C^{hi} monocytes in diverse models of inflammation.

To evaluate the capacity of *in vitro* Ly6C^{hi} monocytes to modulate inflammation after administration in different mice models of inflammation.

EXPERIMENTAL PROCEDURES

IV. EXPERIMENTAL PROCEDURES

1. Experimental mice

BALB/cByJRj and C57BL/6JRj 6- to 11-week-old female mice were purchased from Janvier laboratories, Le Genest-Saint-Isle, France.

DsRED$^{+/+}$ transgenic mice on the C57BL/6JRj background were kindly offered by Dr. Javier Diaz-Nido from the Center of Molecular Biology Severo Ochoa, Madrid, Spain (Vadivelu, Ooi et al. 2015).

LysM^{Cre}:YFP$^{+/-}$ conditional knock-in mice were kindly supplied by Dr. Annabel Valledor from the Department of Physiology and Immunology, Faculty of Biology, University of Barcelona, Spain.

CX3CR1-EGFP$^{+/-}$ knock-in mice were kindly offered by Dr. Paul Heppenstall from the Molecular Physiology Group, EMBL center, Monterotondo, Italy (Paolicelli, Bolasco et al. 2011).

STAT1$^{-/-}$ and STAT6$^{-/-}$ knock-out mice were kindly provided by Dr. Anna M. Planas from the Clinical and Experimental Brain Ischemia Group, IDIBAPS center, Barcelona, Spain (Meraz, White et al. 1996; Chitnis, Najafian et al. 2001).

Experiments were all based on females on the BALB/cByJRj background except for the EAE model and the experiments involving the DsRED transgenic mice where we based our experiments in females on the C57BL/6JRj background. STAT1 and STAT6 mice knockouts were backcrossed at least for 8 generations into the BALB/cByJRj and C57BL/6JRj backgrounds.

Mice were maintained under specific pathogen-free conditions in the Scientific Park of Barcelona animal house (SEA-PCB) or the Faculty of Pharmacy of the University of Barcelona animal house (UEA).

Experiments and animal manipulation were always performed in accordance with the policies of the ethics committee of the Government of Catalonia as well as national and international guidelines.

2. In vitro generation of Ly6C^{hi} monocytes and in vitro experiments

2.1. In vitro monocytes and BMDM generation

BALB/cByJRj or C57BL/6JRj 8-week-old female mice were euthanized by cervical dislocation and bone marrow was aseptically perfused by flushing 37°C DMEM into the isolated bones. Extracted bone marrow was homogenized to obtain a cell suspension and counted with a Neubawer cell counting camera.

Induction of bone marrow-derived Ly6C^{hi} monocytes was attempted by culturing bone marrow cells at a determined concentration. Cells were cultured during six days in a defined cocktail of growth factors in a 37°C 5%CO$_2$ incubator. The specific combination and concentration of growth factors and cells is still under patent pending process.

Induction of bone marrow-derived macrophages was attempted by culturing bone marrow cells in DMEM (10% FCS; 1%P-S; 20% L929 conditioned media) during six to seven days in a 37°C 5%CO$_2$ incubator (Comalada, Xaus et al. 2004).

2.2. *In vitro* produced Ly6Chi monocytes purification

Ly6C^{hi} cells cultures were recovered after six days of differentiation. Cell suspensions were centrifuged and resuspended in fresh ice-cold DMEM media specific for sorting procedure (10% FCS; 4mM EDTA; 1%P-S). Cells were counted and resuspended to reach a concentration of 20×10^6cell/mL.

Neutralization of the FcR receptors was made with the anti-CD16/CD32 (BD Pharmingen; San Diego, CA, USA) antibody used at a concentration of 1:200. Cells were incubated for 15 minutes at 4°C.

Ly6C labelling was made with the anti-Ly6C-FITC (BD Pharmingen; San Diego, CA, USA) antibody used at a concentration of 1:200. When necessary, Ly6C labelling was made with the anti-Ly6C-PE (BD Pharmingen; San Diego, CA, USA) antibody used at a concentration of 1:100. Cells were incubated for 30 minutes at 4°C. Isotype control was performed with the correspondent Rat IgM,κ monoclonal antibody isotype control (BD Pharmingen; San Diego, CA, USA).

Ly6C^{hi} cell sorting was accomplished using the FACS Aria or the FACS Fusion (Becton Dickinson; Franklin Lakes, NJ, USA) sorters. Sorting was effectuated at highest speed with the tip70. Ly6C^{hi} gated fraction was recovered and the final cell purity reached 99%. Ly6C^{lo} and Ly6C^{neg} fractions were only purified as controls for determined experiments. All cells were kept on ice during the whole process.

For recovery, cells were maintained in the same cocktail of growth factors used for the generation including 4mM EDTA in a 37°C 5%CO$_2$ incubator till the sorting procedure was over.

2.3. *In vitro* produced monocytes and BMDM culture

Well-plates were previously coated overnight with 100µg/ml poly-L-Lysine Borate Buffer and washed several times with PBS prior to use. BMDM were recovered and plated in coated 24 well-plates with poly-L-Lysine at a $0,5\times10^6$ cells/well concentration. Purified Ly6C^{hi}, Ly6C^{lo} and Ly6C^{neg} fractions from the *in vitro* produced monocytes culture

34

were recovered and plated in coated 24 well-plates with poly-L-Lysine at a $2x10^6$ cells/well concentration. Plates were centrifuged 5minutes at 500g to ensure proper cell adherence. After 2 hours of incubation culture plates were gently washed to remove non-adherent cells.

2.4. *In vitro* stimulation of *in vitro* produced monocytes and BMDM

For the *in vitro* experiments, BMDM and purified Ly6C^{hi}, Ly6C^{lo} and Ly6C^{neg} fractions from the *in vitro* produced monocytes culture were plated and stimulated with starved media or recombinant IFN-γ, IL-4, IL-10, LPS, CpGB, M-CSF or GM-CSF for 6 hours.

Table1. Cytokines, growth-factors and TLR ligands

Stimuli	Final Concentration	Initial concentration	Required dilution
rIFN-γ	10ng/ml	20ug/ml	1:2000
rIL-4	10ng/ml	10ug/ml	1:1000
rIL-10	10ng/ml	10ug/ml	1:1000
LPS	10ng/ml	10ug/ml	1:1000
CpGB	0,1uM	500uM	1:5000
R848	1ug/ml	1mg/ml	1:1000
rM-CSF	10ng/ml	50ug/ml	1:5000
rGM-CSF	10ng/ml	50ug/ml	1:5000

For the *in vivo* experiments, purified Ly6C^{hi} cells were maintained in suspension at a concentration of $1x10^6$cells/mL and stimulated with starved media, recombinant IFN-γ or IL-4 for 1 hour in DMEM (10% FCS; 4%EDTA; 1%P-S).

Recombinant IFN-γ, IL-4 and IL-10 were purchased from R&D Systems (Minneapolis, MN, USA), recombinant M-CSF and GM-CSF were purchased from Peprotech (Rocky Hill, NJ, USA), LPS was purchased from (Sigma; St Louis, MO, USA) and CpGB was purchased from Invivogen (San Diego, CA, USA).

Samples destined to FACS analysis were harvested after Tripsine (Sigma; St Louis, MO, USA) enzymatic treatment and resuspended in FACS Buffer (PBS; 10% FCS; 4%EDTA).

Samples destined to RT-PCR analysis were kept with Ambion Lysis Buffer (Thermo Fisher Scientiphic; Waltham, MA USA) at -80°C until RNA extraction.

3. Tissue and cell treatments

3.1. Isolation of tissue samples

Tissues destined to FACS analysis without previous enzymatic dissociation included peripheral blood, bone-marrow, spleen and intraperitoneal cells. Peripheral blood was recovered with heparinized 25G syringes after cardiac puncture. Bone-marrow was extracted as mentioned before. Splenocytes were obtained after crushing the spleen through a 100μm nylon cell strainer. Intraperitoneal cells were recovered after intraperitoneal lavage with 5mL of ice-cold PBS. Single cell suspensions were obtained from all tissues and treated for erythrocyte lysis.

Tissues destined to RT-PCR analysis were harvested with a surgical kit and quickly stored in Trizol reagent (Sigma; St Louis, MO, USA) at -80°C until disruption and RNA extraction.

Tissues destined to LSFCM analysis were extracted after transcardiac perfusion. Mice were injected with lethal dose of Ketamine-Xilamine (1:10). Animals were monitored for the loss of nociceptive reflexes and then perfused transcardiacally with PBS 4% paraformaldehyde at 25°C. Tissues of interest were extracted with a surgical kit, post-fixated for 24h in 4% paraformaldehyde at 4°C, and crioprotected in PBS 30% sucrose 0.02% azide solution for 24h at 4°C. Following crioprotection, tissues were embedded in OCT Optimal Cutting Temperature compound in standard Tissue-Tek Cryomolds purchased from Sakura (Torrance, CA, USA), frozen in dry ice, and finally stored at -80°C for at least 24h. Serial criosections of 30μm thickness were obtained with Leica Criotome and microtome blades (Feather635), and then disposed into adhesive microscope slides from Starfrost (Little Rock, AK, USA) . Criosections were maintained at -20°C until treated for immunohistochemistry.

3.2. Enzymatic tissue dissociation

Tissues destined to FACS analysis requiring previous enzymatic dissociation included ear tissue from the DNFB model and muscular tissue from the NTX model. During the experiments of fluorescent-cells transfer tissues were covered from light during the whole process. DNAse I (ref. AMPD1), Dispase I (ref. D4818), Collagenase IV (ref. C5138) and Hyaluronidase (ref. H3506) were all purchased from Sigma (St Louis, MO, USA).

Ear tissues harvested from the DNFB model were incubated in DMEM (0,5% Dispase I; 1%P-S) at 37°C for 60 minutes. The epidermis and dermis were mechanically separated and the epidermal sheet was discarded. The dermis was incubated in DMEM

(1mg/mL Collagenase IV; 0,5mg/mL DNAse I; 1mg/mL Hyaluronidase; 1%P-S) at 37°C for 60 minutes in a thermomixer at 650rpm. Samples were filtrated through a 100μm nylon mesh, centrifuged at 500g for 5 minutes and resuspended in ice-cold PBS.

Muscle tissues from the NTX model were mechanically disaggregated with surgical scissors and then incubated in DMEM (1mg/mL Collagenase IV; 0,5mg/mL DNAse I; 1mg/mL Hyaluronidase; 1%P-S) at 37°C for 60 minutes in a thermomixer at 650rpm. Samples were filtrated through a 100μm nylon mesh, centrifuged at 500g for 5 minutes and resuspended in ice-cold PBS.

3.3. Erythrocyte lysis

Single cell suspensions obtained from all tissues were treated for erythrocyte lysis. Samples were centrifuged at 500g for 5 minutes, resuspended in 5mL of Lysis Buffer (NH_4Cl 0,155M; EDTA 0,1mM; $KHCO_3$ 0,01M; pH 7,5) and incubated for 10 minutes on ice. This process was repeated till three times until complete erythrocyte lysis.

3.4. Percoll gradient leucocyte isolation

Samples coming from enzymatic dissociation and erythrocyte lysis were destined to density gradient centrifugation with Percoll. Percoll was purchased from GE Healthcare Life Sciences (Little Chanfont, UK).

Percoll 30% and 70% solutions were prepared in DMEM. Cell pellets were resuspended in 5mL of 30% Percoll, then overlaid slowly to 5mL of 70% Percoll to avoid mixing and centrifuged at 20g for 20 minutes at room temperature without brakes. Leucocytes were collected from the interface of the gradient using a micropipette, washed in PBS and resuspended in FACS Buffer (PBS; 10% FCS; 4mM EDTA).

3.5. DIR tracer labelling

Ly6C^{hi} sorted cells were labelled with the lipophilic tracer DIR (Invitrogen; Carlsbad, CA, USA). DIR 10μM stock solution was prepared in 37°C PBS. Cells were resuspended at a concentration of $10x10^6$cell/mL in 37°C PBS. DIR labelling was accomplished by a 1:1 mixture and incubation for 10 minutes at 37°C. Three washing steps with 37°C DMEM (20% FCS) were performed in order to eliminate the excess of unbound tracer. Samples were always protected from light (Hoffman 2002; Hillman 2007).

3.6. PKH26 tracer labelling

Ly6C^{hi} sorted cells were labelled with the lipophilic tracer PKH26 (Sigma; St Louis, MO, USA). PKH26 4µM stock solution was prepared in 37°C PBS. Cells were resuspended at a concentration of $20x10^6$cell/mL in 37°C PBS. PKH26 labelling was accomplished by a 1:1 mixture and incubation for 30 minutes at 37°C. Three washing steps with 37°C DMEM (20% FCS) were performed in order to eliminate the excess of unbound tracer. Samples were always protected from light (Fischer, Andreesen et al. 2002).

4. Flow cytometric analysis

4.1. Flow cytometry characterization (FACS)

Single cell suspensions were centrifuged and resuspended in FACS Buffer (PBS; 10% FCS; 4%EDTA) and plated in a 96-well plate at a concentration of $1x10^6$ cell/100µL/well.

Neutralization of the FcR receptors was made with the anti-CD16/CD32 (BD Pharmingen; San Diego, CA, USA) antibody used at a concentration of 1:50. Cells were incubated for 15 minutes at 4°C.

FACS labelling was made incubating the cells in the corresponding antibodies dilution for 30 minutes at 4°C. Isotype controls were performed in the same way.

FACS analysis was accomplished using FACS Gallios (Beckman Coulter; Brea, CA, USA) analyser, and flow cytometry data was analyser using FlowJo10 (Treestar; Ashland, OR, USA) analysis software.

Table2. Antibodies

Antigen	Company	Reference	Fluorochrome	Dilution
CCR2	RD Systems	RYD-FAB5538P	PE	1:25
CD115	eBioscience	12-1152-82	PE	1:500
CD11b	BD Pharmingen	557397	PE	1:500
CD11b	Biolegend	101241	Brilliant Violet 711	1:500
CD11c	Biolegend	117322	Pacific Blue	1:25
CD11c	eBioscience	56-0114	Alexa Fluor 700	1:100
CD16/CD32	BD Pharmingen	553142	Non-Labeled	1:50
CD45	Miltenyi Biotec	130-091-910	PE	1:500
CD45	eBioscience	25-0451-82	PE/CY7	1:1000

CD62L	eBioscience	12-0621-81	PE	1:500
CD62L	eBioscience	56-0621	Alexa Fluor 700	1:25
CD68	AbD serotec	MCA1957A700T	Alexa Fluor 700	1:100
CD68	Bioloegend	137010	PerCP.CY5.5	1:1000
CD80	BD Pharmingen	553769	PE	1:500
CD86	eBioscience	15-0862	PE/CY5	1:800
CX3CR1	RD Systems	FAB5825A	APC	1:25
F4/80	eBioscience	17-4801	APC	1:100
F4/80	Biolegend	123132	Brilliant Violet 421	1:500
Ly-6C	BD Pharmingen	560562	PE	1:500
Ly-6C	BD Pharmingen	553104	FITC	1:50
Ly-6G (Gr-1)	eBioscience	47-5931-82	APC/Efluor 780	1:1000
Ly-6G (Gr-1)	eBioscience	11-5931	FITC	1:100
MHC II I-A/I-E	eBioscience	56-5321	A700	1:25
MHC II I-A/I-E	eBioscience	12532181	PE	1:500
MHC II I-A/I-E	BD Pharmingen	553623	FITC	1:200
MHC II I-Ad	BD Pharmingen	06281D/553611	FITC	1:50
MHC II I-Ad	BD Pharmingen	562823	APC	1:1000
Viability Fixable Dye	eBioscience	65-0865	eFLUOR 780	1:1000
Viability Fixable Dye	eBioscience	65-0863-14	eFLUOR 450	1:1000

5. Gene expression characterization

Cells were homogenized in Ambion Lysis Buffer and RNA was extracted and DNAse treated using Ambion RNA extraction Kit (Life Technologies; Waltham, MA USA).

Tissues were homogenized in Trizol Reagent (Sigma; St Louis, MO, USA) with an UltraTurrax (IKA; Breisgrau, DE) and RNA was extracted and DNAse treated following ReliaPrep RNA system Kit (Promega; Madison, WI, USA).

DNA was retrotranscribed using 400ng of RNA using the Moloney murine leukaemia virus reverse transcriptase RNase H Minus (Promega; Madison, WI, USA). DNA retrotranscription program: 70ºC 5min; ICE; 40°C 10min; 42°C 50min; 72°C 15min.

RT-PCR was performed using SYBR Green Master Mix purchased from Applied Biosystems (Waltham, MA USA). RT-PCR program: STAGE 1: 95° 10:00; STAGE 2: 95° 0:30 / 60° 0:30 / 72° 0:30 [35 REPEATS]; STAGE 3: 95° 0:15 / 60° 0:15 / 95° 0:15.

All procedures were performed as recommended by the manufacturer. Data was normalized using *hprt1*, *l14* and *sdha* as reference genes. Primer sequences are presented in the following table. Data was analysed using the Biogazelle Qbaseplus (Gent, BE) analysis software.

Table3. Primer sequences

NAME	SYMBOL	NCBI NUMBER	PRIMERS	INTER-INTRONIC
ARGINASE-1	ARG1	NM_007482.3	FORWARD:TTGCGAGACGTAGACCCTGG	YES
			REVERSE:CAAAGCTCAGGTGAATCGGC	
FIZZ1	RETNLA	NM_020509.3	FORWARD:TCTGCCCCAGGATGCCAACTTTGA	YES
			REVERSE:GTCCAGTCAACGAGTAAGCACAGGC	
HPRT1	HPRT1	NM_013556.2	FORWARD:ATCATTATGCCGAGGATTTGG	YES
			REVERSE:GCAAAGAACTTATAGCCCCC	
IL 10	IL10	NM_010548.2	FORWARD:ACCAGCTGGACAACATACTGC	YES
			REVERSE:TCACTCTTCACCTGCTCCACT	
IL 12 B	IL12B	NM_008352	FORWARD:TGGTTTGCCATCGTTTTGCTG	YES
			REVERSE:ACAGGTGAGGTTCACTGTTTCT	
IL 1B	IL1B	NM_008361.3	FORWARD:TGGGCCTCAAAGGAAAGAAT	YES
			REVERSE:CAGGCTTGTGCTCTGCTTGT	
IL 6	IL6	NM_031168.1	FORWARD:CCAGAGATACAAAGAAATGATGG	YES
			REVERSE:ACTCCAGAAGACCAGAGGAAAT	
L14	RPL14	NM_025974.2	FORWARD:TCCCAGGCTGTTAACGCGGT	YES
			REVERSE:GCGCTGGCTGAATGCTCTG	
NOS2	NOS2	NM_001313921.1	FORWARD:GCCACCAACAATGGCAACA	YES
			REVERSE:CGTACCGGATGAGCTGTGAATT	
SDHA	SDHA	NM_023281.1	FORWARD:TGGGGAGTGCCGTGGTGTCA	YES
			REVERSE:CATGGCTGTGCCGTCCCCTG	
TGF B	TGF	NM_011577.1	FORWARD:GAGACGGAATACAGGGCTTTC	YES
			REVERSE:TCTCTGTGGAGCTGAAGCAAT	
TNF A	TNF	NM_013693.2	FORWARD:CCAGACCCTCACACTCAGATC	YES
			REVERSE:CACTTGGTGGTTTGCTACGAC	
YM1	CHI3L3	NM_009892.2	FORWARD:GCCAGCAGAAGCTCTCCAGAAGCA	YES
			REVERSE:GCACTGAACGGGGCAGGTCC	
YWHAZ	YWHAZ	NM_011740.3	FORWARD:TCATCGTGCGTGTGGTGCCC	YES
			REVERSE:TCGGCCAGCTTGGCCTTCTG	

6. *In vivo* imaging (IVIS)

Mice destined to *in vivo* imaging analysis were anesthetized with isoflurane and placed inside the IVIS chamber (Xenogen; Cranbury, NJ, USA). IVIS basal background calibration was done before each measurement to avoid any background.

Fluorescence detection was accomplished using ICG channel as it presents very similar emission and excitation wavelengths to the ones from the DIR tracer, 1 second exposition was chosen, and ICG fluorescence was simultaneously acquired to the ICG

background. IVIS data were analysed using LivingImage 2.6.0.1 (Xenogen; Cranbury, NJ, USA) analysis software.

7. Microscopy analysis

7.1. Immunohistochemistry

Immunohistochemistry was performed in dark humid chambers to avoid evaporation and bleaching of the fluorophores. Slides were first incubated for 30 minutes room temperature in Glycine Buffer (Glycine 0,1M; pH 7.4) to eliminate OCT. Permeabilization step was accomplished by a 5 minutes incubation with Permeabilization Buffer (PBS; 0.2% Triton). Neutralization of FcR was made incubating the slides 2h at room temperature with Blocking Buffer (PBS; 0.2% Triton; 1:1000 rat anti-mouse-CD16/CD32). For F4/80 labelling we used the primary antibody rat anti-mouse-F4/80 (eBioscience; San Diego, CA, USA) and the secondary antibody chicken anti-rat-IgG-AlexaFluor647 Invitrogen (Carlsbad, CA, USA). During the blocking step and we did not use the rat anti-mouse-CD16/CD32 (BD Pharmingen; San Diego, CA, USA) because of antibody cross-reaction. Primary antibody labelling was performed by incubating the slides overnight at 4°C in anti-F4/80 labelling solution (PBS; 0.2% Triton; 1:200 anti-F4/80). Secondary antibody step was performed by incubating the slides 1h room temperature in anti-IgG-AlexaFluor647 labelling solution (PBS; 0.2% Triton; 1:200 anti-IgG-AlexaFluor647). For NOS2 labelling we used the primary antibody rabbit anti-mouse-NOS2 (Abcam; Cambridge, UK) and the secondary antibody goat anti-rabbit-IgG-AlexaFluor680 (ThermoFisher; Waltham, MA USA). Primary antibody labelling was performed by incubating the slides overnight at 4°C in anti-NOS2 labelling solution (PBS; 0.2% Triton; 1:250 anti-NOS2). Secondary antibody step was performed by incubating the slides 1h room temperature in anti-IgG-AlexaFluor680 labelling solution (PBS; 0.2% Triton; 1:200 anti-IgG-AlexaFluor680).

Nuclear DNA labelling was accomplished by incubation of the slides during 10 minutes room temperature in DAPI (Sigma; St Louis, MO, USA) labelling solution (PBS; 1:1000 DAPI). Slides were then dried and mounted in Prolong Gold (ThermoFisher; Waltham, MA USA) fluorescent mounting media and stored at -20°C.

7.2. Fluorescence confocal microscopy (LSFCM)

Microscope analysis was performed using the SP5 and SP2 Leica Laser Scanning Fluorescence Confocal Microscopes and the Fluorescence Stereoscope Leica

Lupa. Fluorescence-based microscopy data was analysed using the Leica LAS AF (Wetzlar; DE) analysis software and the Fiji/ImageJ analysis software.

7.3. Optical microscopy

Microscope analysis was conducted using the Optical Inverted Microscope Nikon TE200, the Optical Upright Microscope Nikon E600 and the Optical Upright Microscope Nikon E800, all of them coupled to an Olympus DP72 camera. Peroxidase-based and haematoxylin-eosin microscopy data were analysed using the Fiji/ImageJ analysis software.

8. ELISAs

Enzyme linked immunosorbent assay (ELISA) was used to detect serum TNF-α. ELISAs were purchased from eBioscience (San Diego, CA, USA) and achieved following the commercial protocol.

9. Animal models

9.1. Thyoglicollate-induced inflammation model (TII)

Thyoglicollate 5% media was prepared with distilled water, autoclaved and kept at 4°C covered from light for three weeks prior to use. The model was generated in BALB/cByJRj 8-week female by injecting intraperitoneally 1mL of 5% aged thyoglicollate or PBS as a control. Thyoglicollate was purchased from Oxoid (Hampshire, UK).
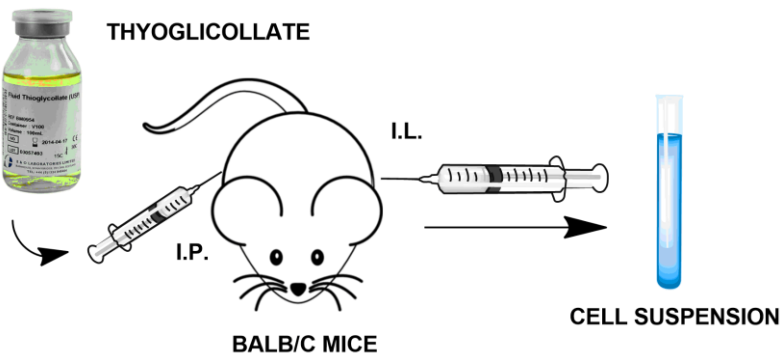
Figure1. Thyoglicollate-induced intraperitoneal inflammation model, (I.P.) Intraperitoneal injection, (I.L.) Intraperitoneal lavage

Ly6C^{hi} purified cells were injected the same day of the generation of the model. Following 24, 48 or 72 hours, leucocyte infiltrates were recovered by peritoneal lavage as described before (Figure1).

9.2. Dinitrofenolbenzene contact-induced inflammation model (DNFB)

Dinitrofenolbenzene was diluted in acetone to reach a concentration of 1%. BALB/cByJRj 8-week female mice were anesthetized with isoflurane and 10µL of DNFB1% were applied homogeneously to the whole extension of the right ear. Acetone was applied to the left ear as a control. Dinitrofenolbenzene was purchased from Sigma (St Louis, MO, USA). Ly6C^{hi} purified cells were injected the same day of the generation of the model. Samples were recovered at different times depending on the experiment (Figure2).
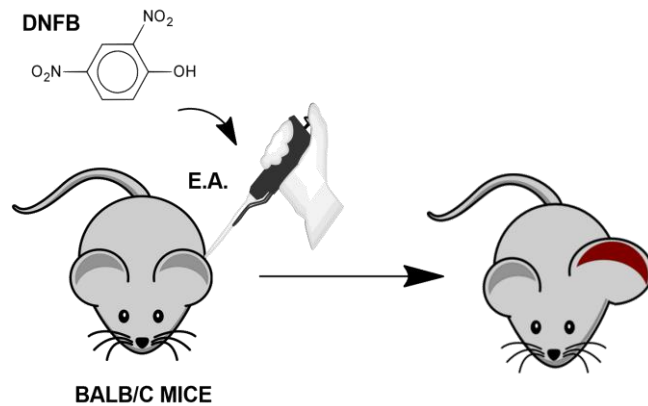
Figure2. Dinitrophenolbenzene-induced inflammation model, (E.A.) Ear application

9.3. Notexin-induced myoinjury model (NTX)
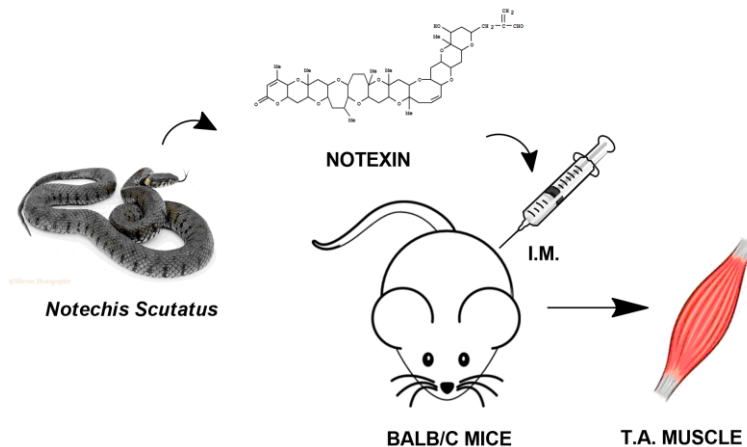
Figure3. Notexin-induced chronic myoinjury inflammation model, (I.M.) Intramuscular injection, (T.A.) *Tibialis anterioris* muscle

Notexin venom was resuspended at a concentration of 25µg/mL. Then, female BALB/cByJRj 8-week mice were anesthetized with isoflurane and 20uL of total Notexin volume was injected intramuscular in the right leg *tibiallis anterioris* muscle. The left leg

tibiallis anterioris muscle was injected with PBS as a control. Notexin venom was purchased from Latoxan (Valence, FR).

Ly6C^{hi} purified cells were injected intravenously 24 hours after the generation of the model. Samples were recovered at days 0, 1, 2, 4, 6 and 8 after Notexin injection (Figure3).

9.4. *Klebsiella pneumoniae* systemic infection model (KP)

Klebsiella pneumoniae was cultured to determinate its specific growth curve under established conditions. *K. pneumoniae* was then inoculated in brain heart infusion broth (BHIB) liquid media (Fluka; St Louis, MO, USA) and cultured overnight at 37°C 5%CO_2 under agitation. The day after, fresh BHIB was inoculated at a dilution of 1:100. Vials were incubated at 37°C 5%CO_2 under agitation until the culture reached a DO in between of 0,6-0,8. Following the growth curve equation we could extrapolate the concentration of bacteria CFUs. Female C57BL/6JRj 8-week mice were anesthetized with isoflurane and 8.10^6 CFU were injected intranasally with a micropipette. Control mice were injected with PBS (Figure4).
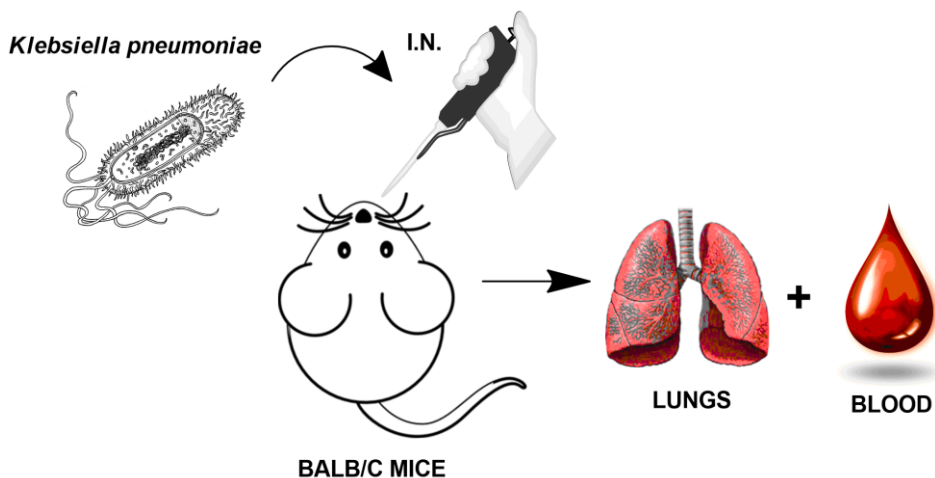
Figure4. *Klebsiella pneumoniae* systemic infection model, (I.N.) Intranasal injection

Ly6C[hi] purified monocytes were injected the same day of bacteria inoculation. Samples destined to ELISA quantification of serum cytokines, lungs CFU counting and immunohistochemistry were recovered after 48 hours. For the experiments of survival and clinical scoring mice were evaluated for a week.

Klebsiella pneumoniae was gently offered by Dr. Susana Merino from the Department of Microbiology, Faculty of Biology, University of Barcelona, Spain (Tomas, Camprubi et al. 1991).

9.5. Experimental autoimmune encephalomyelitis model (EAE)

C57BL/6JRj 11-week female mice were immunized by axillary and inguinal subcutaneous injections of the oligodendrocyte myelin peptide MOG40-55 (100µg/mice) emulsified in complete Freund´s adjuvant (CFA) (Sigma; St Louis, MO, USA) containing 4mg/mL *Mycobacterium tuberculosis* extract (Difco; Franklin Lakes, NJ, USA). MOG40-55 was previously diluted in PBS and a 1:1 emulsion was performed with CFA. The final injected volume per mice was 200µL. Mice were also intravenously injected with *Bordetella pertussis* toxin (Sigma; St Louis, MO, USA) (250ng/mice) on the days 0 and 2 post-immunization (Figure5).
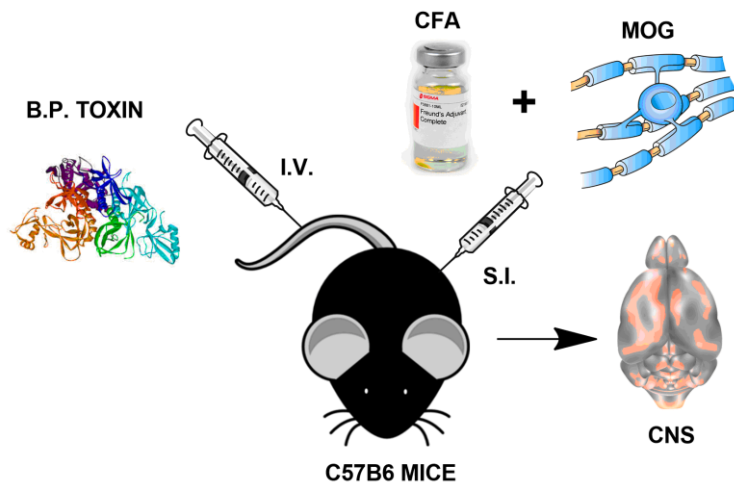
Figure5. Experimental autoimmune encephalopathy model, (B.P.) *Bordetella pertussis* toxine, (I.V.) Intravenous injection, (CFA) Complete Freund´s Adjuvant, (MOG) Myelinic Oligodendrocyte Glycoprotein, (S.I.) Subcutaneous injection, (CNS) Central Nervous System

Ly6C^{hi} purified cells were injected the days 10 and 12 after generation of the model. Samples destined to IVIS evaluation and immunohistochemistry were recovered after 48 hours. For the experiments of survival and clinical scoring mice were evaluated for two weeks.

This model was gently offered by Eva-Maria Martinez Caceres from the Division of Immunology, Germans Trias i Pujol University Hospital and Research Institute, Campus Can Ruti, Badalona, Spain (Mansilla, Selles-Moreno et al. 2015).

10. Experimental analysis

10.1. Statistical analysis

Whenever it is not specified in each particular figure legend, all results show collected data corresponding to at least three separate experiments. In some cases, only the most representative experiment is shown. *In vitro* experiments were always performed with three replicates per point. Each *in vivo* experiment was performed with at least three mice per group, but the majority was effectuated with five to eight animals per group. *In vivo* experiments involving survival and clinical scoring involved from eight till ten animals. Both *in vitro* and *in vivo* experiments were expressed as the mean$^+$SD except when specified. Statistical analysis used was dependent on each type of experiment.

Linear regressions were effectuated with second order polynomial (quadratic) based equations.

In experiments involving simple comparison of two groups of in vitro or in vivo data we used the non-parametric t-Test or Mann-Whitney test.

In experiments involving simple comparison of various groups of in vitro or in vivo data we used the One-way ANOVA non-parametric or Kruskal-Wallis test, followed in some cases by the Dunn´s multiple comparison post-test.

In experiments involving multiple comparison of in vivo data we used the Two-way ANOVA, followed by the Bonferroni´s multiple comparison post-test.

Survival curves statistical analysis of in vivo data was analysed with the Log-rank or Mantel-Cox test, and the Gehan-Breslow-Wilcoxon test.

The significance level depended on the experiments as was expressed in the form of the four different symbols mentioned here after:

Significance level alpha > 0.05 (95% Confidence interval) #
Significance level alpha ≤ 0.05 (95% Confidence interval) *
Significance level alpha ≤ 0.01 (99% Confidence interval) **
Significance level alpha ≤ 0.001 (99.9% Confidence interval) ***

10.2. Software analysis

The software used for analysis of Flow Cytometry, Gene Expression and Microscopy Optical and Confocal data is specified at the end of each section.

The software used for statistical analysis was Graphpad Prism5, Graphpad Prism6 and Microsoft Excel 2016.

The software used for graphing purposes was Graphpad Prism5, Graphpad Prism6 and Microsoft Excel 2016.

The software used for text treatment purposes was Microsoft Word 2016.

The software used image treatment and drawing was Adobe Photoshop CS3, ChemBioDraw Ultra 12.

The software used for image and text design was Adobe InDesign, Inkscape, Microsoft Powerpoint 2016.

The software used for bibliographic purposes was Endnote and Zotero.

RESULTS

V. RESULTS

I. SECTION. *IN VITRO* GENERATION OF LY6C^{hi} CELLS

1. Titration of the optimal conditions for the *in vitro* generation

In a first step we optimized the *in vitro* generation of Ly6C^{hi} cells. This method was first established in our laboratory by Catalina Rincon (M.Sc.). For the optimization of the protocol, we performed extensive titration experiments to determine the ideal number of cultivated bone marrow cells and specific concentrations for each one of the components of the growth-factors cocktail (under patent process).

In these experiments we observed that either low or high concentrations of cells or growth-factors were detrimental to Ly6C^{hi} cell production. Using low concentrations of growth-factors induced low percentages of Ly6C^{hi} CD11b$^+$ cells and Ly6C^{hi} CCR2$^+$ cells. Using high concentrations of growth-factors also resulted in poor recovery of populations of interest (Figure 1.A and B).
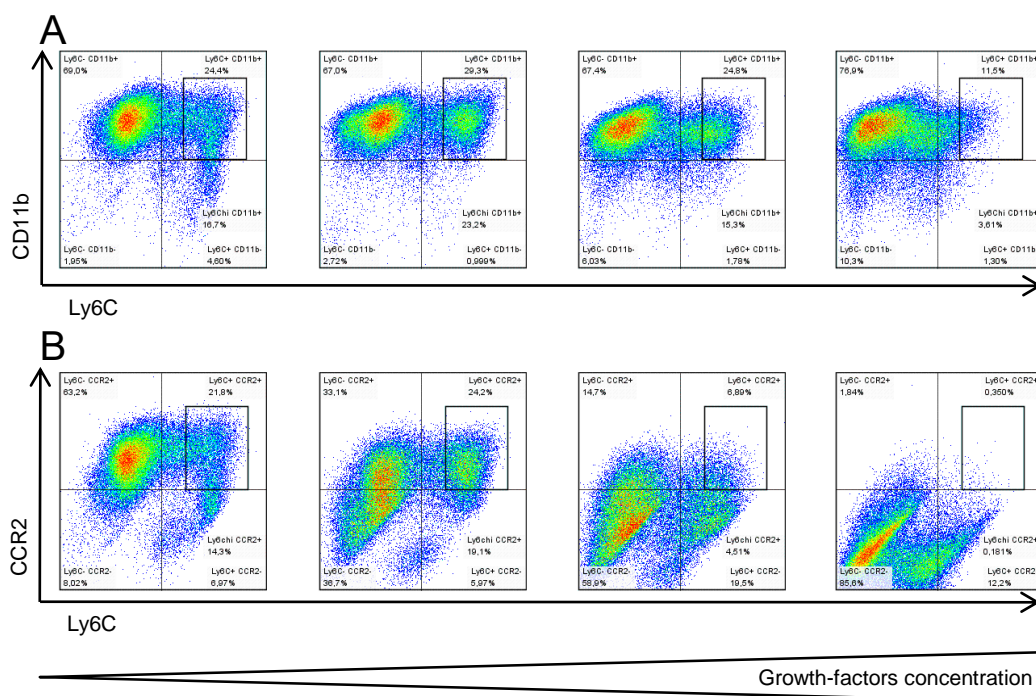
Figure1. Specific combination and concentration of growth factors is required for the correct *in vitro* generation of Ly6C^{hi} CD11b⁺ CCR2⁺ cells.
(A)   Dot-blots of the titration of growth-factor concentrations showing the emergence of the characteristic monocyte markers CD11b and Ly6C.
(B)   Dot-blots of the titration of growth-factor concentrations showing the emergence of the characteristic monocyte markers CCR2 and Ly6C.
Results are representative of three experiments. Mean and ±SD performed with three mice/ group.

Optimal conditions corresponded to a narrow range of concentrations of both cells and growth-factors. Additional data can be found in the Supplementary data section (Figure 1.A and B).

2. Kinetics of the *in vitro* generation of Ly6C^{hi} cells

After that, we evaluated the phenotype characterization of the *in vitro* culture of Ly6C^{hi} cells. The aim was to study the evolution through time of the expression of extracellular markers characteristic for recruited monocytes. This was done in terms of increase or diminution of the expressing cells percentage and the levels of expression for each marker. We developed an eight colours flow cytometry panel to analyse the expression of eight markers specific of the Ly6C^{hi} cell subtype. The chosen markers for this method were Ly6C, CD11b, CD11c, F4/80, CD115, CD62L, CCR2 and CX3CR1.

When we assessed the kinetics of expression of all markers in an independent manner we observed distinct patterns. During the differentiation process, monocyte cultures show a substantial increase in the percentage of CCR2 and CD115 positive cells. Whereas the percentage of Ly6C, CD11b and CD62L positive cells remained high and stable until day 7. The percentage of F4/80, CX3CR1 and CD11c positive cells remained moderate to low and stable also until day 7. There was a strong decay after day 7 in the percentage of cells positive for each one to the markers. This fact strongly suggested an exhaustion of the cultures and corresponded with increased cell death and high decrease in the total cell suspension number (Figure 2.A). *In vitro* cultures reached a pick in suspension cell yield at day 6 after bone marrow plating (Figure 2.B). After 6 days of culture, cell death percentages were still acceptable showing that cultures were not exhausted (Figure 2.B). The day 6 after culture corresponded to the point where we observed maximum percentage of cells of interest.

When we assessed the expression of markers in combination with Ly6C^{hi} expression we observed clearer results. *In vitro* monocyte cultures increase the percentage of Ly6C^{hi} CD11b$^+$, Ly6C^{hi} CCR2$^+$, Ly6C^{hi} CD115$^+$ and Ly6C^{hi} CD62L$^+$ populations reaching their maximum at day 6 after culture. Oppositely, the percentage of Ly6C^{hi} F4/80$^+$, Ly6C^{hi} CX3CR1$^+$ and Ly6C^{hi} CD11c$^+$ cells remained low and stable (Figure 2.C). Additional data is included in the Supplementary data section (Figure2).

In vitro bone marrow cells cultures observed under optic microscope showed that the initial homogeneous suspension of bone marrow cells was soon forming a monolayer of adherent cells (Day4). This monolayer turned to generate dividing clusters from where cells were progressively released into the media (Day6). After culture exhaustion, the fraction of suspension cells decreased dramatically and only the macrophage-like adherent monolayer of cells remained (Day8) (Figure 3.A and Supplementary Figure3).

Our results defined a final protocol for *in vitro* generation of Ly6C^{hi} cells, establishing the days of culture for a proper differentiation, cell yield and viability.
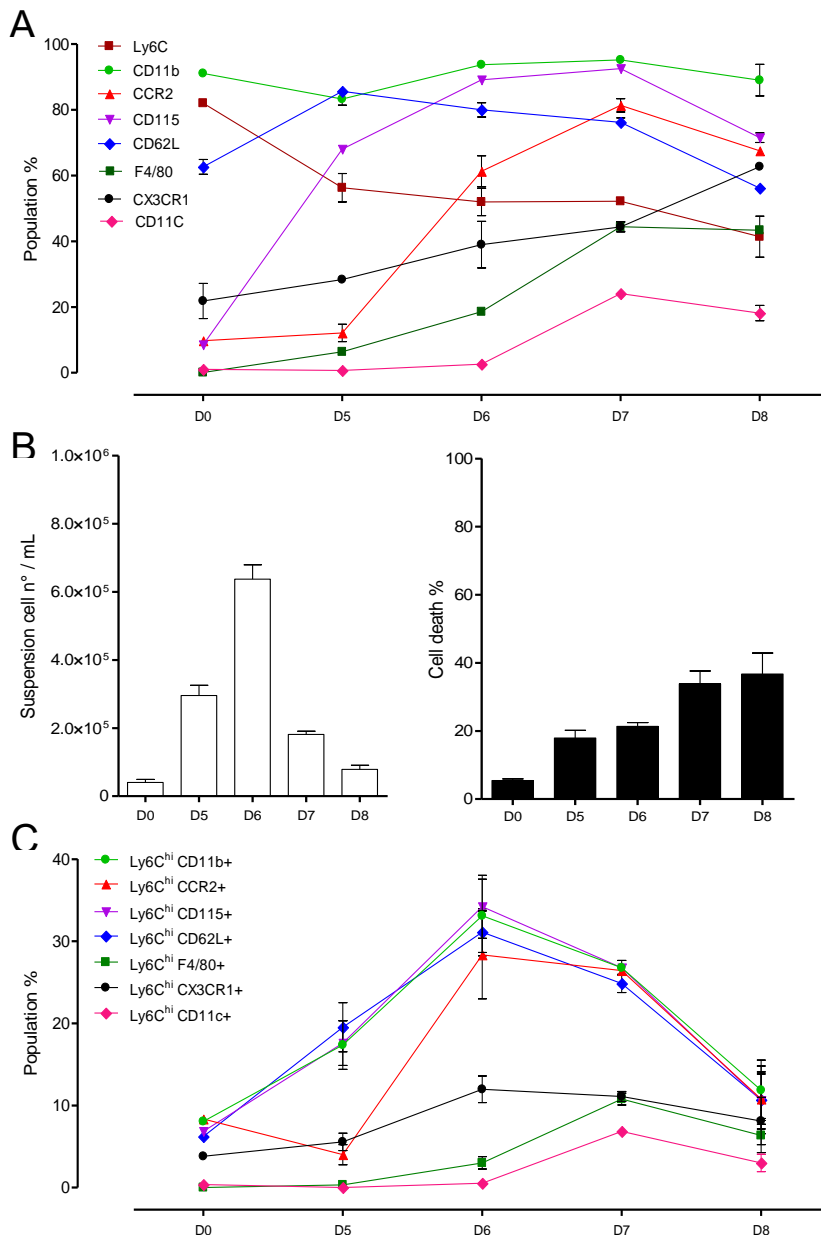
Figure2. Under specific growth factor conditions bone marrow suspensions give raise to pro-inflammatory Ly6C^{hi} CD11b^{+} CCR2^{+} cells.
(A) Kinetics of the positive cell percentage for distinct characteristic monocyte markers during the *in vitro* generation of Ly6C^{hi} cells.
(B) Kinetics of the suspension cell number and dead DAPI[+] cell percentage.
(C) Kinetics of the population percentage during monocyte generation.
Results are representative of three experiments. Mean and ±SD are performed with three mice per group.

A
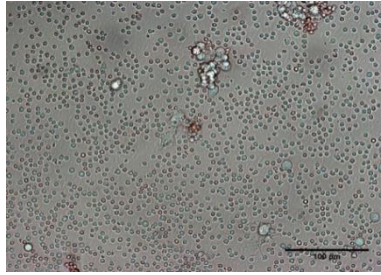
Day2
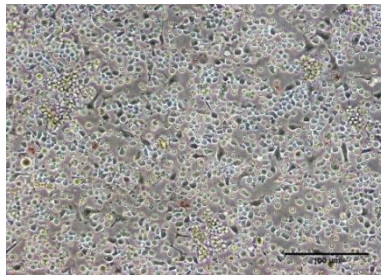
Day4
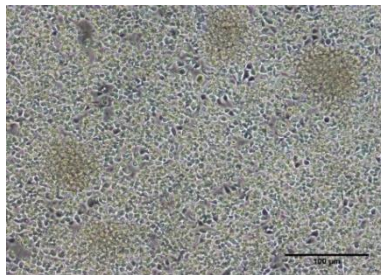
Day6
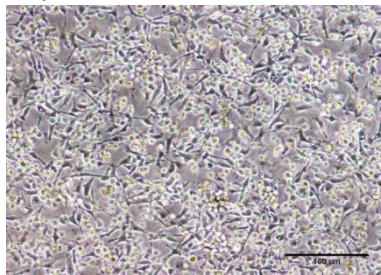
Day10

Figure3. Optic microscope images of different stages and different purified subpopulations of the *in vitro* culture of Ly6C^{hi} cells.
(A) *In vitro* bone marrow cells cultures at days 2, 4, 6 and 10.
Results are representative of three experiments. Mean and ±SD are performed with three mice per group.

3. Distinct populations regarding the Ly6C marker expression emerge from the *in vitro* produced monocyte cultures

Once the procedure was completely optimized we were able to obtain a high concentration of Ly6C^{hi} cells in our cultures. In optimal conditions we reached percentages of 60% of Ly6C^{hi} cells from the total of Ly6C positive generated cells. We could differentiate four different subpopulations attempting to the Ly6C marker expression: Ly6C^{negative} (Ly6C^{neg}), Ly6C^{lo} (Ly6C^{low}), Ly6C^{intermediate} (Ly6C^{int}), and Ly6C^{high} (Ly6C^{hi}) population (Figure 4.B). We focused our analysis on the three majoritarian populations that corresponded to the Ly6C^{neg}, Ly6C^{lo} and Ly6C^{hi} fractions.

We decided to further analyse the expression of extracellular markers such as CD11b, CCR2, CD115, CD62L, F4/80, CX3CR1 and CD11c. Each one of the previous three distinct populations expressed distinct combinations of cell markers suggesting distinct properties and functions (Figure 4.C). Supplementary data section (Figure 4).

The Ly6C^{hi} fraction presented high expression of the markers Ly6C, CD11b, CCR2, CD115 and CD62L, and low or no expression of the markers F4/80, CX3CR1 and CD11c. This was in complete accordance with the expected classical monocyte phenotype as previously described in the introduction.

The Ly6C^{lo} fraction differentiated from the Ly6C^{hi} fraction exclusively from the expression of CCR2 and CD115. These two markers are specifically associated to the function of Ly6C^{hi} monocytes and their expression was strongly reduced in Ly6C^{lo} cells.

The Ly6C^{neg} fraction differentiated from the Ly6C^{hi} fraction from the expression of F4/80, CX3CR1 and CD11c. These three markers are not expressed by Ly6C^{hi} monocytes. F4/80 is usually associated to a macrophage phenotype, CX3CR1 and CD11c are usually associated to dendritic cell phenotypes. Their expression was strongly increased in Ly6C^{neg} cells.

4. Enrichment of the Ly6C^{hi}, Ly6C^{low} and Ly6C^{neg} cell populations

The objective was to obtain a purified fraction of Ly6C^{hi} cells from the whole culture. For this purpose, we performed a cell sorting of the desired Ly6C^{hi} population based only in the Ly6C marker which is known to be a differentiation marker with no specific function. We excluded CCR2, CD11b and other markers from the sorting procedure to avoid the blockage of receptors and ligands which are known to be essential for the monocyte functionality.

In vitro produced Ly6C^{hi} cells were generated as previously described and purified following the sorting procedure, ensuring a minimum 95% of Ly6C^{hi} cell purity. The other cell fractions Ly6C^{lo} and Ly6C^{neg} were only purified and used as experimental controls (Figure 4.A and B).
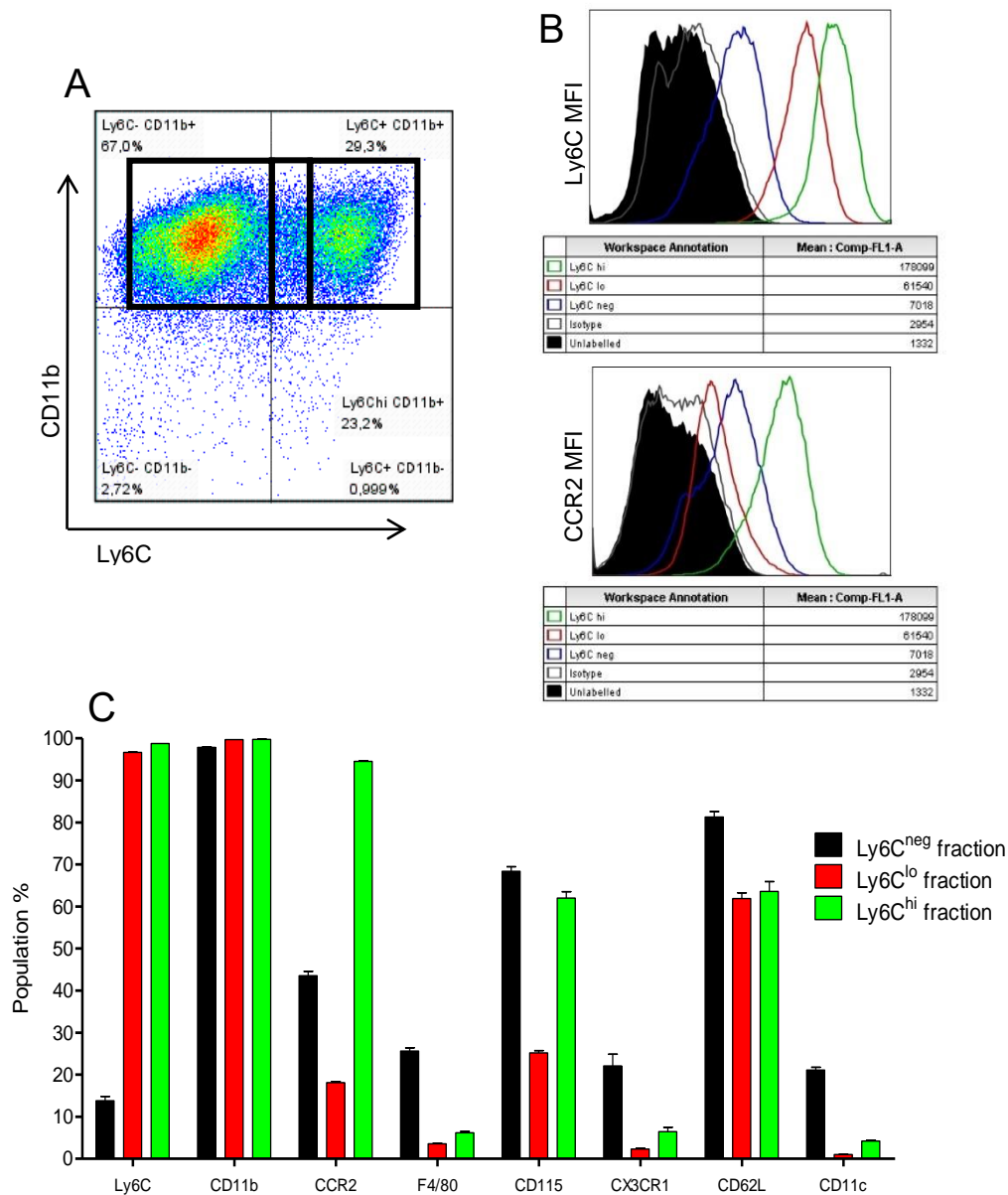
Figure4. Following the Ly6C expression, distinct types of populations emerge from the in vitro produced monocyte cultures.
(A) Dot-blot showing the Ly6C^{neg}, Ly6C^{lo} and Ly6C^{hi} distinct fractions of the bone-marrow derived cells culture.
(B) Histograms of the Ly6C and CCR2 expression comparing the distinguishable populations.
(C) Flow cytometric comparative analysis for characteristic monocyte markers of the different fractions of the *in vitro* cells culture.
Results are representative of three experiments. Mean and ±SD are performed with three mice per group.

II. SECTION. STUDIES FOR CHARACTERIZATION OF *IN VITRO* Ly6C^{hi} CELLS

1. *In vitro* produced Ly6C^{hi} cells and peripheral blood Ly6C^{hi} monocytes show equivalent extracellular surface markers

Subsequently, we compared the phenotype of *in vitro* Ly6C^{hi} cells and tissue Ly6C^{hi} monocytes by flow cytometry. For that, we analysed the expression of previously described markers Ly6C, CD11b, CCR2, CD115, CD62L, F4/80, CX3CR1 and CD11c.

In vitro generated Ly6C^{hi} cells were recovered six days after culture. Simultaneously, bone marrow, peripheral blood, spleen and intraperitoneal cells were extracted and a cell suspension was obtained from each one of the tissues. *In vitro* cells and mice tissue cell suspensions were labelled in parallel for FACS comparative analysis. The gating strategy included exclusively single viable cells.

FACS data showed that the yield of Ly6C^{hi}CD11b^{hi} cells was around 3-5% in spleen and blood, and around 20-30% in the bone-marrow and monocyte cultures. However, after the enrichment procedure the yield of Ly6C^{hi}CD11b^{hi} cells from the Ly6C^{hi} fraction was extremely high (almost 100%) (Figure 5.A).

Following the analysis of all markers we could asses the similarities and differences between tissue and *in vitro* produced Ly6C^{hi}CD11b^{hi} cells (Figure 5.B and D). *In vitro* and peripheral blood Ly6C^{hi}CD11b^{hi} cells similarly expressed CCR2 in almost 85% of the cells, whether bone marrow, spleen and intraperitoneal Ly6C^{hi}CD11b^{hi} cells presented the marker only in 50-60% of the total population. *In vitro*, peripheral blood and bone marrow Ly6C^{hi}CD11b^{hi} cells similarly expressed CD115 (around 65%). Spleen and intraperitoneal Ly6C^{hi}CD11b^{hi} cells presented reduced numbers of CD115 expressing cells (around 40-50%). Peripheral blood, bone marrow and spleen Ly6C^{hi}CD11b^{hi} cells showed high numbers of CD62L expressing cells (around 80%). *In vitro* Ly6C^{hi}CD11b^{hi} cells had slightly decreased levels of cells expressing this marker (around 65%). *In vitro*, peripheral blood, bone marrow and spleen Ly6C^{hi}CD11b^{hi} cells showed reduced and almost inexistent numbers of F4/80, CX3CR1 and CD11c expressing cells (around 2-5%). Intraperitoneal Ly6C^{hi}CD11b^{hi} cells had slightly increased levels of cells expressing these markers (around 10-20%). Supplementary data section (Figure 5).

Integration of FACS data and comparative analysis determined that the pattern of expression of Ly6C^{hi}CD11b^{hi} *in vitro* produced cells was almost identical to the one found in the Ly6C^{hi}CD11b^{hi} subpopulation from peripheral blood. Even thou *in vitro* Ly6C^{hi}CD11b^{hi} monocytes present similar chemotactic and adhesion molecules of that of peripheral blood Ly6C^{hi}CD11b^{hi} monocytes it is still necessary to confirm these functional features and others with further analysis.
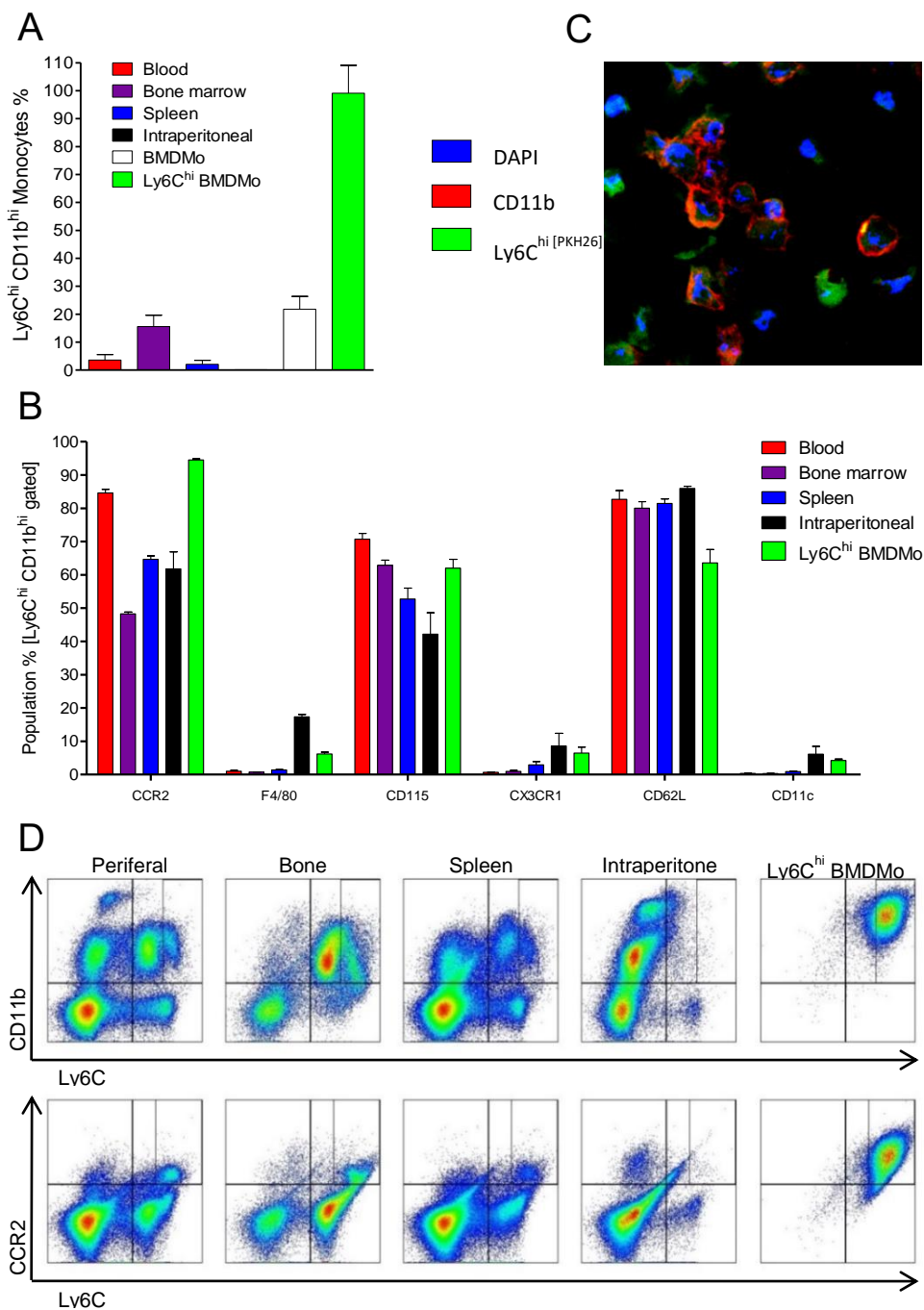
Figure5. *In vitro* and peripheral blood Ly6C^hi monocytes present equivalent surface markers
(A, B) FACS comparative analysis of the Ly6C^{hi} CD11b^{hi} percentage (A) and distinct monocyte markers percentage after Ly6C^{hi} CD11b^{hi} gating (B) in the distinct tissues of mice and the bone-marrow-derived monocytes (BMDMo).
(C) Fluorescence microscopy showing the expression the Ly6C and CD11b markers of BMDMo.
(D) Dot-blots of Ly6C/CD11b and Ly6C/CCR2 expression in distinct tissues and BMDMo.
Results are representative of three experiments. Mean and ±SD are performed with three mice per group.

2. Gene expression plasticity following stimulation is a feature of Ly6C^{hi} cells

Afterwards, to characterize the expression profile of these cells we studied the gene expression plasticity of *in vitro* produced Ly6C^{hi} cells following pro-inflammatory and anti-inflammatory stimulation. For this purpose, we focused on RT-PCR gene expression analysis following a wide range of stimulations. BMD macrophages, Ly6C^{hi}, Ly6C^{lo} and Ly6C^{neg} cells were purified as described previously and cultured in poly-L-lysine pre-coated well-plates to ensure proper adherence and survival. Cells were then starved for 6 hours and stimulated with IFN-γ, LPS, CpGB, IL-4 or IL-10 for comparative analysis.

In a first row of experiments and following six hours of stimulation, RNA was recovered, DNA retrotranscribed and gene expression evaluated by qPCR (Figure 6).

Stimulation with LPS and CpGB induced in all cell types a strong pro-inflammatory polarization, increasing the expression of pro-inflammatory mediators such as *tnf-α, il-1β, nos2, il-6* and the suppressor cytokine *il-10*. Stimulation with IFN-γ induced the same effect to a much minor extent. In its turn, stimulation with IL-4 induced in all cell types a strong anti-inflammatory polarization, increasing the expression of various anti-inflammatory mediators such as *arg1, mrc, fizz1* and *ym1*. There was no altered expression of the suppressor cytokine *tgf-β* in any cell type by any type of stimulation.

In vitro Ly6C^{hi} cells and BMD macrophages presented strong pro-inflammatory polarization capacity in terms of *tnf-α, il-1β, nos2* and *il-6* expression, when compared to Ly6C^{lo} and Ly6C^{neg} cells. However, *in vitro* produced Ly6C^{hi} cells and BMDM also demonstrated to be capable to polarize to an anti-inflammatory phenotype. Ly6C^{lo} cells showed an intermediate phenotype when compared to all other cell types in terms of expression of all the genes studied. Ly6C^{neg} cells showed stronger anti-inflammatory polarization capacity in terms of *arg1* and *fizz1* expression, and higher expression of *il-10,* than the rest of these cell types.

In a second row of experiments, cells were only stimulated for one hour but incubated for another five hours in starved media. Then, following six hours, RNA was recovered, DNA retrotranscribed and gene expression evaluated by qPCR (Figure 7). This was done in order to check the effectivity of *ex vivo* treatments before cell administration into *in vivo* mice models.

Stimulation for one hour with IFN-γ was sufficient to observe a polarization of i*n vitro* Ly6C^{hi} cells to a pro-inflammatory phenotype. *In vitro* Ly6C^{hi} cells increased the expression of pro-inflammatory mediators such as *tnf-α, il-1β* and *nos2* and decreased the expression of anti-inflammatory mediators such as *arg1, mrc* and *ym1* compared to unstimulated controls and IL-4 treated cells.
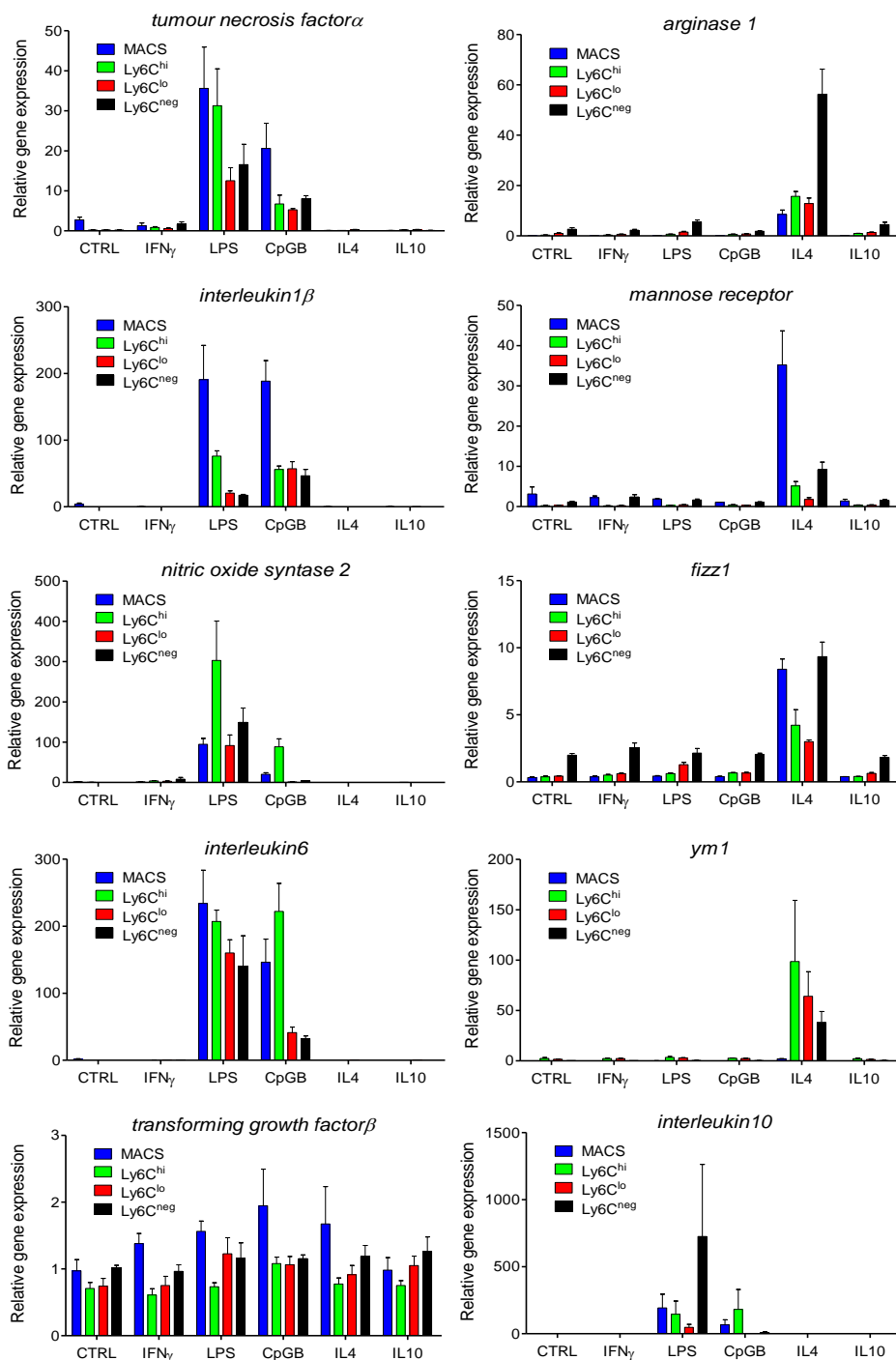
Figure6. Gene expression profile in a comparative analysis of stimulated bone marrow-derived macrophages and the *in vitro* produced Ly6C^{hi}, Ly6C^{lo} and Ly6C^{neg} fractions.
Relative gene expression assessed by qPCR following six hours of stimulation with pro-inflammatory and anti-inflammatory cytokines and ligands.
Results are representative of two experiments. Mean and ±SD are performed with three mice per group.

Stimulation for one hour with IL-4 was not sufficient to observe a polarization of Ly6C^{hi} cells to an anti-inflammatory phenotype. *In vitro* Ly6C^{hi} cells did not increased the expression of anti-inflammatory mediators such as *arg1, mrc* and *ym1* neither decrease the expression of pro-inflammatory mediators such as *tnf-α, il-1β* and *nos2* compared to unstimulated controls.

RT-PCR confirmed an extraordinary plasticity of Ly6C^{hi} cells to modulate gene-expression depending on the stimuli. This phenotypic characteristic is intrinsic to the natural subpopulation of *in vitro* Ly6C^{hi} monocytes.
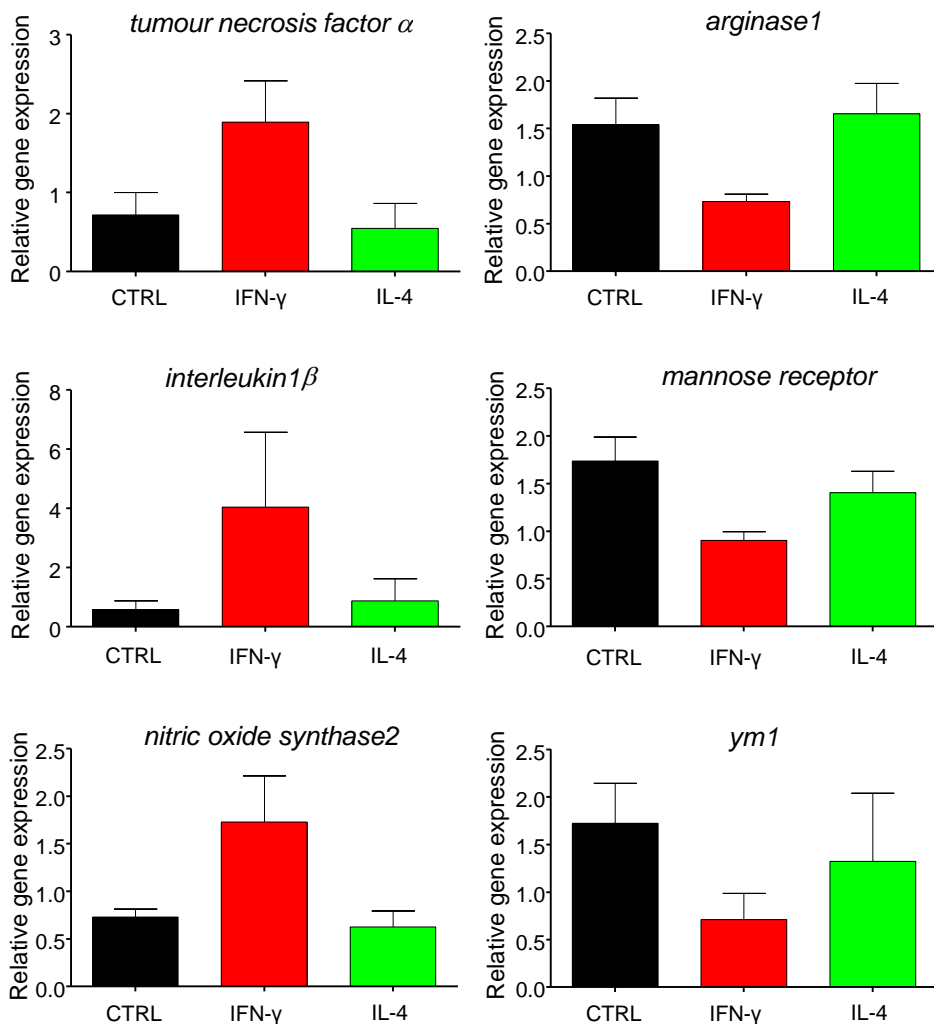
Figure7. Gene expression profile of the *in vitro* produced Ly6C^{hi} monocytes following short pro- and anti-inflammatory cytokine stimulations.
Relative gene expression was assessed by qPCR following one hour of stimulation with interferon-γ or interleukin-4 and five hours of resting the cells in starved media.
Results are representative of one experiment. Mean and ±SD are performed with three mice per group.

3. *In vitro* produced Ly6C^{hi} cells show *in vitro* differentiation, activation and maturation capacities

Following the initial phenotypical characterization of extracellular markers and gene expression capacity, we wanted to test the *in vitro* differentiation, activation and maturation features of *in vitro* Ly6C^{hi} cells. This time we focused on FACS analysis following a wide range of stimulations to test the variation of differentiation, activation and maturation cell markers. BMD macrophages, Ly6C^{hi}, Ly6C^{lo} and Ly6C^{neg} cells were purified and cultured as described previously, and stimulated for 48 hours with M-CSF, GM-CSF, IFN-γ or IL-4 for comparative analysis. Then we analysed the expression of differentiation markers such as Ly6C, CD11b, F4/80 and CD11c. We also analysed the expression of CD80 an activation cell marker, and the expression of MHC class II a cell marker for maturation. Here we only show the analysis of the Ly6C^{hi} monocyte population, extensive data can be found in the Supplementary data section (Figure 6-9).

First, we determined the variation in the expression of all markers in an independent manner. F4/80, the macrophage differentiation marker, behaved equally in all conditions (Figure 8A). After some hours of starvation, the percentage of F4/80^{+} cells already raised (35%) when compared to recently sorted cells (5%). After 48 hours of stimulation with any compound the percentage of F4/80^{+} cells reached almost 100% in all conditions. Ly6C, the monocyte differentiation marker, was expressed by almost all cells in the beginning of the experiment (Figure 8B). After 48 hours of stimulation with any compound the percentage of Ly6C^{+} cells diminished to 30% in all conditions except for IFN-γ treated cells where its expression remained at around 60% of all cells. CD11b, a pan-myeloid differentiation marker, was not altered either by starvation or stimulation for 48 hours (Figure 8C). CD11c, a dendritic cell differentiation marker, was only expressed by around 5% of the cells in the beginning of the experiment and remained very low in all conditions (<5%) except for GM-CSF and IL-4 treated cells where it reached 25% of total cells (Figure 8D). MHC class II, a cell marker for maturation, was expressed by around 25% of the cells in the beginning of the experiment. It was expressed by almost 50% of total cells after 48 hours of stimulation with IFN-γ (Figure 9B). CD80, a cell marker for activation, was expressed by 25% of the cells prior to the experiment (Figure 9C). Its expression increased till 50% after 48 hours of stimulation with M-CSF and 75% after 48 hours of stimulation with GM-CSF and IL-4.

Second, in order to associate this markers profile to specific cell types, we determined the variation of expression of markers in a combinatorial manner. We seek to evaluate the variation in the percentage of Ly6C^{hi} cells, Ly6C^{lo} cells, macrophages and dendritic cells after 48 hours of stimulation compared to control condition (Figure 9). In combination, the evolution of cell markers indicated a ubiquitous differentiation of *in vitro*

Ly6C^{hi} cells into macrophages. Ly6C^{lo} cells proportion remained constant in all conditions, and dendritic cells proportion was slightly increased after stimulation with GM-CSF or IL-4.

Therefore, these results confirm the *in vitro* differentiation, activation and maturation capacities of *in vitro* Ly6C^{hi} cells.
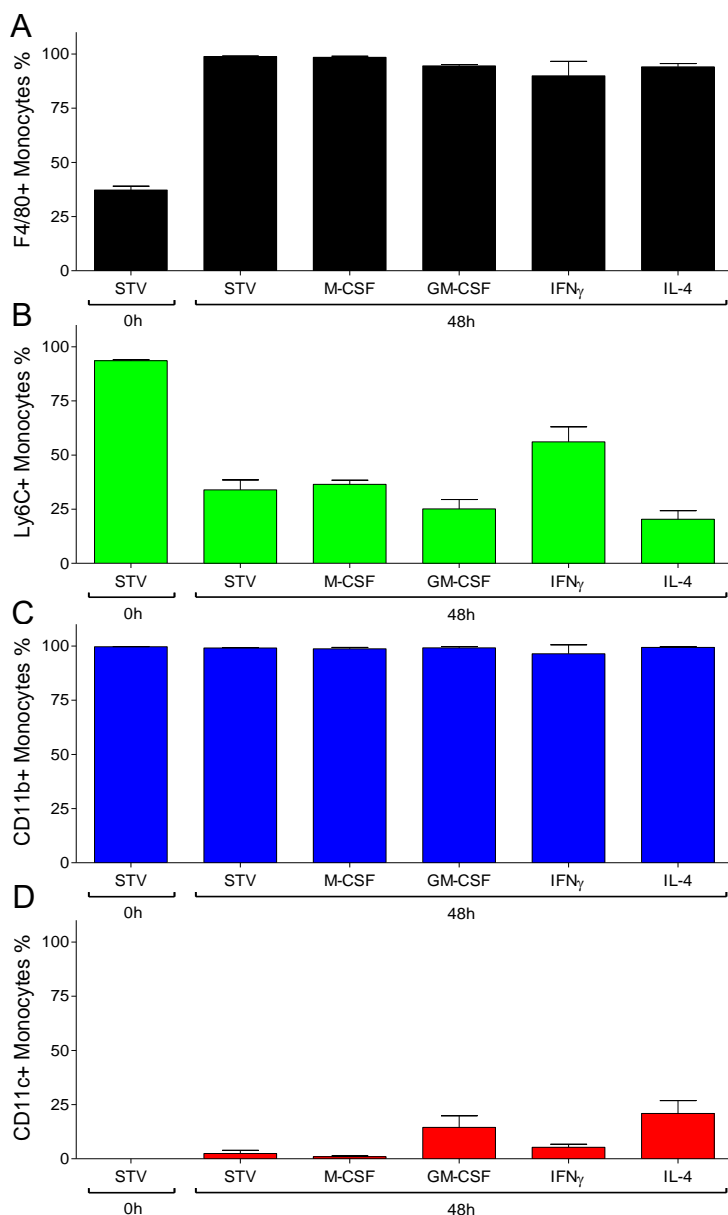
Figure8. *In vitro* produced Ly6C^{hi} cells present *in vitro* differentiation capacity.
(A, B, C, D) Flow cytometric analysis of the Ly6C^{hi} fraction cultured for forty-eight hours under distinct pro- and anti-inflammatory stimuli. Expression percentage of F4/80$^+$ cells (A), Ly6C$^+$ cells (B), CD11b$^+$ cells (C) and CD11c$^+$ cells (D).
Results are representative of one experiments. Mean and ±SD are performed with three mice per group.
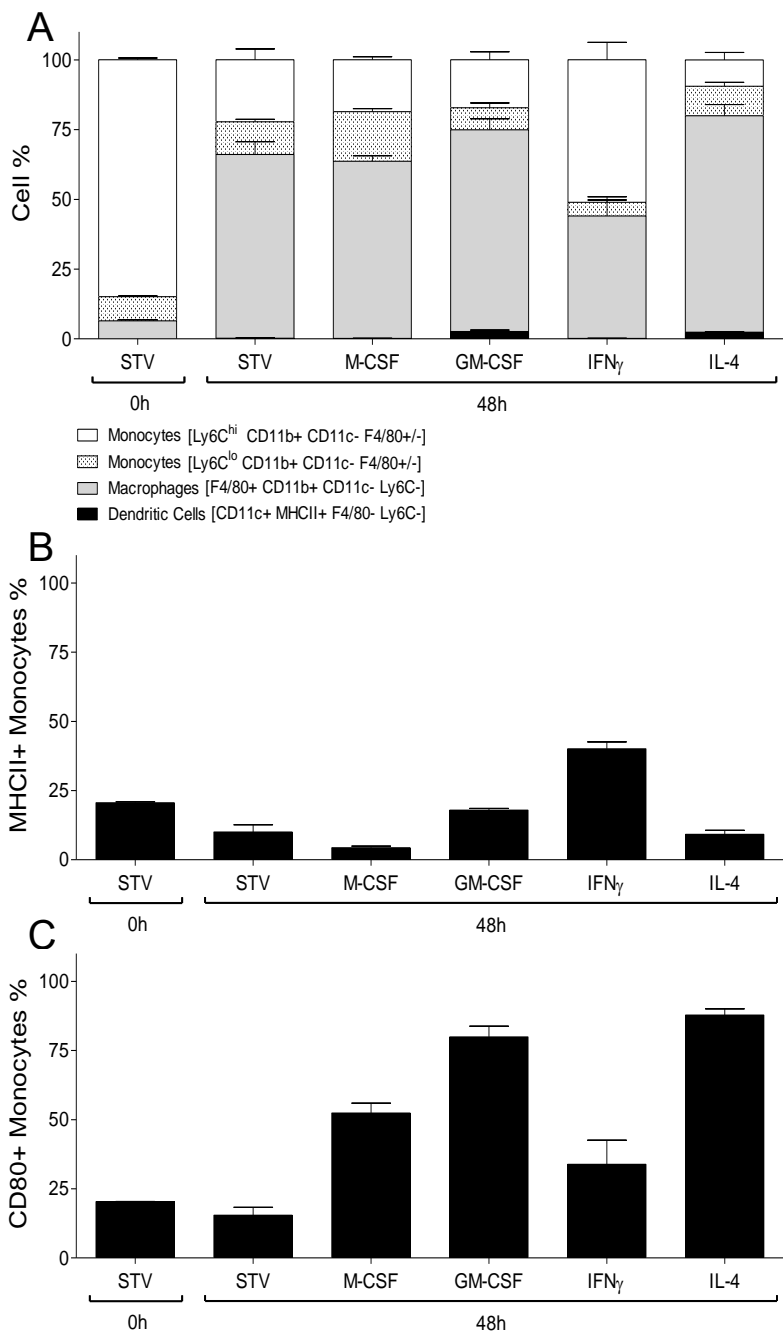
Figure9. *In vitro* **produced Ly6C^{hi} cells show** *in vitro* **activation and maturation capacity.**
(A, B, C) Flow cytometric analysis of the Ly6C^{hi} fraction cultured for forty-eight hours under distinct pro- and anti-inflammatory stimuli. Total percentage of profiled macrophages, Ly6C^{hi} monocytes, Ly6C^{lo} monocytes and dendritic cells (A). Expression percentage of MHCII^{+} cells (B) and CD80^{+} cells (C).
Results are representative of one experiment. Mean and ±SD are performed with three mice per group.

III.   **SECTION. STUDY OF THE Ly6C^{hi} ADMINISTRATION IN THE MODEL OF THYOGLICOLLATE-INDUCED INTRAPERITONEAL ACUTE INFLAMMATION**

1.   ***In vitro* Ly6C^{hi} monocytes are able to migrate and differentiate selectively in a model of intraperitoneal inflammation**

The similarities in extracellular markers, gene expression plasticity and differentiation capacity between the *in vitro* Ly6C^{hi} cells and peripheral blood Ly6C^{hi} monocytes, made us consider the *in vitro* Ly6C^{hi} cells as *in vitro* Ly6C^{hi} monocytes.

Next, our aim was to evaluate the capacity of *in vitro* Ly6C^{hi} monocytes to infiltrate selectively into the inflamed loci in an *in vivo* model of inflammation. Thyoglicollate-induced inflammation (TII) model was the first *in vivo* model used to evaluate infiltration during inflammation. This model was extremely useful for transfer and recovery experiments in terms of simple and soft extraction of the infiltrates, since no tissue disaggregation was required.

To do so we used the *in vivo* imaging (IVIS), flow cytometry (FACS) and laser scanning fluorescence confocal microscopy (LSFCM). We performed two different cell labelling techniques based in two fluorescent tracers, the dialkylcarbocyanine lipophilic tracer (DIR) and the red fluorescent cell linker (PKH26). For IVIS and FACS detection the DIR lipophilic tracer was used. DIR has the property to stain unspecifically living cells with fluorescence without disturbing cell functionality. Moreover, its characteristics make it an extremely suitable product for IVIS and FACS detection. DIR excitation and emission maxima in the near infrared region where many tissues are optically transparent is optimal for IVIS cell tracing. The quantum yield of DIR compound is very high which allows the detection of transferred cells by FACS. For LSFCM detection the PKH26 tracer was used because it shares with DIR the capacity to label living cells in an unspecific way that does not disturb the cell functionality, but its excitation and emission maxima are optimal for LSFCM detection. PKH26 quantum yield is also very high which makes easier to differentiate the transferred cells from the background Supplementary data section (Figure 10).

TII model was generated by single intraperitoneal injection of thyoglicollate media. *In vitro* Ly6C^{hi} monocytes were generated and purified. In addition, native bone-marrow cell suspensions were recovered. Then, Ly6C^{hi} and bone marrow cells were labelled with DIR. All methods were accomplished as described in the experimental procedures section. TII-induced mice were injected intravenously with 10.10^6 purified *in vitro* Ly6C^{hi} monocytes or bone marrow cells labelled with DIR as a positive control, or PBS as a negative control. Control mice intraperitoneally injected with only PBS were also injected with DIR⁺Ly6C^{hi} cells as a control. TII model induction and cell transfer were

effectuated the same day. Mice were recovered after 0, 24, 48 or 72 hours and intraperitoneal infiltrates were recovered for FACS evaluation.

FACS analysis of the cell suspensions allowed us to detect already at 24 hours several numbers of infiltrated DIR+ cells in TII-induced mice injected with *in vitro* Ly6Chi monocytes (0.4% from total cells), whether TII-induced mice injected with bone marrow cells presented only few numbers of DIR+ infiltrates in all time points. TII-induced mice injected with PBS and control mice injected with DIR+ Ly6Chi cells showed no infiltration of DIR+ cells in all time points confirming that our results were reliable (Figure 10.A, D). Supplementary data section (Figure 11).These results confirmed the selective homing capacity of *in vitro* Ly6Chi monocytes from the vascular system to the inflammatory loci.

In addition, we decided to evaluate the expression of diverse myeloid markers (Ly6C, F4/80 and CD11b) of the recovered cell infiltrates. Our objective was to check the evolution of Ly6C marker in infiltrated *in vitro* Ly6Chi monocytes and to test the kinetics of monocyte and macrophage populations within the inflamed peritoneum. FACS analysis shows that infiltrated DIR+ Ly6Chi cells were losing the Ly6C marker progressively between 24 and 72 hours after generation of the model and administration of cells (Figure 10.B). This result strongly suggested a differentiation process may occur after extravasation of cells from the blood flow and establishment into the tissues.

FACS data also exposed that there was no difference in the total number of infiltrated monocytes within the peritoneum between TII-induced mice injected with Ly6Chi cells, bone marrow cells or PBS. However, the total number of macrophages within the peritoneum was significantly increased after 48 and 72 hours in TII-induced mice injected with *in vitro* Ly6Chi monocytes and to a lesser extent in TII-induced mice injected with bone marrow cells (Figure 10.C). We hypothesized that there was a limit threshold of monocyte infiltration, and because we did not use any depletion treatment injected monocytes and monocytes from the recipient mice would be competing for the chemokines and ligands essential for extravasation into the peritoneum. This would explain why we could not see increased population of monocytes in mice injected with Ly6Chi cells or bone marrow cells, even though the population of macrophages was. These results again suggested a process of differentiation of the infiltrated DIR+ *in vitro* Ly6Chi monocytes.

Globally, our results confirmed the selective migratory capacity of *in vitro* Ly6Chi monocytes and advanced a possible process of differentiation within the tissues.
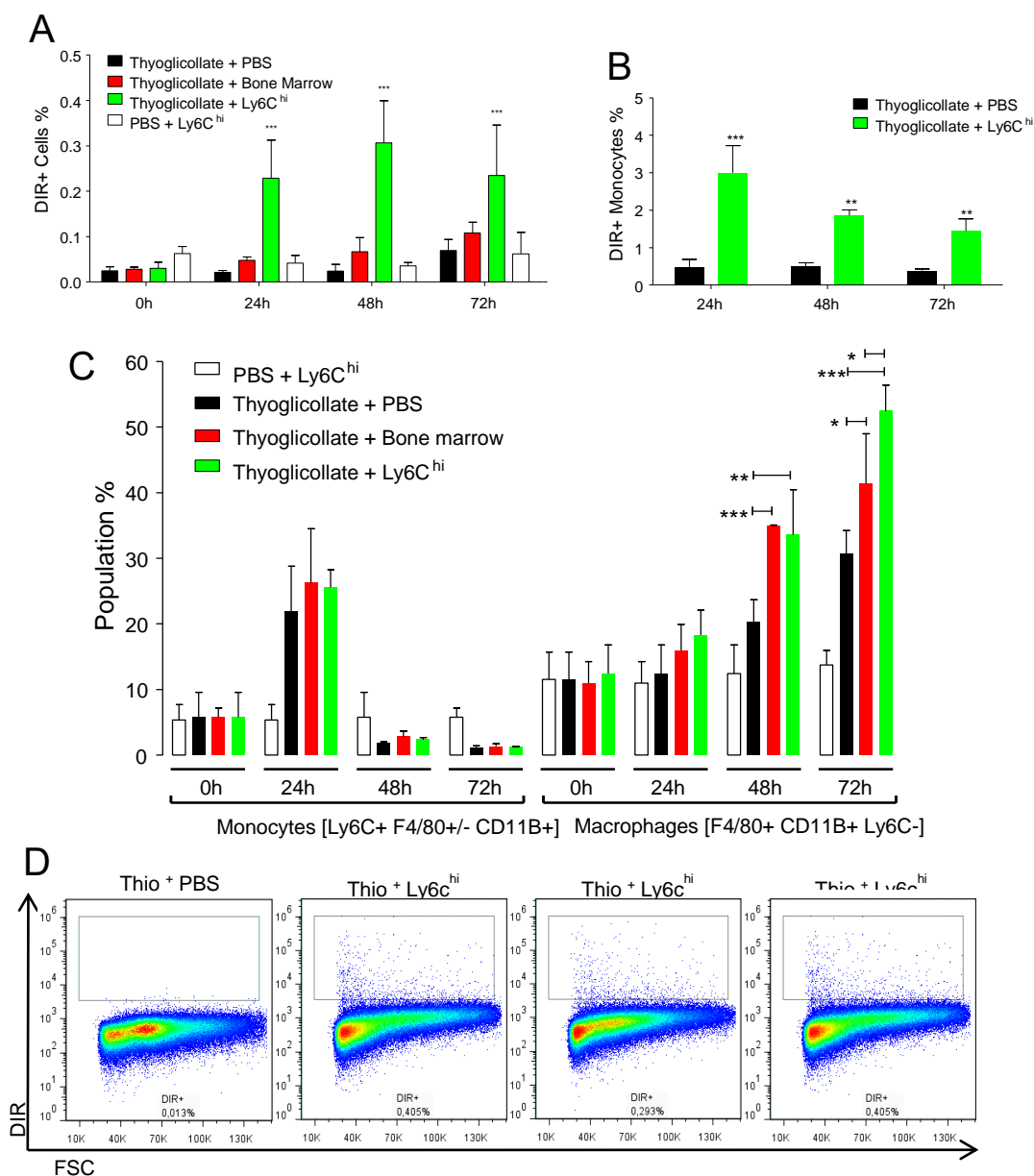
Figure10. *In vitro* Ly6c^{hi} monocytes are able to migrate and differentiate selectively in a model of intraperitoneal inflammation

(A) Flow cytometric analysis of the DIR$^+$ cell percentage recovered after intraperitoneal lavage from each experimental condition, 0, 24, 48 and 72 hours after intravenous injection of DIR labelled cells.

(B) Flow cytometric analysis of the DIR$^+$ monocytes recovered in the same conditions after Ly6C^{hi} CD11b^{hi} gating.

(C) Flow cytometric analysis of the percentage of total monocytes and macrophages recovered in the same conditions.

(D) Representative dot-blots showing the DIR$^+$ recovered cells in the control mice compared with the Ly6C^{hi} intravenous injected mice.

Results are representative of three experiments. Mean and ±SD are performed with three mice per group.

IV.   SECTION. STUDY OF THE Ly6C^{hi} ADMINISTRATION IN THE MODEL OF DNFB-INDUCED INFLAMMATION

1.   *In vitro* produced Ly6C^{hi} monocytes infiltrate, differentiate and induce inflammation in the *in vivo* model of DNFB

Furthermore, we assessed the infiltration as well as the modulatory capacity of *in vitro* Ly6C^{hi} monocytes in the DNFB model of inflammation. Dinitrofenolbenzene-induced contact inflammation (DNFB) model was employed to avoid the presence of important resident populations of myeloid cells, such as the resident macrophages found in the peritoneum.

DNFB model was generated as described in the experimental procedures section. DNFB was applied in the right ear and its solvent the acetone was applied in the left ear as a control. Ly6C^{hi} purified cells labelled with DIR (10.10^6 per mice) or PBS were injected intravenously in DNFB-induced mice. DNFB model induction and cell transfer were performed the same day. Mice were recovered after 48 and tissues of interest were recovered. DNFB applied ear, control ear and spleen were extracted from each mice and weighted. Then, ear tissue cell suspensions were obtained after enzymatic tissue dissociation procedures. When desired, cell suspensions were labelled for distinct characteristic markers of myeloid cells such as Ly6C, CD11b, CD68 and CD11c, to evaluate the differentiation stage of infiltrating cells.

FACS analysis once more confirmed infiltration of DIR$^+$ Ly6C^{hi} cells into the inflamed tissues. DNFB applied ears of DNFB-induced mice injected with *in vitro* Ly6C^{hi} monocytes presented 0.4% of DIR$^+$ cells from total cells. DNFB-induced mice injected with PBS and control ears applied with acetone of DNFB-induced mice injected with Ly6C^{hi} cells did not show any infiltration of DIR$^+$ cells, supporting the accuracy of our results (Figure 11.A and Figure 12.C). When we gated our samples to evaluate the percentage of DIR$^+$ cells from the macrophage population, we found that 4% of total CD68$^+$ CD11b$^+$ Ly6C- macrophages within inflamed ears were positive for DIR (Figure 11.B). Similar to TII model results, FACS analysis also showed an increase in 4% of the macrophage population in DIR$^+$ Ly6C^{hi} injected mice compared to PBS injected mice (Figure 11.C). Supplementary data section (Figure 12). Therefore, our results confirmed selective infiltration of *in vitro* Ly6C^{hi} monocytes in the DNFB inflammation model. Moreover, *in vitro* Ly6C^{hi} monocytes seemed to differentiate into macrophages, increasing their number within the inflamed tissues.

Most significantly, there was an increase of weight of the DNFB applied ears from mice injected with Ly6C^{hi} cells compared to the ones from mice injected with PBS (Figure 11.D). This fact strongly suggested that infiltrating *in vitro* Ly6C^{hi} monocytes could be modulating and enhancing inflammation in some way. Yet, this fact had to be proved. Spleens from the DNFB-induced mice injected with *in vitro* Ly6C^{hi} cells also increased their weight compared to the ones from mice injected with PBS (Figure 11.E). The increase of spleen weight may be explained by an expansion of the splenic monocytic reservoir from the *in vitro* Ly6C^{hi} monocytes injected mice. This last hypothesis could not be validated.

FACS also determined that there was a variation within the extracellular markers composition of infiltrated *in vitro* Ly6C^{hi} monocytes when compared to Ly6C^{hi} cells prior to injection (Figure 12.A and B). The Ly6C^{hi} cells prior to injection were composed of two different populations, 75% of Ly6C^{hi} CD11b^{hi} cells, and 20% of Ly6C^{hi} CD11b^{lo} cells.
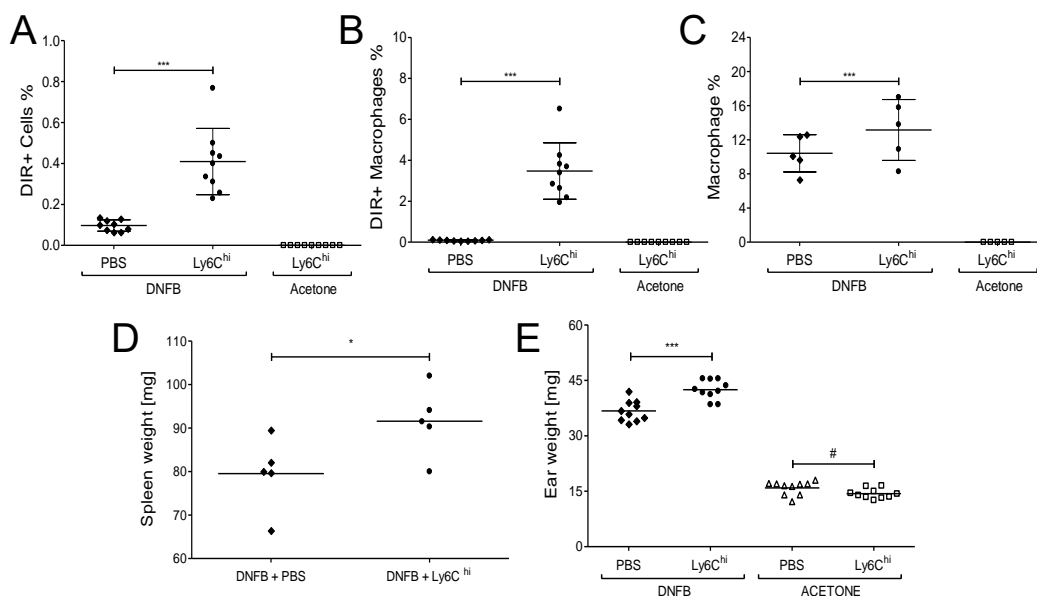
Figure11. *In vitro* produced Ly6C^{hi} monocytes infiltrate, differentiate and induce inflammation in the *in vivo* model of DNFB
(A, B, C) Flow cytometric analysis of the DIR[+] cell percentage (A), the DIR[+] macrophage percentage (B), and the total macrophage percentage (C), recovered after enzymatic dissociation from each experimental condition at 48 hours after intravenous injection of DIR labelled cells.
(D, E) Weight measures of spleens (D), and ears (E), at 48 hours after intravenous injection of Ly6C^{hi} cells.
Results are representative of three experiments. Mean and ±SD are performed with three, five or ten mice per group.

Once infiltrated and 48 hours later, the Ly6C^{hi} CD11b^{hi} cell fraction was reduced to 25% and the Ly6C^{hi} CD11b^{lo} cell fraction increased to 30%. Above all, a new population of Ly6C^{lo} CD11b^{hi} cells corresponding to 30% of total cells expanded. No CD11c^{+} cells were found to derive from infiltrating *in vitro* Ly6C^{hi} monocytes.

Our results again implied an *in vivo* differentiation process occurring to *in vitro* Ly6C^{hi} monocytes after infiltration. *In vitro* Ly6C^{hi} monocytes loosed progressively the expression of Ly6C or CD11b and did not differentiate into CD11c positive cells in the DNFB model.
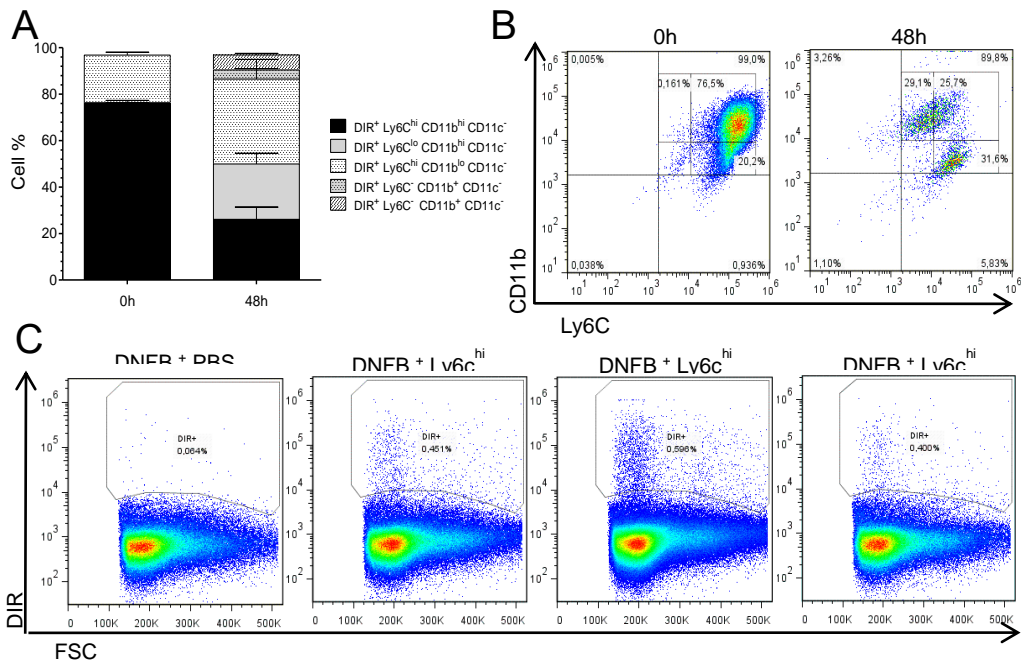
Figure12. *In vitro* produced Ly6C^{hi} monocytes infiltrate, differentiate and induce inflammation in the *in vivo* model of DNFB

(A, B) Flow cytometric analysis (F) and dot-blots (G) of the DIR^{+} monocytes before and after injection when recovered from tissues at 48 hours.

(C) Representative dot-blots showing the DIR^{+} recovered cells in the control mice compared with the Ly6C^{hi} intravenous injected mice.

Results are representative of three experiments. Mean and ±SD are performed with three, five or ten mice per group.

2. There is a dose-dependent correlation between the number of infiltrated *in vitro* Ly6C^{hi} monocytes and inflammation

Following the evaluation of the infiltration of *in vitro* Ly6C^{hi} monocytes in the DNFB model, we decided to effectuate titration experiments with increasing numbers of administered Ly6C^{hi} cells. The DNFB model was generated as before. DNFB was applied in the right ear and its solvent the acetone was applied in the left ear as a control. *In vitro* produced Ly6C^{hi} monocytes were generated, sorted and labelled with DIR as previously described. DNFB-induced mice were injected intravenously with purified Ly6C^{hi} cells labelled with DIR or PBS as a control. Mice were recovered after 24 hours for IVIS evaluation, and ears were extracted for weight and microscopy measurements. DNFB applied ears and control ears were extracted after IVIS evaluation and weighted. After, ear tissues were fixed, dehydrated with ethanol, embedded in paraffin, sectioned and labelled with haematoxylin/eosin. Slides were analysed using the E800 optical microscope and images were treated with Fiji/ImageJ software to quantify ear width.

IVIS evaluation of the DNFB-induced DIR$^+$ Ly6C^{hi} administered mice was performed *in vivo*. IVIS analysis showed substantial net fluorescence emission increase in treated animals. Fluorescence emission increased proportionally to the amount of cells injected (Figure 12.A and E). This fact confirmed that specific homing of DIR$^+$ Ly6C^{hi} cells was occurring from blood circulation to the inflamed loci.

There was an increase of ear weight from the DNFB-induced mice administered with DIR$^+$ Ly6C^{hi} cells compared to mice injected with PBS. Ear weight increase was also proportional to the amount of cells administered except for the highest concentration of cells where strong variability was found (Figure 12.B). There was also an increase of ear thickness from the DNFB-induced mice that were injected with DIR$^+$ Ly6C^{hi} cells compared to control mice. Ear thickness increase was once more proportional to the amount of injected cells except for the highest cell concentration where we found high variability presumably due to system saturation (Figure 12.C). These results indicate that there is a dose-dependent correlation between the number of administered *in vitro* Ly6C^{hi} monocytes and inflammation.

Combining FACS results of the number of infiltrated DIR$^+$ Ly6C^{hi} cells within the DNFB-applied ears and the corresponding ear weights, we found a strong correlation between the number of DIR$^+$ recovered cells and ear weight increase (Figure 12.D).These results indicate that there is a dose-dependent correlation between the number of infiltrated *in vitro* Ly6C^{hi} monocytes and inflammation.
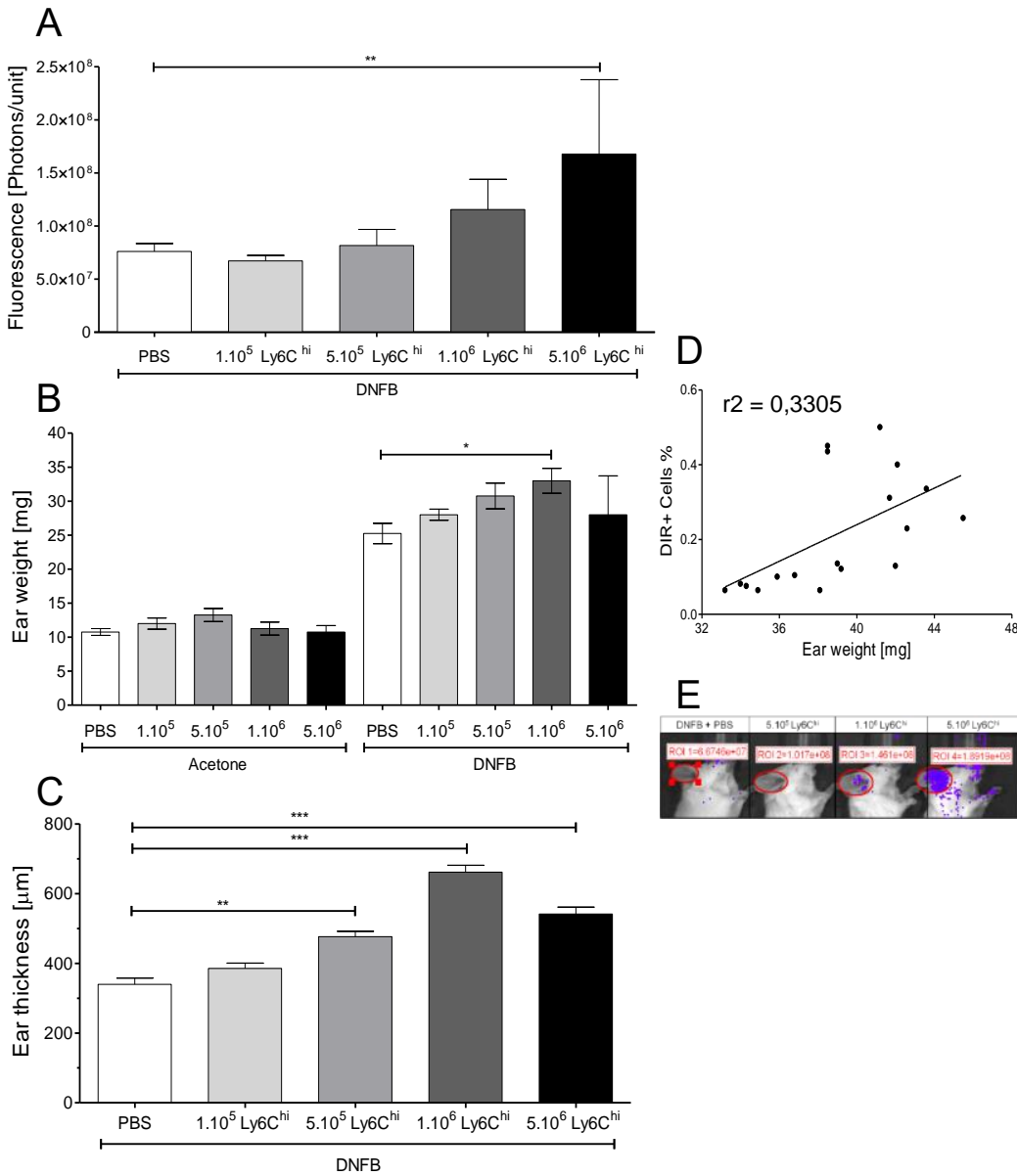
Figure13. There is a dose-dependent correlation between the number of infiltrated *in vitro* Ly6C^{hi} monocytes and inflammation

(A) IVIS analysis of ear fluorescence emission 24 hours after intravenous injection of DIR+ cells.

(B) Weight measures of the ears from each experimental condition 24 hours after intravenous injection of Ly6C^{hi} cells.

(C) Fiji/ImageJ microscopy analysis of ear thickness 24 hours after injection of Ly6C^{hi} cells.

(D) Linear correlation between the percentage of DIR+ cells and inflammation as ear weight.

(E) IVIS images of the ears fluorescence emission 24 hours after injection of DIR+ Ly6C^{hi} cells.

Results are representative of two experiments. Mean and ±SD are performed with five or twenty mice per group.

3.   *In vitro* Ly6C^{hi} monocytes enhance inflammation in the model of DNFB-induced contact inflammation

Later on, our aim was to further evaluate the capacity of infiltrating *in vitro* Ly6C^{hi} monocytes to modulate inflammation in the *in vivo* model of DNFB used in this study. For that we performed experimental kinetics following the same previous procedures.

DNFB model was generated as described previously. Purified DIR$^+$ Ly6C^{hi} cells (5.10^6 per mice) were injected intravenously in DNFB-induced mice, PBS was also injected as a control. Mice were recovered after 0, 24, 48 and 72 hours, evaluated with IVIS, euthanized and the inflamed and control ears were extracted and weighted. Half of the auricular tissues were fixed, dehydrated with ethanol, embedded in paraffin and processed for haematoxylin/eosin labelling. The slides were analysed using the E800 optical microscope and images were treated with Fiji/ImageJ software to quantify ear width. The other half of the samples were homogenized in Trizol® reagent for RNA extraction. Once high purity RNA was obtained we proceeded to DNA retrotranscription and evaluated the auricular gene expression profile by real-time qPCR. IVIS analysis again evidenced fluorescence emission increase in treated animals. Fluorescence emission was maximal at 24 hours and decreased progressively at 48 and 72 hours (Figure 13.A). DNFB-induced a fast inflammatory reaction that could be detected already at 24 hours by measuring the ear weight and ear thickness as before. Acetone appliance did not induce any inflammatory response. Administration of *in vitro* Ly6C^{hi} monocytes increased the ear weight and ear thickness when compared to animals only injected with PBS. Ear weight and ear thickness increase were maintained at 48 and 72 hours (Figure 13.B and C). Supplementary data section (Figure 13).

4.   Enhanced inflammation in the DNFB model after *in vitro* Ly6C^{hi} monocytes administration is due to up-regulation of pro-inflammatory genes

In vitro Ly6C^{hi} monocytes administration induced the upregulation of pro-inflammatory genes within the inflamed tissue such as *tnf-α*, *il-1β* and *nos2*, when compared to the PBS condition. In contrast, *in vitro* Ly6C^{hi} monocytes did not cause the upregulation of anti-inflammatory genes such as *mrc* and *fizz1* but induced up-regulation of *arg1*. There was no basal expression of pro-inflammatory genes in the tissues where only acetone was applied, as opposed with the anti-inflammatory genes expression (Figure 14).

The pro-inflammatory auricular gene expression profile enhanced by monocyte administration could explain the increase of ear weight and thickness and therefore the inflammation occurred upon *in vitro* Ly6C^{hi} monocytes treatment.
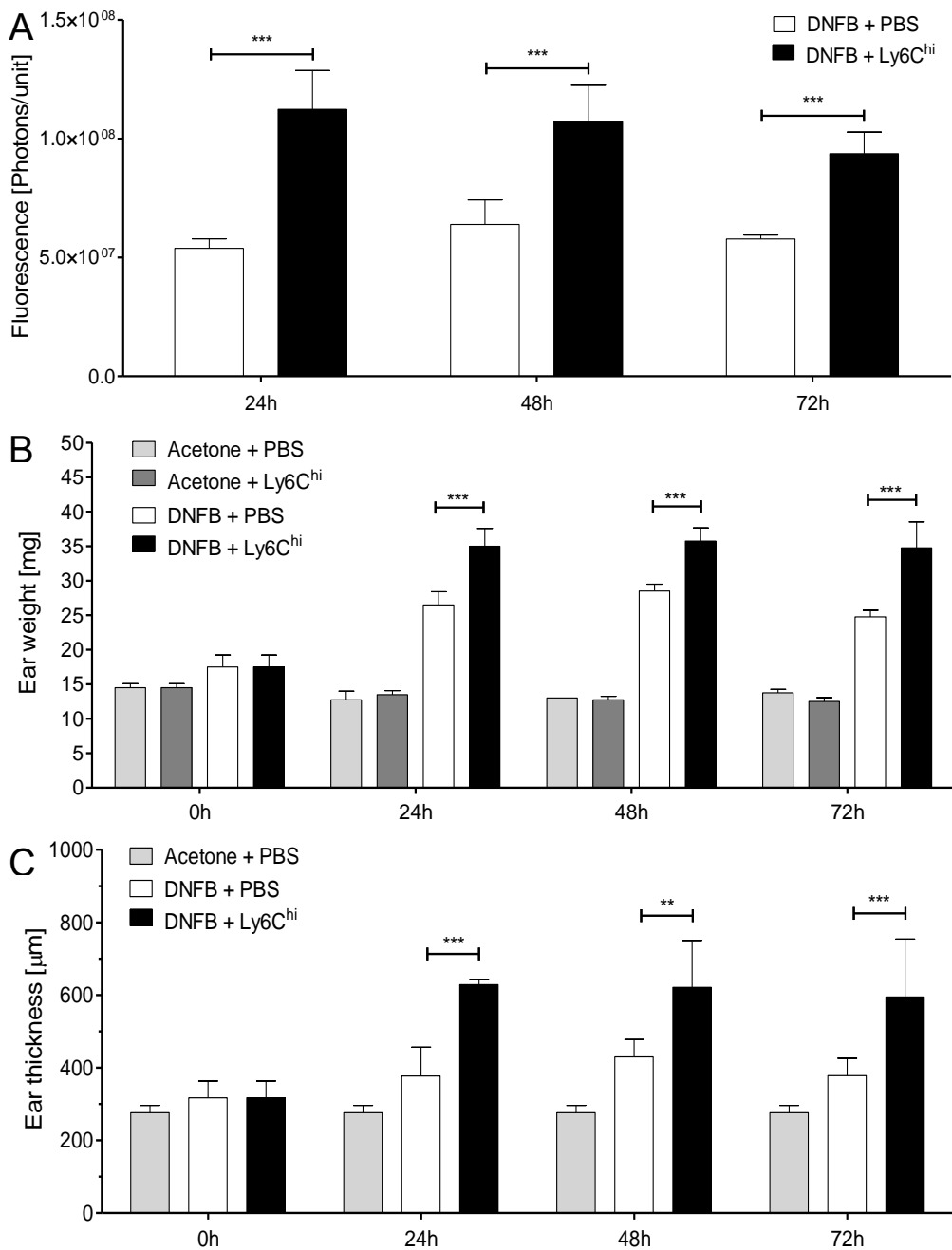
Figure14. *In vitro* Ly6C^{hi} monocytes enhance inflammation in a model of DNFB-induced contact inflammation

(A) IVIS analysis of the fluorescence emitted by the ear tissue 24, 48 and 72 hours after intravenous injection of DIR labelled cells.

(B) Weight ear measures from each experimental condition 24, 48 and 72 hours after intravenous injection of Ly6C^{hi} cells.

(C) Fiji/ImageJ microscopy analysis of the ear thickness 24, 48 and 72 hours after intravenous injection of Ly6C^{hi} cells.

Results representative of three experiments. Mean and ±SD performed with five mice per group.
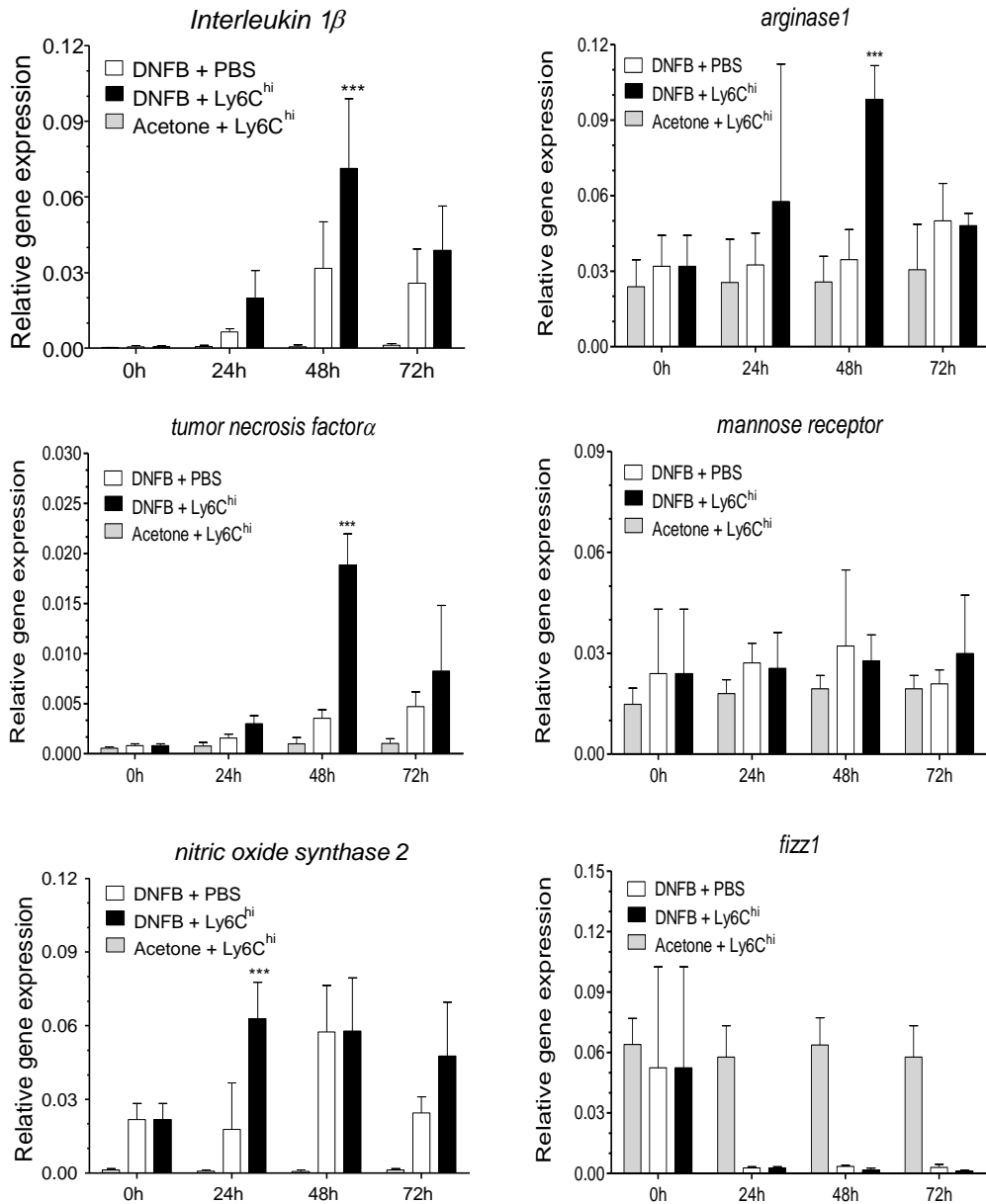
Figure15. Enhanced inflammation in the DNFB model after *in vitro* Ly6C^{hi} monocytes administration is due to up-regulation of pro-inflammatory genes
Relative gene expression kinetic assessed by qPCR from each experimental condition following 0, 24, 48 and 72 hours after intravenous injection of Ly6C^{hi} cells.
Results are representative of one experiment. Mean and ±SD are performed with four mice per group.

5. IFN-γ and IL-4 treated *in vitro* Ly6C^{hi} monocytes modulate inflammation in the DNFB model

Continuing with the evaluation of the modulatory capacity of inflammation of the *in vitro* Ly6C^{hi} monocytes in the *in vivo* model of DNFB, we decided to test the influence of *ex vivo* pre-treatment of our cells with pro-inflammatory and anti-inflammatory cytokines such as IFN-γ and IL-4 respectively.

DNFB model was generated as described. *In vitro* Ly6C^{hi} monocytes were purified and treated *ex vivo* for one hour with IFN-γ, IL-4 or starved media. Then, 5.10^6 of *in vitro* IFN-γ-Ly6C^{hi}, IL-4- Ly6C^{hi} or Ly6C^{hi} monocytes were injected intravenously in DNFB-induced mice, PBS was again injected as a control. Mice were recovered after 48 euthanized and the inflamed and control ears were extracted and weighted. As before, the auricular tissue was fixed, dehydrated, embedded in paraffin and processed and labelled with haematoxylin/eosin. We analysed the slides with an E800 optical microscope and quantified the ear width with Fiji/ImageJ software.

DNFB-induced inflammation in all conditions as expected, increasing the ear thickness as compared to the controls. No inflammatory reaction was observed in any experimental condition were acetone was applied as a control instead of DNFB. Once more, administration of *in vitro* Ly6C^{hi} monocytes induced an increase in inflammation, ear weight and thickness when compared to mice administered with PBS. Treatment with IFN-γ-Ly6C^{hi} cells boosted inflammation, ear weight increase and ear thickness increase, when compared to mice administered with non-treated Ly6C^{hi} cells. Oppositely, treatment with IL-4-Ly6C^{hi} cells reduced inflammation as well as ear weight and thickness, compared to mice administered with treated with IFN-γ-Ly6C^{hi} cells. However, reduction of inflammation, ear weight and ear thickness was slight when compared mice administered with non-treated Ly6C^{hi} cells (Figure 15.A, B and C). Supplementary data section (Figure 14).

Ex vivo pre-treatment of *in vitro* Ly6C^{hi} monocytes balanced inflammation in a negative way when IL-4-Ly6C^{hi} cells were administered. On the other hand, *ex vivo* pre-treatment of *in vitro* Ly6C^{hi} monocytes with IFN-γ balanced inflammation in a positive way. These contrasting results corroborate our hypothesis that not only *in vitro* Ly6C^{hi} monocytes are highly plastic cells that are able to modulate gene expression depending on the environment of cytokines, but also that modulation of gene expression is capable to balance inflammation in vivo. Our results seem to indicate that the IFN-γ STAT1-dependent pathway and the IL-4 STAT6-dependent pathway play both an essential role in *in vitro* Ly6C^{hi} monocytes functionality.
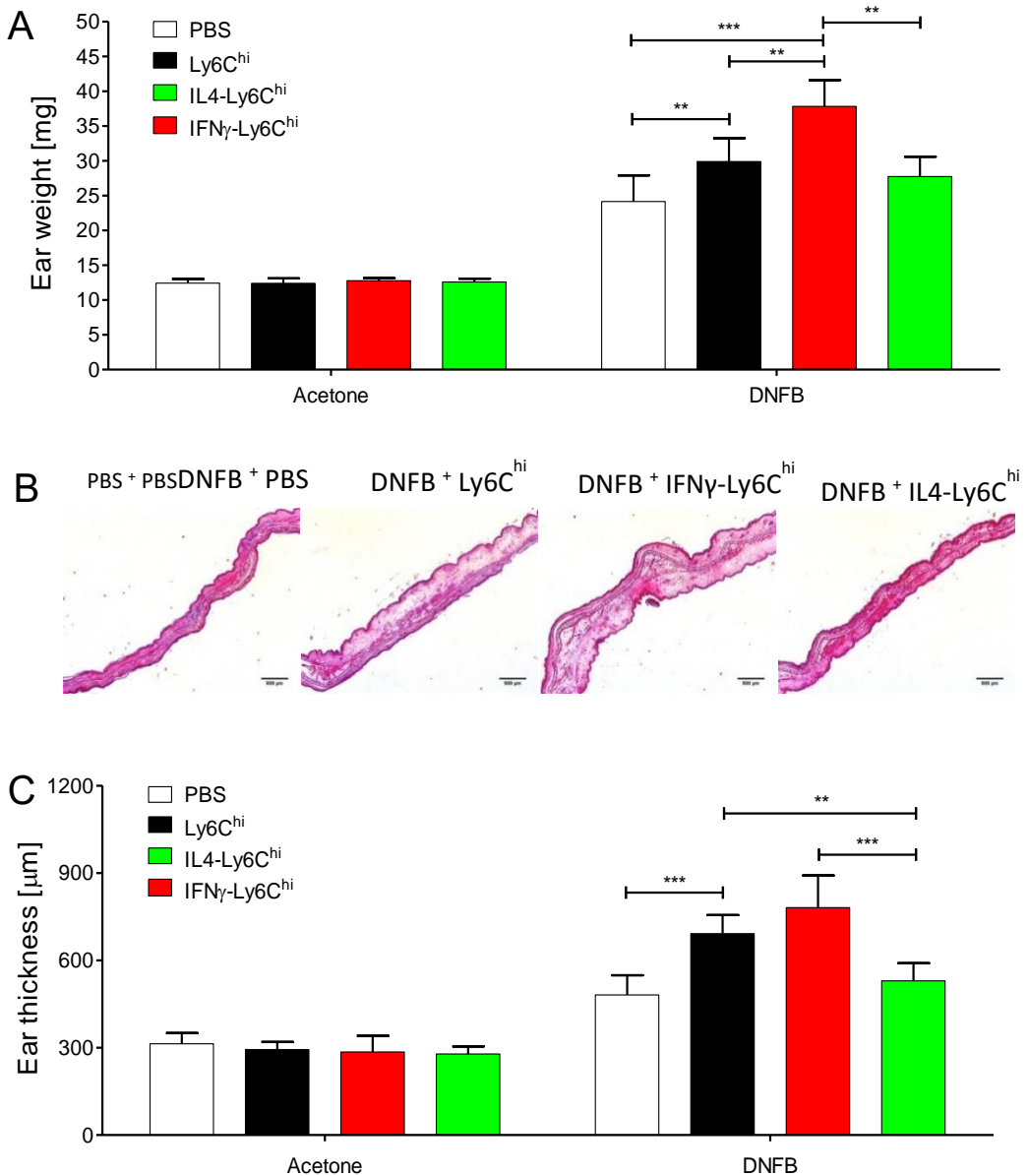
Figure16. IFN-γ and IL-4 treated *in vitro* Ly6C^{hi} monocytes modulate inflammation in the DNFB model

(A) Weight measures of the ear from each experimental condition 48 hours after intravenous injection of non-treated, IL-4 treated or IFN-γ treated Ly6C^{hi} cells.

(B) Optic microscope images of transversal ear cuts from each experimental condition.

(C) Fiji/ImageJ microscopy analysis of the ear thickness 48 hours after intravenous injection of non-treated, IL-4 treated or IFN-γ treated Ly6C^{hi} cells.

Results are representative of two experiments. Mean and ±SD are performed with five mice per group.

6. STAT1$^{-/-}$ and STAT6$^{-/-}$ derived *in vitro* Ly6C^{hi} monocytes are unable to modify the inflammation profile in the DNFB model

To confirm the results obtained with IFN-γ and IL-4 treated cells, and unravel the molecular pathways involved in the capacity of *in vitro* Ly6C^{hi} monocytes to modulate inflammation in the *in vivo* model of DNFB, we decided to test the functionality of *in vitro* Ly6C^{hi} monocytes derived from STAT1 and STAT6 knock-out mice. Our aim was to determinate whether if, as already hypothesized, the IFN-γ STAT1-dependent pathway or the IL-4 STAT6-dependent pathway were essential or not to the function of *in vitro* Ly6C^{hi} monocytes to infiltrate and balance inflammation. Prior to the *in vivo* studies in DNFB, we checked the capacity of STAT1$^{-/-}$ and STAT6$^{-/-}$ derived *in vitro* Ly6C^{hi} monocytes to express IFN-γ dependent genes such as *nos2* and IL-4-dependent genes such as *arg1*, after IFN-γ or IL-4 stimulation. As expected, STAT1$^{-/-}$ derived *in vitro* Ly6C^{hi} monocytes were unable to induce the expression of *nos2* after IFN-γ stimulation, and STAT6$^{-/-}$ derived *in vitro* Ly6C^{hi} monocytes were unable to induce the expression of *arg1* after IL-4 stimulation (Figure 16.A). Therefore, confirming that the pathways involved in IFN-γ and IL-4 signal transduction were impaired in STAT1 and STAT6 knock-out mice respectively.

DNFB model was generated and $5·10^6$ purified Ly6C^{hi} cells derived from wild-type, STAT1$^{-/-}$ or STAT6$^{-/-}$ mice were injected intravenously in DNFB-induced mice. As always intravenous injection of PBS was performed as a control. Mice were recovered after 6 days and after being euthanized the DNFB-applied inflamed ear and the acetone-applied control ears were extracted and weighted. Once more, part of the auricular tissue was fixed, dehydrated, embedded in paraffin and labelled with haematoxylin/eosin. Slides were again analysed with the E800 optical microscope and data was processed with Fiji/ImageJ software. The rest of the auricular tissue was homogenized in Trizol® reagent, RNA was extracted and retrotranscribed to DNA. RT-PCR was performed to evaluate the auricular gene expression profile.

DNFB induced the previously observed inflammatory reaction that did not occur in acetone-applied ears. Reproducing the previous results, injection of Ly6C^{hi} cells increased inflammation in terms of ear weight and ear thickness when compared to the control condition injected with PBS. Neither injection of STAT1$^{-/-}$- or STAT6$^{-/-}$-derived Ly6C^{hi} cells was capable to balance inflammation as seen in mice injected with Ly6C^{hi} cells derived from wild-type animals (Figure 16.B, C, D and supplementary (Figure 15).
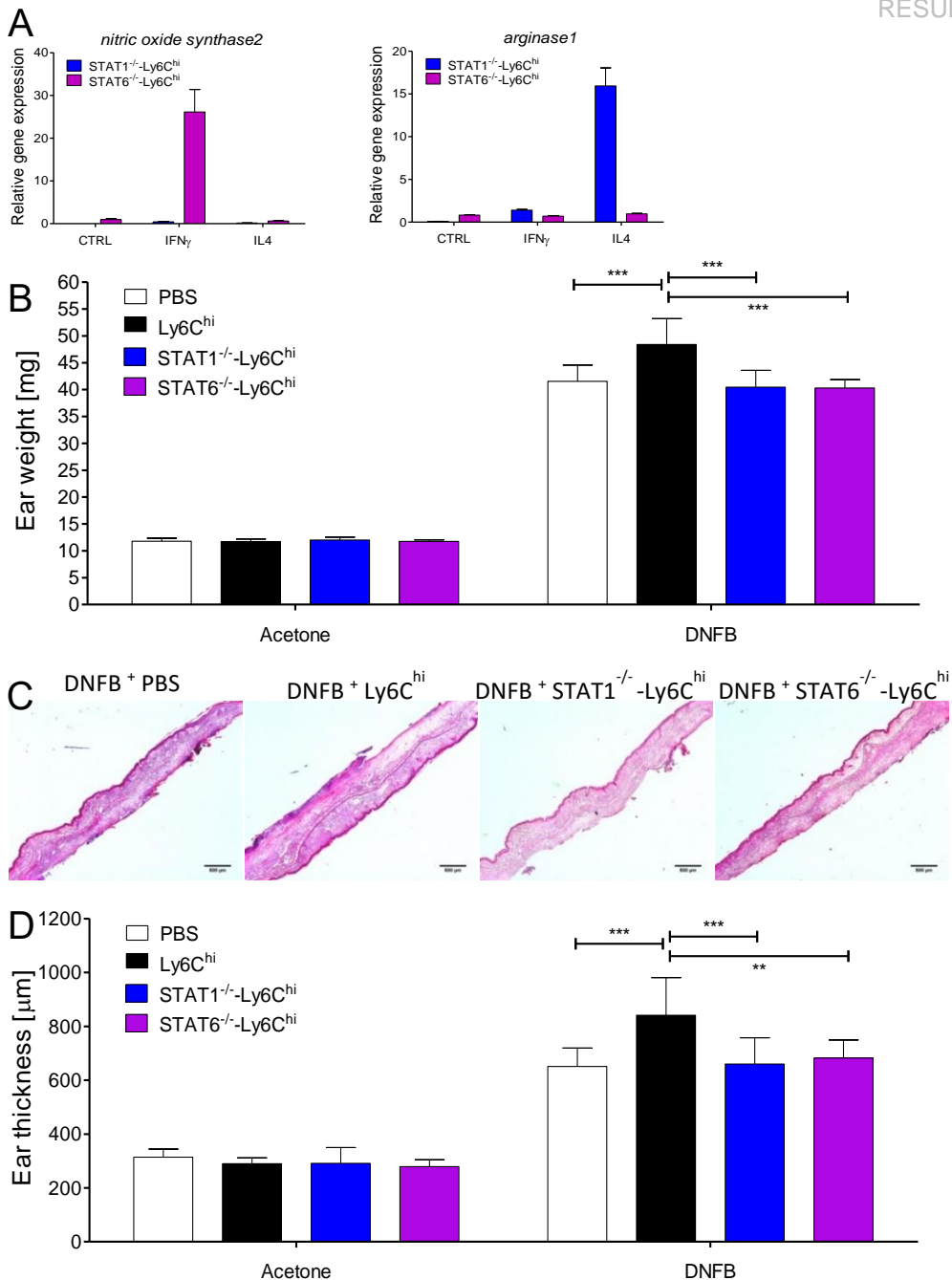
Figure17. STAT1$^{-/-}$ and STAT6$^{-/-}$ derived *in vitro* Ly6C^{hi} monocytes are unable to enhance inflammation in the DNFB model

(A) Gene expression assessed by qPCR from stat1$^{-/-}$ and stat6$^{-/-}$ Ly6C^{hi} cells six hours after stimulation.

(B) Weight measures of the ear from each experimental condition six days after intravenous injection of wild-type, stat1$^{-/-}$ and stat6$^{-/-}$ Ly6C^{hi} cells.

(C) Optic microscope images of transversal ear cuts from each experimental condition.

(D) Fiji/ImageJ microscopy analysis of the ear thickness six days after intravenous injection of wild-type, stat1$^{-/-}$ and stat6$^{-/-}$ Ly6C^{hi} cells.

Results are representative of two experiments. Mean and ±SD are performed with five mice per group.

Treatment with STAT1$^{-/-}$-derived *in vitro* Ly6C^{hi} monocytes was unable to induce inflammation nor ear weight and ear thickness increase as previously observed with wild-type-derived *in vitro* Ly6C^{hi} monocytes or IFN-γ-treated *in vitro* Ly6C^{hi} monocytes. Treatment with STAT6$^{-/-}$-derived *in vitro* Ly6C^{hi} monocytes did not reduce or increase inflammation nor ear weight and ear thickness. Our results confirm that both the IFN-γ STAT1-dependent pathway and the IL-4 STAT6-dependent pathway are essential to the function of *in vitro* Ly6C^{hi} monocytes to balance inflammation in the model of DNFB.

7. **Inability to balance inflammation of STAT1$^{-/-}$ and STAT6$^{-/-}$ derived *in vitro* Ly6C^{hi} monocytes is not due to reduced migration capacity but to reduced gene expression profiles**

Treatment with wild-type-derived *in vitro* Ly6C^{hi} monocytes induced the upregulation of pro-inflammatory genes in the ear of DNFB-treated mice such as *il-1β* and *il-6* but not *tnf-α*, when compared to PBS controls. Again, Ly6C^{hi} monocytes treatment did not upregulate the expression of anti-inflammatory genes such as *mrc* but did induce the up-regulation of *ym1* and slightly the one of *arg1* (Figure 17.A). Globally, all these effects were reversed when mice were treated with STAT1$^{-/-}$ or with STAT6$^{-/-}$ derived *in vitro* Ly6C^{hi} monocytes. In both cases, Ly6C^{hi} cells from STAT1$^{-/-}$ or STAT6$^{-/-}$ mice were not capable to induced upregulation of pro-inflammatory genes neither the upregulation of anti-inflammatory genes (Figure 17.A).

In parallel experiments, 5.10^6 purified Ly6C^{hi} cells derived from STAT1$^{-/-}$ or STAT6$^{-/-}$ mice were labelled with PKH26 and injected intravenously in DNFB-induced mice. We recovered the mice after 48 hours and tissues were processed for immunohistochemistry using only DAPI to stain cellular DNA. Slides were analysed using the confocal microscope Leica TCS SP5 and images were treated with Fiji/ImageJ software. Interestingly, LSFCM demonstrated that Ly6C^{hi} cells derived from STAT1 or STAT6 knock-out mice were indeed capable to infiltrate inflamed tissues, as PKH26$^+$ cells were observed. However, further quantification needs to be performed to discard a reduction. In contrast, no PKH26$^+$ cells were found in PBS-injected mice (Figure 17.B).

Thus, the inability of STAT1$^{-/-}$- or STAT6$^{-/-}$-derived *in vitro* Ly6C^{hi} monocytes to balance inflammation in the *in vivo* model of DNFB could not be explained by impaired cell homing within inflamed tissues. Yet, it could be explained by the reduced gene expression profiles observed in mice treated with those cells. STAT1$^{-/-}$- or STAT6$^{-/-}$-derived *in vitro* Ly6C^{hi} monocytes seem to fail in inducing the gene expression patterns previously observed in mice administered with wild-type-derived *in vitro* Ly6C^{hi} monocytes.
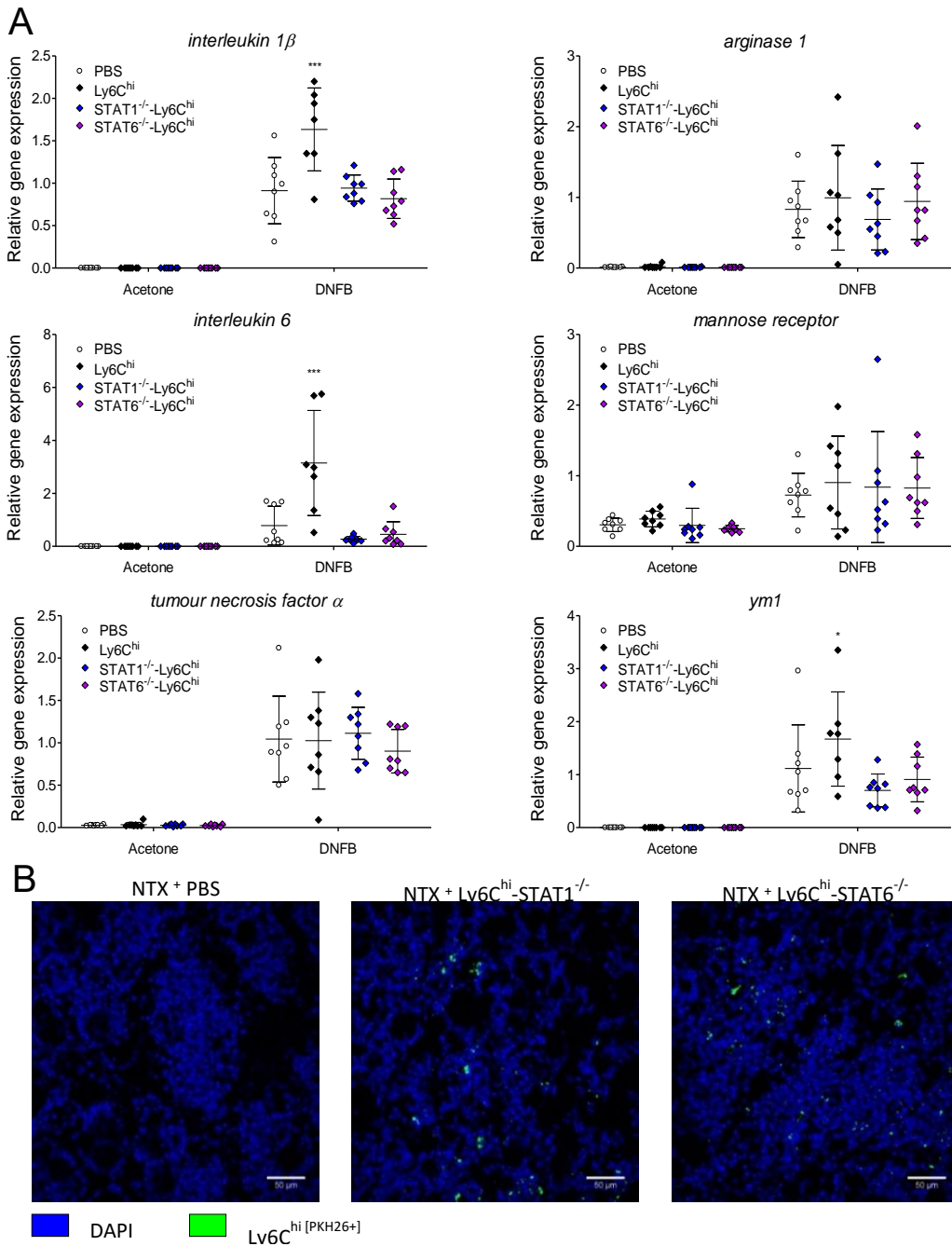
Figure18. Inability to balance inflammation of STAT1^{-/-} and STAT6^{-/-} derived *in vitro* Ly6C^{hi} monocytes is not due to reduced migration capacity but to reduced gene expression profiles

(A) Relative gene expression assessed by qPCR from each experimental condition following six days after intravenous injection of wild-type, stat1-/- and stat6-/- Ly6Chi cells.

(B) Fluorescence microscopy showing infiltration of the injected PKH26+ stat1-/- and stat6-/- Ly6Chi cells.

Results are representative of one experiment. Mean and ±SD are performed with eight mice per group.

V. SECTION. STUDY OF THE Ly6C^{hi} ADMINISTRATION IN THE MODEL OF NOTEXIN-INDUCED INFLAMMATION

1. Infiltrated *in vitro* produced monocytes differentiate and give rise to a macrophage population in the inflammatory model of Notexin

In addition to studies with the DNFB model, the Notexin-induced myoinjury (NTX) model was disposed to test the fate of infiltrating cells in a model of inflammation where macrophages have proved to be essential for the resolution of inflammation.

In a first time, Notexin model was generated as described in the material and methods section, NTX was applied by intramuscular injection to the right *tibialis anterioris* muscle and its solvent the PBS to the left muscle as a control. Ly6C^{hi} purified cells were labelled with DIR and injected intravenously (10.10^6 per mice) in NTX-induced mice 24 hours after generation of the model, PBS was also injected intravenously in control mice. Mice were euthanized after 48 of the generation of the model and legs were excised. NTX-injected and PBS-injected legs were recovered and evaluated with IVIS. Following that step, muscular tissues were dissociated enzymatically and cell suspensions were obtained. In certain experiments cells were labelled for FACS analysis with antibodies against myeloid cell markers such as Ly6C and CD11b to evaluate infiltration.

IVIS was performed *ex vivo* and demonstrated substantial net fluorescence emission increase in NTX-applied legs of animals treated with DIR$^+$ Ly6C^{hi} cells compared to PBS-applied legs of the same animals (Figure 18.A). Supplementary data section. These results corroborated previous data obtained from the DNFB model, suggesting infiltration of DIR$^+$ *in vitro* Ly6C^{hi} monocytes from peripheral blood circulation to the inflamed muscles.

FACS analysis of cell suspensions obtained from muscle tissues indicated over again infiltration of DIR$^+$ Ly6C^{hi} cells. NTX-applied legs of animals treated with DIR$^+$ *in vitro* Ly6C^{hi} monocytes showed 0.4% of DIR$^+$ cells from total. PBS-applied legs of animals treated with DIR$^+$ *in vitro* Ly6C^{hi} monocytes and NTX-applied legs of animals injected only with PBS did not show any positive cell for DIR, confirming the reliability of the data (Figure 18.B and F). Supplementary data section (Figure 16). Similar to TII model results, and DNFB model results, FACS showed an increase of the total monocyte population of 4% in intravenously DIR$^+$ *in vitro* Ly6C^{hi} monocytes-injected mice compared to PBS-injected mice (Figure 18.C).

Accordingly, our results confirmed that *in vitro* Ly6C^{hi} monocytes undergo a selective homing process from the blood flow into inflamed muscle tissues in the chronic inflammation model of Notexin.

In a second time, we used two different types of *in vitro* Ly6C^{hi} monocytes to quantify infiltration into the tissues and to evaluate differentiation. Ly6C^{hi} cells were generated from DsRed transgenic mice or wild-type mice, purified and wild-type cells were labelled with PKH26. NTX-induced mice were injected with purified PKH26$^+$ Ly6C^{hi} cells, DsRed$^+$ Ly6C^{hi} cells or PBS as a control. Mice were recovered after 48 hours of damage-induction, anesthetized, perfused transcardiacally with 4% paraformaldehyde and the inflamed and control muscular tissues were extracted. Tissues were then crioprotected and finally frozen in OCT with dry ice. The frozen pieces of tissue were cut with a criotome and the criosections were destined to the immunostaining procedure. Immunohistochemistry was performed using two different fluorophores, DAPI staining cellular DNA and anti-F4/80 staining a typical marker of macrophages. The slides were analysed using the Leica TCS SP5 confocal microscope and images were treated with Fiji/ImageJ software.

LSFCM confirmed IVIS and FACS previous results as DsRed$^+$ and PKH26$^+$ cells were detected within the inflamed tissues of *in vitro* Ly6C^{hi} monocytes injected mice. In contrast, no DsRed$^+$ or PKH26$^+$ injected cells were found in the control muscle neither in the intravenously PBS-injected control mice, confirming that our findings were reliable (Figure 18.E). Moreover, the presence of PKH26$^+$ and DsRed$^+$ cells was found colocalizing with the F4/80 marker for macrophages. This fact strongly suggested a differentiation process occurred after infiltration toward functional recruited macrophages. No macrophages were observed in the healthy control tissues. Note that not all the macrophages within the damaged tissues were PKH26$^+$ nor DsRed$^+$, meaning that also *in vitro* Ly6C^{hi} monocytes from the receptor mice had homed into the inflamed loci and differentiated into recruited macrophages (Figure 18.E). Quantification of the cell infiltrates where colocalization of F4/80 and DsRed occurred, demonstrated that 12% of total macrophages from inflamed muscle tissues were coming from our administered *in vitro* Ly6C^{hi} monocytes. Quantification of cell infiltrates where colocalization of F4/80 and PKH26 occurred showed more modest results, 8% of total macrophages seemed to be derived from our administered *in vitro* Ly6C^{hi} monocytes (Figure 18.D). This could be explained by the simple fact that DsRed fluorophore presents much higher quantum yield than PKH26, and that it is intrinsically produced by the cells, weather PKH26 is an artificial labelling that could be lost through time. Supplementary data section.

Collectively, our results demonstrate a selective infiltration process of *in vitro* Ly6C^{hi} monocytes into the inflamed tissues, followed by a differentiation process into recruited F4/80 macrophages. Subsequently to transmigration, these cells establish into the tissues and fill the pool of recruited macrophages in consistent numbers.
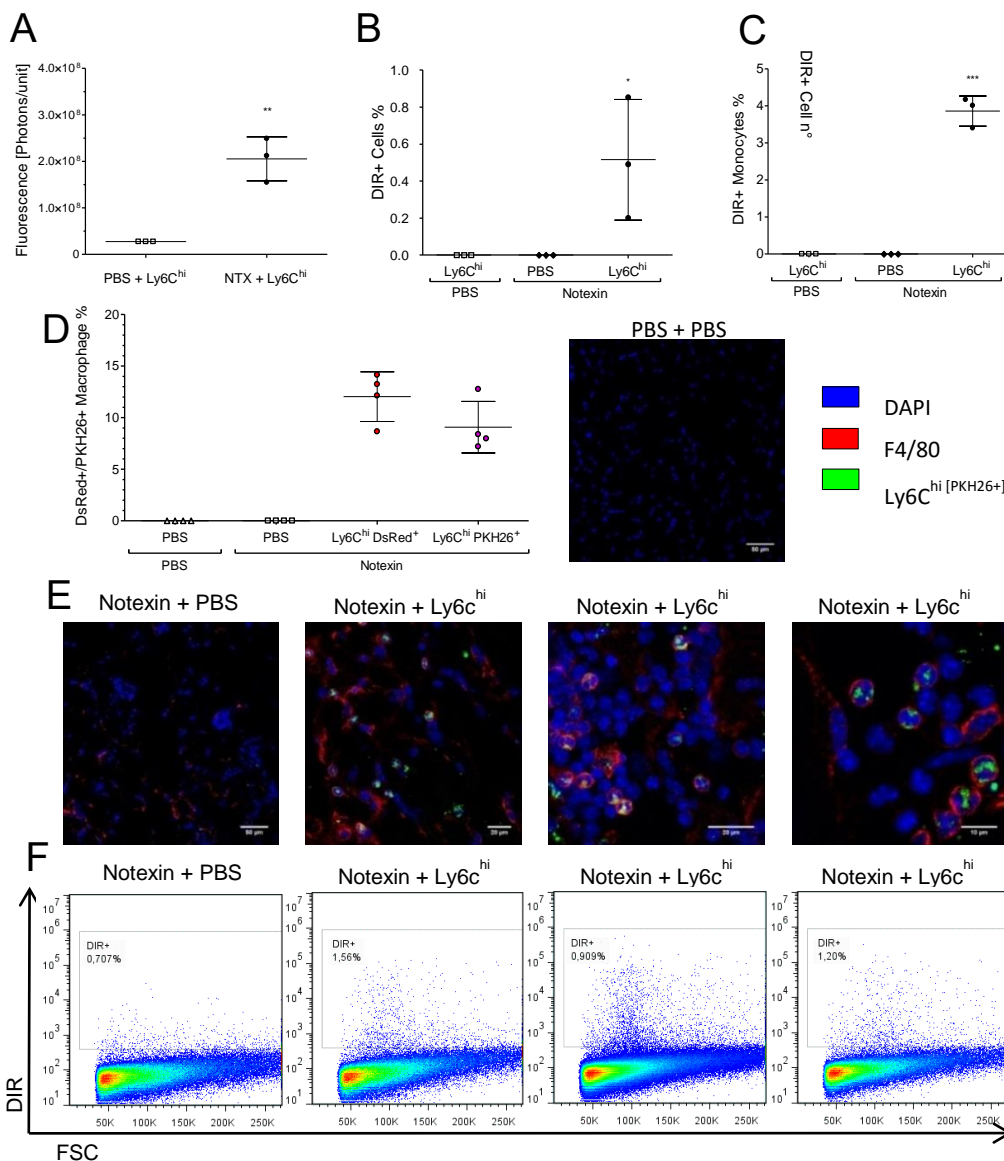
Figure19. Infiltrated *in vitro* produced Ly6Chi monocytes differentiate and give rise to a macrophage population in the chronic inflammatory model of Notexin

(A) IVIS analysis of the fluorescence emitted by the tissues 48 hours after intravenous injection of DIR labelled cells.

(B, C) Flow cytometric analysis of the DIR+ cell percentage and number of cells (B), and the DIR+ monocyte percentage (C), recovered after enzymatic dissociation from each experimental condition at 48 hours after intravenous injection of DIR labelled cells.

(D) Fiji/ImageJ microscopy quantification of the DsRed+ and PKH26+ monocytes infiltrated into the inflamed tissues.

(E) Fluorescence microscopy showing infiltration and differentiation of injected PKH26+ Ly6C*hi* cells in muscle.

(F) Representative dot-blots showing the DIR+ recovered cells in the control mice compared with the Ly6Chi intravenous injected mice.

Results are representative of three experiments. Mean and ±SD are performed with three or four mice per group.

2. *In vitro* produced Ly6C^{hi} monocytes treated with IFN-γ and IL-4 also modulate inflammation in the Notexin myoinjury model

Following the initial homing experiments with the inflammatory model of NTX-induced myoinjury, we wanted to examine the effect that administration of *in vitro* Ly6C^{hi} monocytes may have in inflammation. Similar to the DNFB model, we also decided to check weather pre-treatment of Ly6C^{hi} cells with IFN-γ or IL-4 would enhance the pro-inflammatory or anti-inflammatory effect of cell administration. NTX model was generated as described before and purified non-treated, IFN-γ-treated or IL-4 treated Ly6C^{hi} cells were injected intravenously in NTX-induced mice 24 hours after generation of the model, PBS was also injected as a control.

During a first row of experiments mice were recovered at days 0, 1, 2, 4, 6 and 8 after Notexin injection, euthanized and the inflamed and control *tibialis anterioris* muscles were extracted. A first section of the muscles was fixed, dehydrated with ethanol, embedded in paraffin and processed for haematoxylin/eosin labelling. The slides were analysed using the E1000 optical microscope and images were treated with free Fiji software to quantify necrotic and regenerative myofibers. The other sections were homogenized in Trizol® reagent for RNA extraction. RNA was isolated, DNA retrotranscribed and muscular gene expression profile was evaluated by real-time qPCR.

During a second row of experiments injected cells were not treated and previously labelled with PKH26 as described before. Mice were recovered after 48 hours, anesthetized, perfused transcardiacally with 4% paraformaldehyde and the inflamed and control *tibialis anterioris* muscles were extracted. We crioprotected the tissues, froze them in OCT with dry ice and then cut them with a criotome to proceed to immunostaining. Immunohistochemistry was performed using two different fluorophores, DAPI staining cellular DNA and anti-NOS2 or anti-ARG1 labelling nitric oxide synthase 2 and arginase 1 expressing cells. The slides were analysed using the Leica TCS SP5 confocal microscope and we treated the images with Fiji/ImageJ software.

NTX-induced mice showed a fast degeneration of the muscle myofibers already at day1. We could observe leucocyte infiltration and myofiber digestion starting around day 2 and 3. Tissue regeneration and multiplication of growing myofibers started around day4 reaching a maximum pick at day 6. PBS injection without Notexin did not cause any inflammatory response nor muscle damage. No differences in muscle necrosis or regeneration were found between NTX-induced mice injected intravenously with PBS or non-treated Ly6C^{hi} cells. IFN-γ treated *in vitro* Ly6C^{hi} monocytes enhanced inflammation and tissue necrosis, and delayed the regeneration of muscle tissue. Oppositely, IL-4 treated *in vitro* Ly6C^{hi} monocytes attenuated inflammation and tissue necrosis, and

boosted the regeneration of muscle tissue (Figure 19. A, B and C). Supplementary data (Figure 17).
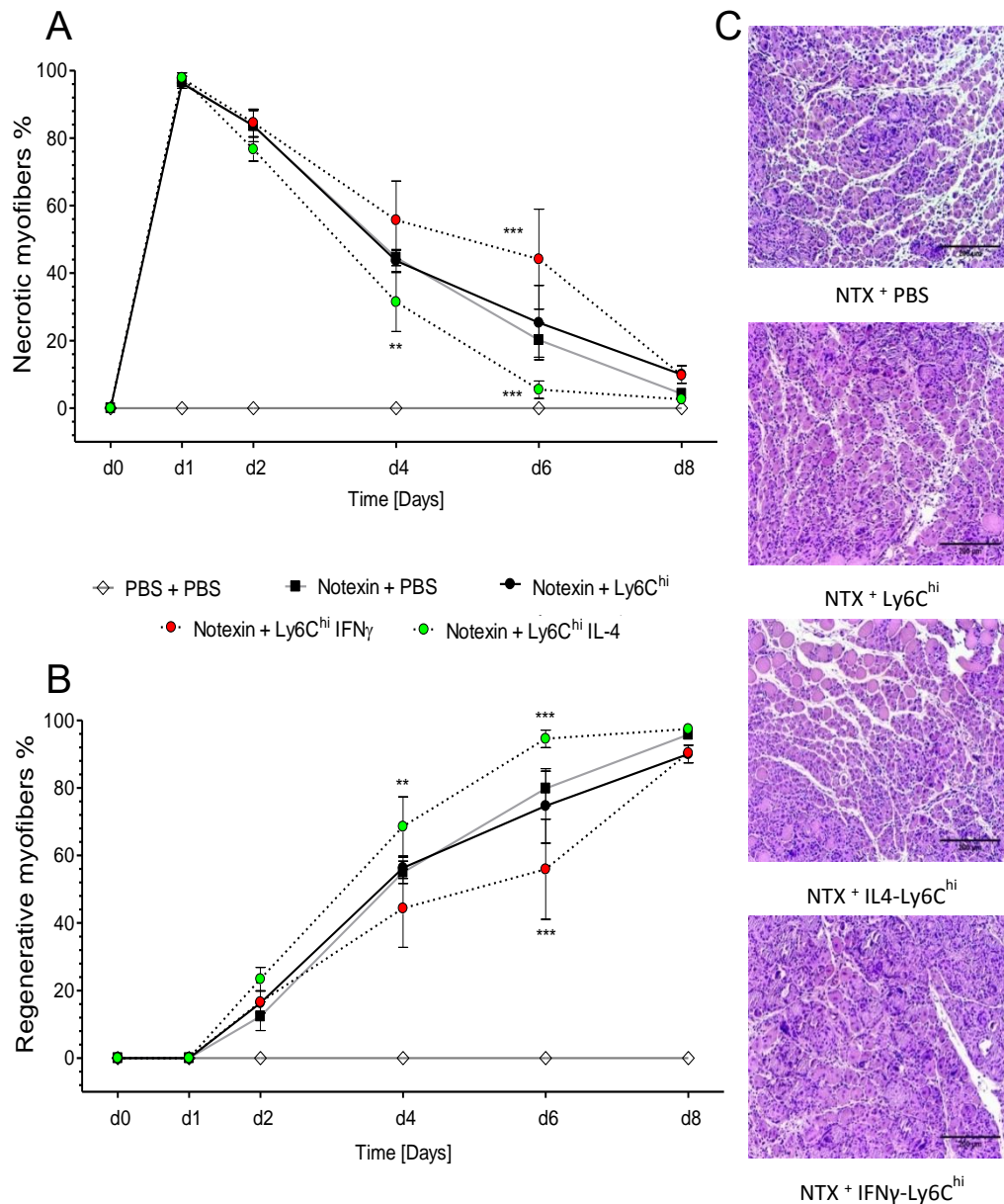
Figure20. IFN-γ and IL-4 treated *in vitro* Ly6C^{hi} monocytes also modulate chronic inflammation in the Notexin myoinjury model

(A, B) Fiji/ImageJ microscopy quantification of the necrotic (A) and regenerative (B) myofibers 0, 1, 2, 4, 6 and 8 days after intravenous injection of non-treated, IL-4 treated or IFN-γ treated Ly6C^{hi} cells.

(C) Optic microscope images of muscle sections from each experimental condition at day 6 after intravenous injection of non-treated, IL-4 treated or IFN-γ treated Ly6C^{hi} cells.

Results are representative of two experiments. Mean and ±SD are performed with four mice per group.

Our results show that treatment with *in vitro* Ly6C^{hi} monocytes, whether non-treated, IFN-γ or IL-4 pre-treated, are able to balance the evolution of inflammation in *in vivo* models. *In vitro* Ly6C^{hi} monocytes treatments are able to reduce or increase the extent of inflammation and therefore the extent of tissue damage.

3.   IFN-γ and IL-4 treated *in vitro* Ly6C^{hi} monocytes alter inflammation in the Notexin model altering the expression profile

RT-PCR analysis of the gene expression demonstrated that already at day 4 there was an increase in the expression of pro-inflammatory genes tissue such as *tnf-α* and *il-1β* when NTX was injected compared to the PBS condition. Surprisingly, *nos2* was downregulated after muscle damage induction. The expression of *myogenin*, a marker for muscle regeneration was also upregulated upon damage induction. The expression of anti-inflammatory genes varied depending on the genes analysed. NTX injection induced up-regulation of *arg1,* but also induced downregulation *fizz1* (Figure 20.A). *In vitro* Ly6C^{hi} monocytes administration induced a variety of modification within the pro-inflammatory gene expression pattern of the muscle (Figure 20.A). Non-treated Ly6C^{hi} cells infusion increased the expression of *tnf-α,* this upregulation seemed to be boosted when administered cells were previously treated with IFN-γ and decreased when cells were pre-treated with IL-4. Infusion of non-treated *in vitro* Ly6C^{hi} monocytes, cells treated with IFN-γ or cells treated with IL-4 reduced the expression of *il-1β*. Infusion of non-treated *in vitro* Ly6C^{hi} monocytes but not the one of cells treated with IFN-γ or cells treated with IL-4 increased the expression of *nos2.*

In vitro Ly6C^{hi} monocytes administration also induced very variable alteration within the anti-inflammatory gene expression pattern of the muscle (Figure 20.A). Infusion of non-treated Ly6C^{hi} cells increased the expression of *myogenin,* this effect was not seen when infused cells were pre-treated with IFN-γ or IL-4*.* Non-treated Ly6C^{hi} cells administration increased the expression of *arg1,* this upregulation seemed to be also present when we administered IFN-γ treated cells and decreased with administration of cells treated with IL-4. Non-treated Ly6C^{hi} cells treatment induced lesser downregulation of *fizz1, t*his result was seen in the same way when we administered IFN-γ treated cells, and to a major extend when cells were pre-treated with IL-4.

The pro-inflammatory and anti-inflammatory muscular gene expression profile seem to correspond to a very complex process. Indeed, administration of non-treated *in vitro* Ly6C^{hi} monocytes, cells treated with IFN-γ or cells treated with IL-4 induced changes in the gene expression, confirming the modulatory capacity that *in vitro* Ly6C^{hi} monocytes have in inflammation. However, more experiments shall be performed in order to truly unravel how this mechanism take place.
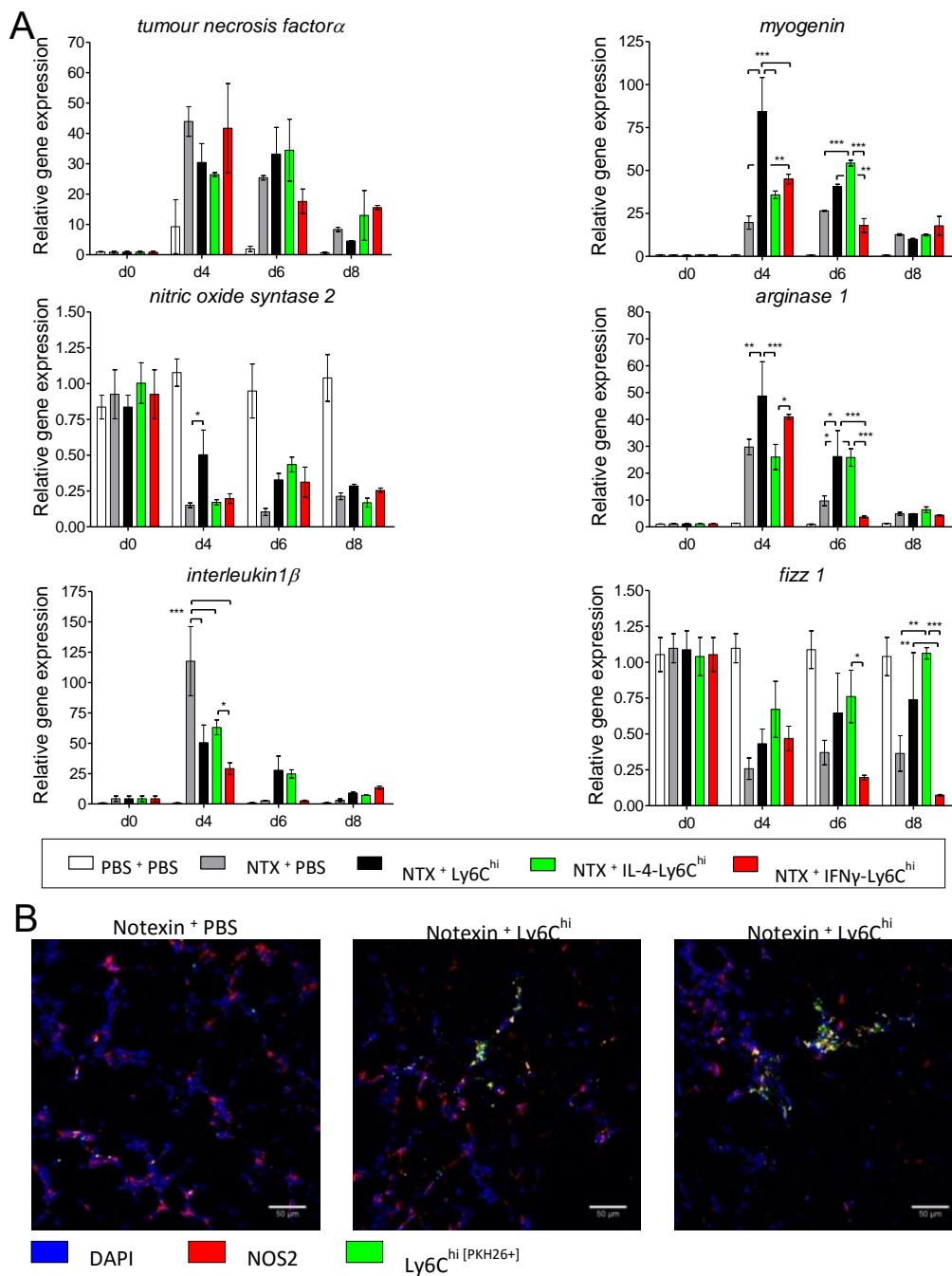
Figure21. IFN-γ and IL-4 treated *in vitro* Ly6C^hi monocytes alter inflammation in the Notexin model up-regulating pro- or anti-inflammatory genes

(A) Relative gene expression assessed by qPCR from each experimental condition following 0, 1, 2, 4, 6 and 8 days after intravenous injection of non-treated, IL-4 treated or IFN-γ treated Ly6C^hi cells.

(B) Fluorescence microscopy showing muscular tissue infiltrated PKH26^+ cells expressing NOS2. Results are representative of one experiment. Mean and ±SD are performed with five mice per group.

LSFCM helped us to detect PKH26$^+$ cells reproducing the previous results of transfer and recovery experiments. Ly6C^{hi} PKH26$^+$ cells were again detected infiltrating the inflamed muscular tissue. No PKH26$^+$ cells were found in PBS-injected control legs of the mice, confirming that migration of *in vitro* Ly6C^{hi} monocytes is specific and requires a chemoattractant inflammatory environment (Figure 20.B). PKH26$^+$ cells were colocalizing with the NOS2 marker. No PKH26$^+$ cells were found to colocalize with ARG1 marker, instead the ARG1 was distributed within myofibers. Supplementary data (Figure 18). Note that all the PKH26$^+$ cells were NOS2$^+$. This indicated that *in vitro* Ly6C^{hi} monocytes acquired almost invariably a pro-inflammatory phenotype after infiltration into the damaged muscle. Again, no macrophages were observed in the healthy control tissues. Large amounts of NOS2$^+$ PKH26- cells were also found, confirming the expression of NOS2 also from the recipient mice cells (Figure 20.B).

This result again further confirms the *in situ* function that infiltrated *in vitro* Ly6C^{hi} monocytes have in inflammation and the implication of *in vitro* Ly6C^{hi} monocytes in the inflammatory model of NTX.

VI.   SECTION. STUDY OF THE Ly6C^{hi} ADMINISTRATION IN THE *KLEBSIELLA PNEUMONIAE* MODEL OF SYSTEMIC INFECTION

1.   *In vitro* Ly6C^{hi} monocytes infusion boost mortality rate in a model of systemic infection with *Klebsiella pneumoniae*

Further on, we wanted to assess the impact of *in vitro* Ly6C^{hi} monocytes infusion in a model of septic inflammation. For that we used the gram-negative bacteria *Klebsiella pneumoniae*. Our aim was to determinate if Ly6C^{hi} cell administration would be beneficial or detrimental for infection resolution, survival and recovery.

Initially, since all the *in vivo* experiments were performed with exponentially growing bacteria, the growth curve of *Klebsiella pneumoniae* was determined. This was done in order to extrapolate the optical density of growth cultures to a specific number of living CFU. Supplementary data (Figure 19). Furthermore, multiple experiments were performed to determine the lethal dose 50% (DL50) of *Klebsiella pneumoniae* in mice for subsequent *in vivo* experiments. Supplementary data (Figure 20).

In first row of experiments KP model was generated as described in the material and methods section*,* and purified Ly6C^{hi} cells, purified Ly6C^{neg} cells or PBS were injected intravenously the same day. Mice were evaluated daily for clinical signs, scoring, weight loss and mortality rate. The clinical scoring system used the following criteria: score 0 – no clinical signs; score 1 – hunched, ruffled hair, ocular protrusion,

conjunctivitis; score 2 – ataxia, neurologic placement deficits, diarrhoea; score 3 – lethargy, unresponsiveness; score 4 – moribund, lateral recumbence; score 5 – dead.
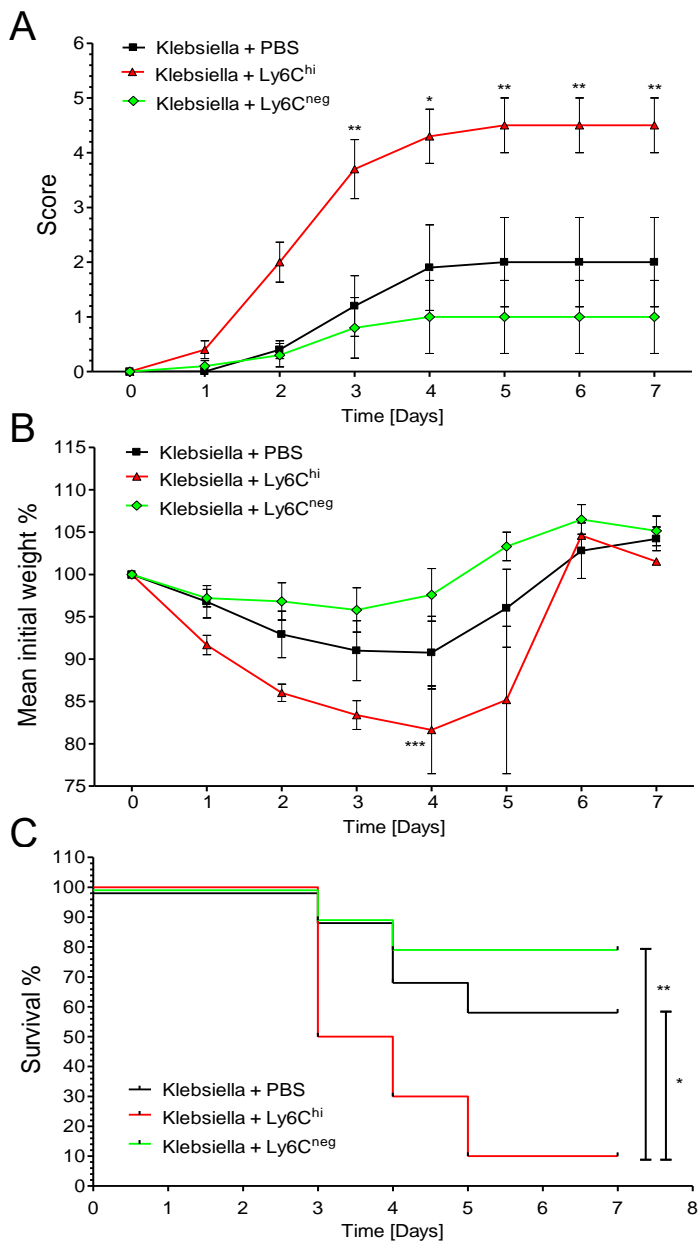
Figure22. *In vitro* produced Ly6C^{hi} monocytes infusion boost mortality rate in a model of systemic infection with *Klebsiella pneumoniae*

(A) Score curves from each experimental condition at days 0 till 7 after intranasal inoculation of *Klebsiella pneumoniae* and intravenous injection of PBS, Ly6C^{hi} or Ly6C^{neg} cells.

(B) Mean initial weight percentage curves from each experimental condition at days 0 till 7.

(C) Survival curves from each experimental condition at days 0 till 7 after intranasal inoculation of bacteria and intravenous injection of cells or PBS.

Results are representative of two experiments. Mean and ±SD are performed with ten mice per group.

Infected mice with *Klebsiella pneumoniae* also injected with *in vitro* Ly6C^hi monocytes showed at day 4 highly increased clinical scoring and loss of weight. Clinical scores were reaching score 5 and the loss of weight percentage reached 25%. This data was in total correspondence with survival rates data. Mice from this experimental group died at a rate of 50% within the first 72 hours, suggesting that the cause of the death was septic shock. Final mortality rate of infected mice administered with Ly6C^hi cells was 90%. Only 10% of the whole experimental condition survived after 7 days of experiment (Figure 21.A, B and C). Infected mice with *Klebsiella pneumoniae* injected with Ly6C^neg cells did not show such exacerbation in clinical scores, weight loss nor rate of mortality, neither within the first 72 hours nor after 7 days. These three values were closer or even more moderate than the ones from the PBS injected group of mice. Final mortality rate of infected mice administered with Ly6C^neg cells was only 20%. Almost 80% of Ly6C^neg injected mice survived after 7 days of experiment (Figure 21.A, B and C). Infected mice with *Klebsiella pneumoniae* injected only with PBS showed mild clinical scoring and the loss of weight was moderate. Clinical scores were never reaching up to score 3 and the loss of weight percentage was less than 12%. PBS injected mice did not show such a high rate of mortality, neither within the first 72 hours nor after 7 days. Final mortality rate of infected mice administered with PBS was almost 40%, more than 60% of PBS injected mice survived after 7 days of experiment (Figure 21.A, B and C).

From these results we can extract the conclusion that treatment with *in vitro* Ly6C^hi monocytes was extremely detrimental for infection resolution, survival and recovery. Surprisingly, mice treated with Ly6C^neg cells seemed to have even better prognosis than mice only treated with PBS. We rather confirm the exceptional implication that *in vitro* Ly6C^hi monocytes have in controlling inflammation, in this case exacerbating inflammation and boosting mortality, in the *in vivo* model of systemic infection with *Klebsiella pneumoniae*. Further experiments need to be done to specify the function of Ly6C^neg cells in this model.

2. TNF-α production from infiltrated *in vitro* Ly6C^hi monocytes causes septic-shock increased mortality and also reduces pulmonary bacterial load

In a second row of experiments mice were infected with *Klebsiella pneumoniae* and PBS or purified *in vitro* Ly6C^hi monocytes were injected intravenously the same day. We also performed a control group of mice which was injected intranasal only with PBS. Mice were euthanized after 48 hours. Total blood was recovered after cardiac puncture for cytokine evaluation in serum. Lung tissues were recovered under sterile conditions for tissue homogenization, culture in agar plates and colony forming units (CFUs) count. Blood and lung tissue samples were processed as described in the experimental

procedures section. ELISA quantification of serum TNF-α determined a high concentration in blood of the septic shock causing cytokine in mice infected with *Klebsiella pneumoniae* injected with Ly6C^{hi} cells (≈6000pg/mL). Nevertheless, infected mice with *Klebsiella pneumoniae* injected only with PBS also presented high concentrations of TNF-α but four times lower than the other experimental group (≈2000pg/mL). No TNF-α production was found in the non-infected mice injected with PBS or Ly6C^{hi} cells (Figure 22.A). CFU counting showed that mice infected with *Klebsiella pneumoniae* injected with Ly6C^{hi} cells presented much less bacterial burden in lungs than infected mice with *Klebsiella pneumoniae* injected only with PBS. There was a 2 logarithms difference in bacterial load between both experimental conditions. Lungs of mice injected with Ly6C^{hi} cells had around 1.10^5 CFUs/mg of tissue, whether lungs of mice injected only with PBS presented values around 1.10^7 CFUs/mg of tissue (Figure 22.B).

In a third row of experiments mice were infected with *Klebsiella pneumoniae* and purified PKH26$^+$ Ly6C^{hi} cells or PBS were injected intravenously. Mice were recovered after 48 hours, anesthetized, perfused transcardiacally with paraformaldehyde and lungs were extracted. After crioprotection, tissues were frozen in OCT with dry ice and cut with a criotome for immunohistochemistry. Two immunohistochemistry techniques were used. The first immunohistochemistry was peroxidase-based TNF-α labelling. We aimed to compare the tissue expression of TNF-α between both experimental conditions. The second immunohistochemistry was fluorescence-based TNF-α labelling. We wanted to determinate weather Ly6C^{hi} PKH26$^+$ cells were colocalizing or not with TNF-α and therefore actively producing the cytokine. We used the E1000 optical microscope for peroxidase detection and the Leica TCS SP5 confocal microscope for fluorescence detection. Afterwards images were treated with Fiji/ImageJ software (data not shown). Peroxidase-based immunohistochemistry of lung tissues demonstrated a substantial increase of TNF-α labelling in lungs from mice infected with *Klebsiella pneumoniae* and injected with Ly6C^{hi} cells compared to infected mice injected only with PBS. TNF-α positive labelling affected extensive zones of the tissue and was also found to be more intense in mice administered with Ly6C^{hi} cells (Figure 22.C and D). Supplementary data (Figure 21). Fluorescence-based immunohistochemistry of lung tissues revealed TNF-α labelling colocalizing with PKH26 in lungs from mice infected with *Klebsiella pneumoniae* and injected with *in vitro* Ly6C^{hi} monocytes. There was also extensive labelling of TNF-α in lungs from infected mice and injected with PBS. This fact shows that mice that were not transferred with *in vitro* Ly6C^{hi} monocytes also present TNF-α producing cells in lungs. No PKH26 labelling was found in tissues from mice injected with PBS, which supported the validity of our findings (Figure 22.E). Supplementary data (Figure 22).
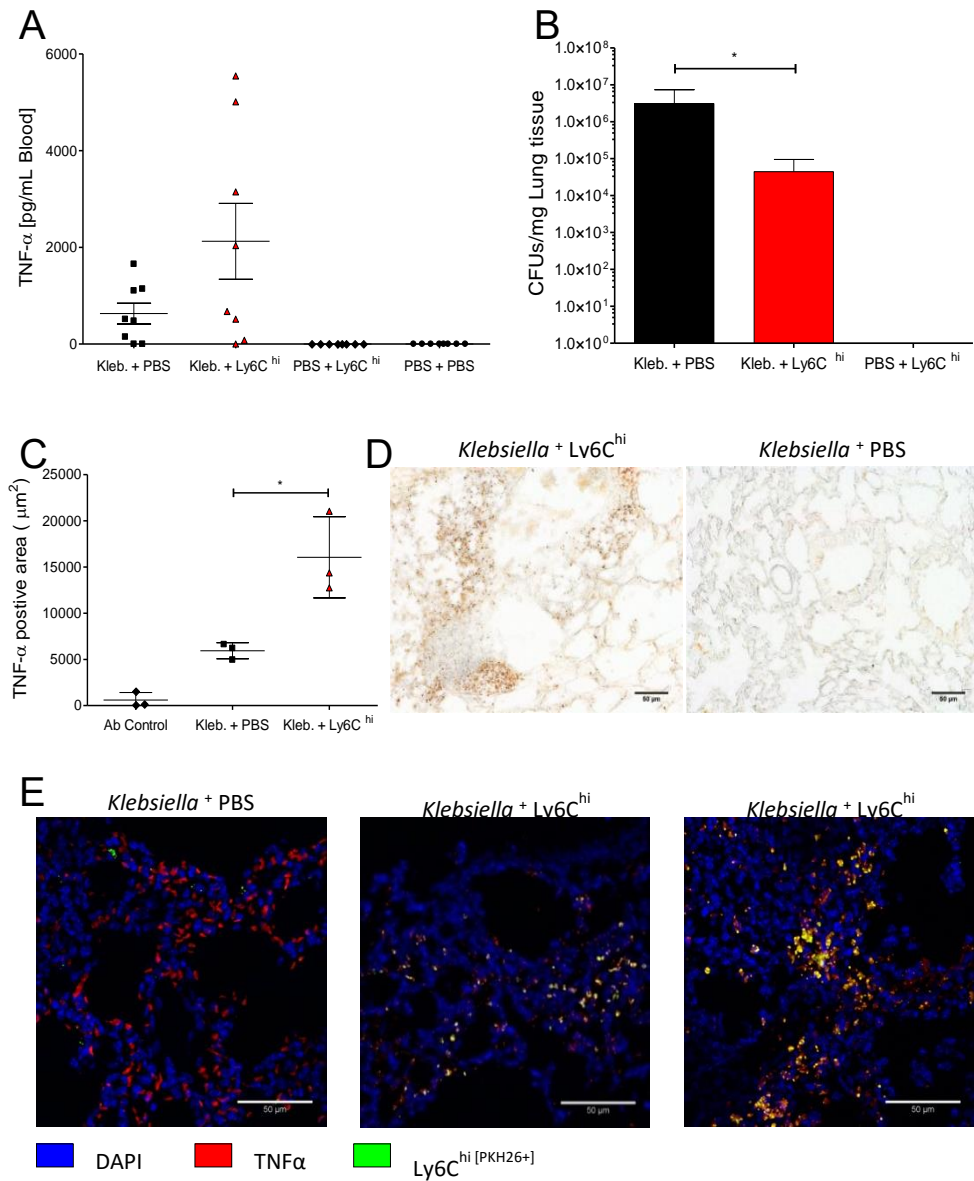
Figure23. TNF-α production from infiltrated *in vitro* Ly6C^{hi} monocytes causes septic-shock increased mortality and also reduces pulmonary bacterial load

(A) ELISA quantification of serum TNF-α from both experimental conditions 48 hours after intranasal inoculation of *Klebsiella pneumoniae* and intravenous injection of PBS or Ly6C^{hi} cells.

(B) CFU counting per mg of lung tissue 48 hours after intranasal and intravenous administrations.

(C) Fiji/ImageJ quantification of the TNF-α positive area in lung tissue from both experimental conditions 48 hours.

(D) Optical microscopy showing TNF-α peroxidase labelling in lung tissue.

(E) Fluorescence microscopy showing lung tissue infiltrated PKH26^{+} Ly6C^{hi} cells expressing TNF-α at 48 hours.

Results are representative of one experiment. Mean and ±SD are performed with eight or three mice per group.

Taking in account all this data we can extract different conclusions. *In vitro* Ly6C^{hi} monocytes are able to infiltrate selectively into the inflamed lungs from mice infected with *Klebsiella pneumoniae* and differentiate actively into recruited macrophages. These cells are able to reduce bacterial burden from the lungs of infected mice, but the mechanism how this process is overcome has yet to be proven. However, these cells are also able to secrete large amount of TNF-α that can be detected within the tissues and peripheral blood. In its turn, the TNF-α cytokine causes septic shock-induced mortality increasing the mortality rate in mice treated with *in vitro* Ly6C^{hi} monocytes.

VII.   SECTION. STUDY OF THE Ly6C^{hi} ADMINISTRATION IN THE EXPERIMENTAL AUTOIMMUNE ENCEPHALOMYELITIS MODEL

1.   *In vitro* produced Ly6C^{hi} monocytes are able to migrate and differentiate within the CNS in a chronic inflammatory model of EAE

Finally, we decided to test the influence of the *in vitro* Ly6C^{hi} monocytes administration in a chronic model of experimental autoimmune encephalomyelitis (EAE). We focused in the chronic-progressive model of EAE induced by active immunization. This model facilitates the study of bone-marrow myeloid cell migration within the central nervous system in contrast with the relapsing-remitting form of the EAE. Extensive data was previously obtained by Juan A. Calatayud (M.Sc) and can be found in the Master Thesis script.

EAE chronic model was generated as described in the materials and methods section. First we performed an initial subcutaneous injection of myelinic oligodendrocyte protein (MOG) peptide in emulsion with Complete Freund Adjuvant (CFA). This initial immunization was followed the same day and the day after by two intraperitoneal injections of *Bordetella pertussis* toxin. The immunization with MOG protein causes the generation of autoreactive peripheral T cells that will later on infiltrate the CNS and induce the illness. The injection of *Bordetella pertussis* toxin breaks the hematoencephalic endothelial barrier permitting the autoreactive T cells to reach their destination within the CNS.

In a first row of experiments EAE was generated as described and mice were separated in five different groups. Ly6C^{hi} cells and Ly6C^{lo} cells were purified, fluorescently labelled with DIR or PKH26 tracers for IVIS and LSFCM detection respectively, and injected at different scores (0, 1, 2, 3, 4) to check for infiltration. Mice were recovered 24 hours after cell administration, anesthetized, perfused transcardiacally with paraformaldehyde and the whole CNS was extracted. Extracted CNS tissues from mice injected with DIR⁺ Ly6C^{hi} cells were analysed by IVIS *ex vivo*.

Extracted tissues from mice injected with PKH26^{+} Ly6C^{hi} cells were crioprotected, frozen in OCT with dry ice and then cut with a criotome for immunohistochemistry. Immunohistochemistry was performed using three different fluorophores, DAPI staining nuclei, anti-F4/80 labelling macrophages and FluoroJade C a marker of myelin destruction. The slides were analysed using the Leica TCS SP5 confocal microscope and the images were treated with Fiji/ImageJ software.

IVIS demonstrated no increase in total fluorescence when mice were injected with DIR[+] *in vitro* Ly6C^{hi} monocytes during scores 0, 1, 2 and 4. However, when mice were injected during score 3 we observed an increment in fluorescence from the tissues. Increase of fluorescence was maximal in the lumbar spinal cord compared to cervical spinal cord where it happened to a minor extent. Encephalon showed no increase in fluorescence at all. There was no increase in total fluorescence from tissues of mice that were treated with DIR[+] Ly6C^{lo} monocytes (Figure 23.A, B and C). Supplementary data (Figure 23.B).

This data suggested that also in the chronic autoimmune inflammatory model of EAE, the Ly6C^{hi} cells but not the Ly6C^{lo} cells are able to transmigrate selectively from the blood flow into the inflamed tissues. It is also suggested that migration occurs mainly during score 3 and within the spinal cord, mainly the lumbar spinal cord, but not the encephalon.

LSFCM revealed PKH26^{+} Ly6C^{hi} cell infiltration within the lumbar and cervical spinal cord at scores 2 and 3, therefore confirming IVIS results. Homing of administered cells occurred mainly within the lumbar spinal cord during score 3 and was undetectable at scores 0, 1 and 4. Infiltration was also undetectable within the brain. Moreover, infiltrated PKH26^{+} cells were distributed forming aggregates and patches close to vessels and along the spinal cord. Infiltrates colocalized with the macrophage marker F4/80, suggesting a differentiation process within the CNS tissue. Note again that not all F4/80^{+} cells were positive for PKH26. Extravasated cells were also colocalizing near areas positive for the fluorescent dye FluoroJade C a chemical marker for axonal damage, indicating the possibility of an active role within the disease (Figure 23.D and E). Supplementary data (Figure 23.A and C and 24).

This data confirmed that *in vitro* Ly6C^{hi} monocytes are able to overcome the hematoencephalic endothelial barrier, colonize the inflamed CNS and differentiate into recruited macrophages in the chronic autoimmune inflammatory model of EAE. Its distribution along vessels, forming patches close to demyelinating areas also suggests a possible role within the disease progression.
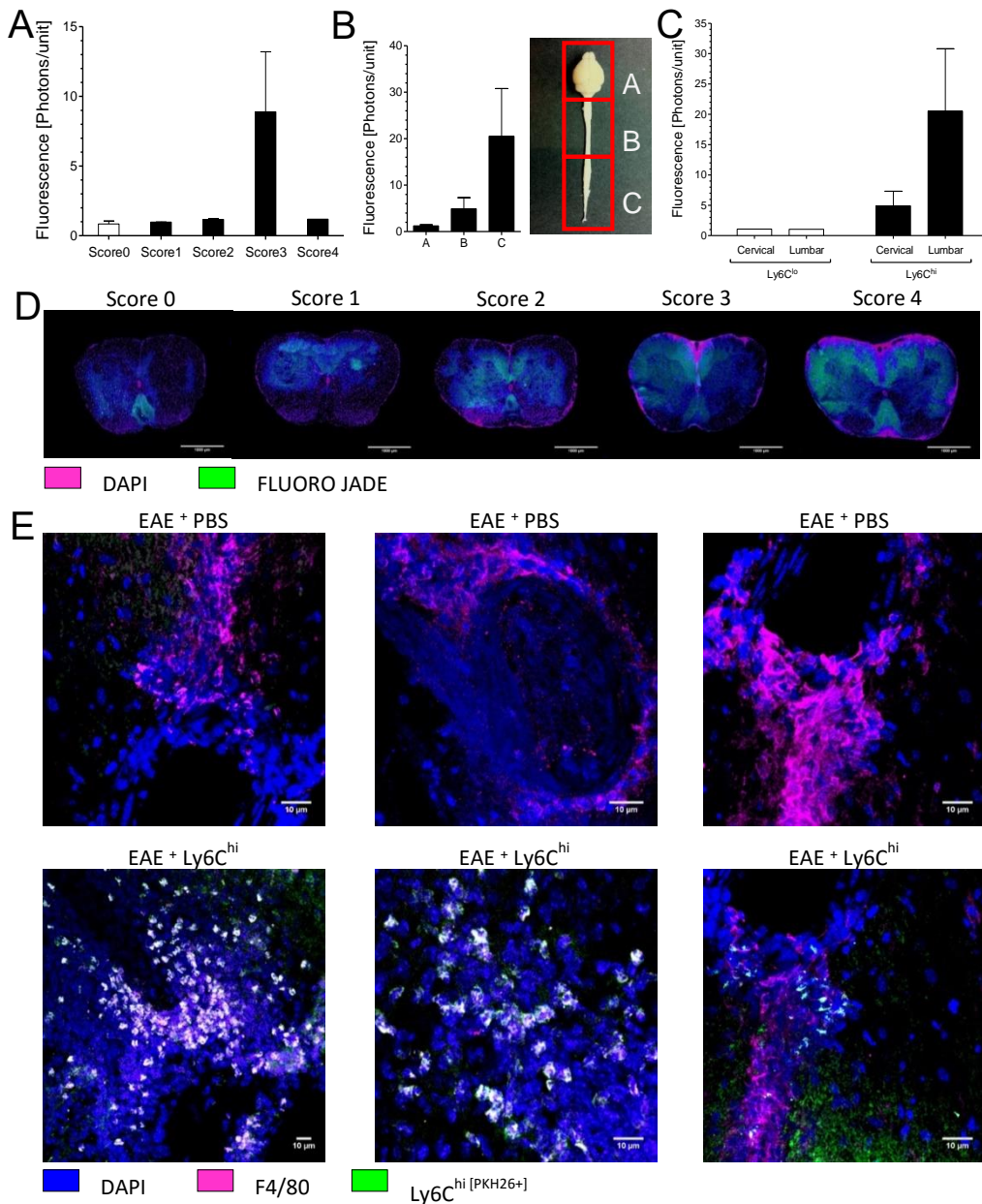
Figure24. *In vitro* Ly6C^{hi} monocytes are able to migrate and differentiate within the spinal cord in a chronic inflammatory model of EAE

(A) IVIS analysis of the fluorescence emitted by the central nervous system at scores 0 to 4 of EAE, 48 hours after intravenous injection of DIR labelled cells.
(B) IVIS analysis of the fluorescence emitted by the encephalon, cervical and lumbar spinal cord at score 3.
(C) IVIS analysis of the fluorescence emitted by the cervical and lumbar spinal cord at score 3 of EAE, 48 hours after intravenous injection of DIR labelled Ly6C^{hi} or Ly6C^{lo} cells.
(D) Fluorescence microscopy showing progressive cell infiltration and axonal damage in lumbar spinal cord.
(E) Fluorescence microscopy showing CNS tissue infiltrated with F4/80$^+$ cells and PKH26$^+$ cells.
Results are representative of two experiments. Mean and ±SD are performed with three mice per group.

2. *In vitro* Ly6C^{hi} monocytes reduce severity of the experimental autoimmune encephalomyelitis chronic model

In a second row of experiments EAE was generated as previously described in the experimental procedures section and purified *in vitro* Ly6C^{hi} monocytes or PBS were administered in two consecutive days, at day 12 and day 14. These two specific days corresponded to the time point where mice were reaching the score 2 of EAE. We evaluated all mice daily for clinical signs, scoring, weight loss and mortality rate.

The following criteria were used for clinical scoring: score 0 – no clinical signs; score 1 – decreased tail tone, tail weakness; score 2 – tail paralysis, spasticity, ataxia; score 3 – paraparesis, hind limb weakness; score 4 – paraplegia, complete hind limb paralysis; score 5 – quadriparesis, fore limb weakness; score 6 – quadriplegia, complete fore limb paralysis. Due to ethical statements mice were always euthanized prior to reach score 6.

EAE-induced mice injected with *in vitro* Ly6C^{hi} monocytes showed slower disease progression than EAE-induced mice injected with PBS. Furthermore, mice injected with *in vitro* Ly6C^{hi} monocytes showed moderate weight loss compared to the ones injected with PBS. Nevertheless, final disease severity and weight loss was identical between mice injected with Ly6C^{hi} cells and mice injected with PBS. No differences were found in mortality rate between both experimental conditions (Figure 24.A, B and C).

Globally, all these data confirm once again the capacity of *in vitro* Ly6C^{hi} monocytes to balance inflammation. *In vitro* Ly6C^{hi} monocytes are able to transmigrate from the blood flow, establish within the tissues, give rise to a population of recruited macrophages and modulate the evolution of the clinical symptoms of the EAE. However, there is still an extensive work to be done to truly unravel the mechanism by which *in vitro* Ly6C^{hi} monocytes control inflammation.
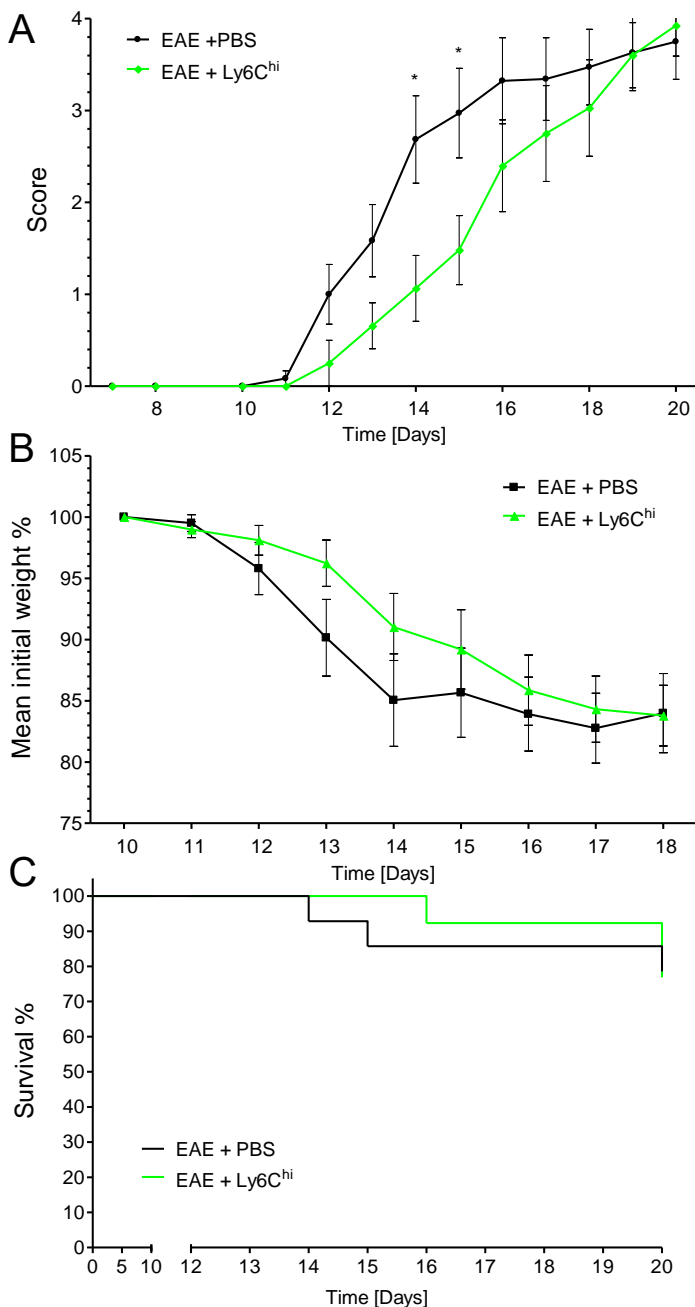
Figure25. EAE severity is reduced after administration of *in vitro* Ly6C^{hi} monocytes
(A) Score curves from each experimental condition at days 0 till 20 after EAE induction and intravenous injection of PBS or Ly6C^{hi} cells at days 10 and 12.
(B) Mean initial weight percentage curves from each experimental condition at days 10 till 18 after EAE induction and intravenous injection of PBS or Ly6C^{hi} cells at days 10 and 12.
(C) Survival curves from each experimental condition at days 0 till 20 after EAE induction and intravenous injection of PBS or Ly6C^{hi} cells at days 10 and 12.
Results are representative of two experiments. Mean and ±SEM are performed with ten mice per group.

DISCUSSION

VI. DISCUSSION

The term monocyte suggests, following its Latin etymology "single-cell", a homogeneous population of leucocytes. However, studies performed by a number of laboratories around the world have clearly established the heterogeneity of monocyte population. Monocytes are composed of several subsets which differ in sizes, morphology, ontogeny, localization, gene expression, fates and functions. Two principal and functionally distinct subsets have been identified in human, mice and other species. The short-lived recruited Ly6C^{hi} CCR2$^+$ CX3CR1^{lo} subset, CD14$^+$ CD16$^-$ in humans, is believed to be recruited in an active manner during inflammation in a wide range of pathologies varying from acute to chronic, septic an aseptic, autoimmune and oncologic inflammatory pathologies. The long-lived patrolling Ly6C^{lo} CCR2$^-$ CX3CR1^{hi}, CD14^{lo} CD16$^+$ in humans, subset is believed to patrol the vascular system for repair, refill the pool of resident macrophages and contribute substantially during inflammation and resolution processes again in the same wide range of pathologies.

Monocytes are key players of the innate immune system. This is due to two different capacities of all monocytes, their ability to be recruited, migrate and infiltrate the tissues when required, and their extreme functional and genetic plasticity. Their implication in the early events of inflammation makes them extremely attractive to uncover the initial processes that drive multiple pathologies. Even more, monocytes not only actively contribute to inflammation and resolution, but also contribute extensively to coordination, recruitment and balance of many other leucocyte subsets such as neutrophils, NK cells, lymphocytes and non-immune cells. Not only monocytes are able to give rise to recruited populations of macrophages and/or dendritic cells, but they also are able to skew through opposed pro-inflammatory and anti-inflammatory phenotypes. Additionally, regulatory, tolerogenic and immunomodulatory subsets have been identified and characterized (Geissmann, Jung et al. 2003; Gordon and Taylor 2005; Mantovani, Sica et al. 2005; Mosser and Edwards 2008; Auffray, Sieweke et al. 2009; Geissmann, Gordon et al. 2010; Yona and Jung 2010; Murray and Wynn 2011; Yona, Kim et al. 2013; Ginhoux and Jung 2014; Guilliams, Ginhoux et al. 2014; Mitchell, Roediger et al. 2014).

In this study we present a technique for *in vitro* generation of Ly6C^{hi} monocytes produced *in vitro*. Until that moment, studies regarding Ly6C^{hi} cells obtained the cellular subset from subsequent blood purifications with very low efficiency. This new technique developed and optimized in our laboratory allows us to directly generate through primary bone marrow cell cultures large amounts of highly pure Ly6C^{hi} cells. Initially, we demonstrated that *in vitro* generated monocytes showed similar markers to the natural Ly6C^{hi} monocyte population found in the blood stream of mice. For this purpose, we focused on diverse techniques to check whether the phenotype and functional

characteristics of our cells corresponded or not to the natural subpopulation of peripheral blood Ly6C^{hi} monocytes.

Monocyte subpopulations are well characterized following differential expression of extracellular markers. Blood circulating monocytes are heterogeneous and this heterogeneity is conserved in humans, mice and other species. The distinct monocyte subsets seem not only to reflect distinct developmental states but also distinct mature populations with different physiologic roles during homeostasis and inflammation (Gordon and Taylor 2005). Extensively reviewed before, monocyte subsets can be classified in two main subpopulations, the recruited Ly6C^{hi} monocyte and the patrolling Ly6C^{lo} monocyte subsets. Our study focuses in the Ly6C^{hi} population of recruited monocytes. Blood-derived recruited Ly6C^{hi} monocytes and patrolling Ly6C^{lo} monocytes both share the following pattern of expression CD11b^{+} CD115^{+} F4/80^{-} CD11c^{-}. Furthermore, Ly6C^{hi} monocytes can be differentiated from Ly6C^{lo} monocytes through their pattern of expression of CCR2^{+} CX3CR1^{lo} CD62L^{+} and obviously Ly6C^{hi} (Geissmann, Jung et al. 2003; Ziegler-Heitbrock 2014).

First of all, optimization of the protocol was critical to obtain the maximum efficiency in Ly6C^{hi} cell production. *In vitro* generation of monocytes showed four patterns of expression of the Ly6C marker. We could differentiate between a Ly6C^{neg} population, a Ly6C^{lo} population, a Ly6C^{int} population and a Ly6C^{hi} population showing no expression, low expression, intermediate expression and high expression of the marker respectively. We focused our studies exclusively in the Ly6C^{hi} population. The Ly6C^{lo} and Ly6C^{neg} populations were only used as experimental controls. For purification of the Ly6C^{hi} fraction we performed cytometric sorting. FACS sorting purification procedure was only based in the Ly6C marker, other markers such as chemokine receptors and adhesion molecules were avoided preventing functional alterations. In our study of *in vitro* generated monocytes, we performed FACS comparative analysis between them and the tissue pro-inflammatory monocyte subpopulations. We analysed the pattern of expression of a specific combination of extracellular markers known to be specific for the non-classical Ly6C^{hi} monocytes subpopulation. *In vitro* generated Ly6C^{hi} monocytes were compared to peripheral blood, bone-marrow, spleen and intraperitoneal monocytes. Ly6C, CD11b, F4/80, CD115, CD11c, CD62L, CCR2 and CX3CR1 were the chosen markers for this study.

The integration of FACS data determined that Ly6C^{hi} cells and peripheral blood Ly6C^{hi} monocytes present equivalent surface markers. Thus, suggesting that the Ly6C^{hi} subpopulation found in our cultures could also share other phenotypical properties with peripheral blood Ly6C^{hi} monocytes.

Monocytes are defined as highly plastic cells capable to develop remarkable phenotypic and functional changes depending on signals from local microenvironment. This capacity of monocytes allows them to effectively perform the required functions during homeostasis, inflammation or pathogen specific immune responses. Monocyte polarization, similarly to macrophage polarization can be driven by an extremely wide range of stimuli that induce differential patterns of gene expression and functions. Therefore, monocyte as well as macrophage polarization is far more complex than the initially established paradigm of M1/M2 polarization duality (Mosser and Edwards 2008; Murray, Allen et al. 2014).

However, Th1 pro-inflammatory or Th2 anti-inflammatory cytokines provide potent polarizing stimulus that unequivocally induce dramatic and opposite gene expression and functional changes. These two antagonistic states correspond to opposite ends of a phenotypic spectrum that is extraordinarily complex (Mantovani, Sica et al. 2005; Murray and Wynn 2011; Martinez and Gordon 2014; Mitchell, Roediger et al. 2014; Das, Sinha et al. 2015). In particular, monocyte polarization driven by GM-CSF, IFN-γ or LPS occur *in vivo* in response to extracellular and intracellular pathogens as well as in sterile inflammatory conditions such as autoimmune pathologies. M1-like polarization of monocytes induce, as expected, increased gene expression of pro-inflammatory genes such as *tnf-α*, *il-1β*, *nos-2*, *il-6* and *ifn-γ*. Increased expression of these genes is essential for reactive oxygen and nitrogen species production during pathogen killing. Additionally, expression of pro-inflammatory cytokines enhances the pro-inflammatory reaction mediated by other cells types. Even more, expression of chemokine receptors and chemoattractant proteins such as MCP-1, IL-8 or IP-10 boosts the recruitment and coordination of additional monocytes and other cell types such as neutrophils, B and T cells. Oppositely, monocyte polarization driven by M-CSF, IL-4 or IL-13 occur *in vivo* in response to parasite pathogens as well as in allergic and pro-fibrotic inflammatory pathologies. M2-like polarization of monocytes causes increased gene expression of anti-inflammatory genes such as *arg-1*, *mrc*, *fizz-1* and *ym-1*. Heightened expression of anti-inflammatory genes contributes to processes such as uptake of particles, inhibition of inflammation and tissue repair and remodelling processes. In a similar way to the M1-like polarization, expression of anti-inflammatory cytokines and chemoattractant proteins enhances the anti-inflammatory reaction and recruitment of other leucocytes.

Real-time PCR analysis was performed in our model to test the expression of pro-inflammatory and anti-inflammatory genes under different types of stimulation. Bone marrow-derived macrophages, *in vitro* produced Ly6C^{hi} cells, Ly6C^{lo} cells and Ly6C^{neg} cells were purified, cultured in vitro and stimulated with diverse pro- and anti-inflammatory

ligands and cytokines. When activated by pro-inflammatory stimuli Ly6C^{hi} expressed the *tnf-α, il-1β, nos2* and *il-6* expected genes. Oppositely, when activated by ant-inflammatory stimuli they expressed *arg1, mrc, fizz1* and *ym1*.

Indeed, gene expression analysis confirmed the plasticity of Ly6C^{hi} cells indicating their potential modulatory effects during inflammation.

Migratory and differentiation capacities are intrinsic to monocyte function and essential for their contribution during inflammation and resolution in multiple pathologies. Recruitment of these cells from the blood stream requires orchestrated chemokine and adhesion molecules interaction between monocytes and vascular or lymphatic endothelium (Imhof and Aurrand-Lions 2004; Shi and Pamer 2011). Once infiltrated, monocytes activate their differentiation program and generate a population of recruited macrophages or dendritic cells. Monocyte differentiation into recruited macrophages can lead to the generation of multiple macrophage phenotypes, including the M1-like and the M2-like phenotypes. It is still a matter of debate whether monocytes and macrophages can be crossly differentiated into different subsets in response to environmental changes or not (Italiani and Boraschi 2014; Yang, Zhang et al. 2014).

Monocytes Ly6C^{hi} express high levels of monocyte chemokine receptor 2 (CCR2) and low levels of CX3C-chemokine receptor 1 (CX3CR1). They also express a wide variety of adhesion molecules including the L-selectin (CD62L), the macrophage receptor 1 (CD11b) between others such as LFA1, PECAM1 and VLA4. Additionally, monocytes lack the expression of EGF-like module-containing mucin-like hormone receptor-like 1 (F4/80) and express high levels of the macrophage colony stimulating factor (CD115).

CCR2 deficiency markedly reduces monocyte trafficking to sites of inflammation which indicates a crucial role for the CCR2 receptor during infiltration. The same conclusion can be extracted from experiments related with CCR2 ligands deficiency, the monocyte chemoattractant protein 1 (CCL2 or MCP-1) and the monocyte chemoattractant protein 3 (CCL7 or MCP-3). CCR2 has also demonstrated to be essential for monocyte emergence from the bone marrow into the blood flow (Kurihara, Warr et al. 1997; Kuziel, Morgan et al. 1997; Jia, Serbina et al. 2008; Si, Tsou et al. 2010). CX3CR1 deficiency results in diminished recruitment of the Ly6C^{hi} population to the splenic sites of bacterial infection. Even though CX3CR1 has demonstrated to perform an active role during Ly6C^{hi} monocyte recruitment, its deletion has much less dramatic effects than the CCR2 deletion, which confirms again the essential function of CCR2 in Ly6C^{hi} monocytes (Auffray, Fogg et al. 2009). CCR1, CCR5, CCR6 and CXCR2 deficiencies have demonstrated non-redundant roles for these chemokine receptors during inflammation recruitment in diverse pathologies. CCR1 and CXCR2 mediate the

arrest of monocytes. CCR6 mediates the extravasation of monocytes into the tissues. CCR5 seems to contribute to the spreading of monocytes within the tissues (Kaufmann, Salentin et al. 2001; Mack, Cihak et al. 2001; Vanbervliet, Homey et al. 2002; Bernhagen, Krohn et al. 2007). CD62L deficiency and CD11b blockage with monoclonal antibodies they both inhibited monocyte recruitment during inflammation models (Rosen and Gordon 1987; Tedder, Steeber et al. 1995). CD115 deficient mice have a decreased number of monocytes in the bone marrow and circulation, in addition to a decrease in osteoclasts. Experimentally blocking CD115 with monoclonal antibodies leads to a reduction in Ly6C^{lo} monocytes and is also associated with an increase in Ly6C^{hi} monocytes, suggesting the involvement of CD115 in the maturation of (Dai, Ryan et al. 2002).

In addition to our initial *in vitro* studies with the *in vitro*-derived monocytes, we tested the differentiation, maturation and activation capacity of the cells under different *in vitro* stimulation conditions. Again, bone marrow-derived macrophages, Ly6C^{hi} cells, Ly6C^{lo} cells and Ly6C^{neg} cells were purified, cultured *in vitro* and stimulated during 48 hours with diverse pro- and anti-inflammatory ligands, cytokines and growth-factors.

FACS analysis revealed a differentiation capacity of our cells. Ly6C^{hi} cells loosed the Ly6C expression and acquired a high expression of the F4/80 macrophage marker. Only few cells expressed the CD11c dendritic cell marker and CD11b expression was stable in all cases. FACS analysis also revealed a maturation and activation capacity. Ly6C^{hi} cells increased their expression in MHCII marker upon IFN-γ stimulation demonstrating maturation ability. Ly6C^{hi} cells also increased their expression in CD80 marker upon M-CSF, GM-CSF and IL-4 stimulation demonstrating their potential.

Therefore, FACS data confirmed that Ly6C^{hi} cells were capable to differentiate, maturate and activate *in vitro*.

Subsequently, our aim was to evaluate the migratory and differentiation capacities of Ly6C^{hi} cells *in vivo*. For this purpose, we carried out transfer, track and recovery experiments in diverse *in vivo* models of inflammation. *In vitro* produced Ly6C^{hi} monocytes were labelled with fluorescent dyes that did not alter cell functionality but allowed us to detect, track and isolate infiltrated cells by IVIS, FACS and LSFCM. To begin with, *in vivo* fluorescence-based imaging (IVIS) was chosen as the first technique to evaluate transmigration of our cells from the blood flow to the inflamed tissues. IVIS allows the detection of slight fluorescence increases of living and death tissues.

IVIS results encouraged us to believe that a homing process was taking place. We observed an increase in the total fluorescence emitted by the inflamed tissues when Ly6C^{hi} cells were injected compared to control mice. Secondly, laser scanning fluorescence confocal microscopy (LSCFM) confirmed the infiltration process that was

occurring within inflamed tissues after infusions of *in vitro* Ly6C^{hi} monocytes. LSFCM offers much more resolution and sensibility compared to IVIS technique, and allowed us to detect infiltrated aggregates of fluorescence-labelled Ly6C^{hi} cells. Transmigrated Ly6C^{hi} cells acquired the expression of F4/80 a macrophage marker expressed only by a small percentage of cells before injection, as previously observed in our *in vitro* studies of differentiation. Infiltrates localized preferentially close to vessels. We could then conclude that our injected *in vitro* Ly6C^{hi} monocytes are localized in the inflammatory loci close to vasculature. Lately, fluorescence activated cell sorting (FACS) helped us to detect and isolate the infiltrated cells. The pattern of expression of diverse extracellular markers suffered alterations when compared to the cells prior to injection. FACS demonstrated again that infiltrated cells change their phenotype after transmigration. After infiltration *in vitro* Ly6C^{hi} monocytes start losing the Ly6C marker and expressing the CD68 marker, a macrophage marker similar to F4/80. Another marker CD11b presented two different patterns of differentiation. CD11c was not expressed at all by infiltrated cells, confirming that our Ly6C^{hi} cells did not differentiate into dendritic cells. FACS also determined that the number of macrophages was increasing after cell administration.

Taking together all these results, we confirm the infiltration capacity of *in vitro*-derived Ly6C^{hi} monocytes as well as their ability to differentiate into recruited macrophages *in vivo*.

Finally, we tested the impact that administration of Ly6C^{hi} cells may have in the inflammation onset and progression in several *in vivo* models. We decided to evaluate this effect in two mice models of inflammation, the dinitrofenolbenzene contact-induced inflammation model (DNFB model) and the Notexin-induced myoinjury model (NTX model). We decided as well to evaluate the effect of Ly6C^{hi} cells administration in a model of septic infection with *Klebsiella pneumoniae* (KP model) and the chronic inflammatory model of experimental autoimmune encephalopathy (EAE model). In the first place, we used the dinitrofenolbenzene contact-induced inflammation (DNFB) model as a model of aseptic inflammation.

DNFB contact-induced inflammation model consists in a delayed-type hypersensitivity response to cutaneous contact with the chemical irritant 2,4-dinitrofluorobenzene (DNFB). DNFB is applied in the right ear of mice and acetone is applied in the left ear as a control, all this is performed as described in the experimental procedures section. DNFB exposure induce an increase in the expression of adhesion molecules from the activated endothelium. Endothelial activation enhances leukocyte binding from the circulation, transmigration and trafficking to the site of inflammation. Furthermore, in this skin model of inflammation, DNFB diffuses from the epidermis to the

dermis and reacts with amino-acid chains of extracellular proteins. Langerhans cells process this modified proteins and migrate to the regional lymph nodes through the lymphatic vessels. This process enables the generation of hapten-specific T lymphocytes.

This model provides a fast and useful tool to study inflammation and extravasation of leukocytes to the site of DNFB application (Klimuk, Semple et al. 1999; Tuckermann, Kleiman et al. 2007; Tang, Zou et al. 2012; Tamoutounour, Guilliams et al. 2013; Christensen, Skov et al. 2014).

Myeloid cells including monocytes, macrophages and neutrophils are thought to play an important role during contact inflammation mediated by DNDB. This was proved during depletion experiments with anti-Ly6G/C mAb, where all three populations were eliminated, causing a substantial suppression of the inflammatory response to DNFB. In addition, treatments with anti-Ly6G mAb targeting only the neutrophil population, reduced inflammation to a much lesser extent. DNFB-induced mice treated with anti-Ly6G/C mAb compared to DNFB-induced mice treated with anti-Ly6G mAb not only showed reduced ear swelling but very significant reduction in the local tissue expression of multiple pro-inflammatory genes including *tnf-α* and *il-1β*. (Christensen, Skov et al. 2014).

Suppressive treatments with glucocorticoids directed to monocyte and macrophage populations strongly downregulated the inflammatory response. Contrary, when the same treatment was specifically directed to keratinocytes, T or B lymphocyte populations, there was no suppressive effect of dexamethasone. Even more, when animals treated with glucocorticoids were also injected with recombinant cytokines such as TNF-α and IL-1β, suppression of the inflammation was partially reversed (Tuckermann, Kleiman et al. 2007). Extensive analysis of epidermal and dermal CD11b+ populations of monocytes, dendritic cells and macrophages during hapten-mediated inflammation confirmed again the important role of myeloid cells in the model of DNFB. Myeloid infiltration following DNFB exposure triggered a massive and rapid infiltration of myeloid cells dominated by monocytes. Importantly, many type-I IFN simulated genes were induced in infiltrated monocytes, which suggests important roles for the type I IFN transcriptional routes including the STAT1 transcriptional signaling (Tamoutounour, Guilliams et al. 2013).

In our model of study, Ly6C^{hi} cells administration boosted inflammation. Tissue swelling was enhanced as ear weight and width increased when mice were treated with Ly6C^{hi} cells. There was a dose dependent correlation between inflammation and injected cells determined by ear weight measures and infiltrate quantification by FACS. Cell treatment induced the expression of diverse pro-inflammatory genes such as the *tnf-α*, *il-1β*, *il-6* and *nos2* genes and anti-inflammatory genes such as the *arg1*. We hypothesized

that infiltrating Ly6C^{hi} cells differentiate into recruited macrophages and polarize following the microenvironment of cytokines. Once polarized, recruited macrophages synthesize new pro-inflammatory mediators that may exacerbate the inflammation.

Consistently reviewed before, extensive data can be found related with monocyte and macrophage activation states and its plasticity (Sica and Mantovani 2012; Natoli and Monticelli 2014). In contrast to the IFN-γ polarization which induces NOS2 enzyme, IL-4 polarizing stimuli is in charge to induce the arginase-1 enzyme. Both iNOS and arginase-1 enzymes show a range of effects that include opposing actions, they both require L-arginine as a substrate and compete for the same pool of the amino acid. Therefore, IFN-γ and IL-4 induce opposite reactions in terms of gene expression patterns, functional alterations and roles in monocytes and macrophages (Mitchell, Roediger et al. 2014). IFN-γ-mediated activation clearly drives monocytes into a pro-inflammatory phenotype accompanied by pro-inflammatory cytokine production. IFN-γ polarization of monocytes is essential not only for production of antimicrobial species and clearance of pathogens, but also to establish the pro-inflammatory and chemoattractant microenvironment that will boost inflammation mediated by monocytes and other leucocytes (Becker 1984;(Delneste, Charbonnier et al. 2003). IL-4-mediated activation distinctly induced an anti-inflammatory phenotype in monocytes followed by anti-inflammatory cytokine production. IL-4-driven polarization of monocytes is fundamental during anti-inflammatory reactions to settle regeneration and pro-fibrotic events carried out by monocytes and additional cell types (Hart, Vitti et al. 1989; Lehtonen, Ahlfors et al. 2007).

Our experimental data concerning the DNFB model shows that the inflammatory effect mediated by Ly6C^{hi} cell treatments was increased when cells were stimulated *ex vivo* with IFN-γ prior to administration. Contrary, reduced inflammation was found when cells were stimulated with IL-4. Reinforcing the hypothesis that pro-inflammatory monocytes may be regulating the inflammation *in vivo* through expression of cytokines and that this effect could be balanced by the microenvironment as well as directed through *ex vivo* treatments.

Transcriptional studies involving targeted disruption of the STAT1 and STAT6 genes demonstrated their essential implication during signal transduction after IFN-γ and IL-4 stimulation. Thus, STAT1 activity is crucial for M1-like polarization as STAT6 is for M2-like polarization in monocytes and macrophages (Lawrence and Natoli 2011). During IFN-γ activation, right after receptor ligation, a rapid phosphorylation of a tyrosine-containing sequence of the α-chain receptor forms a specific docking site for STAT1. Once STAT1 proteins bind to the IFN-γ receptor the JAK proteins phosphorylate them provoking their activation, homodimerization and migration to the nuclei where they perform their transcriptional functions (Darnell, Kerr et al. 1994). STAT1-deficient mice

did not show deficiencies in development but displayed a complete lack of response to IFN-γ. Indeed, STAT1 exhibits an indispensable and unexpected level of physiologic specificity for the IFN-γ signal transduction and its functions *in vivo* (Durbin, Hackenmiller et al. 1996; Meraz, White et al. 1996). During IL-4 signalling, in a similar way of that of IFN-γ signalling, phosphorylation of tyrosine-containing sequences of the α-chain receptor create specific docking sites for STAT6. STAT6 binding to the IL-4 receptor is followed by its phosphorylation mediated by the JAK proteins. This sequence of events causes its activation, homodimerization and nuclear migration, allowing its transcriptional functions (Takeda, Tanaka et al. 1996; Gordon and Martinez 2010). However, some anti-inflammatory effects caused by IL-4 signalling have been found to be independent of STAT6 transcriptional routes (Levings and Schrader 1999). STAT6-deficient mice did not show morphologic nor developmental alterations but as expected IL-4 and IL-13 signalling pathways were impaired. Thus, STAT6 is confirmed as an essential mediator for signal transduction and functions mediated by IL-4 *in vivo* (Takeda, Kamanaka et al. 1996; Brombacher, Arendse et al. 2009). Therefore, the use of STAT1 and STAT6 knock-out mice is an exceptional tool for the study of the IFN-γ and IL-4 signalling implication during inflammation.

During our study of the DNFB-mediated inflammation we observed an impaired function when administered Ly6C^{hi} cells were derived from STAT1 and STAT6 knock-out mice. STAT1^{-/-} and STAT6^{-/-} Ly6C^{hi} cells were able to infiltrate inflamed tissues as they were detected by LSFCM. Even though this infiltration process occurred, further quantification needs to be performed in order to discard its reduction compared to wild-type- derived Ly6C^{hi} cells. But although migratory function was not impaired, the administration of cells did not have the pro-inflammatory neither the anti-inflammatory effects observed before. Gene expression analysis determined that there was a reduced pro-inflammatory profile when injected cells were derived from both STAT1 and STAT6 knock-outs. This data suggests strong interdependence between both signal transduction pathways.

Regarding our results, we suggest an essential contribution to inflammation through cytokine production that *in vitro* generated Ly6C^{hi} monocytes perform in the inflammatory model of DNFB. Additionally, we propose a fundamental role of the cytokine-mediated polarization of *in vitro* generated Ly6C^{hi} monocyte in balancing inflammation during hapten-mediated inflammation. Furthermore, we advance an important if not crucial role of both functional STAT1 and STAT6 transcriptional pathways in the establishment of inflammation during allergic contact dermatitis mediated by the *in vitro* generated Ly6C^{hi} monocytes.

Following with *in vivo* studies in relation with our *in vitro* generated Ly6C^{hi} monocytes, we focused on the notexin-induced myoinjury (NTX) model as another model of aseptic inflammation and regeneration.

NTX-mediated myoinjury model aims to mimic the myofiber injury typically observed in inflammatory myopathies such as the Duchenne's syndrome and other muscular dystrophies, where a variety of poorly understood immune reactions take place. NTX skeletal muscle injury model presents a pro-inflammatory phase followed by an anti-inflammatory regenerative phase. During the generation of this model an intramuscular injection of the *Notechis scutatus* venom or Notexin venom is applied in the right *Tibialis anterioris* (TA) muscle of the mice, while intramuscular injection of PBS is applied in the left TA muscle as a control. Notexin venom inhibits Ca2+ uptake into fragmented sarcoplasmic reticulum from skeletal muscle, causing muscle myofibers necrosis. Skeletal muscle necrosis causes massive release of pro-inflammatory mediators and extensive infiltration of leucocytes in charge to digest dead tissues and contribute to regeneration. Monocytes and macrophages are known to present an essential role in tissue regeneration in this animal model (Chazaud, Brigitte et al. 2009). The Notexin model provides an extremely useful tool to study monocyte infiltration and its role during inflammation and regeneration.

Experiments of bone-marrow transplantation carried out with CAG-GFP-transgenic mice allowed to differentially identify resident macrophages and recruited monocytes/macrophages. During NTX-mediated skeletal muscle injury the resident population of macrophages located in the connective tissue surrounding the muscle plays (epimysium/perimysium) an essential role. Right after muscle damage resident mast cells release a variety of pro-inflammatory mediators including TNF-α. Soon after this initial damage signal, resident macrophages selectively secrete two chemoattractant proteins, the cytokine induced neutrophil chemoattractant protein (CINC-1) and the monocyte chemoattractant protein 1 (MCP-1). The first chemokine CINC-1 is in charge to recruit a massive amount of neutrophils that enhance the pro-inflammatory mediators signalling. The second chemokine MCP-1 will induce the recruitment of pro-inflammatory monocytes at around 24 to 48 hours post-injury. The initially infiltrated monocytes *in vitro* Ly6C^{hi} monocytes progressively differentiate into an intermediate Ly6C^{lo} stage. NTX skeletal muscle injury model is characterized by massive infiltration of these pro-inflammatory monocytes that will differentiate into beneficial recruited macrophages (Brigitte, Schilte et al. 2010). Monocytes and recruited macrophages are indispensable players during skeletal muscle regeneration as demonstrated in experiments with CD11b-difteria toxin receptor transgenic mice experiments. In this model monocytes and macrophages were transiently depleted at multiple stages before and after skeletal

muscle injury. Early ablation of macrophages resulted in delayed but exaggerated monocyte/macrophage accumulation, poor myofiber regeneration and increased adipose tissue accumulation. Infiltrated monocytes and macrophages actively expressed pro-inflammatory and anti-inflammatory genes such as *mcp-1*, *tnf-α* and *arg-1*. Impairment of muscle regeneration was explained by dysfunctional or delayed switch of recruited macrophages to an anti-inflammatory state (Wang, Melton et al. 2014).

Treatment with *in vitro*-derived Ly6C^{hi} cells did not have an effect in inflammation, tissue necrosis or tissue regeneration when the injected cells were not stimulated previously. This could be explained by the possibility that the system is already saturated by the massive infiltration of Ly6C^{hi} monocytes from the own animal. However, injections of Ly6C^{hi} cells treated with IFN-γ boosted tissue necrosis and delayed the regeneration of myofibers. In the opposite way, when we injected Ly6C^{hi} cells treated with IL-4 tissue necrosis was reduced and muscle regeneration was enhanced. Indeed, we found altered gene expression profiles of pro- and anti-inflammatory genes when animals were treated with Ly6C^{hi} cells stimulated with IFN-γ or IL-4. Pro-inflammatory genes such as *tnf-α* or *nos2* were over expressed at day 4 post-injury when mice were injected with IFN-γ treated Ly6C^{hi} cells or non-treated Ly6C^{hi} cells respectively. The same genes were down regulated at day 4 post-injury in mice injected with IL-4 treated Ly6C^{hi} cells. Anti-inflammatory genes such as *fizz1* were over expressed at days 4, 6 and 8 post-injury in mice injected with IL-4 treated Ly6C^{hi} cells, and down regulated in mice injected with IFN-γ treated Ly6C^{hi} cells. Muscle regeneration related genes such as *myogenin* were over expressed at day 4 post-injury in mice injected with non-treated Ly6C^{hi} cells and at day 6 post-injury in mice injected with IL-4 treated Ly6C^{hi} cells. Moreover, intrinsic expression of NOS2 protein was found in infiltrated Ly6C^{hi} cells when we analysed tissue sections by LSFCM, once more confirming functional activity of the Ly6C^{hi} cells homed into the inflamed tissues.

Again, we confirm the infiltration, differentiation and modulatory capacity of *in vitro*-derived Ly6C^{hi} monocytes. These particular results globally confirm the contribution of infiltrated *in vitro* Ly6C^{hi} monocytes to balance inflammation during skeletal muscle injury. However, more experiments including previous selective monocyte depletion shall be performed in order to truly unravel the contribution that *in vitro* Ly6C^{hi} monocytes do to tissue regeneration and myogenesis.

Besides our *in vivo* studies, related with the inflammatory models of DNFB inflammation and NTX-mediated myoinjury, we assessed the effect of administration of *in vitro*-derived Ly6C^{hi} monocytes in the *in vivo* model of systemic infection with the gram-negative bacteria *Klebsiella pneumoniae* (KP).

The KP systemic infection model wants to reproduce the inflammatory state occurred during systemic infection in human patients. *Klebsiella pneumoniae* bacteria is ubiquitous in nature and common inhabitant of the upper respiratory tract in mammals. *Klebsiella pneumoniae* causes a wide range of infections from urinary tract infections to pneumonia and systemic infection, and it is particularly devastating in immunodepressed subjects. Systemic infection with this pathogen rarely occurs in healthy individuals and its mortality rates are between 25 to 60% (Yu, Hansen et al. 2007; Regueiro, Moranta et al. 2009; Moranta, Regueiro et al. 2010). The KP systemic infection model is generated by intranasal administration of living *Klebsiella pneumoniae* bacteria from the virulent serogroup O1:K2. We used a group of control mice injected intranasal only with PBS. *Klebsiella pneumoniae* fast multiplies in the respiratory tract of mice affecting the totality of the lungs and soon inducing septic shock-mediated death. The human pathogen *Klebsiella pneumoniae* is known to be highly resistant to macrophage phagocytosis. The capsule of polysaccharide which contains LPS plays a crucial role in resistance to phagocytosis. In addition, LPS is also the direct cause of septic shock-mediated death after systemic infection with this bacterium. This ability to resist phagocytosis is essential for the bacteria to escape its natural predator the amoeba *Dictyostelium discoideum*. This mechanism is thought to be employed in a similar means to counteract amoebae and mammalian macrophage phagocytosis (Rukavina, Ticac et al. 1997; March, Cano et al. 2013).

Therefore, the KP systemic infection model serves as a great means to study monocyte and macrophage function during septic inflammation.

Monocytes infiltrate infected tissues during septic immune assaults and following stimulation with growth-factors, pro-inflammatory cytokines and microbial products they differentiate into recruited macrophages. Moreover, monocytes mediate direct antimicrobial activity at this sites before differentiation occurs carrying microbial antigens to lymph nodes and secreting pro-inflammatory cytokines such as TNF-α, reactive nitrogen species after expression of NOS-2 and chemokines. Recruitment of Ly6C^{lo} monocytes to sites of infection seems to be even earlier than recruitment of Ly6C^{hi} monocytes. Once homed into the tissues, Ly6C^{lo} monocytes participate into the early response to pathogens by secreting TNF-α and chemokines. However, infiltration of Ly6C^{hi} monocytes is usually more prominent and robust. After differentiation the resultant macrophage population up-regulates series of genes involved in M1-like polarization, including genes encoding for cytokines such as TNF-α, IL-6, IL-12, IL-1β, cytokine receptors, chemokines, chemokine receptors, costimulatory molecules and enzymes such as NOS-2 in charge of the NO synthesis. Recruitment of monocytes is essential for effective control and clearance of bacterial infections, but excessive infiltration of

recruited monocytes contribute to pathogenesis. Indeed, excessive myeloid cell infiltration including monocytes and the resultant recruited macrophages are poor prognosis markers during systemic infection (Benoit, Desnues et al. 2008; Mege, Mehraj et al. 2011; Shi and Pamer 2011; Indramohan, Sieve et al. 2012).

Experimental approaches using infection models with *Salmonella typhi* the agent of typhoid fever, *Salmonella typhimurium* a gastroenteritis agent, and *Mycobacterium tuberculosis* the responsible of pulmonary tuberculosis, demonstrated the importance of M1-like polarization in macrophages for infection resolution (Ehrt, Schnappinger et al. 2001; Chacon-Salinas, Serafin-Lopez et al. 2005). The use of IFN-γ-deficient and IFN-γR-deficient mice was tested during infection with *Chlamydia* and again demonstrated the protective effect of M1-like polarization (Rottenberg, Gigliotti-Rothfuchs et al. 2002). Experiments involving the use of MIF-deficient mice gave special emphasis to the importance of monocyte/macrophage-mediated TNF-α production during bacterial infections. The cytokine macrophage migration inhibitory factor MIF presents a regulatory role for the Toll-like receptor 4. MIF-deficient mice showed reduced TNF-α production, impaired bacterial killing by macrophages and reduced survival after systemic infection (Roger, Delaloye et al. 2013). Additional experiments testing the susceptibility of TNF-α-deficient or IFN-γ-deficient mice and mice deficient in their respective receptors showed again how essential pro-inflammatory cytokines signalling is during infectious disease. All mice deficient for TNF-α, IFN-γ, TNF-αR or IFN-γR died after challenge with *Listeria monocytogenes (Pfeffer, Matsuyama et al. 1993).* However, as mentioned before, excessive or prolonged M1-like polarization is deleterious for the host and can lead between other to septic shock and death. In baboon experimental peritonitis with *Escherichia coli* the M1-like phenotype was prominent in all dead individuals while surviving animals displayed a mixed M1/M2 phenotype (Mehta, Brewington et al. 2004). In human patients with severe sepsis, high concentrations of circulating M1 cytokines and macrophage phenotypes expressing high levels of pro-inflammatory cytokines were correlated with mortality (Lopez-Bojorquez, Dehesa et al. 2004; Bozza, Salluh et al. 2007).

In our model of *Klebsiella pneumoniae* systemic infection, there was a great impact in illness progression, prognosis and survival when infected mice were treated with *in vitro*-derived Ly6C^{hi} cells. Administration of cells accelerated weight loss and dumped survival. Treated mice with Ly6C^{hi} cells reached a mortality rate of 90% within the first three days after inoculation. This fact strongly suggested that the cause of death was septic shock. Reduced numbers of *Klebsiella pneumoniae* CFUs were found in the lungs of mice treated with Ly6C^{hi} cells. This fact could be explained by the presence of the *in vitro* Ly6C^{hi} monocytes. Therefore, the increased mortality rate of mice treated with

Ly6C^{hi} cells was not due to increased spreading of the bacteria. Serum TNF-α levels were boosted in mice treated with Ly6C^{hi} cells compared to control mice. We hypothesized that administered Ly6C^{hi} cells may be the cause of TNF-α lung production and septic shock mediated dead. Likewise, we found increased levels of lung tissue TNF-α in mice treated with Ly6C^{hi} cells, suggesting that the origin of serum TNF-α was the infected lungs. Intrinsic expression of TNF-α from infiltrated Ly6C^{hi} cells was found when we analysed lung tissue sections with LSFCM. This evidence gives strength to our hypothesis that the Ly6C^{hi} cells infiltrated into the infected lungs were the origin of TNF-α production and the cause of the mortality rate increase.

These results again confirm the functional activity of *in vitro*-derived Ly6C^{hi} monocytes i*n vivo*. Once more, we confirm that *in vitro*-derived Ly6C^{hi} monocytes are able to infiltrate within inflamed tissues, differentiate into recruited macrophages and perform active functions. Taken together, we can affirm the detrimental effect that excessive infiltration of monocytes and TNF-α production has in survival prognosis during systemic infection.

In the last place, we decided to test the treatment of Ly6C^{hi} cells in an autoimmune inflammatory model such as the experimental autoimmune encephalomyelitis model (EAE).

The EAE model is a well-studied and generally considered to be a relevant model for the human immune mediated demyelinating disease multiple sclerosis. EAE model is characterized by extensive infiltration of the central nervous system (CNS) by inflammatory cells from both the innate and adaptive immune compartments. During EAE progression several components of the immune system coordinate and counteract to generate progressive demyelination of axonal tracks in the CNS and the final characteristic phenotype of motor paralysis. Even thou the EAE model has extensively demonstrated to be a useful tool for the study of multiple sclerosis, many differences still exist between the human pathology and the mice model (Miller, Karpus et al. 2010; Ajami, Bennett et al. 2011). The experimental autoimmune encephalomyelitis model was induced in C57/B6 mice by active immunization with a myelinic oligodendrocyte glycoprotein peptide (MOG$_{35-55}$) in emulsion with complete Freund´s adjuvant (CFA) containing *Mycobacterium tuberculosis* extract. MOG$_{35-55}$ peptide corresponds to the immunodominant epitope of MOG protein. Immunization was performed by single subdermal injection of the emulsion, and followed by two daily separated intravenous injections of *Bordetella pertussis* toxin. *Bordetella pertussis* toxin administration is essential to permeabilize the hematoencephalic barrier and allow the immune response generated in the periphery to reach the CNS.

Thence, the EAE model allows us to study in a deeper way monocyte infiltration, differentiation and functionality in complex model of autoimmune inflammation.

EAE development consists in two differentiated phases, the induction phase and the effector phase. Initiation of the EAE during the induction phase involves the priming of myelin epitope–specific T cells following immunization and the consequent generation and activation of peripheral myelin-specific TH1 or TH17 cells. Following their peripheral generation, during the effector phase, activated myelin-specific T cells migrate into the CNS after extravasation through the hematoencephalic barrier. Once there, T cells start producing chemokines and cytokines which in turn trigger the expansion of resident microglia and the recruitment of blood-borne myelomonocytic cells into the CNS parenchyma. Resident microglia and recruited monocytes and macrophages activate within the CNS and initiate the process of demyelination of CNS axonal tracts by their phagocytic activity and by the inflammatory and cytotoxic effects of cytokines such as IFN-γ, LT, IL-17, TNF- α, ROS and NO. Myeloid-derived chemokines and pro-inflammatory cytokines will also enhance the pro-inflammatory reaction and recruitment of additional leucocytes (Miller, Karpus et al. 2010; (Saijo and Glass 2011; Jung and Schwartz 2012; Ransohoff and Engelhardt 2012; Heneka, Kummer et al. 2014; Walsh, Muruve et al. 2014). It is proposed that immune-privileged sites such as the CNS allow the entrance of immune cells through two distinct types of gates. The first type of barriers, including the blood-brain barrier (BBB) and the blood-leptomeningeal barrier (BLMB), are composed of tight junction-interconnected endothelium. The BBB and BLMB are associated with destructive inflammation and infiltration of encephalitogenic Th1, Th17 and recruited Ly6C^{hi} monocytes precursors of pro-inflammatory M1-like macrophages. Oppositely, the second type of barrier, the blood-CSF barrier (BCSFB), consists in border structures comprised of fenestrated vasculature enveloped by tightly regulated epithelium, and serve as active and selective immune-skewing gates. The BCSFB is associated with immune regulating properties and infiltration of protective Th2, Treg and recruited Ly6C^{lo} monocytes precursors anti-inflammatory M2-like macrophages. (Shechter, London et al. 2013).

Experimental data with the EAE model using a combination of parabiosis and myeloablation allowing to differentiate properly between resident microglia and recruited populations. The data extracted from this experiments confirmed a strong correlation between monocyte infiltration and progression to the paralytic stage of EAE. Moreover, it was also confirmed that following remission infiltrating monocytes did not contribute to refill the pool of myeloid cells of the CNS. Therefore, infiltrating monocytes play an essential role during pathogenesis and the EAE, but its function is transitory and they do not establish resident populations (Ajami, Bennett et al. 2011). Additional experiments

using the EAE model confirmed an elevation of pro-inflammatory Ly6C^{hi} monocytes in blood at the disease onset. At peak of disease severity, clinical scores were inversely correlated with the proportion of Ly6C^{hi} monocytes in blood and directly correlated with the proportion of Ly6C^{hi} monocytes in the spinal cord. Therapeutic treatment resulting in retention of Ly6C^{hi} monocytes into the blood and reduced entry of Ly6C^{hi} monocytes into the CNS diminished the severity of EAE, confirming the essential role of Ly6C^{hi} monocytes in the pathogenesis of EAE (Mishra, Wang et al. 2012). Multiple experiments including the use of disrupted chemokine receptors in mice settled the strong role of CCR2 during infiltration of Ly6C^{hi} monocytes. CCR2 or CCL2 knock-out or silenced mice showed milder or no progression of the EAE (Gaupp, Pitt et al. 2003; Mahad and Ransohoff 2003; Eltayeb, Berg et al. 2007). Combination of bone-marrow chimerism and gene targeting systems permitted to selectively deplete the Ly6C^{hi} CCR2+ monocyte subset through engagement of CCR2. This caused strong reduction in CNS autoimmunity. This allowed to confirm once more the fundamental role of CCR2-mediated infiltration of Ly6C^{hi} monocytes in the promotion of disease in the EAE model (Mildner, Mack et al. 2009). Further experiments using selective blockage of the granulocyte-macrophage colony stimulating factor (GM-CSF) suggest that Ly6C^{hi} monocytes are mobilized into the bloodstream by a granulocyte-macrophage colony stimulating factor-dependent pathway. These data also suggest that GM-CSF-driven release of Ly6C^{hi} precursors from the bone marrow prevents exhaustion of CNS myeloid populations during chronic autoimmune demyelination (King, Dickendesher et al. 2009; Croxford, Lanzinger et al. 2015). Other experiments based in spinal cord injury models demonstrated that two distinct waves of infiltrating monocytes are recruited through different structures and develop different functions during CNS inflammation. Infiltrating Ly6C^{hi} monocytes are recruited through the BBB in a CCR2-dependent manner and give rise to a pro-inflammatory population of recruited M1-like macrophages. On the other hand, infiltrating Ly6C^{lo} monocytes are recruited through the choroid plexus, included in the BCSFB, in a VCAM1-dependent manner and are primed to provide an anti-inflammatory function and differentiate into resolving M2-like macrophages. Hence, we can affirm that different subsets of monocytes infiltrate the CNS through different gates and have opposite detrimental and beneficial contribution to CNS inflammation (Shechter, Miller et al. 2013). Supplementary experiments with the spinal cord injury model confirmed that only M1-like macrophages are neurotoxic and M2-like alternatively activated macrophages promote a regenerative growth response in adult sensory axons, even in the context of inhibitory substrates that dominate sites of CNS injury. Therefore, modulating monocyte, macrophage and microglia polarization toward an anti-

inflammatory phenotype could promote CNS repair while limiting secondary inflammatory-mediated damage (Kigerl, Gensel et al. 2009).

Treatment with *in vitro*-derived Ly6C^{hi} cells in EAE-induced mice had an impact in illness progression but not average survival. Mice injected with Ly6C^{hi} cells presented reduced clinical scores and weight loss in the acute phase of the disease but reached the same final illness severity as their PBS injected counterparts. IVIS and LSFCM confirmed the capacity of our cells to cross the hematoencephalic barrier, transmigrating from the blood flow into the inflamed CNS. This homing process was not occurring before inflammation was established into the CNS neither when the inflammation reached an advanced stage. There was a specific time window for infiltration in which cells were able to establish within the inflamed tissue. Infiltrating Ly6C^{hi} cells were found to express F4/80. Those cells were localized close to vessels and demyelinating areas of the lumbar spinal cord, and at a less extent in areas of the cervical spinal cord. Thus, we hypothesized a possible implication of infiltrated *in vitro*-generated Ly6C^{hi} cells in tissue protection and better prognosis. More experiments shall be performed in order to truly unravel the effect that *in vitro*-produced Ly6C^{hi} monocyte administration has in CNS inflammation and pathology progression within the EAE model.

These results confirm the functional activity of *in vitro*-derived Ly6C^{hi} monocytes *in vivo*. Once more, we confirm that *in vitro*-derived Ly6C^{hi} monocytes are able to infiltrate within inflamed tissues, differentiate into recruited macrophages and perform active functions.

In conclusion, considering the obtained results from this experimental project we can affirm the phenotypical, migratory and differentiation capacities of *in vitro*-generated Ly6C^{hi} monocytes. *In vitro* Ly6C^{hi} cells are able to transmigrate from the blood flow into the tissues, differentiate into recruited macrophages, actively induce modifications in gene expression, synthetize pro-inflammatory cytokines and induce changes in pathology progression.

Our findings show that *in vitro* generation of Ly6C^{hi} monocytes represents a technique to study the immune involvement, pathogenesis as well as new therapeutic approaches for inflammation-related pathologies. Because of the possibility to manipulate *in vitro* monocytes through cytokine stimulation or using knock-out bone marrow as precursors, monocytes could be a valuable tool to determine the cellular and molecular mechanisms involved in pathogenic inflammation Pre-treatment of Ly6C^{hi} cells with neutralizing antibodies against adhesion molecules and chemokine receptors may help to understand the process of infiltration into the inflamed tissues and lead to new monoclonal antibody therapies. Treatment with knock-out or pre-treated *in vitro* monocytes could induce changes into the adaptive immune system response.

Reprogramming the immune balances through modulation of interleukin microenvironment and antigen presentation could bias the T-cell populations to an anti-inflammatory Th2/Treg or pro-inflammatory Th1/Th17 immune response. Knock-out-derived *in vitro* Ly6C^{hi} monocytes or gene-silenced *in vitro* Ly6C^{hi} monocytes could be a powerful tool to study the genes implicated in the polarization process of monocytes into M1 or M2 macrophage phenotypes during the inflammatory response. Discovery of new therapeutic targets is essential in research for the subsequent design of targeted therapies based on appropriate drugs. Selective migration of monocytes could represent a novel specific targeting technique for drugs.

Essentially*, in vitro* generation of Ly6C^{hi} monocytes seem a living tool that can provide many insights into the mechanisms required for the development of inflammatory diseases. Our hope is to be able to study in a deeper way how the infiltration process occurs and to develop new strategies to modify the microenvironment in different pathologies.

CONCLUSIONS

VII. CONCLUSIONS

In vitro generated Ly6C^{hi} monocytes and mice peripheral blood Ly6C^{hi} pro-inflammatory monocytes present very similar surface markers profile.

Gene expression plasticity following pro- and anti-inflammatory stimuli is a feature of *in vitro* generated Ly6C^{hi} monocytes.

In vitro Ly6C^{hi} monocytes present in vitro differentiation, activation and maturation capacity.

In vitro generated Ly6C^{hi} monocytes are able to infiltrate selectively within the tissues and differentiate into recruited macrophages in diverse *in vivo* models of inflammation.

In vitro generated Ly6C^{hi} monocytes modulate inflammation in diverse mice models up-regulating the expression of pro- or anti-inflammatory genes.

BIBLIOGRAPHY

VIII. BIBLIOGRAPHY

Ajami, B., J. L. Bennett, C. Krieger, K. M. McNagny, and F. M. Rossi. "Infiltrating Monocytes Trigger Eae Progression, but Do Not Contribute to the Resident Microglia Pool." [In eng]. *Nat Neurosci* 14, no. 9 (Sep 2011): 1142-9.

Ajuebor, M. N., A. M. Das, L. Virag, R. J. Flower, C. Szabo, and M. Perretti. "Role of Resident Peritoneal Macrophages and Mast Cells in Chemokine Production and Neutrophil Migration in Acute Inflammation: Evidence for an Inhibitory Loop Involving Endogenous Il-10." [In eng]. *J Immunol* 162, no. 3 (Feb 1 1999): 1685-91.

Arnold, L., A. Henry, F. Poron, Y. Baba-Amer, N. van Rooijen, A. Plonquet, R. K. Gherardi, and B. Chazaud. "Inflammatory Monocytes Recruited after Skeletal Muscle Injury Switch into Antiinflammatory Macrophages to Support Myogenesis." [In eng]. *J Exp Med* 204, no. 5 (May 14 2007): 1057-69.

Arnold, L., H. Perrin, C. B. de Chanville, M. Saclier, P. Hermand, L. Poupel, E. Guyon*, et al.* "Cx3cr1 Deficiency Promotes Muscle Repair and Regeneration by Enhancing Macrophage Apoe Production." [In eng]. *Nat Commun* 6 (2015): 8972.

Auffray, C., D. Fogg, M. Garfa, G. Elain, O. Join-Lambert, S. Kayal, S. Sarnacki*, et al.* "Monitoring of Blood Vessels and Tissues by a Population of Monocytes with Patrolling Behavior." [In eng]. *Science* 317, no. 5838 (Aug 3 2007): 666-70.

Auffray, C., D. K. Fogg, E. Narni-Mancinelli, B. Senechal, C. Trouillet, N. Saederup, J. Leemput*, et al.* "Cx3cr1+ Cd115+ Cd135+ Common Macrophage/Dc Precursors and the Role of Cx3cr1 in Their Response to Inflammation." [In eng]. *J Exp Med* 206, no. 3 (Mar 16 2009): 595-606.

Auffray, C., M. H. Sieweke, and F. Geissmann. "Blood Monocytes: Development, Heterogeneity, and Relationship with Dendritic Cells." [In eng]. *Annu Rev Immunol* 27 (2009): 669-92.

Benoit, M., B. Desnues, and J. L. Mege. "Macrophage Polarization in Bacterial Infections." [In eng]. *J Immunol* 181, no. 6 (Sep 15 2008): 3733-9.

Bernhagen, J., R. Krohn, H. Lue, J. L. Gregory, A. Zernecke, R. R. Koenen, M. Dewor*, et al.* "Mif Is a Noncognate Ligand of Cxc Chemokine Receptors in Inflammatory and Atherogenic Cell Recruitment." [In eng]. *Nat Med* 13, no. 5 (May 2007): 587-96.

Biswas, S. K., and A. Mantovani. "Macrophage Plasticity and Interaction with Lymphocyte Subsets: Cancer as a Paradigm." [In eng]. *Nat Immunol* 11, no. 10 (Oct 2010): 889-96.

Boring, L., J. Gosling, S. W. Chensue, S. L. Kunkel, R. V. Farese, Jr., H. E. Broxmeyer, and I. F. Charo. "Impaired Monocyte Migration and Reduced Type 1 (Th1) Cytokine Responses in C-C Chemokine Receptor 2 Knockout Mice." [In eng]. *J Clin Invest* 100, no. 10 (Nov 15 1997): 2552-61.

Bozza, F. A., J. I. Salluh, A. M. Japiassu, M. Soares, E. F. Assis, R. N. Gomes, M. T. Bozza, H. C. Castro-Faria-Neto, and P. T. Bozza. "Cytokine Profiles as Markers of Disease Severity in Sepsis: A Multiplex Analysis." [In eng]. *Crit Care* 11, no. 2 (2007): R49.

Bradfield, P. F., C. Scheiermann, S. Nourshargh, C. Ody, F. W. Luscinskas, G. E. Rainger, G. B. Nash*, et al.* "Jam-C Regulates Unidirectional Monocyte Transendothelial Migration in Inflammation." [In eng]. *Blood* 110, no. 7 (Oct 1 2007): 2545-55.

Brigitte, M., C. Schilte, A. Plonquet, Y. Baba-Amer, A. Henri, C. Charlier, S. Tajbakhsh*, et al.* "Muscle Resident Macrophages Control the Immune Cell Reaction in a

Mouse Model of Notexin-Induced Myoinjury." [In eng]. *Arthritis Rheum* 62, no. 1 (Jan 2010): 268-79.

Brombacher, F., B. Arendse, R. Peterson, A. Holscher, and C. Holscher. "Analyzing Classical and Alternative Macrophage Activation in Macrophage/Neutrophil-Specific Il-4 Receptor-Alpha-Deficient Mice." [In eng]. *Methods Mol Biol* 531 (2009): 225-52.

Cao, Q., D. C. Harris, and Y. Wang. "Macrophages in Kidney Injury, Inflammation, and Fibrosis." [In eng]. *Physiology (Bethesda)* 30, no. 3 (May 2015): 183-94.

Codarri, L., G. Gyulveszi, V. Tosevski, L. Hesske, A. Fontana, L. Magnenat, T. Suter, and B. Becher. "Rorgammat Drives Production of the Cytokine Gm-Csf in Helper T Cells, Which Is Essential for the Effector Phase of Autoimmune Neuroinflammation." [In eng]. *Nat Immunol* 12, no. 6 (Jun 2011): 560-7.

Comalada, M., J. Xaus, E. Sanchez, A. F. Valledor, and A. Celada. "Macrophage Colony-Stimulating Factor-, Granulocyte-Macrophage Colony-Stimulating Factor-, or Il-3-Dependent Survival of Macrophages, but Not Proliferation, Requires the Expression of P21(Waf1) through the Phosphatidylinositol 3-Kinase/Akt Pathway." [In eng]. *Eur J Immunol* 34, no. 8 (Aug 2004): 2257-67.

Condeelis, J., and J. W. Pollard. "Macrophages: Obligate Partners for Tumor Cell Migration, Invasion, and Metastasis." [In eng]. *Cell* 124, no. 2 (Jan 27 2006): 263-6.

Croxford, A. L., M. Lanzinger, F. J. Hartmann, B. Schreiner, F. Mair, P. Pelczar, B. E. Clausen*, et al.* "The Cytokine Gm-Csf Drives the Inflammatory Signature of Ccr2+ Monocytes and Licenses Autoimmunity." [In eng]. *Immunity* 43, no. 3 (Sep 15 2015): 502-14.

Chacon-Salinas, R., J. Serafin-Lopez, R. Ramos-Payan, P. Mendez-Aragon, R. Hernandez-Pando, D. Van Soolingen, L. Flores-Romo, S. Estrada-Parra, and I. Estrada-Garcia. "Differential Pattern of Cytokine Expression by Macrophages Infected in Vitro with Different Mycobacterium Tuberculosis Genotypes." [In eng]. *Clin Exp Immunol* 140, no. 3 (Jun 2005): 443-9.

Chazaud, B., M. Brigitte, H. Yacoub-Youssef, L. Arnold, R. Gherardi, C. Sonnet, P. Lafuste, and F. Chretien. "Dual and Beneficial Roles of Macrophages During Skeletal Muscle Regeneration." [In eng]. *Exerc Sport Sci Rev* 37, no. 1 (Jan 2009): 18-22.

Chitnis, T., N. Najafian, C. Benou, A. D. Salama, M. J. Grusby, M. H. Sayegh, and S. J. Khoury. "Effect of Targeted Disruption of Stat4 and Stat6 on the Induction of Experimental Autoimmune Encephalomyelitis." [In eng]. *J Clin Invest* 108, no. 5 (Sep 2001): 739-47.

Chow, A., B. D. Brown, and M. Merad. "Studying the Mononuclear Phagocyte System in the Molecular Age." [In eng]. *Nat Rev Immunol* 11, no. 11 (Nov 2011): 788-98.

Christensen, A. D., S. Skov, and C. Haase. "The Role of Neutrophils and G-Csf in Dnfb-Induced Contact Hypersensitivity in Mice." [In eng]. *Immun Inflamm Dis* 2, no. 1 (Jun 2014): 21-34.

Dai, X. M., G. R. Ryan, A. J. Hapel, M. G. Dominguez, R. G. Russell, S. Kapp, V. Sylvestre, and E. R. Stanley. "Targeted Disruption of the Mouse Colony-Stimulating Factor 1 Receptor Gene Results in Osteopetrosis, Mononuclear Phagocyte Deficiency, Increased Primitive Progenitor Cell Frequencies, and Reproductive Defects." [In eng]. *Blood* 99, no. 1 (Jan 1 2002): 111-20.

Darnell, J. E., Jr., I. M. Kerr, and G. R. Stark. "Jak-Stat Pathways and Transcriptional Activation in Response to Ifns and Other Extracellular Signaling Proteins." [In eng]. *Science* 264, no. 5164 (Jun 3 1994): 1415-21.

Das, A., M. Sinha, S. Datta, M. Abas, S. Chaffee, C. K. Sen, and S. Roy. "Monocyte and Macrophage Plasticity in Tissue Repair and Regeneration." [In eng]. *Am J Pathol* 185, no. 10 (Oct 2015): 2596-606.

De Palma, M., M. A. Venneri, R. Galli, L. Sergi Sergi, L. S. Politi, M. Sampaolesi, and L. Naldini. "Tie2 Identifies a Hematopoietic Lineage of Proangiogenic Monocytes Required for Tumor Vessel Formation and a Mesenchymal Population of Pericyte Progenitors." [In eng]. *Cancer Cell* 8, no. 3 (Sep 2005): 211-26.

Delneste, Y., P. Charbonnier, N. Herbault, G. Magistrelli, G. Caron, J. Y. Bonnefoy, and P. Jeannin. "Interferon-Gamma Switches Monocyte Differentiation from Dendritic Cells to Macrophages." [In eng]. *Blood* 101, no. 1 (Jan 1 2003): 143-50.

Dranoff, G. "Cytokines in Cancer Pathogenesis and Cancer Therapy." [In eng]. *Nat Rev Cancer* 4, no. 1 (Jan 2004): 11-22.

Du, R., K. V. Lu, C. Petritsch, P. Liu, R. Ganss, E. Passegue, H. Song*, et al.* "Hif1alpha Induces the Recruitment of Bone Marrow-Derived Vascular Modulatory Cells to Regulate Tumor Angiogenesis and Invasion." [In eng]. *Cancer Cell* 13, no. 3 (Mar 2008): 206-20.

Durbin, J. E., R. Hackenmiller, M. C. Simon, and D. E. Levy. "Targeted Disruption of the Mouse Stat1 Gene Results in Compromised Innate Immunity to Viral Disease." [In eng]. *Cell* 84, no. 3 (Feb 9 1996): 443-50.

Ehrt, S., D. Schnappinger, S. Bekiranov, J. Drenkow, S. Shi, T. R. Gingeras, T. Gaasterland, G. Schoolnik, and C. Nathan. "Reprogramming of the Macrophage Transcriptome in Response to Interferon-Gamma and Mycobacterium Tuberculosis: Signaling Roles of Nitric Oxide Synthase-2 and Phagocyte Oxidase." [In eng]. *J Exp Med* 194, no. 8 (Oct 15 2001): 1123-40.

El-Behi, M., B. Ciric, H. Dai, Y. Yan, M. Cullimore, F. Safavi, G. X. Zhang, B. N. Dittel, and A. Rostami. "The Encephalitogenicity of T(H)17 Cells Is Dependent on Il-1- and Il-23-Induced Production of the Cytokine Gm-Csf." [In eng]. *Nat Immunol* 12, no. 6 (Jun 2011): 568-75.

Eltayeb, S., A. L. Berg, H. Lassmann, E. Wallstrom, M. Nilsson, T. Olsson, A. Ericsson-Dahlstrand, and D. Sunnemark. "Temporal Expression and Cellular Origin of Cc Chemokine Receptors Ccr1, Ccr2 and Ccr5 in the Central Nervous System: Insight into Mechanisms of Mog-Induced Eae." [In eng]. *J Neuroinflammation* 4 (2007): 14.

Epelman, S., K. J. Lavine, and G. J. Randolph. "Origin and Functions of Tissue Macrophages." [In eng]. *Immunity* 41, no. 1 (Jul 17 2014): 21-35.

Fischer, K., R. Andreesen, and A. Mackensen. "An Improved Flow Cytometric Assay for the Determination of Cytotoxic T Lymphocyte Activity." [In eng]. *J Immunol Methods* 259, no. 1-2 (Jan 1 2002): 159-69.

Forbes, S. J., and N. Rosenthal. "Preparing the Ground for Tissue Regeneration: From Mechanism to Therapy." [In eng]. *Nat Med* 20, no. 8 (Aug 2014): 857-69.

Franklin, R. A., and M. O. Li. "Ontogeny of Tumor-Associated Macrophages and Its Implication in Cancer Regulation." [In Eng]. *Trends Cancer* 2, no. 1 (Oct 1 2016): 20-34.

Gaupp, S., D. Pitt, W. A. Kuziel, B. Cannella, and C. S. Raine. "Experimental Autoimmune Encephalomyelitis (Eae) in Ccr2(-/-) Mice: Susceptibility in Multiple Strains." [In eng]. *Am J Pathol* 162, no. 1 (Jan 2003): 139-50.

Geissmann, F., S. Gordon, D. A. Hume, A. M. Mowat, and G. J. Randolph. "Unravelling Mononuclear Phagocyte Heterogeneity." [In eng]. *Nat Rev Immunol* 10, no. 6 (Jun 2010): 453-60.

Geissmann, F., S. Jung, and D. R. Littman. "Blood Monocytes Consist of Two Principal Subsets with Distinct Migratory Properties." [In eng]. *Immunity* 19, no. 1 (Jul 2003): 71-82.

Geissmann, F., M. G. Manz, S. Jung, M. H. Sieweke, M. Merad, and K. Ley. "Development of Monocytes, Macrophages, and Dendritic Cells." [In eng]. *Science* 327, no. 5966 (Feb 5 2010): 656-61.

Ginhoux, F., and S. Jung. "Monocytes and Macrophages: Developmental Pathways and Tissue Homeostasis." [In eng]. *Nat Rev Immunol* 14, no. 6 (Jun 2014): 392-404.

Gordon, S., and F. O. Martinez. "Alternative Activation of Macrophages: Mechanism and Functions." [In eng]. *Immunity* 32, no. 5 (May 28 2010): 593-604.

Gordon, S., and P. R. Taylor. "Monocyte and Macrophage Heterogeneity." [In eng]. *Nat Rev Immunol* 5, no. 12 (Dec 2005): 953-64.

Guilliams, M., F. Ginhoux, C. Jakubzick, S. H. Naik, N. Onai, B. U. Schraml, E. Segura, R. Tussiwand, and S. Yona. "Dendritic Cells, Monocytes and Macrophages: A Unified Nomenclature Based on Ontogeny." [In eng]. *Nat Rev Immunol* 14, no. 8 (Aug 2014): 571-8.

Handel, T. M., Z. Johnson, D. H. Rodrigues, A. C. Dos Santos, R. Cirillo, V. Muzio, S. Riva*, et al.* "An Engineered Monomer of Ccl2 Has Anti-Inflammatory Properties Emphasizing the Importance of Oligomerization for Chemokine Activity in Vivo." [In eng]. *J Leukoc Biol* 84, no. 4 (Oct 2008): 1101-8.

Hart, P. H., G. F. Vitti, D. R. Burgess, G. A. Whitty, D. S. Piccoli, and J. A. Hamilton. "Potential Antiinflammatory Effects of Interleukin 4: Suppression of Human Monocyte Tumor Necrosis Factor Alpha, Interleukin 1, and Prostaglandin E2." [In eng]. *Proc Natl Acad Sci U S A* 86, no. 10 (May 1989): 3803-7.

Helmke, S., and B. D. Howard. "Mechanism of Inhibition of Calcium Uptake into Sarcoplasmic Reticulum by Notexin, a Neurotoxic and Myotoxic Polypeptide." [In eng]. *Membr Biochem* 6, no. 3 (1986): 239-53.

Henderson, R. B., J. A. Hobbs, M. Mathies, and N. Hogg. "Rapid Recruitment of Inflammatory Monocytes Is Independent of Neutrophil Migration." [In eng]. *Blood* 102, no. 1 (Jul 1 2003): 328-35.

Hendriks, J. J., C. E. Teunissen, H. E. de Vries, and C. D. Dijkstra. "Macrophages and Neurodegeneration." [In eng]. *Brain Res Brain Res Rev* 48, no. 2 (Apr 2005): 185-95.

Heneka, M. T., M. P. Kummer, and E. Latz. "Innate Immune Activation in Neurodegenerative Disease." [In eng]. *Nat Rev Immunol* 14, no. 7 (Jul 2014): 463-77.

Hillman, E. M. "Optical Brain Imaging in Vivo: Techniques and Applications from Animal to Man." [In eng]. *J Biomed Opt* 12, no. 5 (Sep-Oct 2007): 051402.

Hoffman, R. M. "In Vivo Imaging of Metastatic Cancer with Fluorescent Proteins." [In eng]. *Cell Death Differ* 9, no. 8 (Aug 2002): 786-9.

Hume, D. A., and K. P. MacDonald. "Therapeutic Applications of Macrophage Colony-Stimulating Factor-1 (Csf-1) and Antagonists of Csf-1 Receptor (Csf-1r) Signaling." [In eng]. *Blood* 119, no. 8 (Feb 23 2012): 1810-20.

Imhof, B. A., and M. Aurrand-Lions. "Adhesion Mechanisms Regulating the Migration of Monocytes." [In eng]. *Nat Rev Immunol* 4, no. 6 (Jun 2004): 432-44.

Indramohan, M., A. N. Sieve, T. J. Break, and R. E. Berg. "Inflammatory Monocyte Recruitment Is Regulated by Interleukin-23 During Systemic Bacterial Infection." [In eng]. *Infect Immun* 80, no. 12 (Dec 2012): 4099-105.

Italiani, P., and D. Boraschi. "From Monocytes to M1/M2 Macrophages: Phenotypical Vs. Functional Differentiation." [In eng]. *Front Immunol* 5 (2014): 514.

Jenkins, S. J., and D. A. Hume. "Homeostasis in the Mononuclear Phagocyte System." [In eng]. *Trends Immunol* 35, no. 8 (Aug 2014): 358-67.

Jenkins, S. J., D. Ruckerl, P. C. Cook, L. H. Jones, F. D. Finkelman, N. van Rooijen, A. S. MacDonald, and J. E. Allen. "Local Macrophage Proliferation, Rather Than

Recruitment from the Blood, Is a Signature of Th2 Inflammation." [In eng]. *Science* 332, no. 6035 (Jun 10 2011): 1284-8.

Jia, T., N. V. Serbina, K. Brandl, M. X. Zhong, I. M. Leiner, I. F. Charo, and E. G. Pamer. "Additive Roles for Mcp-1 and Mcp-3 in Ccr2-Mediated Recruitment of Inflammatory Monocytes During Listeria Monocytogenes Infection." [In eng]. *J Immunol* 180, no. 10 (May 15 2008): 6846-53.

Jung, S., and M. Schwartz. "Non-Identical Twins - Microglia and Monocyte-Derived Macrophages in Acute Injury and Autoimmune Inflammation." [In eng]. *Front Immunol* 3 (2012): 89.

Kaufmann, A., R. Salentin, D. Gemsa, and H. Sprenger. "Increase of Ccr1 and Ccr5 Expression and Enhanced Functional Response to Mip-1 Alpha During Differentiation of Human Monocytes to Macrophages." [In eng]. *J Leukoc Biol* 69, no. 2 (Feb 2001): 248-52.

Kigerl, K. A., J. C. Gensel, D. P. Ankeny, J. K. Alexander, D. J. Donnelly, and P. G. Popovich. "Identification of Two Distinct Macrophage Subsets with Divergent Effects Causing Either Neurotoxicity or Regeneration in the Injured Mouse Spinal Cord." [In eng]. *J Neurosci* 29, no. 43 (Oct 28 2009): 13435-44.

King, I. L., T. L. Dickendesher, and B. M. Segal. "Circulating Ly-6c+ Myeloid Precursors Migrate to the Cns and Play a Pathogenic Role During Autoimmune Demyelinating Disease." [In eng]. *Blood* 113, no. 14 (Apr 2 2009): 3190-7.

Klimuk, S. K., S. C. Semple, P. Scherrer, and M. J. Hope. "Contact Hypersensitivity: A Simple Model for the Characterization of Disease-Site Targeting by Liposomes." [In eng]. *Biochim Biophys Acta* 1417, no. 2 (Mar 4 1999): 191-201.

Kurihara, T., G. Warr, J. Loy, and R. Bravo. "Defects in Macrophage Recruitment and Host Defense in Mice Lacking the Ccr2 Chemokine Receptor." [In eng]. *J Exp Med* 186, no. 10 (Nov 17 1997): 1757-62.

Kuziel, W. A., S. J. Morgan, T. C. Dawson, S. Griffin, O. Smithies, K. Ley, and N. Maeda. "Severe Reduction in Leukocyte Adhesion and Monocyte Extravasation in Mice Deficient in Cc Chemokine Receptor 2." [In eng]. *Proc Natl Acad Sci U S A* 94, no. 22 (Oct 28 1997): 12053-8.

Lam, D., D. Harris, and Z. Qin. "Inflammatory Mediator Profiling Reveals Immune Properties of Chemotactic Gradients and Macrophage Mediator Production Inhibition During Thioglycollate Elicited Peritoneal Inflammation." [In eng]. *Mediators Inflamm* 2013 (2013): 931562.

Lawrence, T., and G. Natoli. "Transcriptional Regulation of Macrophage Polarization: Enabling Diversity with Identity." [In eng]. *Nat Rev Immunol* 11, no. 11 (Nov 2011): 750-61.

Lehtonen, A., H. Ahlfors, V. Veckman, M. Miettinen, R. Lahesmaa, and I. Julkunen. "Gene Expression Profiling During Differentiation of Human Monocytes to Macrophages or Dendritic Cells." [In eng]. *J Leukoc Biol* 82, no. 3 (Sep 2007): 710-20.

Levings, M. K., and J. W. Schrader. "Il-4 Inhibits the Production of Tnf-Alpha and Il-12 by Stat6-Dependent and -Independent Mechanisms." [In eng]. *J Immunol* 162, no. 9 (May 1 1999): 5224-9.

Lopez-Bojorquez, L. N., A. Z. Dehesa, and G. Reyes-Teran. "Molecular Mechanisms Involved in the Pathogenesis of Septic Shock." [In eng]. *Arch Med Res* 35, no. 6 (Nov-Dec 2004): 465-79.

Mack, M., J. Cihak, C. Simonis, B. Luckow, A. E. Proudfoot, J. Plachy, H. Bruhl*, et al.* "Expression and Characterization of the Chemokine Receptors Ccr2 and Ccr5 in Mice." [In eng]. *J Immunol* 166, no. 7 (Apr 1 2001): 4697-704.

Mackler, A. M., L. M. Green, P. J. McMillan, and S. M. Yellon. "Distribution and Activation of Uterine Mononuclear Phagocytes in Peripartum Endometrium and

Myometrium of the Mouse." [In eng]. *Biol Reprod* 62, no. 5 (May 2000): 1193-200.

Mahad, D. J., and R. M. Ransohoff. "The Role of Mcp-1 (Ccl2) and Ccr2 in Multiple Sclerosis and Experimental Autoimmune Encephalomyelitis (Eae)." [In eng]. *Semin Immunol* 15, no. 1 (Feb 2003): 23-32.

Mansilla, M. J., C. Selles-Moreno, S. Fabregas-Puig, J. Amoedo, J. Navarro-Barriuso, A. Teniente-Serra, L. Grau-Lopez, C. Ramo-Tello, and E. M. Martinez-Caceres. "Beneficial Effect of Tolerogenic Dendritic Cells Pulsed with Mog Autoantigen in Experimental Autoimmune Encephalomyelitis." [In eng]. *CNS Neurosci Ther* 21, no. 3 (Mar 2015): 222-30.

Mantovani, A., A. Sica, and M. Locati. "Macrophage Polarization Comes of Age." [In eng]. *Immunity* 23, no. 4 (Oct 2005): 344-6.

March, C., V. Cano, D. Moranta, E. Llobet, C. Perez-Gutierrez, J. M. Tomas, T. Suarez, J. Garmendia, and J. A. Bengoechea. "Role of Bacterial Surface Structures on the Interaction of Klebsiella Pneumoniae with Phagocytes." [In eng]. *PLoS One* 8, no. 2 (2013): e56847.

Martinez, F. O., and S. Gordon. "The M1 and M2 Paradigm of Macrophage Activation: Time for Reassessment." [In eng]. *F1000Prime Rep* 6 (2014): 13.

Mege, J. L., V. Mehraj, and C. Capo. "Macrophage Polarization and Bacterial Infections." [In eng]. *Curr Opin Infect Dis* 24, no. 3 (Jun 2011): 230-4.

Mehta, A., R. Brewington, M. Chatterji, M. Zoubine, G. T. Kinasewitz, G. T. Peer, A. C. Chang, F. B. Taylor, Jr., and A. Shnyra. "Infection-Induced Modulation of M1 and M2 Phenotypes in Circulating Monocytes: Role in Immune Monitoring and Early Prognosis of Sepsis." [In eng]. *Shock* 22, no. 5 (Nov 2004): 423-30.

Meraz, M. A., J. M. White, K. C. Sheehan, E. A. Bach, S. J. Rodig, A. S. Dighe, D. H. Kaplan*, et al.* "Targeted Disruption of the Stat1 Gene in Mice Reveals Unexpected Physiologic Specificity in the Jak-Stat Signaling Pathway." [In eng]. *Cell* 84, no. 3 (Feb 9 1996): 431-42.

Mildner, A., M. Mack, H. Schmidt, W. Bruck, M. Djukic, M. D. Zabel, A. Hille, J. Priller, and M. Prinz. "Ccr2+Ly-6chi Monocytes Are Crucial for the Effector Phase of Autoimmunity in the Central Nervous System." [In eng]. *Brain* 132, no. Pt 9 (Sep 2009): 2487-500.

Miller, S. D., and W. J. Karpus. "Experimental Autoimmune Encephalomyelitis in the Mouse." [In eng]. *Curr Protoc Immunol* Chapter 15 (May 2007): Unit 15 1.

Miller, S. D., W. J. Karpus, and T. S. Davidson. "Experimental Autoimmune Encephalomyelitis in the Mouse." [In eng]. *Curr Protoc Immunol* Chapter 15 (Feb 2010): Unit 15 1.

Mishra, M. K., J. Wang, C. Silva, M. Mack, and V. W. Yong. "Kinetics of Proinflammatory Monocytes in a Model of Multiple Sclerosis and Its Perturbation by Laquinimod." [In eng]. *Am J Pathol* 181, no. 2 (Aug 2012): 642-51.

Mitchell, A. J., B. Roediger, and W. Weninger. "Monocyte Homeostasis and the Plasticity of Inflammatory Monocytes." [In eng]. *Cell Immunol* 291, no. 1-2 (Sep-Oct 2014): 22-31.

Moranta, D., V. Regueiro, C. March, E. Llobet, J. Margareto, E. Larrarte, J. Garmendia, and J. A. Bengoechea. "Klebsiella Pneumoniae Capsule Polysaccharide Impedes the Expression of Beta-Defensins by Airway Epithelial Cells." [In eng]. *Infect Immun* 78, no. 3 (Mar 2010): 1135-46.

Mosser, D. M., and J. P. Edwards. "Exploring the Full Spectrum of Macrophage Activation." [In eng]. *Nat Rev Immunol* 8, no. 12 (Dec 2008): 958-69.

Murray, P. J., J. E. Allen, S. K. Biswas, E. A. Fisher, D. W. Gilroy, S. Goerdt, S. Gordon*, et al.* "Macrophage Activation and Polarization: Nomenclature and Experimental Guidelines." [In eng]. *Immunity* 41, no. 1 (Jul 17 2014): 14-20.

Murray, P. J., and T. A. Wynn. "Protective and Pathogenic Functions of Macrophage Subsets." [In eng]. *Nat Rev Immunol* 11, no. 11 (Nov 2011): 723-37.

Nahrendorf, M., F. K. Swirski, E. Aikawa, L. Stangenberg, T. Wurdinger, J. L. Figueiredo, P. Libby, R. Weissleder, and M. J. Pittet. "The Healing Myocardium Sequentially Mobilizes Two Monocyte Subsets with Divergent and Complementary Functions." [In eng]. *J Exp Med* 204, no. 12 (Nov 26 2007): 3037-47.

Nascimento, M., S. C. Huang, A. Smith, B. Everts, W. Lam, E. Bassity, E. L. Gautier, G. J. Randolph, and E. J. Pearce. "Ly6chi Monocyte Recruitment Is Responsible for Th2 Associated Host-Protective Macrophage Accumulation in Liver Inflammation Due to Schistosomiasis." [In eng]. *PLoS Pathog* 10, no. 8 (Aug 2014): e1004282.

Natoli, G., and S. Monticelli. "Macrophage Activation: Glancing into Diversity." [In eng]. *Immunity* 40, no. 2 (Feb 20 2014): 175-7.

Onai, N., and T. Ohteki. "Bipotent or Oligopotent? A Macrophage and Dc Progenitor Revisited." [In eng]. *Immunity* 41, no. 1 (Jul 17 2014): 5-7.

Paolicelli, R. C., G. Bolasco, F. Pagani, L. Maggi, M. Scianni, P. Panzanelli, M. Giustetto*, et al.* "Synaptic Pruning by Microglia Is Necessary for Normal Brain Development." [In eng]. *Science* 333, no. 6048 (Sep 9 2011): 1456-8.

Peranzoni, E., S. Zilio, I. Marigo, L. Dolcetti, P. Zanovello, S. Mandruzzato, and V. Bronte. "Myeloid-Derived Suppressor Cell Heterogeneity and Subset Definition." [In eng]. *Curr Opin Immunol* 22, no. 2 (Apr 2010): 238-44.

Pfeffer, K., T. Matsuyama, T. M. Kundig, A. Wakeham, K. Kishihara, A. Shahinian, K. Wiegmann*, et al.* "Mice Deficient for the 55 Kd Tumor Necrosis Factor Receptor Are Resistant to Endotoxic Shock, yet Succumb to L. Monocytogenes Infection." [In eng]. *Cell* 73, no. 3 (May 7 1993): 457-67.

Poon, I. K., C. D. Lucas, A. G. Rossi, and K. S. Ravichandran. "Apoptotic Cell Clearance: Basic Biology and Therapeutic Potential." [In eng]. *Nat Rev Immunol* 14, no. 3 (Mar 2014): 166-80.

Prinz, M., and J. Priller. "Microglia and Brain Macrophages in the Molecular Age: From Origin to Neuropsychiatric Disease." [In eng]. *Nat Rev Neurosci* 15, no. 5 (May 2014): 300-12.

Pucci, F., M. A. Venneri, D. Biziato, A. Nonis, D. Moi, A. Sica, C. Di Serio, L. Naldini, and M. De Palma. "A Distinguishing Gene Signature Shared by Tumor-Infiltrating Tie2-Expressing Monocytes, Blood "Resident" Monocytes, and Embryonic Macrophages Suggests Common Functions and Developmental Relationships." [In eng]. *Blood* 114, no. 4 (Jul 23 2009): 901-14.

Ransohoff, R. M., and B. Engelhardt. "The Anatomical and Cellular Basis of Immune Surveillance in the Central Nervous System." [In eng]. *Nat Rev Immunol* 12, no. 9 (Sep 2012): 623-35.

Regueiro, V., D. Moranta, M. A. Campos, J. Margareto, J. Garmendia, and J. A. Bengoechea. "Klebsiella Pneumoniae Increases the Levels of Toll-Like Receptors 2 and 4 in Human Airway Epithelial Cells." [In eng]. *Infect Immun* 77, no. 2 (Feb 2009): 714-24.

Roger, T., J. Delaloye, A. L. Chanson, M. Giddey, D. Le Roy, and T. Calandra. "Macrophage Migration Inhibitory Factor Deficiency Is Associated with Impaired Killing of Gram-Negative Bacteria by Macrophages and Increased Susceptibility to Klebsiella Pneumoniae Sepsis." [In eng]. *J Infect Dis* 207, no. 2 (Jan 15 2013): 331-9.

Rosen, H., and S. Gordon. "Monoclonal Antibody to the Murine Type 3 Complement Receptor Inhibits Adhesion of Myelomonocytic Cells in Vitro and Inflammatory Cell Recruitment in Vivo." [In eng]. *J Exp Med* 166, no. 6 (Dec 1 1987): 1685-701.

Rottenberg, M. E., A. Gigliotti-Rothfuchs, and H. Wigzell. "The Role of Ifn-Gamma in the Outcome of Chlamydial Infection." [In eng]. *Curr Opin Immunol* 14, no. 4 (Aug 2002): 444-51.

Ruckerl, D., and J. E. Allen. "Macrophage Proliferation, Provenance, and Plasticity in Macroparasite Infection." [In eng]. *Immunol Rev* 262, no. 1 (Nov 2014): 113-33.

Rukavina, T., B. Ticac, M. Susa, N. Jendrike, S. Jonjic, P. Lucin, R. Marre, M. Doric, and M. Trautmann. "Protective Effect of Antilipopolysaccharide Monoclonal Antibody in Experimental Klebsiella Infection." [In eng]. *Infect Immun* 65, no. 5 (May 1997): 1754-60.

Saijo, K., and C. K. Glass. "Microglial Cell Origin and Phenotypes in Health and Disease." [In eng]. *Nat Rev Immunol* 11, no. 11 (Nov 2011): 775-87.

Shechter, R., A. London, and M. Schwartz. "Orchestrated Leukocyte Recruitment to Immune-Privileged Sites: Absolute Barriers Versus Educational Gates." [In eng]. *Nat Rev Immunol* 13, no. 3 (Mar 2013): 206-18.

Shechter, R., A. London, C. Varol, C. Raposo, M. Cusimano, G. Yovel, A. Rolls*, et al.* "Infiltrating Blood-Derived Macrophages Are Vital Cells Playing an Anti-Inflammatory Role in Recovery from Spinal Cord Injury in Mice." [In eng]. *PLoS Med* 6, no. 7 (Jul 2009): e1000113.

Shechter, R., O. Miller, G. Yovel, N. Rosenzweig, A. London, J. Ruckh, K. W. Kim*, et al.* "Recruitment of Beneficial M2 Macrophages to Injured Spinal Cord Is Orchestrated by Remote Brain Choroid Plexus." [In eng]. *Immunity* 38, no. 3 (Mar 21 2013): 555-69.

Shi, C., and E. G. Pamer. "Monocyte Recruitment During Infection and Inflammation." [In eng]. *Nat Rev Immunol* 11, no. 11 (Nov 2011): 762-74.

Si, Y., C. L. Tsou, K. Croft, and I. F. Charo. "Ccr2 Mediates Hematopoietic Stem and Progenitor Cell Trafficking to Sites of Inflammation in Mice." [In eng]. *J Clin Invest* 120, no. 4 (Apr 2010): 1192-203.

Sica, A., and A. Mantovani. "Macrophage Plasticity and Polarization: In Vivo Veritas." [In eng]. *J Clin Invest* 122, no. 3 (Mar 2012): 787-95.

Sunderkotter, C., M. Goebeler, K. Schulze-Osthoff, R. Bhardwaj, and C. Sorg. "Macrophage-Derived Angiogenesis Factors." [In eng]. *Pharmacol Ther* 51, no. 2 (1991): 195-216.

Swirski, F. K., M. Nahrendorf, M. Etzrodt, M. Wildgruber, V. Cortez-Retamozo, P. Panizzi, J. L. Figueiredo*, et al.* "Identification of Splenic Reservoir Monocytes and Their Deployment to Inflammatory Sites." [In eng]. *Science* 325, no. 5940 (Jul 31 2009): 612-6.

Takahashi, M., C. Galligan, L. Tessarollo, and T. Yoshimura. "Monocyte Chemoattractant Protein-1 (Mcp-1), Not Mcp-3, Is the Primary Chemokine Required for Monocyte Recruitment in Mouse Peritonitis Induced with Thioglycollate or Zymosan A." [In eng]. *J Immunol* 183, no. 5 (Sep 1 2009): 3463-71.

Takeda, K., M. Kamanaka, T. Tanaka, T. Kishimoto, and S. Akira. "Impaired Il-13-Mediated Functions of Macrophages in Stat6-Deficient Mice." [In eng]. *J Immunol* 157, no. 8 (Oct 15 1996): 3220-2.

Takeda, K., T. Tanaka, W. Shi, M. Matsumoto, M. Minami, S. Kashiwamura, K. Nakanishi*, et al.* "Essential Role of Stat6 in Il-4 Signalling." [In eng]. *Nature* 380, no. 6575 (Apr 18 1996): 627-30.

Tamoutounour, S., M. Guilliams, F. Montanana Sanchis, H. Liu, D. Terhorst, C. Malosse, E. Pollet*, et al.* "Origins and Functional Specialization of Macrophages and of Conventional and Monocyte-Derived Dendritic Cells in Mouse Skin." [In eng]. *Immunity* 39, no. 5 (Nov 14 2013): 925-38.

Tang, Q., P. Zou, H. Jin, J. Fu, J. Yang, L. Shang, and X. Wei. "Grape-Seed Proanthocyanidins Ameliorate Contact Hypersensitivity Induced by 2,4-

Dinitrofluorobenzene (Dnfb) and Inhibit T Cell Proliferation in Vitro." [In eng]. *Toxicol Lett* 210, no. 1 (Apr 5 2012): 1-8.

Tedder, T. F., D. A. Steeber, and P. Pizcueta. "L-Selectin-Deficient Mice Have Impaired Leukocyte Recruitment into Inflammatory Sites." [In eng]. *J Exp Med* 181, no. 6 (Jun 1 1995): 2259-64.

Tomas, J. M., S. Camprubi, S. Merino, M. R. Davey, and P. Williams. "Surface Exposure of O1 Serotype Lipopolysaccharide in Klebsiella Pneumoniae Strains Expressing Different K Antigens." [In eng]. *Infect Immun* 59, no. 6 (Jun 1991): 2006-11.

Tuckermann, J. P., A. Kleiman, R. Moriggl, R. Spanbroek, A. Neumann, A. Illing, B. E. Clausen*, et al.* "Macrophages and Neutrophils Are the Targets for Immune Suppression by Glucocorticoids in Contact Allergy." [In eng]. *J Clin Invest* 117, no. 5 (May 2007): 1381-90.

Vadivelu, R. K., C. H. Ooi, R. Q. Yao, J. Tello Velasquez, E. Pastrana, J. Diaz-Nido, F. Lim*, et al.* "Generation of Three-Dimensional Multiple Spheroid Model of Olfactory Ensheathing Cells Using Floating Liquid Marbles." [In eng]. *Sci Rep* 5 (2015): 15083.

van Furth, R., and Z. A. Cohn. "The Origin and Kinetics of Mononuclear Phagocytes." [In eng]. *J Exp Med* 128, no. 3 (Sep 1 1968): 415-35.

Vanbervliet, B., B. Homey, I. Durand, C. Massacrier, S. Ait-Yahia, O. de Bouteiller, A. Vicari, and C. Caux. "Sequential Involvement of Ccr2 and Ccr6 Ligands for Immature Dendritic Cell Recruitment: Possible Role at Inflamed Epithelial Surfaces." [In eng]. *Eur J Immunol* 32, no. 1 (Jan 2002): 231-42.

Walsh, J. G., D. A. Muruve, and C. Power. "Inflammasomes in the Cns." [In eng]. *Nat Rev Neurosci* 15, no. 2 (Feb 2014): 84-97.

Wang, H., D. W. Melton, L. Porter, Z. U. Sarwar, L. M. McManus, and P. K. Shireman. "Altered Macrophage Phenotype Transition Impairs Skeletal Muscle Regeneration." [In eng]. *Am J Pathol* 184, no. 4 (Apr 2014): 1167-84.

Yang, C. C., and L. S. Chang. "Dissociation of Lethal Toxicity and Enzymic Activity of Notexin from Notechis Scutatus Scutatus (Australian-Tiger-Snake) Venom by Modification of Tyrosine Residues." [In eng]. *Biochem J* 280 (Pt 3) (Dec 15 1991): 739-44.

Yang, J., L. Zhang, C. Yu, X. F. Yang, and H. Wang. "Monocyte and Macrophage Differentiation: Circulation Inflammatory Monocyte as Biomarker for Inflammatory Diseases." [In eng]. *Biomark Res* 2, no. 1 (2014): 1.

Yona, S., and S. Jung. "Monocytes: Subsets, Origins, Fates and Functions." [In eng]. *Curr Opin Hematol* 17, no. 1 (Jan 2010): 53-9.

Yona, S., K. W. Kim, Y. Wolf, A. Mildner, D. Varol, M. Breker, D. Strauss-Ayali*, et al.* "Fate Mapping Reveals Origins and Dynamics of Monocytes and Tissue Macrophages under Homeostasis." [In eng]. *Immunity* 38, no. 1 (Jan 24 2013): 79-91.

Yu, V. L., D. S. Hansen, W. C. Ko, A. Sagnimeni, K. P. Klugman, A. von Gottberg, H. Goossens, M. M. Wagener, and V. J. Benedi. "Virulence Characteristics of Klebsiella and Clinical Manifestations of K. Pneumoniae Bloodstream Infections." [In eng]. *Emerg Infect Dis* 13, no. 7 (Jul 2007): 986-93.

Zaslona, Z., S. Przybranowski, C. Wilke, N. van Rooijen, S. Teitz-Tennenbaum, J. J. Osterholzer, J. E. Wilkinson, B. B. Moore, and M. Peters-Golden. "Resident Alveolar Macrophages Suppress, Whereas Recruited Monocytes Promote, Allergic Lung Inflammation in Murine Models of Asthma." [In eng]. *J Immunol* 193, no. 8 (Oct 15 2014): 4245-53.

Zhu, B., J. K. Kennedy, Y. Wang, C. Sandoval-Garcia, L. Cao, S. Xiao, C. Wu, W. Elyaman*,* and S. J. Khoury. "Plasticity of Ly-6c(Hi) Myeloid Cells in T Cell Regulation." [In eng]. *J Immunol* 187, no. 5 (Sep 1 2011): 2418-32.

BIBLIOGRAPHY

Ziegler-Heitbrock, L. "Monocyte Subsets in Man and Other Species." [

SUPPLEMENTARY

VIII.   SUPPLEMENTARY DATA
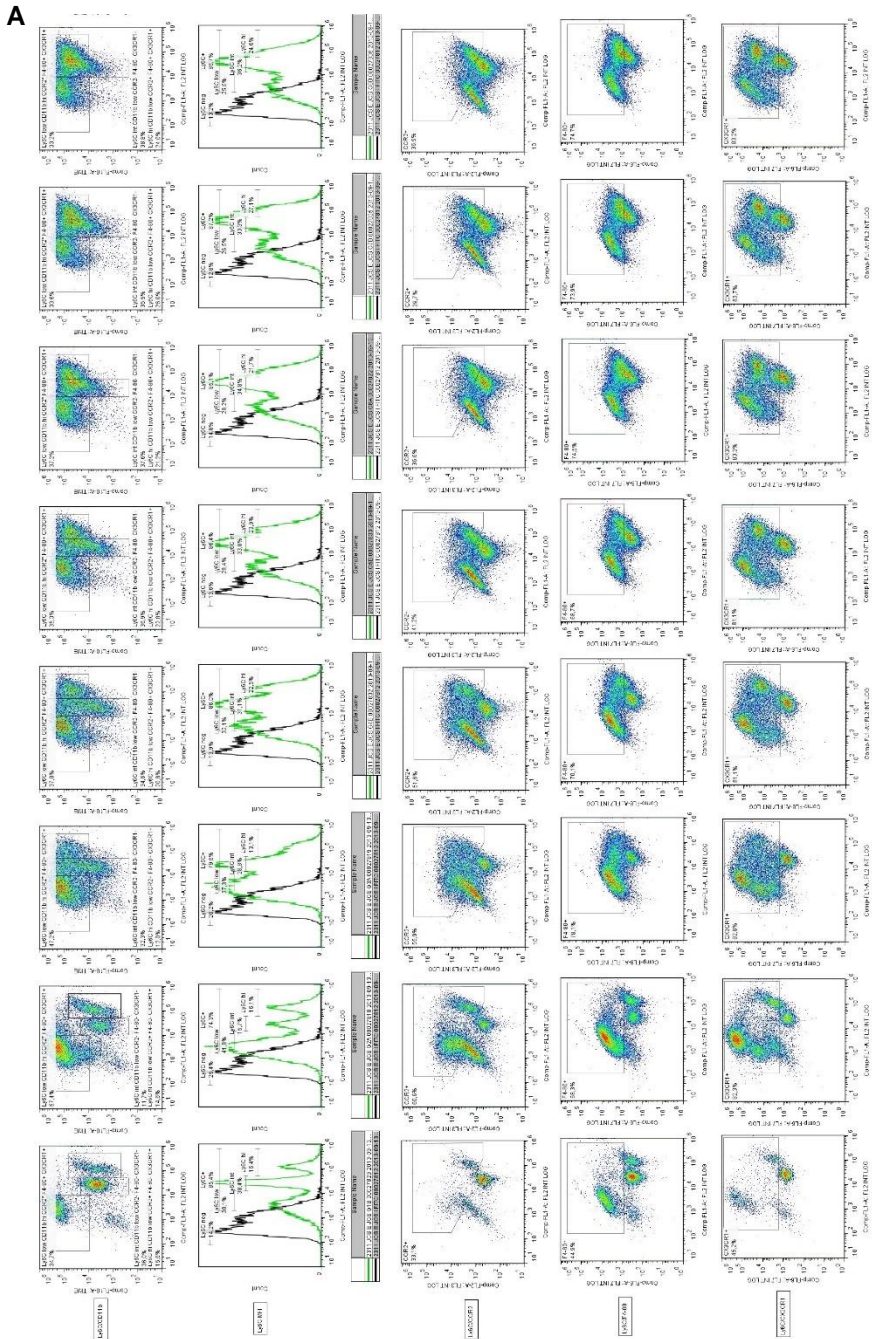
A

Figure1. Growth-factors titration is essential for correct *in vitro* generation of Ly6C^{hi} CD11b⁺ CCR2⁺ monocytes.

(A) Dot-blots of the titration of the growth-factor X concentrations showing the emergence of the characteristic monocyte markers.

Results are representative of three experiments.

B
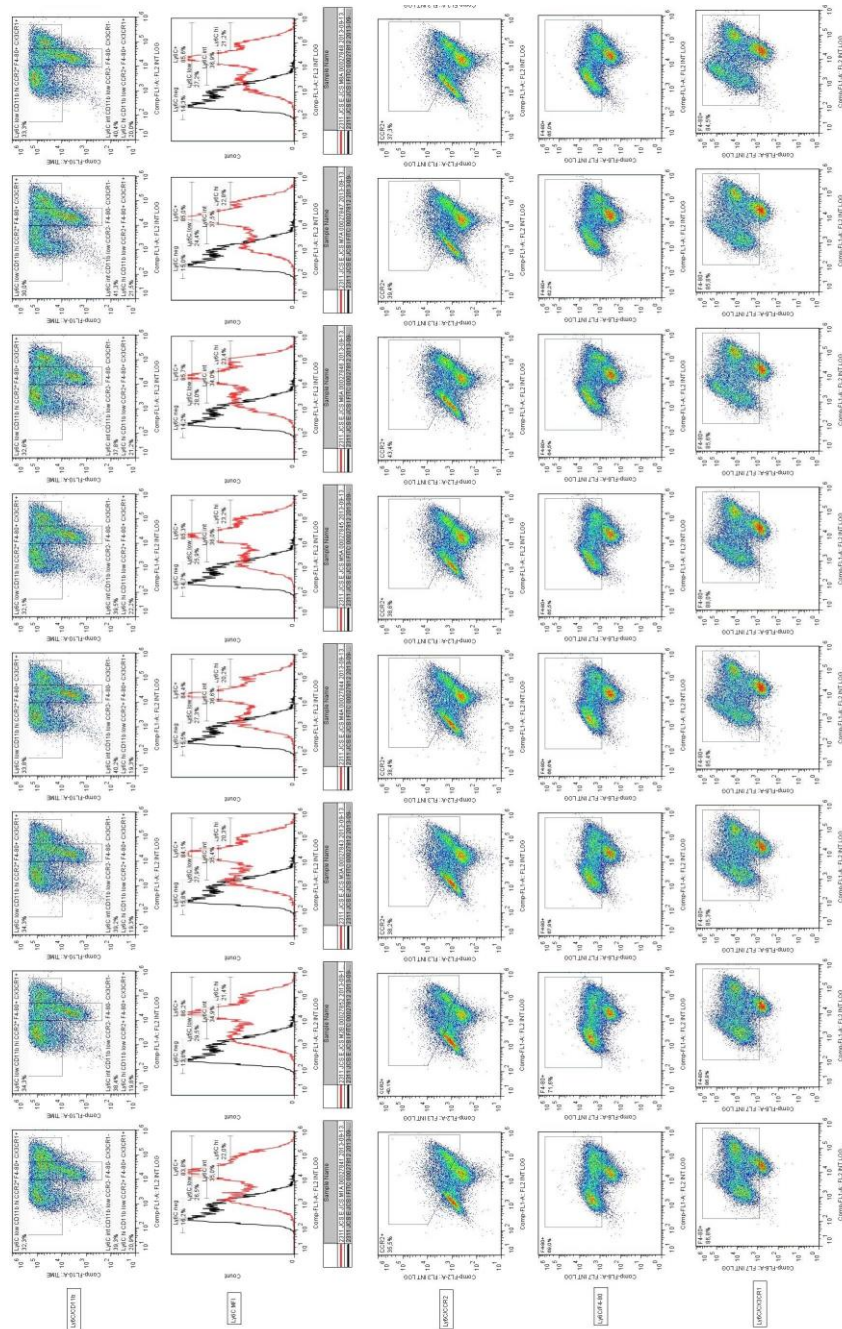
Figure1. Growth-factors titration is essential for correct *in vitro* generation of Ly6C^hi CD11b^+ CCR2^+ monocytes.
(B) Dot-blots of the titration of growth-factor Z concentrations showing the emergence of the characteristic monocyte markers.
Results are representative of three experiments.

A

B
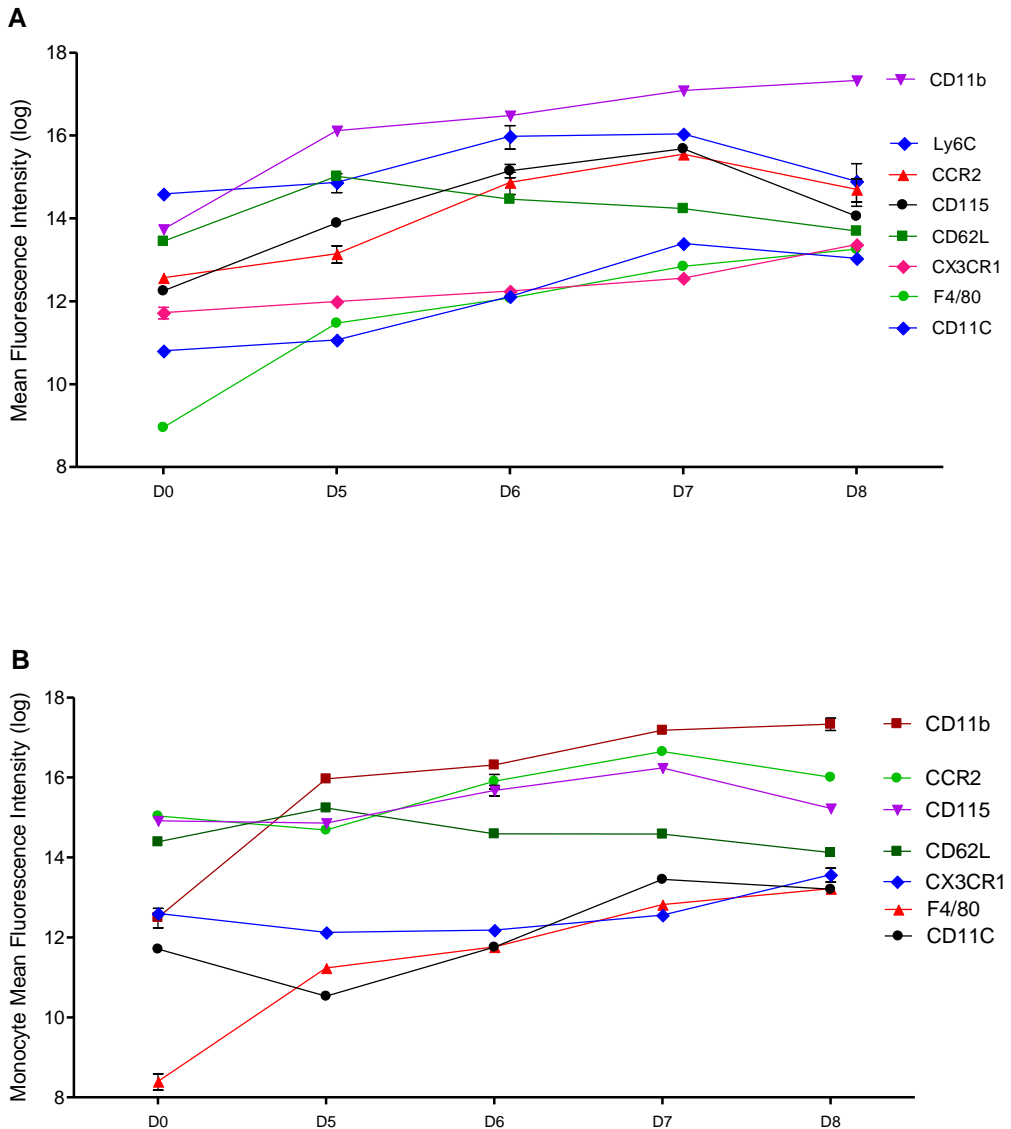
Figure2. Mean fluorescence intensity during kinetics of *in vitro* generation of Ly6C^{hi} CD11b^{+} CCR2^{+} monocytes.

(A) Kinetics of the mean fluorescence intensity for distinct characteristic monocyte markers during the *in vitro* generation of monocytes.

(B) Kinetics of the mean fluorescence intensity gated on the Ly6C^{hi} population during monocyte generation.

Results are representative of three experiments. Mean and ±SD are performed with three mice per group.

A
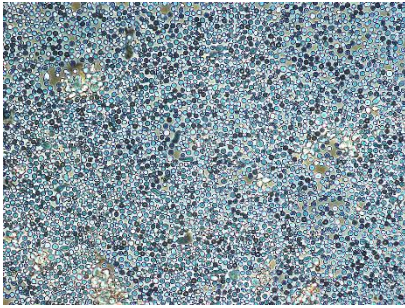
D0
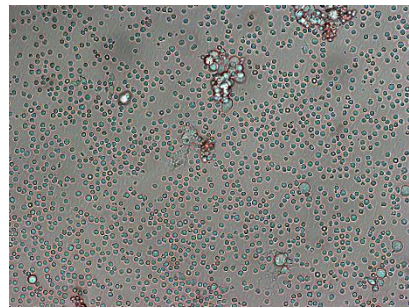
D1
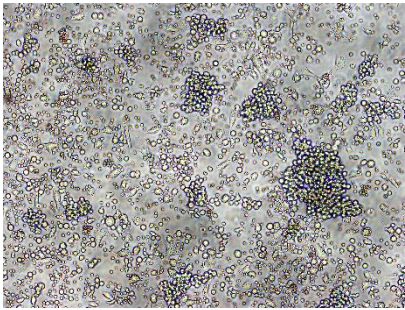
D2

D3

D4

D5

D6

D7

D8

D9

B

D3

D4

D5

D6
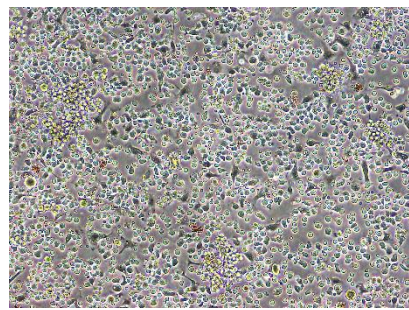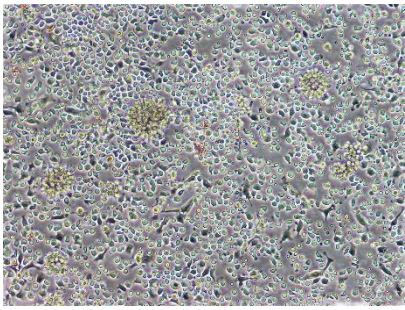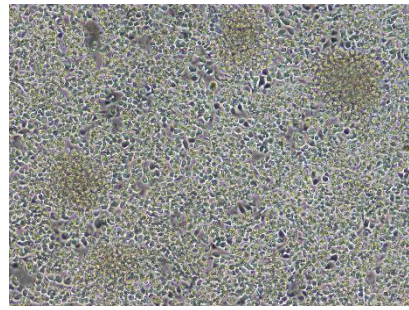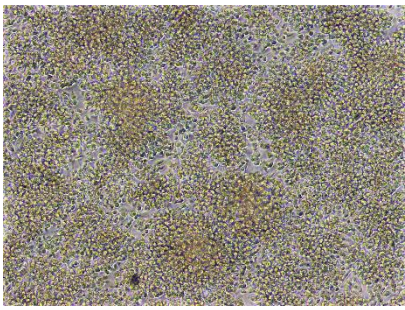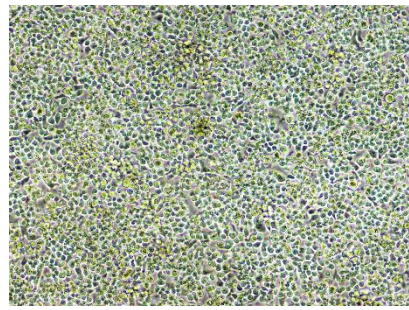
Figure3. Optic microscope images of different stages and different purified subpopulations of the *in vitro* culture of monocytes.
(A) Optic images of i*n vitro* produced monocyte cultures at days 0, 1, 2, 3, 4, 5, 6, 7, 8, and 9 (X10).
(B) Optic images of i*n vitro* produced monocyte cultures at X40.
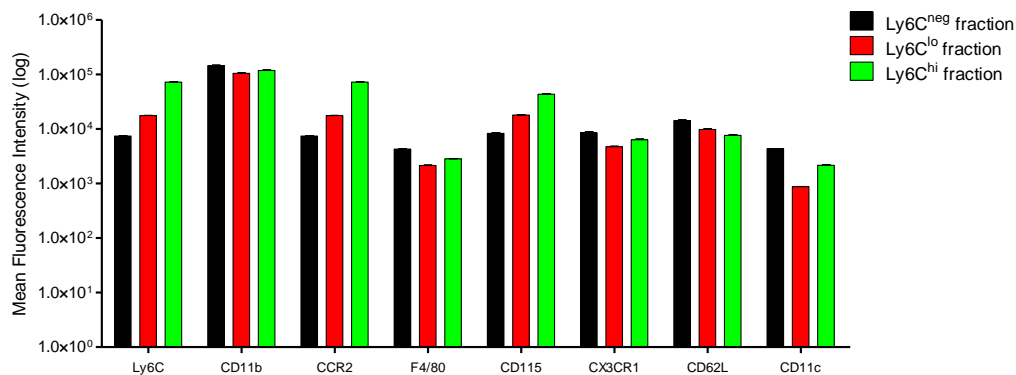
Figure4. Mean fluorescence intensity for characteristic monocyte markers of the distinct Ly6C^{neg}, Ly6C^{lo} and Ly6C^{hi} distinct fractions.
Flow cytometric comparative analysis for characteristic monocyte markers of the different fractions of the *in vitro* monocytes culture.
Results are representative of three experiments. Mean and ±SD are performed with three mice per group.
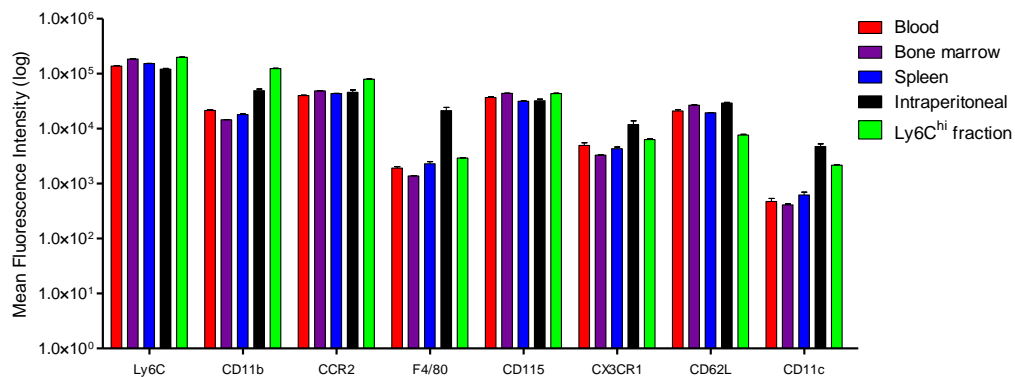
Figure5. Mean fluorescence intensity for characteristic monocyte markers of the distinct tissues of mice and the bone-marrow-derived monocytes
Flow cytometric comparative analysis for characteristic monocyte markers of the distinct tissues of mice and the bone-marrow-derived monocytes.
Results are representative of three experiments. Mean and ±SD are performed with three mice per group.
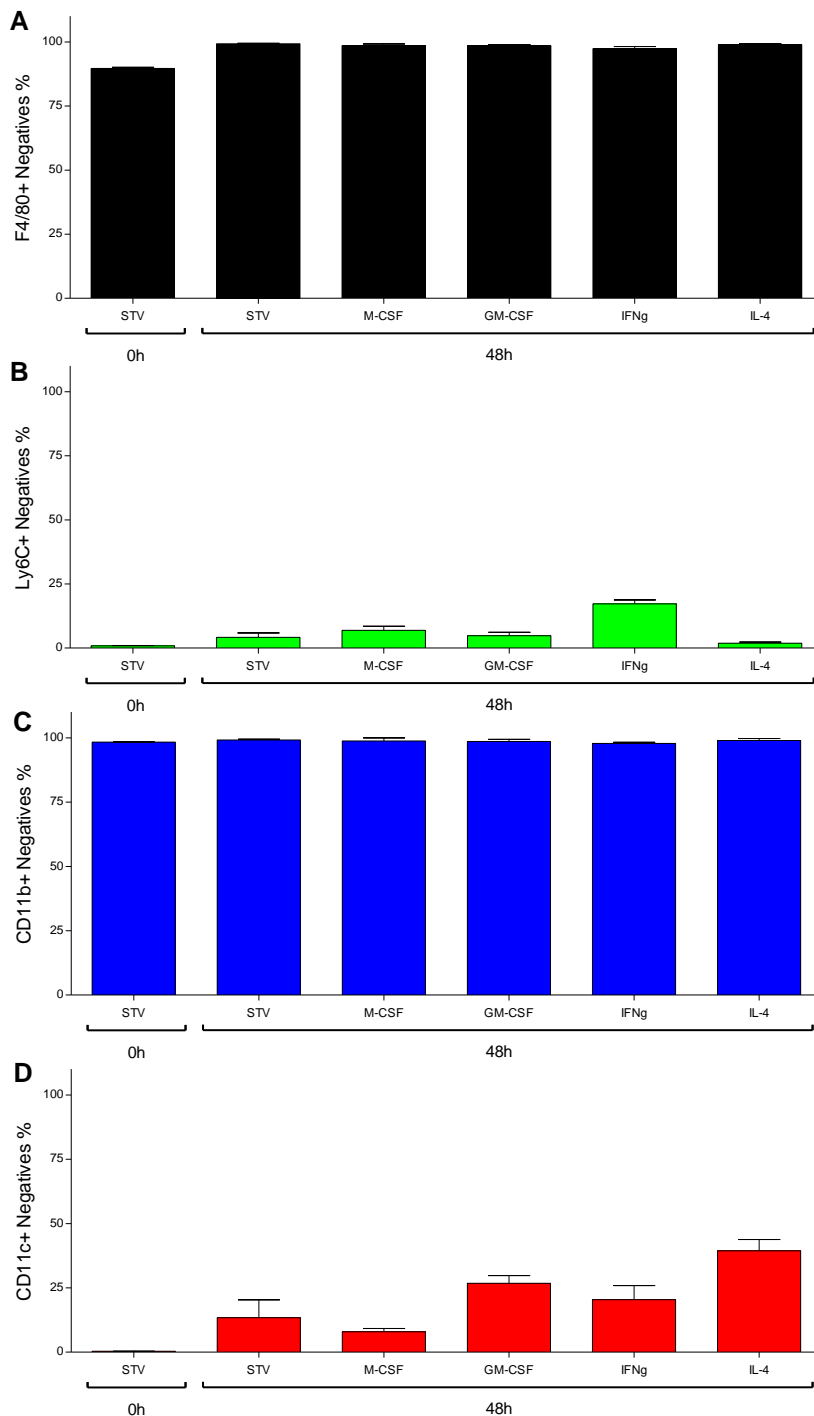
Figure6. *In vitro* produced Ly6C^neg cells present *in vitro* differentiation capacity.
(A, B, C, D) Flow cytometric analysis of the Ly6C^neg fraction cultured for forty-eight hours under distinct pro- and anti-inflammatory stimuli. Expression percentage of F4/80+ cells (A), Ly6C+ cells (B), CD11b+ cells (C) and CD11c+ cells (D).
Results are representative of one experiment. Mean and ±SD are performed with three mice per group.
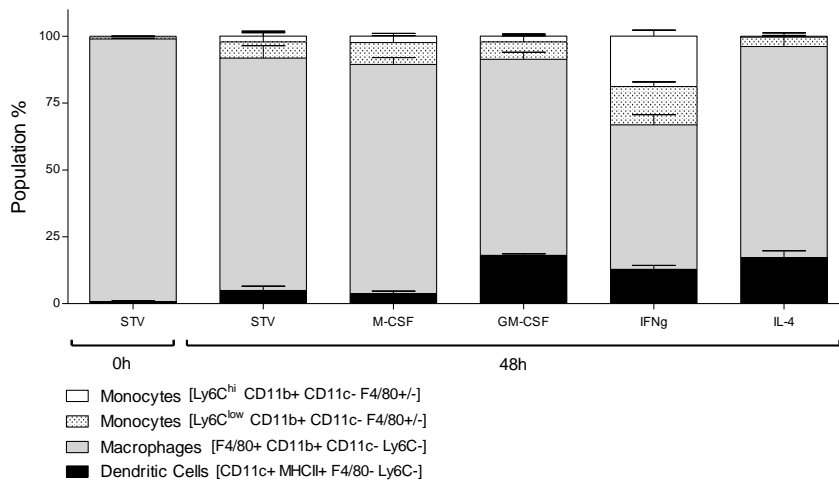
Figure7. *In vitro* produced Ly6C^{neg} monocytes show *in vitro* activation and maturation capacity.

Flow cytometric analysis of the Ly6C^{neg} fraction cultured for forty-eight hours under distinct pro- and anti-inflammatory stimuli. Total percentage of profiled macrophages, Ly6C^{hi} monocytes, Ly6C^{lo} monocytes and dendritic cells.

Results are representative of one experiment. Mean and ±SD are performed with three mice per group.
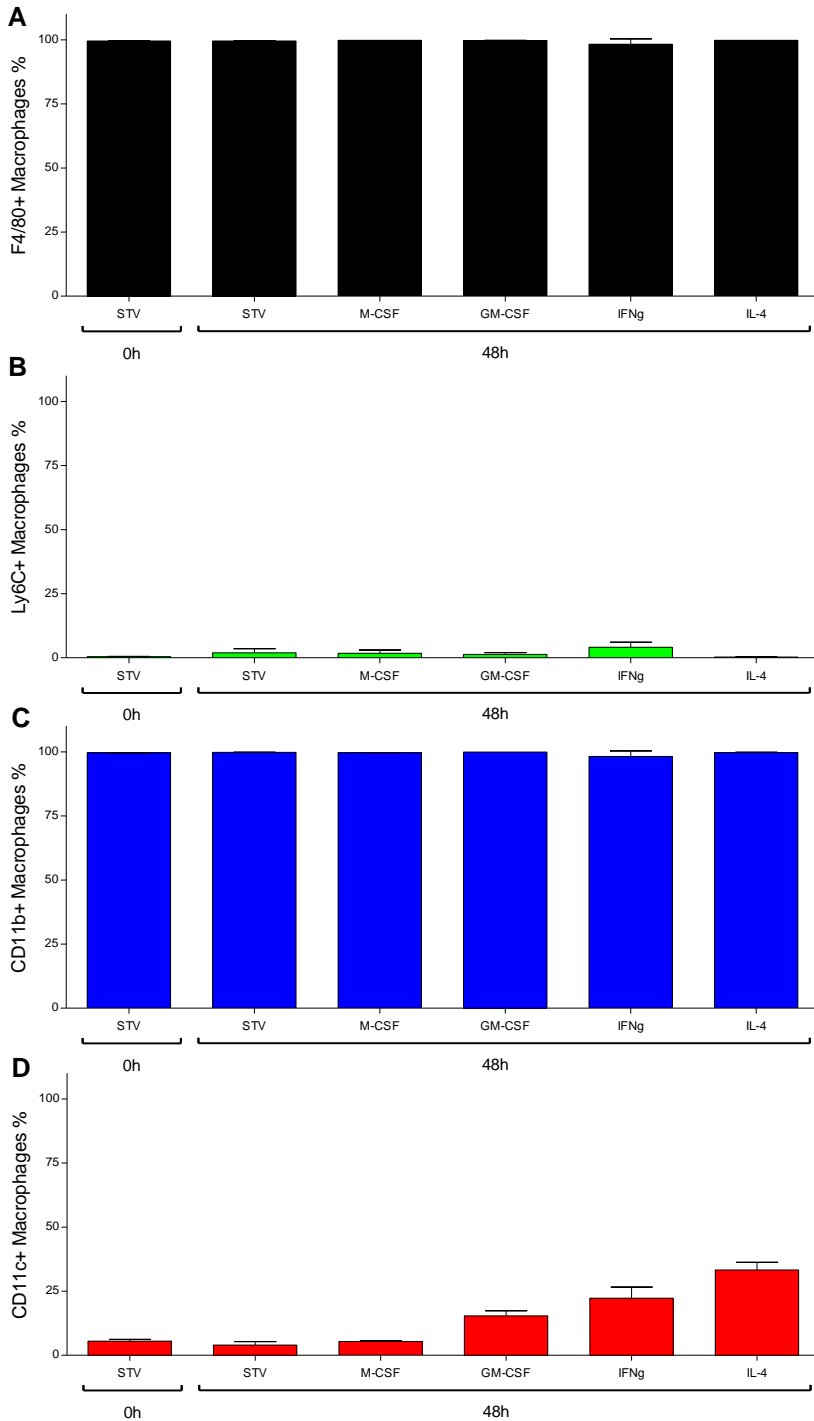
Figure8. *In vitro* produced macrophages present *in vitro* differentiation capacity.
(A, B, C, D) Flow cytometric analysis of the BMDM cultured for forty-eight hours under distinct pro- and anti-inflammatory stimuli. Expression percentage of F4/80+ cells (A), Ly6C+ cells (B), CD11b+ cells (C) and CD11c+ cells (D).
Results are representative of one experiments. Mean and ±SD are performed with three mice per group.
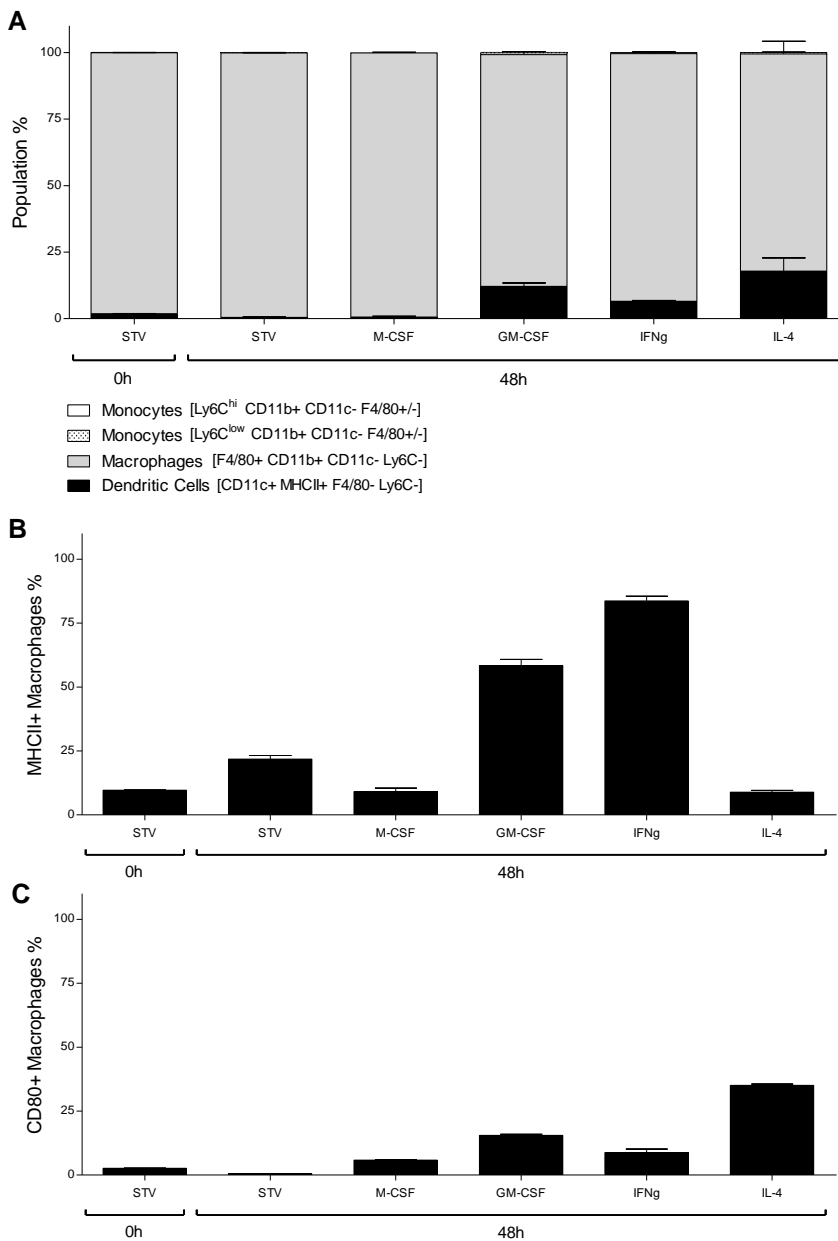
Figure9. *In vitro* produced macrophages show *in vitro* activation and maturation capacity.
(A, B, C) Flow cytometric analysis of the BMDM cultured for forty-eight hours under distinct pro- and anti-inflammatory stimuli. Total percentage of profiled macrophages, Ly6C^{hi} monocytes, Ly6C^{lo} monocytes and dendritic cells (A). Expression percentage of MHCII$^+$ cells (B) and CD80$^+$ cells (C). Results are representative of one experiment. Mean and ±SD are performed with three mice per group.
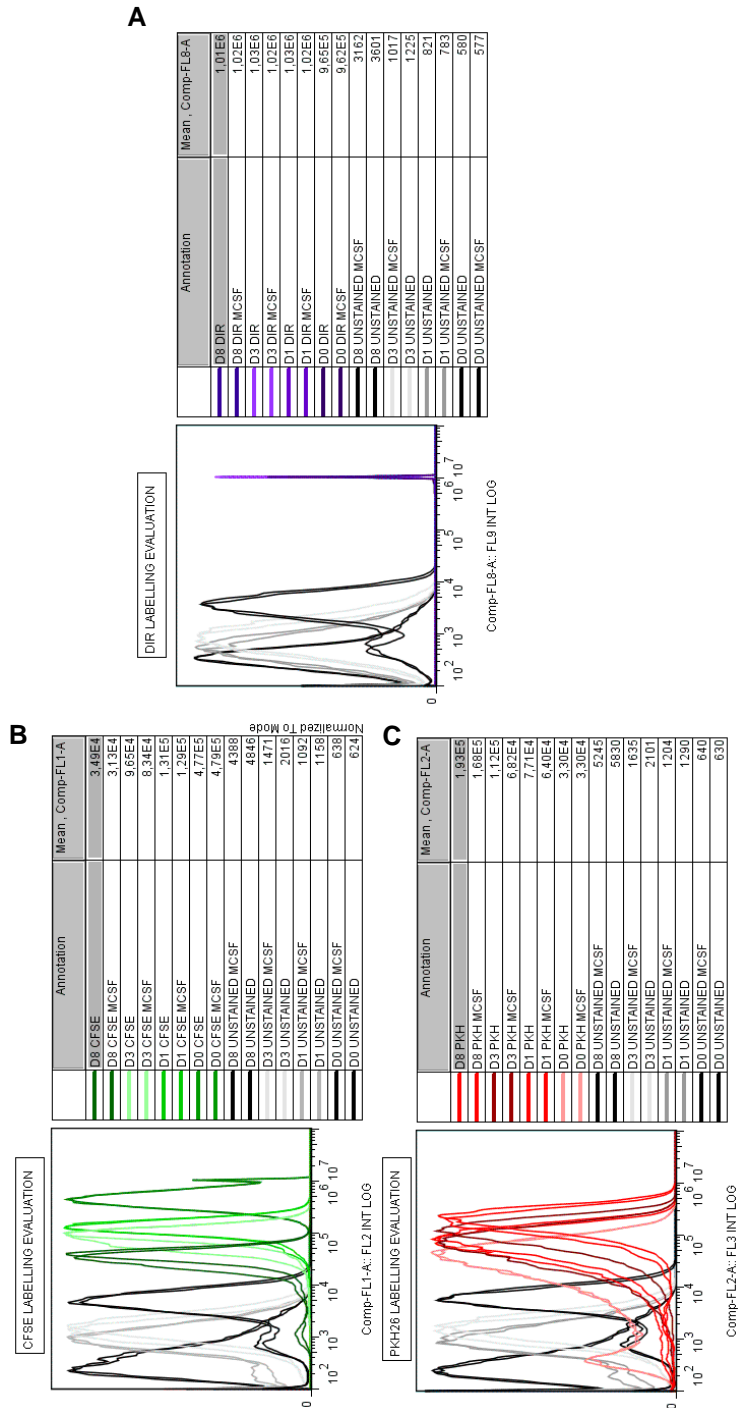
Figure10. Comparative analysis of DIR, CFSE and PKH26 tracers labelling of *In vitro* produced monocytes.
(A, B, C) Mean fluorescence intensity of the *in vitro* Ly6C^hi monocytes after DIR (A), CFSE (B) and PKH26 (C) labelling for different times.
Results are representative of one experiment. Mean and ±SD are performed with three mice per group.
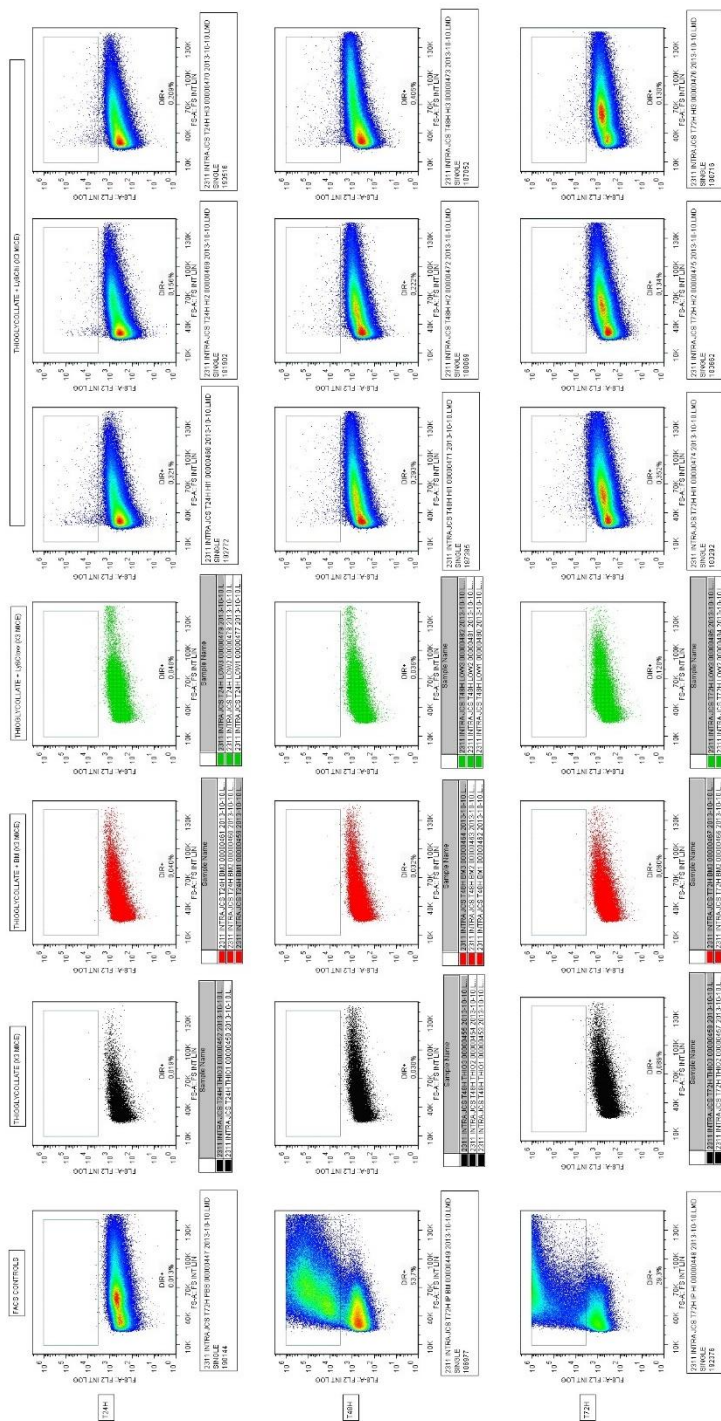
Figure11. *In vitro* Ly6C^{hi} monocytes are able to migrate and infiltrate selectively in a model of intraperitoneal inflammation
Representative dot-blots showing the DIR^{+} recovered cells from all experimental conditions.
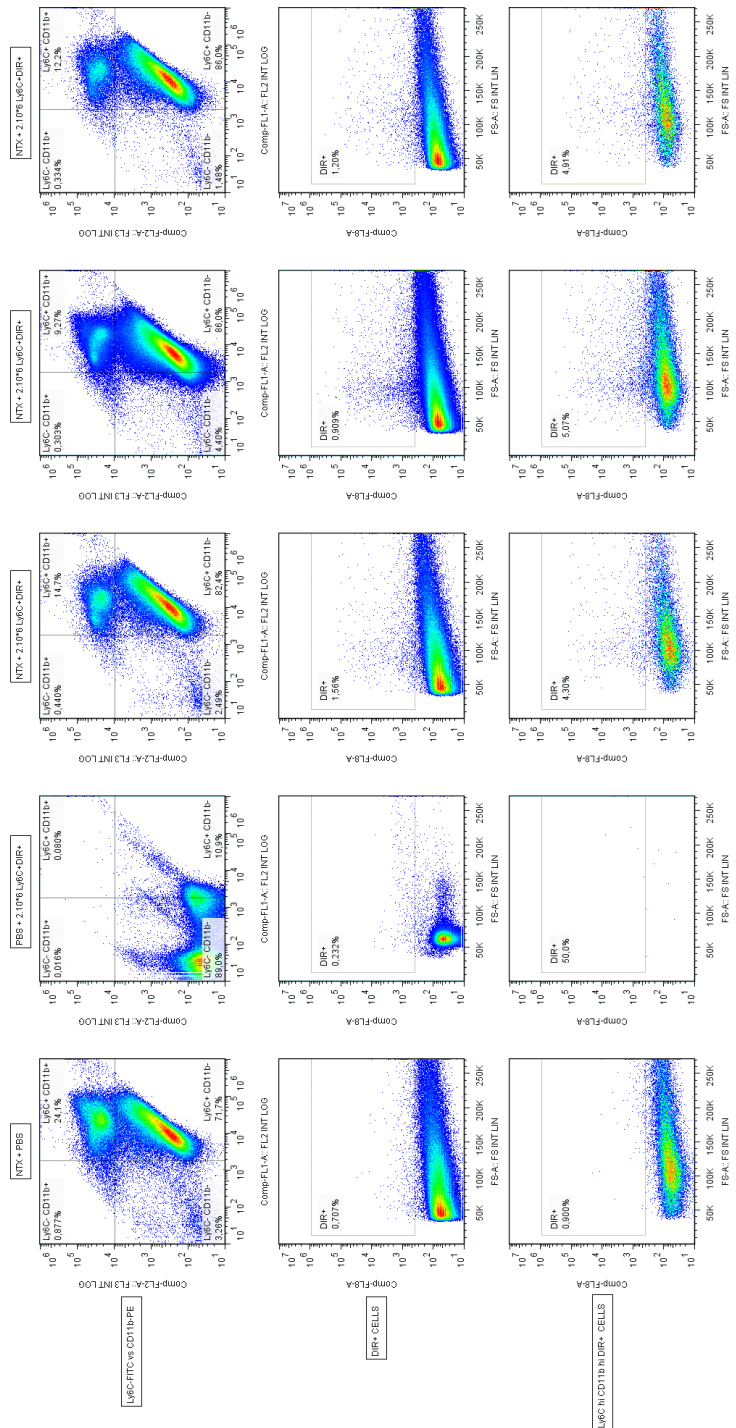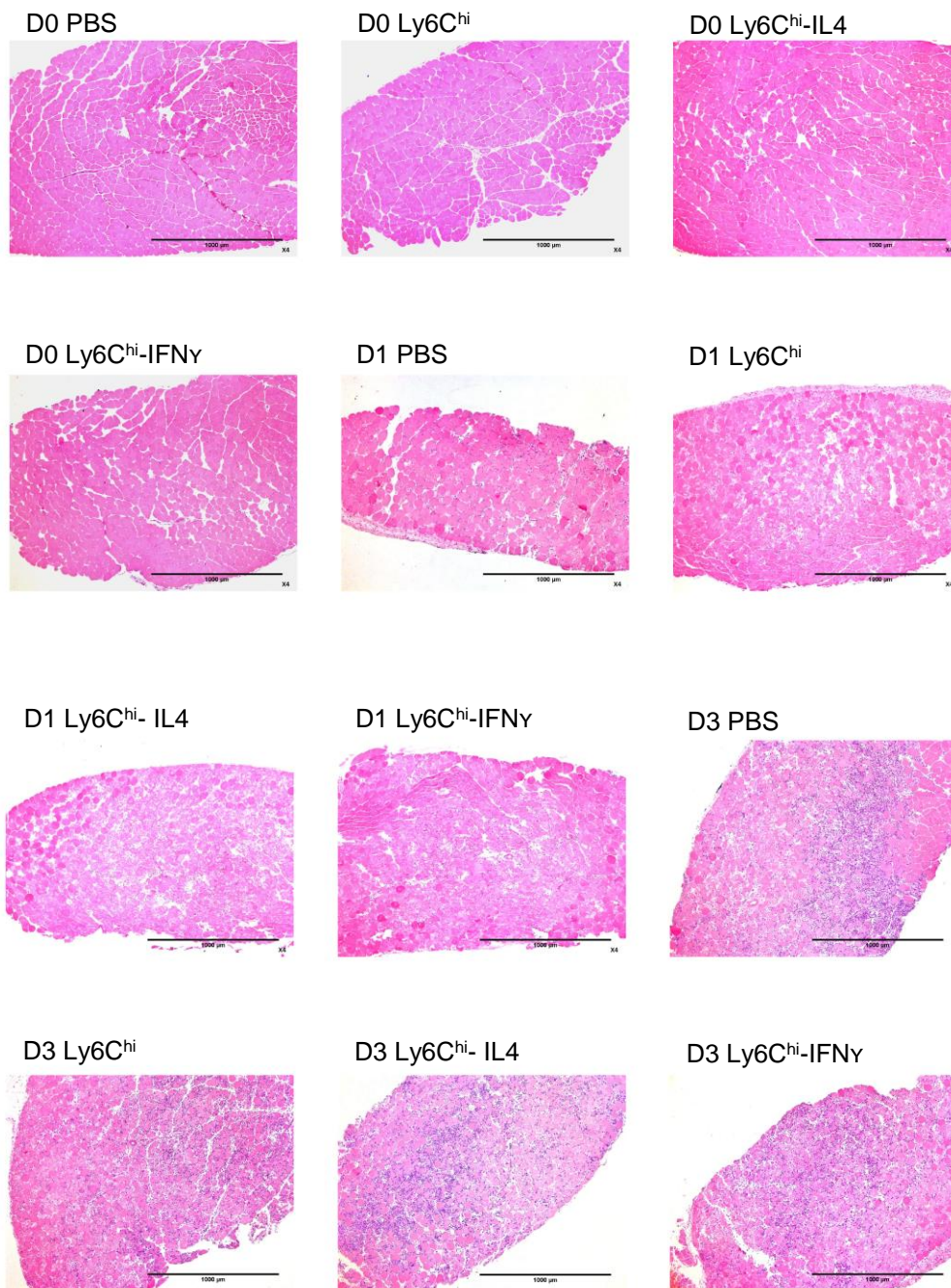Results are representative of three experiments. Mean and ±SD are performed with three mice per group.
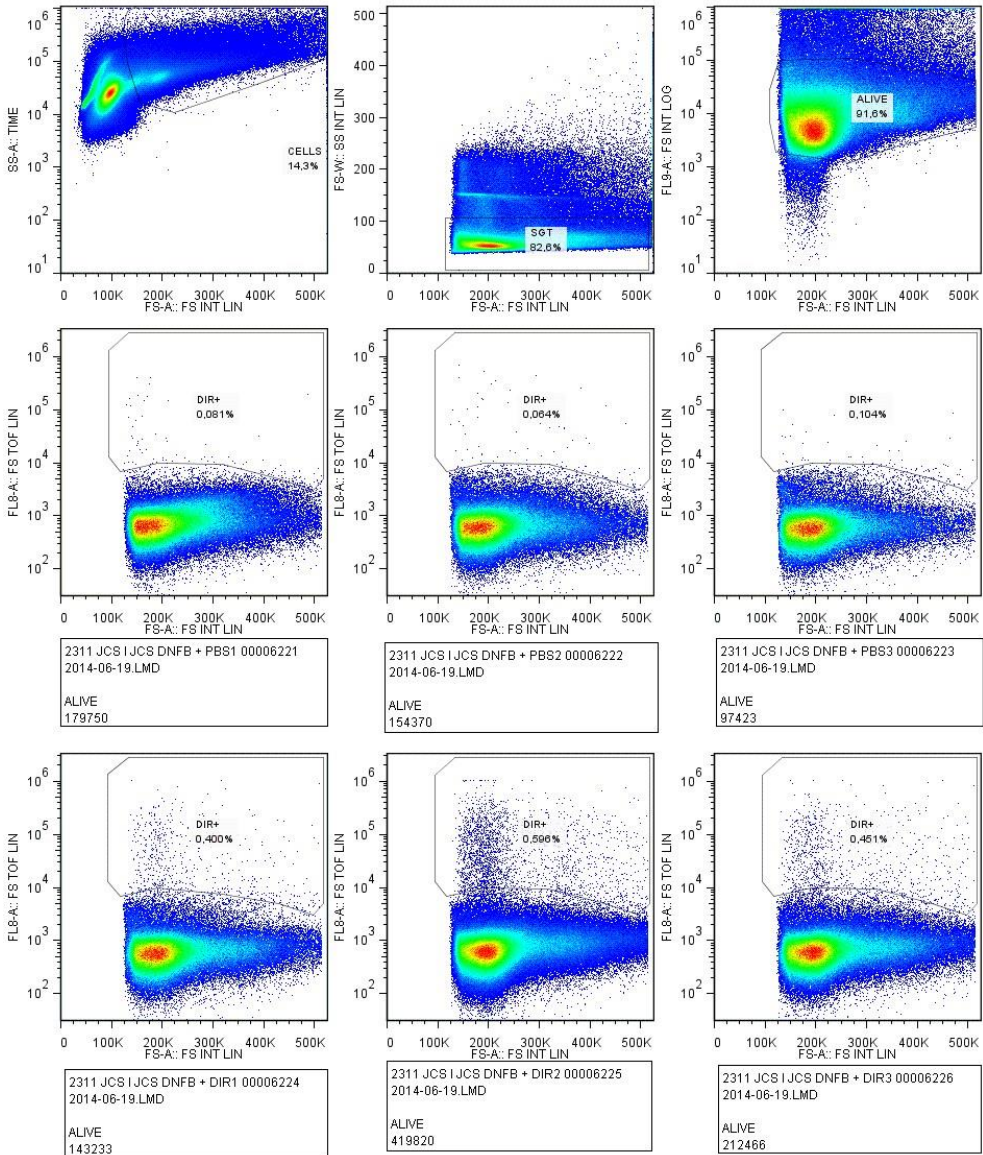
Figure12. *In vitro* **Ly6C**hi **monocytes are able to migrate and infiltrate selectively in the Dinitrofenolbenzene-induced contact inflammation model**
Representative dot-blots showing the DIR+ recovered cells from all experimental conditions.
Results are representative of three experiments. Mean and ±SD are performed with three mice per group.

D0 ACETONE
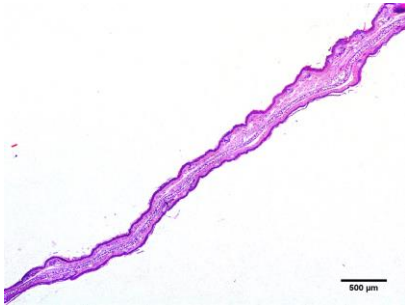
D0 DNFB

D1 Ly6C^hi

D1 PBS
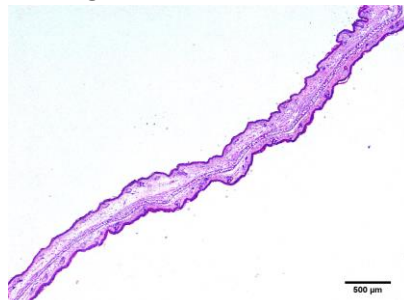
D2 Ly6C^hi

D2 PBS

D3 Ly6C^hi
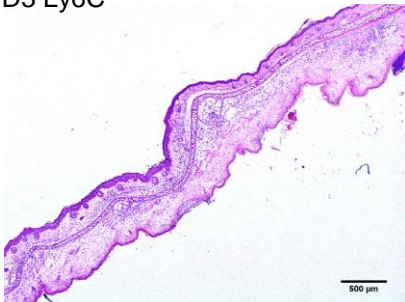
D3 PBS
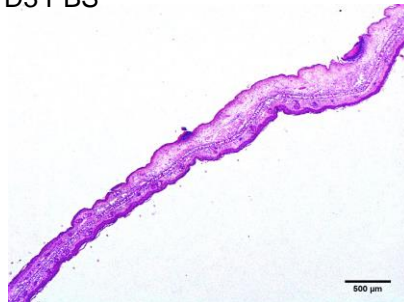
Figure13. Ear thickness after administration and kinetics of *in vitro* generated Ly6C^hi cells in the DNFB model

Optic microscope images of transversal ear cuts from each experimental condition.

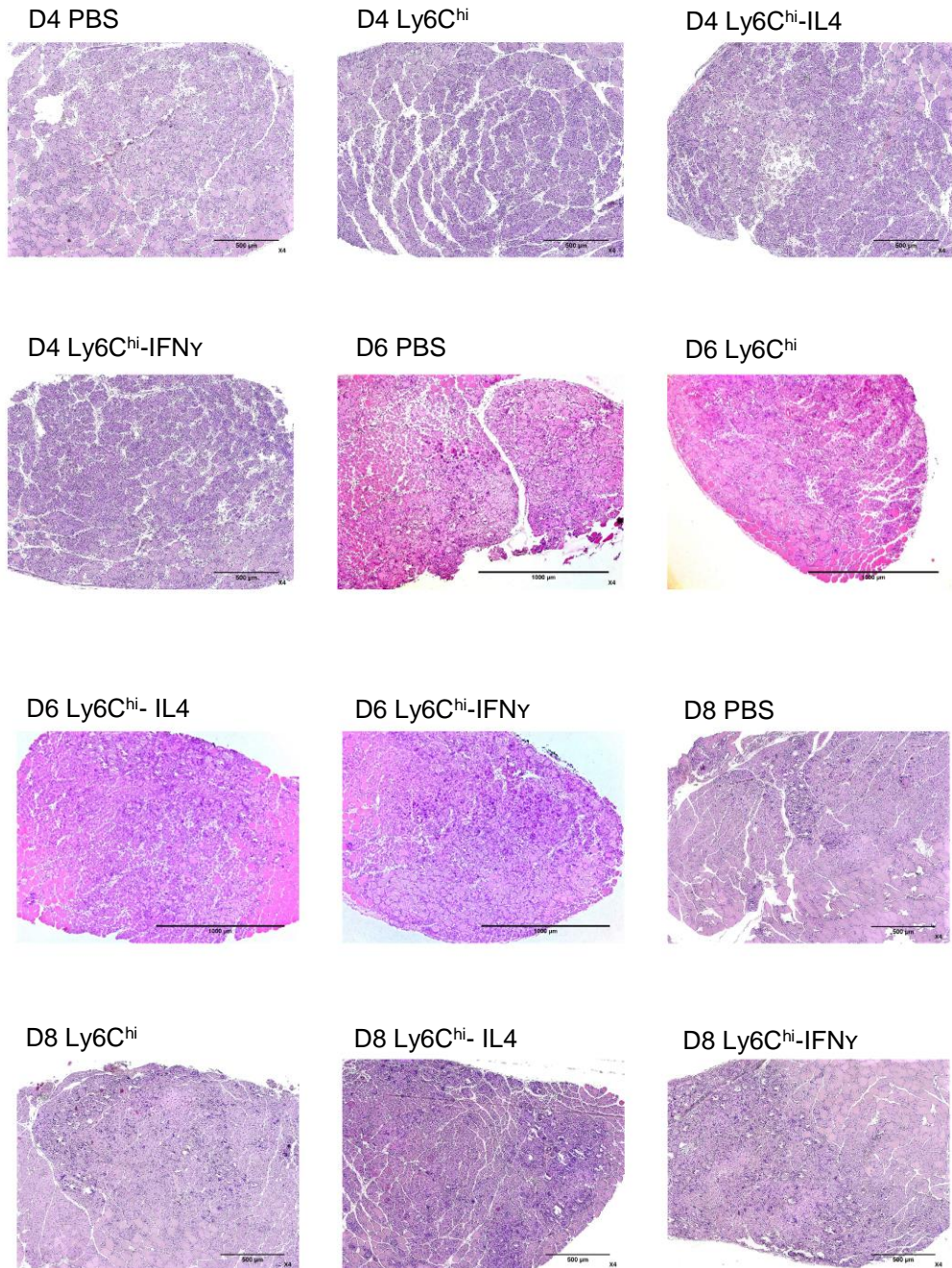Results are representative of two experiments. Mean and ±SD are performed with five mice per group.

D2 PBS

D2 Ly6C^{hi}

D2 Ly6C^{hi}-IL4

D2 Ly6C^{hi}-IFNγ
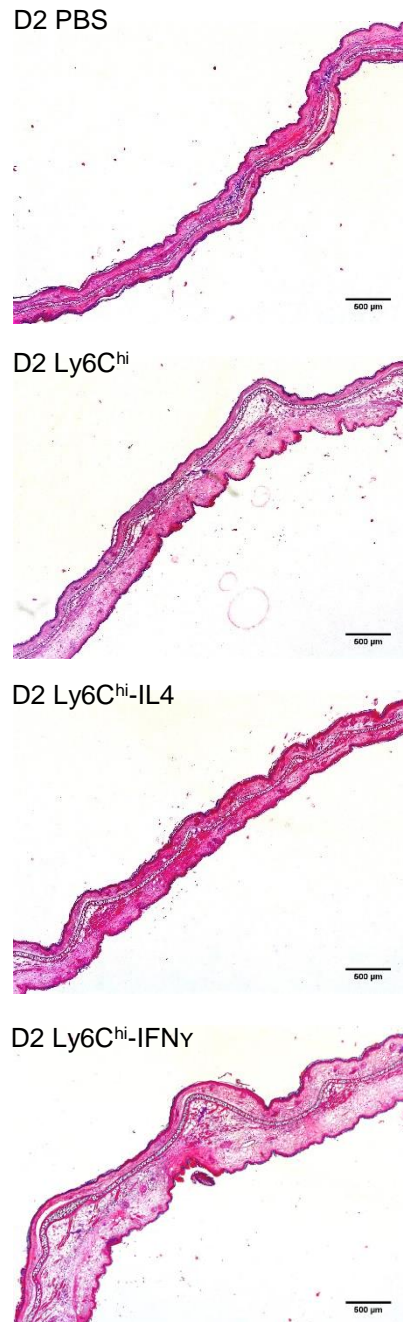
Figure14. Ear thickness after administration of IFN-γ- and IL-4-treated *in vitro* generated Ly6C^{hi} cells in the DNFB model
Optic microscope images of transversal ear cuts from each experimental condition.
Results are representative of two experiments. Mean and ±SD are performed with five mice per group.

D6 PBS

D6 Ly6C^{hi}

D6 Ly6C^{hi}-STAT1$^{-/-}$

D6 Ly6C^{hi}-STAT6$^{-/-}$
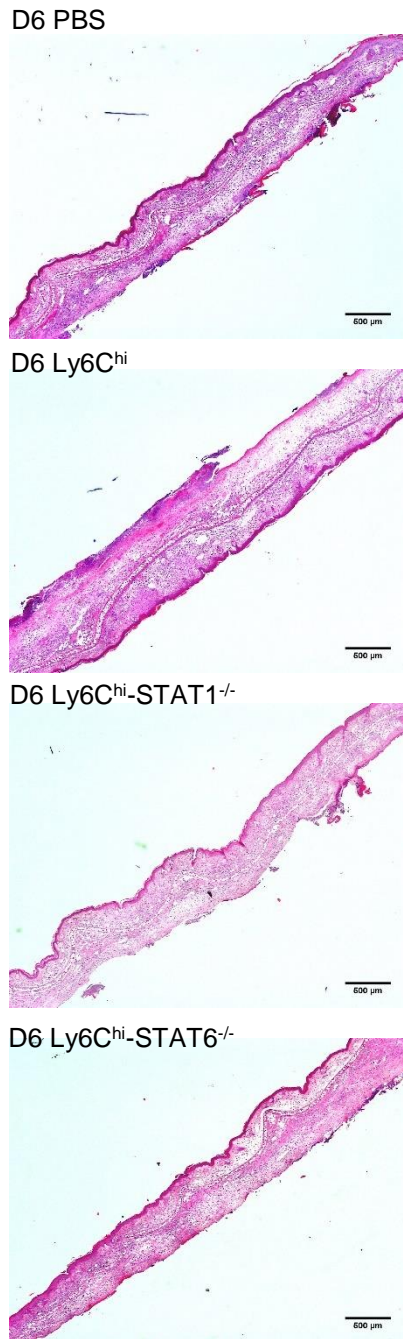
Figure15. Ear thickness after administration of STAT1$^{-/-}$- and STAT6$^{-/-}$-derived *in vitro* generated Ly6C^{hi} cells in the DNFB model
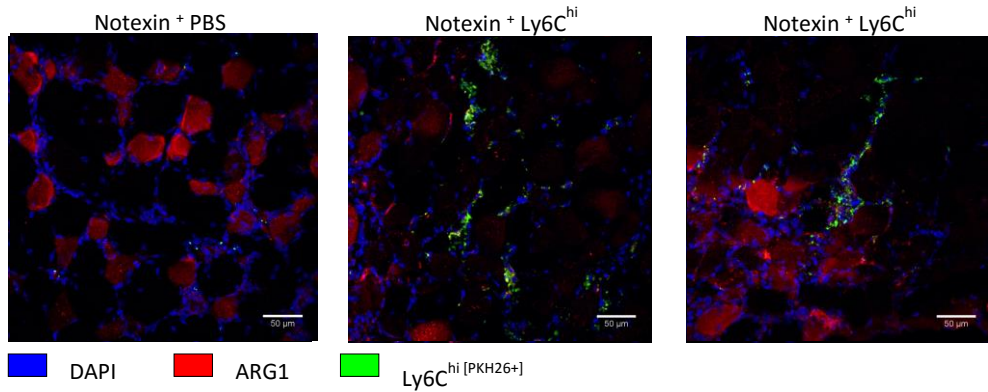Optic microscope images of transversal ear cuts from each experimental condition.
Results are representative of two experiments. Mean and ±SD are performed with five mice per group.

Figure16. *In vitro* Ly6C^{hi} monocytes are able to migrate and infiltrate selectively in the Notexin-induced myoinjury model
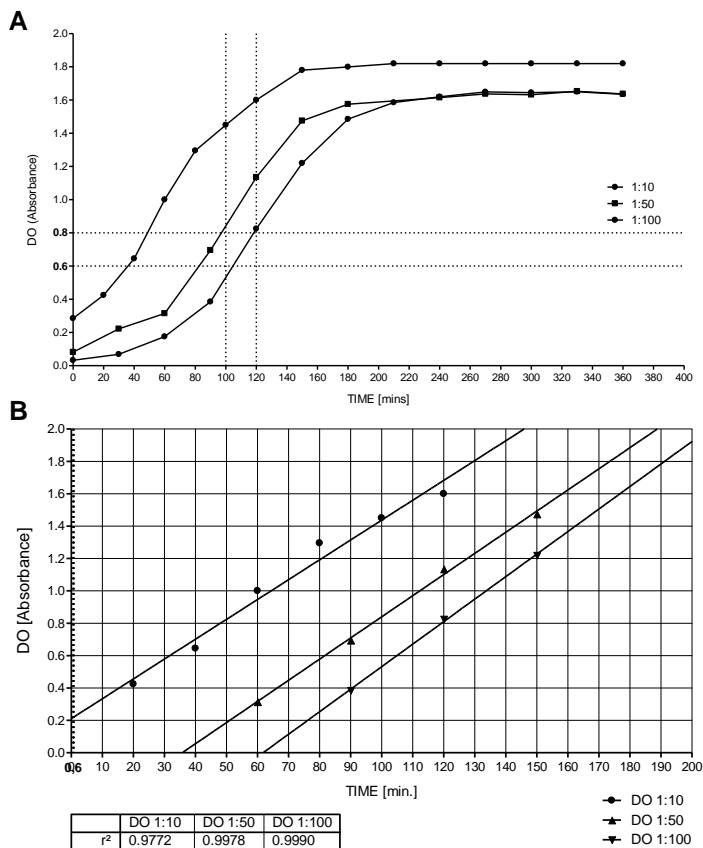
Representative dot-blots showing the DIR⁺ recovered cells from all experimental conditions.
Results are representative of three experiments. Mean and ±SD are performed with three mice per group.

D0 PBS

D0 Ly6C^{hi}

D0 Ly6C^{hi}-IL4

D0 Ly6C^{hi}-IFNɣ

D1 PBS

D1 Ly6C^{hi}

D1 Ly6C^{hi}- IL4

D1 Ly6C^{hi}-IFNɣ

D3 PBS

D3 Ly6C^{hi}

D3 Ly6C^{hi}- IL4

D3 Ly6C^{hi}-IFNɣ

Figure17. Ly6C^{hi} monocytes are able to migrate and infiltrate selectively in the Notexin-induced myoinjury model

Optic microscope images of muscle sections from each experimental condition after intravenous injection of non-treated, IL-4 treated or IFN-ɣ treated Ly6C^{hi} cells.

Results are representative of two experiments. Mean and ±SD are performed with four mice per group.

D4 PBS | D4 Ly6C^hi | D4 Ly6C^hi-IL4

D4 Ly6C^hi-IFNγ | D6 PBS | D6 Ly6C^hi

D6 Ly6C^hi- IL4 | D6 Ly6C^hi-IFNγ | D8 PBS

D8 Ly6C^hi | D8 Ly6C^hi- IL4 | D8 Ly6C^hi-IFNγ

Figure17. *In vitro* Ly6C^hi monocytes are able to migrate and infiltrate selectively in the Notexin-induced myoinjury model

Optic microscope images of muscle sections from each experimental condition after intravenous injection of non-treated, IL-4 treated or IFN-γ treated Ly6C^hi cells.

Results are representative of two experiments. Mean and ±SD are performed with four mice per group.

155

Notexin $^+$ PBS	Notexin $^+$ Ly6C^{hi}	Notexin $^+$ Ly6C^{hi}

DAPI   ARG1   Ly6C$^{hi\ [PKH26+]}$

Figure18. Immunohistochemistry of ARG1 after infiltration of *in vitro* Ly6C^{hi} monocytes in the Notexin model

Fluorescence microscopy showing muscular tissue infiltrated PKH26$^+$ cells and ARG1 expression. Results are representative of one experiment. Mean and ±SD are performed with five mice per group.

	DO 1:10	DO 1:50	DO 1:100
r²	0.9772	0.9978	0.9990

Figure19. Establishment of the growth-curve of *Klebsiella pneumoniae*

(A) Growth-curve of *Klebsiella pneumoniae* (B) Linear regression extracted from the growth-curve of *Klebsiella pneumoniae.* Results are representative of three experiments. Mean and ±SD are performed with five triplicates.

156
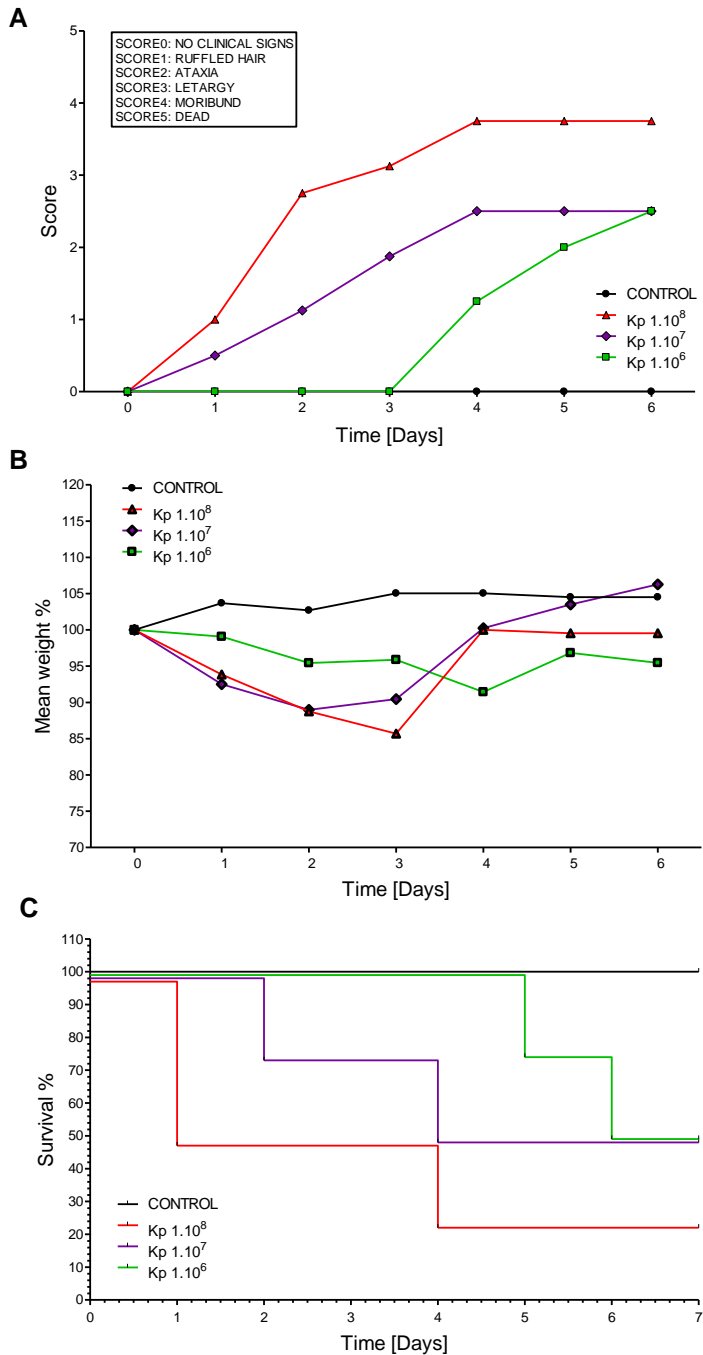
Figure20. Establishment of lethal dose 50% of *Klebsiella pneumoniae* in C57/B6 mice
(A) Score curves from each experimental condition at days 0 till 7 after intranasal inoculation of *Klebsiella pneumoniae*.
(B) Mean initial weight percentage curves from each experimental condition at days 0 till 7.
(C) Survival curves from each experimental condition at days 0 till 7 after intranasal inoculation of bacteria.
Results are representative of two experiments. Mean and ±SD are performed with ten mice per group.

A

KP + Ly6C^{hi}
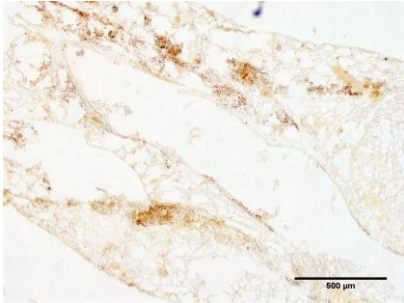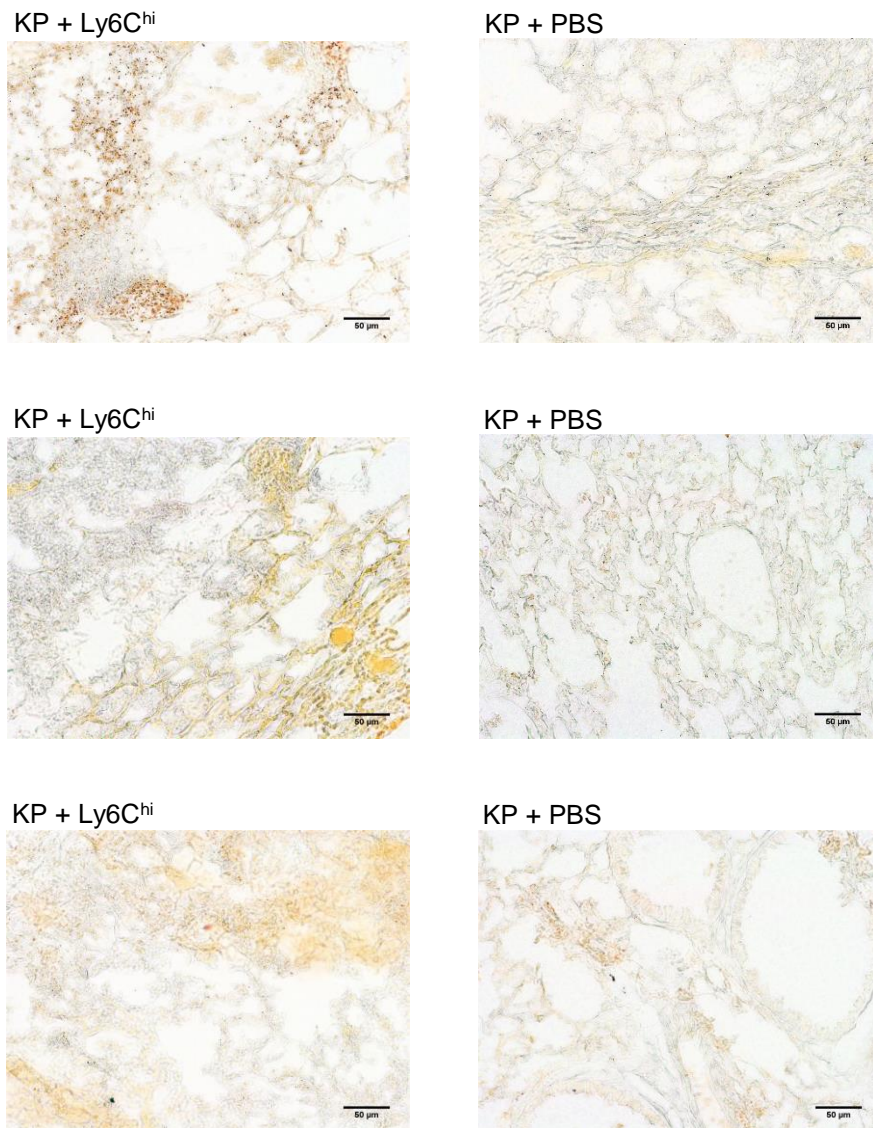
KP + PBS
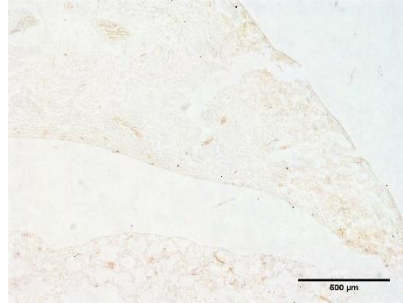
KP + Ly6C^{hi}
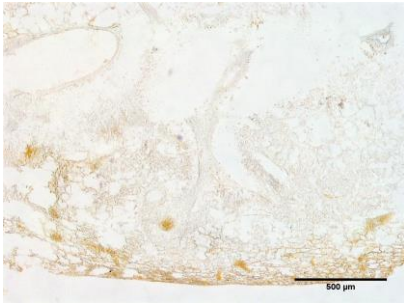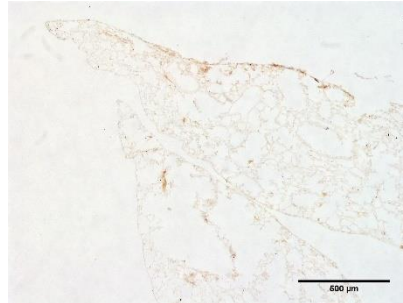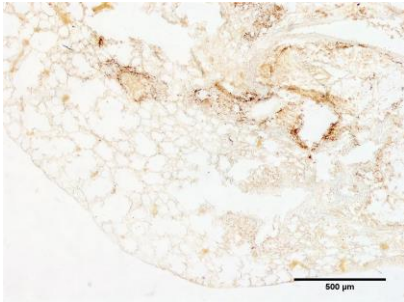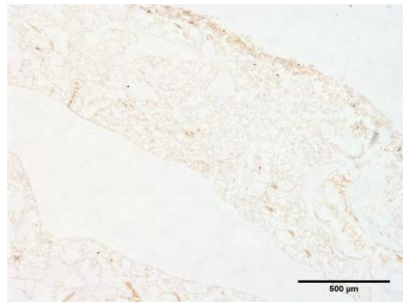
KP + PBS

KP + Ly6C^{hi}

KP + PBS

Figure21. Peroxidase based immunohistochemistry against TNF-α in the model of *Klebsiella pneumoniae*
(A) Optical microscopy showing TNF-α peroxidase labelling in lung tissue from mice injected intravenously with PBS or Ly6C^{hi} cells (X4).
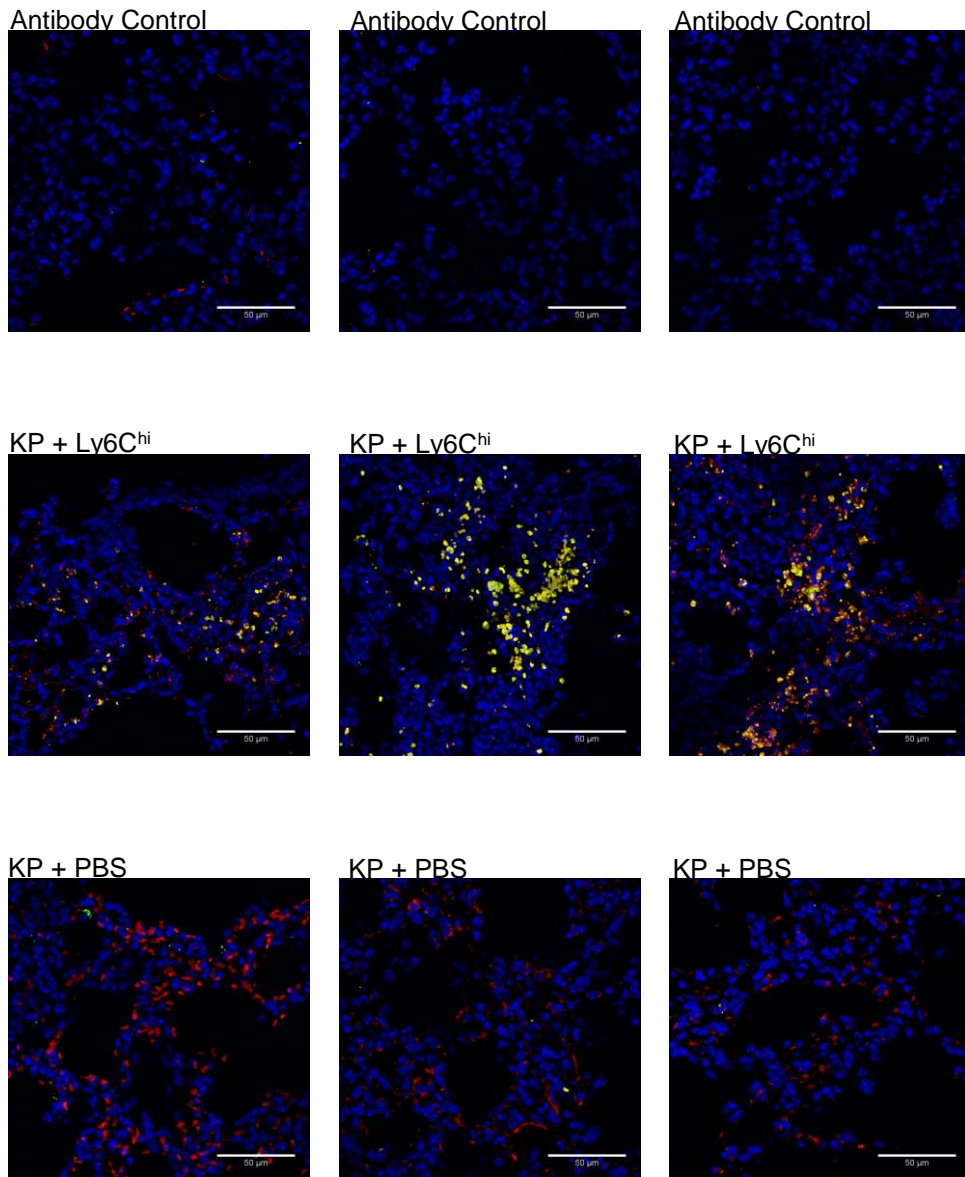Results are representative of one experiment. Mean and ±SD are performed with three mice per group.

B

KP + Ly6C^{hi}

KP + PBS

KP + Ly6C^{hi}

KP + PBS

KP + Ly6C^{hi}

KP + PBS

Figure21. Peroxidase based immunohistochemistry against TNF-α in the model of *Klebsiella pneumoniae*
(B) Optical microscopy showing TNF-α peroxidase labelling in lung tissue from mice injected intravenously with PBS or Ly6C^{hi} cells (X20).
Results are representative of one experiment. Mean and ±SD are performed with three mice per group.

Figure22. Fluorescence based immunohistochemistry against TNF-α in the model of *Klebsiella pneumoniae*

 Fluorescence microscopy showing lung tissue infiltrated PKH26$^+$ Ly6C^{hi} cells expressing TNF-α at 48 hours.
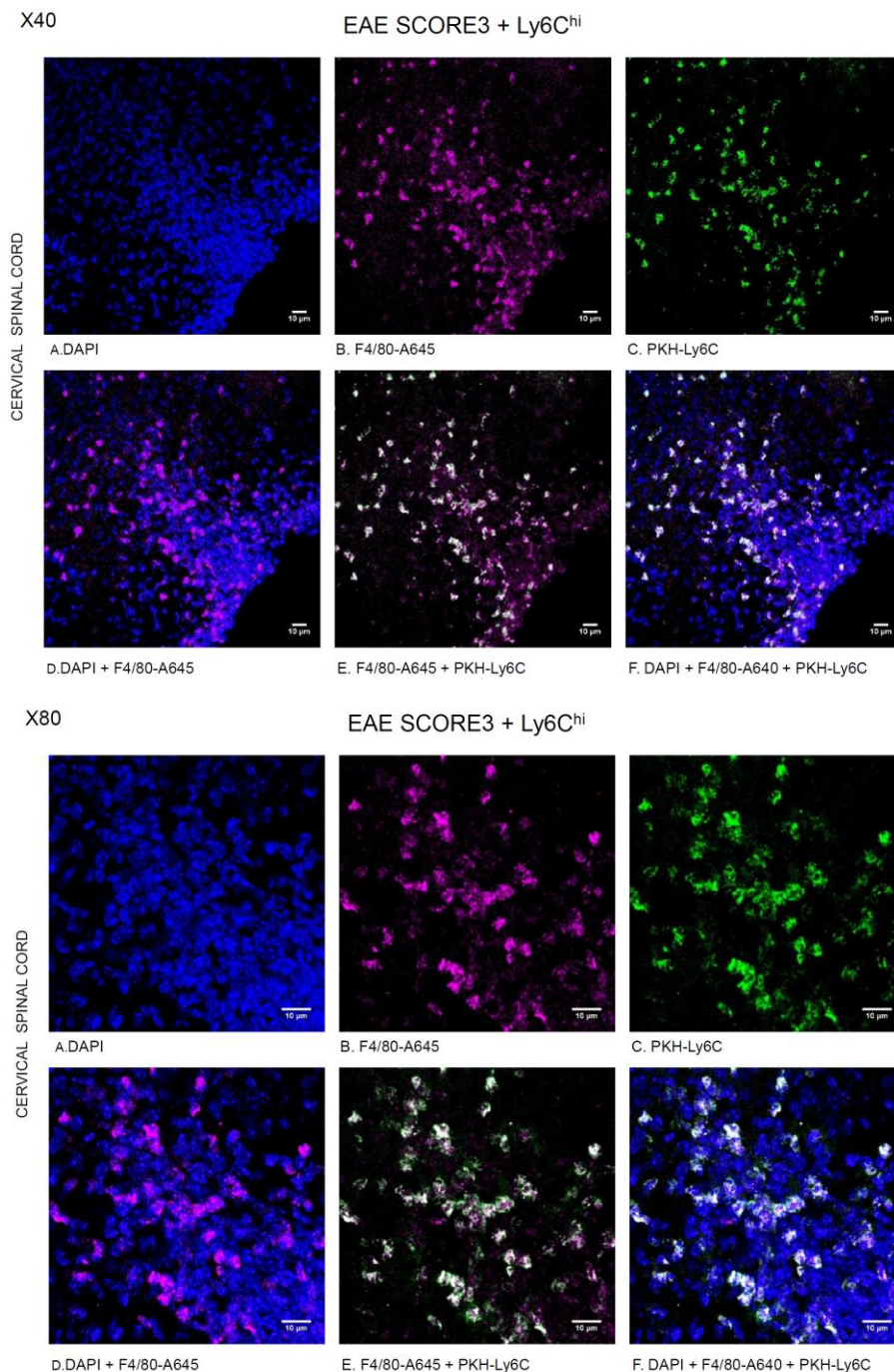
Results are representative of one experiment. Mean and ±SD are performed with three mice per group.
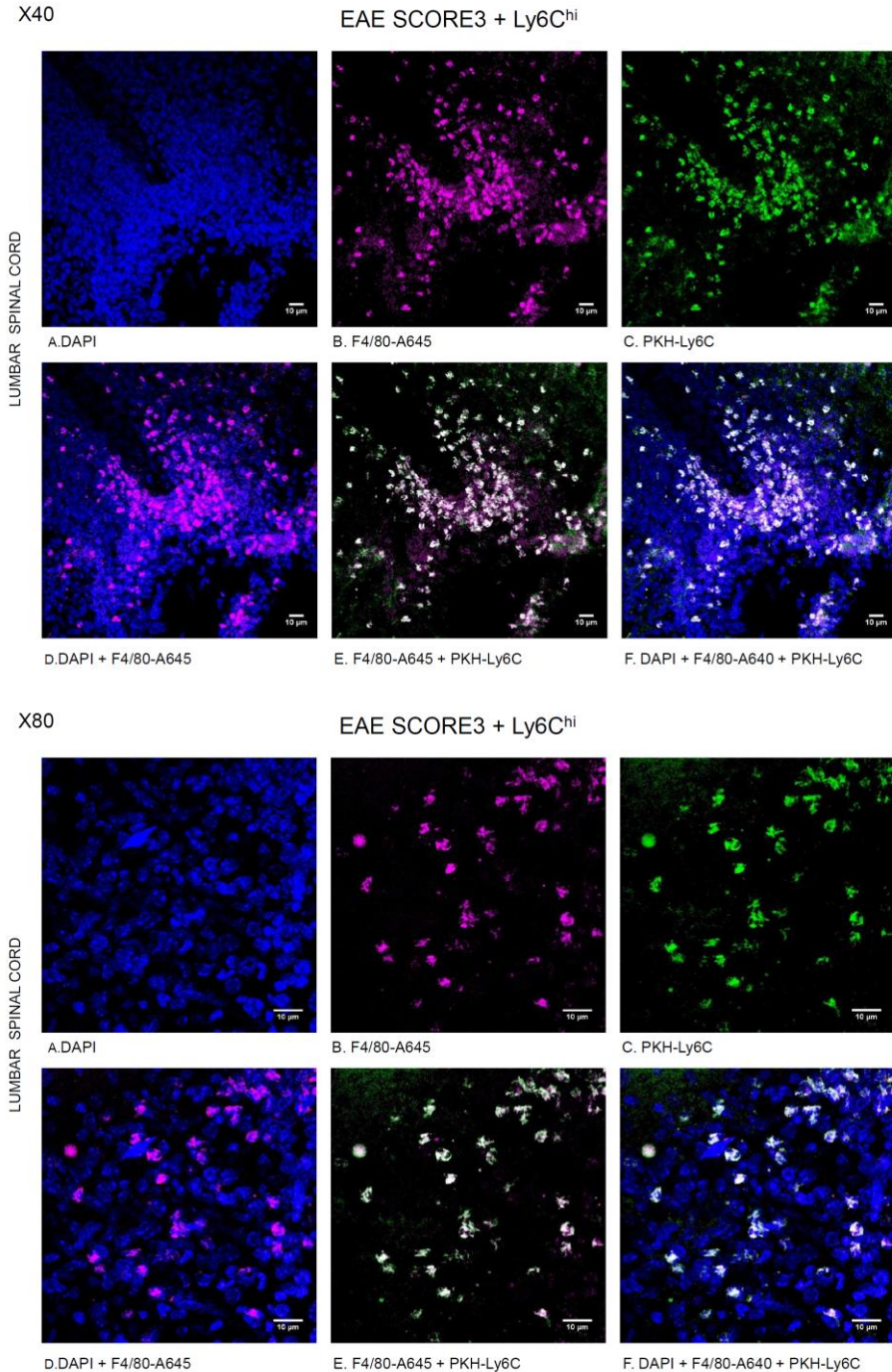
A

B

C
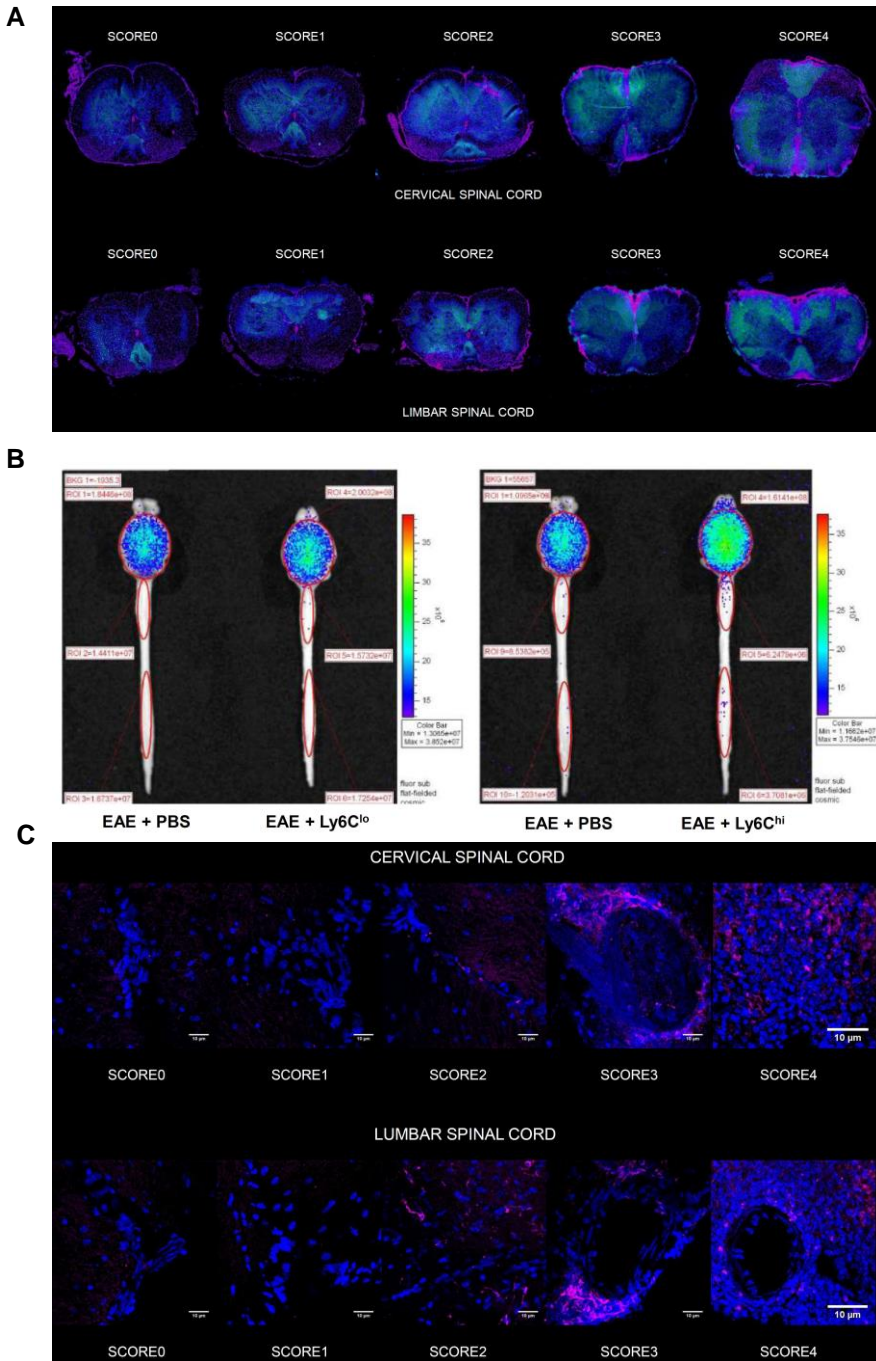
Figure23. Infiltration of *in vitro* Ly6C^{hi} monocytes within the spinal cord of EAE mice
(A) Fluorescence microscopy showing CNS tissue infiltrated with F4/80$^+$ cells and PKH26$^+$ cells.
(B) IVIS images of the fluorescence emitted by the central nervous system at score 3 of EAE, 48 hours after intravenous injection of DIR labelled cells.
(D) Fluorescence microscopy showing cell infiltration of F4/80+ macrophages at score 3 of EAE.
Results are representative of two experiments. Mean and ±SD are performed with three mice per group.

Figure24. Infiltration of PKH26+ *in vitro* Ly6C^hi monocytes within spinal cord of EAE mice
Fluorescence microscopy showing cell infiltration of F4/80+ macrophages and PKH26+ injected Ly6C^hi cells at score 3 of EAE.
Results are representative of two experiments. Mean and ±SD are performed with three mice per group.

Figure24. Infiltration of PKH26+ *in vitro* Ly6C^hi monocytes within spinal cord of EAE mice
Fluorescence microscopy showing cell infiltration of F4/80+ macrophages and PKH26+ injected Ly6C^hi cells at score 3 of EAE.
Results are representative of two experiments. Mean and ±SD are performed with three mice per group.